

**Aus dem Institut für Prophylaxe und Epidemiologie der Kreislaufkrankheiten  
der Ludwig-Maximilians-Universität München  
Vorstand: Prof. Dr. med. P. C. Weber**

# **Dual function of LIMK2 in endothelial cells**

**Dissertation  
zum Erwerb des Doktorgrades der Humanbiologie  
an der Medizinischen Fakultät der  
Ludwig-Maximilians-Universität zu München**

**vorgelegt von  
Pankaj Goyal**

**aus  
Agra, Indien**

**2005**

**Mit Genehmigung der Medizinischen Fakultät  
der Universität München**

**1. Berichterstatter: Prof. Dr. med. Wolfgang Siess**

**2. Berichterstatter: Prof. Dr. M. Schleicher**

**Mitberichterstatter: Priv. Doz. Dr. R. Wienecke  
Prof. Dr. W. M. Franz**

**Dekan: Prof. Dr. med. D. Reinhardt**

**Tag der mündlichen Prüfung: 13.07.2005**

# **Table of contents**

Table of contents .....	i
Abbreviations and units .....	vii
1. Introduction .....	1
1.1. Physiological properties of the endothelium .....	1
1.2. Pathophysiological activation of endothelium .....	2
1.3. Endothelial dysfunction and cytoskeleton .....	3
1.3.1. Actin cytoskeleton .....	4
1.3.2. Actin filament-turnover .....	4
1.3.3. Cellular organization of the actin cytoskeleton .....	5
1.3.4. Regulation of actin dynamics by actin binding proteins .....	7
1.3.5. ADF/Cofilin Family .....	8
1.3.6. Rho GTPases and actin dynamics .....	11
1.3.7. Rho-GTPases activated protein Kinases .....	12
1.4. LIM-kinase .....	14
1.4.1. Structure of LIM-Kinases .....	14
1.4.1.1. LIM domain .....	15
1.4.1.2. PDZ domain .....	17
1.4.1.3. Kinase domain .....	19
1.4.2. Gene expression and subcellular localization of LIM-kinases .....	21
1.4.3. Regulation of LIMK activation .....	21
1.5. Regulation of protein transport between nucleus and cytoplasm .....	22
1.6. Cellular functions of LIMK-kinases .....	24
2. Aim of the study .....	26
3. Materials and methods .....	27
3.1. General equipments .....	27
3.2. Materials .....	28
3.2.1. Chemicals .....	28
3.2.2. Enzymes and reagents for molecular biology .....	29

---

3.2.3. Antibodies .....	29
3.2.3.1. Primary antibodies .....	29
3.2.3.2. Secondary antibodies .....	30
3.2.3.3. IgG isotype controls and sera.....	30
3.2.4. Inhibitors .....	30
3.2.5. Ligands.....	30
3.2.6. Commercial Kits and other materials .....	30
3.2.7. Primers .....	31
3.2.7.1. For preparation of cDNA inserts.....	31
3.2.7.2. For deletion mutation.....	31
3.2.7.3. For site directed mutagenesis.....	32
3.2.7.4. Primers for gene expression analysis.....	33
3.2.8. Plasmids .....	33
3.2.8.1. Original plasmids .....	33
3.2.8.2. Plasmid with insert.....	33
3.2.8.3. Plasmid with mutated insert.....	34
3.3. Work with <i>E.coli</i> .....	36
3.3.1. Bacterial strains.....	36
3.3.2. Media for bacterial culture.....	36
3.3.3. General.....	36
3.3.4. Culturing bacteria.....	37
3.3.4.1. Growth on solid media.....	37
3.3.4.2. Growth of liquid cultures .....	37
3.3.4.3. Monitoring the bacterial growth .....	37
3.3.5. Transformation of plasmid in <i>E.coli</i> .....	37
3.3.5.1. Preparation of competent cells by CaCl <sub>2</sub> method .....	37
3.3.5.2. Heat shock transformation of the plasmid .....	37
3.4. Recombinant DNA processing and manipulation.....	38
3.4.1. DNA amplification of LIMK1 and LIMK2 cDNA.....	38

3.4.2. Buffers and solutions.....	39
3.4.3. Restriction endonuclease digestion of DNA .....	39
3.4.4. Purification of the digested DNA .....	40
3.4.5. Ethanol precipitation of DNA .....	40
3.4.6. Dephosphorylation of linearized plasmid DNA by CIP.....	40
3.4.7. Ligation of DNA fragments .....	41
3.4.8. Miniprep: small-scale preparation of plasmid DNA .....	41
3.4.9. Endofree Maxiprep: Large scale preparation of plasmid DNA .....	41
3.4.10. Quantification of DNA and RNA solutions .....	42
3.4.11. Agarose gel electrophoresis.....	42
3.4.12. DNA recovery from agarose gel .....	43
3.4.13. DNA sequencing .....	43
3.5. Mutagenesis of the LIMK2 gene.....	43
3.5.1. PCR based site-directed mutagenesis.....	43
3.5.2. Deletion mutagenesis .....	45
3.6. Gene expression analysis at the RNA level using RT-PCR.....	46
3.6.1. RNA isolation from HUVEC .....	46
3.6.2. Gel electrophoresis of RNA .....	47
3.6.2.1. Buffers and solutions.....	47
3.6.3. Synthesis of cDNA from total RNA and analysis of LIMK gene expression.....	48
3.7. Protein analysis.....	48
3.7.1. Buffers and solutions.....	48
3.7.2. Measurement of protein concentration.....	49
3.7.2.1. Enhanced alkaline copper (Lowry) protein assay .....	49
3.7.2.2. dotMETRIC™ 1µl Protein assay .....	50
3.7.3. Whole cell lysates.....	51
3.7.4. Immunoprecipitation .....	51
3.7.5. SDS-PAGE.....	51
3.7.6. Detection of protein on gel.....	52

---

3.7.6.1. Silver staining of the polyacrylamide gels.....	52
3.7.6.2. Coomassie staining of the polyacrylamide gels.....	53
3.7.7. Western blot analysis.....	53
3.7.8. Densitometric analysis of immunoblots.....	55
3.8. Endothelial cells.....	55
3.8.1. Buffers and solutions.....	55
3.8.2. General.....	55
3.8.3. Isolation of human umbilical vein endothelial cells (HUVECs).....	56
3.8.4. Culturing.....	56
3.8.5. Collagenization.....	56
3.8.6. Cell number determination.....	57
3.8.7. Freezing and thawing of endothelial cells.....	57
3.8.8. Transfection of endothelial cells.....	57
3.8.8.1. Electroporation method.....	57
3.8.8.2. Nupherin <sup>TM</sup> -neuron mediated transfection.....	58
3.8.9. Actin staining.....	58
3.9. Microscopy.....	59
3.9.1. Live cell imaging by confocal microscopy.....	59
3.9.2. Photobleaching techniques.....	61
3.9.2.1. FRAP.....	61
3.9.2.2. FLIP.....	62
3.9.3. Fluorescence data analysis.....	63
4. Results.....	65
4.1. Expression of LIMKs in endothelial cells.....	65
4.2. LIMKs regulate actin dynamics in thrombin-stimulated endothelial cells.....	67
4.2.1. Thrombin induces stress fiber formation by Rho-kinase activation.....	67
4.2.2. Rho-kinase stimulates phosphorylation of LIMK leading to subsequent cofilin phosphorylation in thrombin-stimulated endothelial cells.....	68
4.2.3. Role of LIMKs in stress fiber formation.....	71
4.3. Primary sequence analysis of LIM-kinase.....	72

4.3.1. Prediction of nuclear localization signals and nuclear export signals.....	72
4.3.2. Prediction of PKC phosphorylation sites in LIMK2 .....	74
4.4. Nucleocytoplasmic shuttling of LIMK2 in endothelial cells .....	76
4.4.1. LIM domains of LIMK2 regulate its cytoplasmic localization.....	77
4.4.2. PDZ-kinase domain of LIMK2 is localized in the nucleus and cytosol: Analysis of shuttling by FRAP and FLIP .....	79
4.4.3. EGFP-kinase of LIMK2 is localized in nucleus and nucleolus: comparison with the EGFP-kinase of LIMK1 .....	81
4.4.4. Site directed mutagenesis of the unique basic amino acid-rich motif in LIMK2.....	82
4.4.4.1. Site directed mutagenesis in EGFP-kinase domain of LIMK2 .....	83
4.4.4.2. Site directed mutagenesis in EGFP-PDZK of LIMK2 .....	86
4.4.5. Sub-cellular localization of EGFP- $\Delta$ kinase-LIMK2 .....	87
4.5. Regulation of nucleocytoplasmic shuttling of LIMK2 by PKC-dependent phosphorylation.....	88
4.5.1. Effect of PMA on sub-cellular localization of LIMK2 .....	88
4.5.2. The PKC- $\alpha$ and PKC- $\beta$ isoforms regulate nucleocytoplasmic translocation of LIMK2.....	89
4.5.3. Ser283 (site I) in LIMK2 is phosphorylated in PMA-stimulated endothelial cells.....	90
4.5.4. PKC-mediated Ser283 phosphorylation inhibits the nuclear import of LIMK2 .....	92
4.5.5. Mutation analysis of the putative PKC phosphorylation site at Thr494 (siteII) .....	94
4.5.6. Phosphorylation of both Ser283 and Thr494 blocks the shuttling of LIMK2.....	95
4.6. PMA-induced activation of endothelial cells does not stimulate LIMK-mediated phosphorylation of cofilin .....	96
5. Discussion .....	97
5.1. Expression of LIMKs in endothelial cells.....	97
5.2. Thrombin-induced stress fiber formation is regulated by Rho-kinase/LIMK/cofilin pathway .....	98
5.3. Primary sequence analysis of LIMK.....	100
5.4. Nucleocytoplasmic shuttling of LIMKs .....	101
5.5. Subcellular distribution of LIMKs and their domains.....	101
5.6. Identification of functional NoLS and NLS in LIMK2.....	102

---

5.7. Regulation of nucleocytoplasmic shuttling of LIMK2 by PKC dependent phosphorylation.....	105
5.8. Possible nuclear function of LIMK2.....	108
6. Summary .....	111
7. Zusammenfassung.....	113
8. Reference List .....	116
Acknowledgements.....	134
List of publications .....	135
Curriculum vitae .....	138

# Abbreviations and units

## Abbreviations

A/C	ADF/Cofilin
ADF	Actin depolymerization factor
Approx	Approximately
Amp	Ampicillin
APS	Ammonium persulphate
ATP	Adenosin-5'-triphosphate
BSA	bovine serum albumin
cDNA	complementary DNA
CIP	calcium and integrin-binding protein; calf intestine alkaline phosphatase
CRM1	Chromosomal Region Maintenance 1
DMSO	dimethylsulfoxide
DNA	deoxyribonucleic acid
dNTP	deoxyribonucleotide triphosphates
DTT	dithiothreitol
<i>E. coli</i>	<i>Escherichia coli</i>
EC	endothelial cell
ECM	extracellular matrix
EDTA	ethylenediaminetetraacetic acid
EGFP	enhanced green fluorescent protein
ERK	extracellular signal-related kinase
EST	Expressed sequence tag
FCS	fetal calf serum
fig.	figure
FLIP	Fluorescence loss in photobleaching
FRAP	Fluorescence recovery after photobleaching
GAP	GTPase activating protein
GEF	Guanine nucleotide exchange factor
Hepes	N-(2-Hydroxyethyl)-piperanzine-N-(2-ethane sulfonic acid)
HUVEC	human umbilical vein endothelial cell
Ig	immunoglobulin
IP	Immunoprecipitation
LB	Luria-Bertani
LIM domain	Acronyms for lim-, isl-, mec- domain
LIMK	LIM-kinase

LMB	Leptomycin B
LPS	lipopolysaccharide
mAb	monoclonal antibody
MCS	multiple cloning site
MLC	Myosin light chain
mRNA	messenger RNA
NES	Nuclear export signal
NLS	Nuclear localization signal
NoLS	Nucleolar localization signal
O.D.	Optical density at a wavelength of $x$ nm
ORF	open reading frame
PAK	P21-activated kinase
PBS	phosphate buffered saline
PCR	polymerase chain reaction
PDZ	<u>P</u> SD-95, <u>d</u> isc large, <u>Z</u> O-1
PDZK	PDZ-kinase
PKC	protein kinase C
PLC	phospholipase C
PMA	phorbol-12-myristate-13-acetate
RNA	ribonucleic acid
RT-PCR	reverse transcriptase polymerase chain reaction
SDS-PAGE	sodium dodecyl sulfate - polyacrylamide gel electrophoresis
TJ	tight junction; <i>zonula occludens</i>
Tris	Tris-(dimethylamino)-methane

## **Units**

UV	ultraviolet
°C	degree Celsius
μg	microgram
μl	microliter
μm	micrometer
μM	micromolar
aa	amino acid
bp	base pair
cm	centimeter
g	gram (weight) respective gravity (for centrifugation)

---

h	hour
kb	kilo base pairs
kDa	kilo Dalton
kV	kilo Volt
l	liter
M	molar (= mol/l)
mA	milliampere
mg	milligram
min	minute
ml	milliliter
mm	millimeter
mM	millimolar
mol	mole
ng	nanogram
nm	nanometer
pmol	picomole
rpm	revolutions per minute
v/v	volume per volume
w/v	weight per volume



# 1. Introduction

## 1.1. Physiological properties of the endothelium

A normal muscular artery consists of three distinct layers (Figure 1.1). The outermost layer, known as **adventia**, contains fibroblasts, collagen, proteoglycans and vasa-vasorum, all of which are separated from the media by the external elastic lamina. The **media** consists primarily of smooth muscle cells and collagen fibers and it is separated from the intima by the inner elastic lamina. The **intima** is composed of endothelial cells and underlying connective tissue. The vascular endothelium forms a continuous monolayer lining all the blood vessels and the heart chambers. In an adult, the endothelium covers a surface of almost 1000 m<sup>2</sup> and is considered as one of the largest organs in the body (Bachetti and Morbidelli, 2000; Cines et al., 1998). The endothelium displays so-called cobblestone morphology, representing a homogeneous and tight monolayer of polygonal endothelial cells.

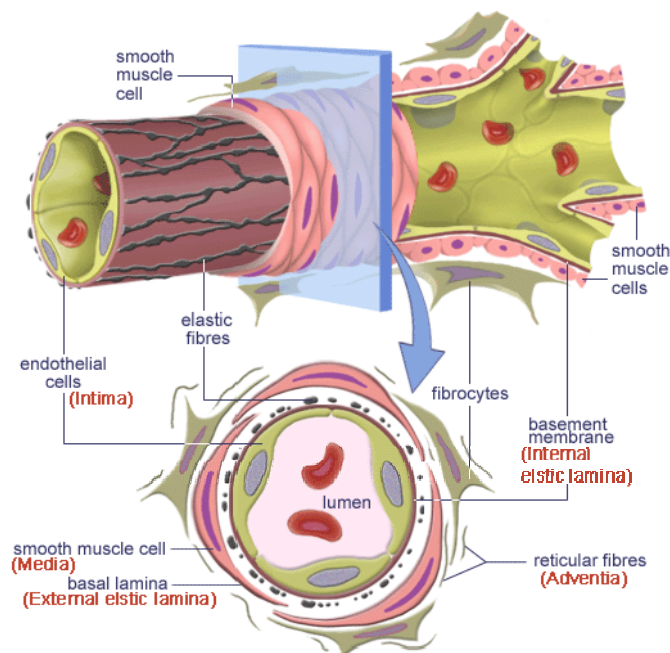


**Figure 1.1: Structure of Blood vessel.** The largest blood vessels are arteries and veins, which have a thick, tough wall of connective tissue and many layers of smooth muscle cells. Vascular endothelial cells (endothelium) form a thin layer on the interior surface of all the vessels, separated from the surrounding outer layers by a basement membrane (basal lamina).

The endothelium regulates cellular and nutrient trafficking, maintains blood fluidity, regulates vasomotor tone, contributes to the local balance of pro-inflammatory and anti-inflammatory mediators and participates in the generation of new blood vessels (Gonzalez and Selwyn, 2003). Endothelial cells in different vascular beds are heterogeneous. They show a highly differentiated structure and function as a consequence of different gene expression and the influence of the surrounding tissue. This functional and structural heterogeneity of endothelial cells may be important for adaptive processes. It also could favor the development of disorders that are

restricted to specific vascular beds (Aird, 2001). In the quiescent state, endothelial cells are non-proliferative and maintain a non-thrombogenic, non-adherent surface and produce vasoactive substances. Cellular and nutrient trafficking is achieved through a specialized trans-cellular system of transport vesicles and by the coordinated opening and closure of cell–cell junctions (Stevens et al., 2000). The specialized trans-cellular vesicle system includes vesiculo-vacuolar organelles, which participate in the regulated transendothelial passage of soluble macromolecules. The trans-cellular vesicle system and the cell-cell junctions must be tightly regulated to maintain endothelial integrity and to protect the vessels from any uncontrolled increase in permeability, inflammation or thrombotic reactions. In addition, the endothelium has secretory functions (Bachetti and Morbidelli, 2000). Endothelial cells regulate the following main biological processes (Datta and Ewenstein, 2001):

**Thrombosis and thromboresistance** are regulated via secretion of molecules such as P-selectin, von Willebrand factor, tissue plasminogen activator, plasminogen activator inhibitor, nitric oxide and prostacyclin (Datta and Ewenstein, 2001; Hayward et al., 1998; Nilius and Droogmans, 2001).

**Vasodilation and vasoconstriction** are regulated via formation of nitric oxide, prostacyclin, endothelin-1, angiotensin II and superoxide radicals (Datta and Ewenstein, 2001; Harrison et al., 1995; Nilius and Droogmans, 2001; Wang et al., 2002).

**Inflammation** is regulated via secretion of IL-8, TNF- $\alpha$  and superoxide radicals (Datta and Ewenstein, 2001; Kaplanski et al., 1997; Nilius and Droogmans, 2001).

**Cell proliferation** is regulated via secretion of aFGF and bFGF (Prudovsky et al., 2002; Swinscoe and Carlson, 1992; Tarantini et al., 2001).

The endothelium regulates vascular hemodynamics under physiological conditions. It is constantly exposed to hemodynamic forces, which consist of pressure acting perpendicular to the vessel wall and mechanical forces exerted by the flowing blood in parallel to the vessel wall. Laminar flow with its high flow rate in the arterial system leads to continuous shear stress of the endothelium. Shear stress stimulates NO formation, which is important for the thromboresistance of the endothelium under physiological conditions.

## **1.2. Pathophysiological activation of endothelium**

Qualitatively or quantitatively abnormal endothelial stimulation, such as bacterial infection and inflammatory stimuli, can result in localized alteration of the endothelium. The endothelium at the arterial branch points, which is exposed to turbulent flow, is more prone to functional disturbances. These will affect the antihaemostatic properties, control of the vascular tone, permeability and anti-adhesive properties of the endothelium. These alterations are collectively

termed “endothelial dysfunction” (Gimbrone et al., 1993). Endothelial dysfunction is one of the important early steps in atherosclerosis (Ross, 1993).

Abnormal endothelial cell activation plays also an important role during inflammation. Vascular inflammation is a key component in several pathological conditions, including atherosclerosis, ischemia/ reperfusion, hypertension, restenosis, angiogenesis and septic shock. It involves a complex series of events: i) dilatation of arterioles, capillaries, and venules, with increased permeability and blood flow; ii) exsudation of fluids and macromolecules such as LDL; and iii) leukocyte migration into the vascular wall. Leukocytes and endothelial cells are the major cellular players of the inflammatory reactions (Nathan, 2002). Endothelial cells coordinate the recruitment of inflammatory cells to sites of tissue injury or infection and produce and release cytokines and growth factors that serve as communication signals for leukocytes (Muller, 2002). In addition, endothelial cells respond to inflammatory stimuli such as lipopolysaccharides (LPS) or cytokines. Finally, a series of cell adhesion molecules expressed on leukocytes and on endothelial cells mediate leukocyte attachment on and migration across the endothelium in a stepwise process. In the normal state, the role of inflammatory endothelial cell activation is to minimize the damage induced by injury and/or infection via the recruitment of blood cells to the site of injury, by initiating blood coagulation and by healing and promoting repair for recovery of function (Jung et al., 1998; Tan et al., 1999).

In adults, the proliferation rate of endothelial cells is very low, and the growth of new vessels only occurs in reproduction, wound healing, or in pathological states such as myocardial infarction, hypoxia and cancer. The construction of this new vascular network requires different sequential steps, including the release of proteases from “activated” endothelial cells with subsequent degradation of the basement membrane, migration of endothelial cells into the interstitial space, endothelial cell proliferation, and differentiation into mature blood vessels in collaboration with other cells such as smooth muscle cells. These processes are mediated by a wide array of angiogenic inducers, including growth factors, chemokines, angiogenic enzymes, endothelial specific receptors, and adhesion molecules (Carmeliet, 2000; Carmeliet and Jain, 2000).

### **1.3. Endothelial dysfunction and cytoskeleton**

The normal function of the endothelium is highly dependent on the endothelial cytoskeleton. Actin microfilaments, their associated adherens junctions and focal adhesions are important regulators of endothelial permeability and cell adhesiveness. After injury of the endothelium, the cytoskeleton is essential for endothelial cell migration and proliferation leading to wound repair. Disruption and dysfunction of the cytoskeleton may result in impairment of endothelial function, subsequently tipping the balance towards vascular disease. Thus, an understanding of the cellular

and molecular biology of the endothelial cytoskeleton is important in our understanding of the pathogenesis of vascular disease such as atherosclerosis and pathological angiogenesis.

### **1.3.1. Actin cytoskeleton**

The term cytoskeleton was originally applied to describe the complex set of protein fibers in the cytoplasm (Darnell et al., 1986). The cytoskeleton is composed of three major types of protein filaments: *microtubules*, *microfilaments*, and *intermediate filaments*. Microfilaments are polymers of actin that together with a large number of actin-binding and associated proteins constitute the actin cytoskeleton (Botstein et al., 1997). Modulation of the actin cytoskeleton network changes the mechanical properties of the cells that are essential for many cellular functions such as **shape change, migration, secretion, cell division, phagocytosis and pinocytosis**. The actin cytoskeleton not only provides mechanical strength to the cells, but it is also dynamic and adaptable, constantly changing through cycles of polymerization/depolymerization, and represents an enormous surface area on which proteins and other cytoplasmic components can bind.

Actin filaments are polar helical assemblages of actin protein (43 kDa) that is found in all eukaryotic cells and is conserved between species (Pollard and Cooper, 1986). In most of the organisms three main actin isotypes ( $\alpha$ -,  $\beta$ -,  $\gamma$ -actin) have been found (Herman, 1993). Actin is the most abundant protein in eukaryotic cells, accounting for as much as 20% of total protein (dos Remedios et al., 2003). Monomeric (G-) actin has 4 sub-domains (numbered 1-4), each having a repeating motif comprising a multi-stranded  $\beta$ -sheet,  $\beta$ -meander, and a right-handed  $\beta\alpha\beta$ unit. The actin cytoskeleton is organized in the cytoplasm in linear bundles as well as 2- and 3-dimensional networks by a plethora of associated actin-binding proteins, which determine structural and dynamic properties and associations with other cell components.

### **1.3.2. Actin filament-turnover**

Actin is an adenosine-nucleotide binding molecule with ATPase activity. In physiological salt conditions, monomeric G-actin spontaneously self-associates to form polar helical microfilaments (F-actin) (Engel et al., 1977). The polymerization of actin can be divided into four steps: 1) Activation (salt-binding and conformational changes in monomers); 2) Nucleation (the formation of oligomers having a higher probability of growing into filaments than decomposing to monomers); 3) Elongation (the bi-directional growth of polymers); and 4) Annealing (the end-to-end joining of two filaments). All of these steps are reversible. Nucleation is the formation of actin trimers which is the rate limiting step and highly unfavorable (Pollard and Cooper, 1986). Once a trimer has formed, polymerization by rapid extension is favored during the growth of the fiber. The rate of extension gradually lessens as the concentration of remaining free G-actin reaches a point where available monomers become exhausted. An equilibrium is then established

when the number of actin monomers joining the filaments equals that leaving the filaments, which is marked by the so-called critical concentration ( $C_c$ ) at steady state. Net polymerization occurs when the G-actin concentration is higher than  $C_c$ , and net depolymerization occurs when the G-actin concentration is lower than  $C_c$  (Figure 1.2).

The structural polarity of the actin filaments is created by the regular, parallel orientation of all of their subunits. Under appropriate conditions, addition of subunits can occur at both ends. However, the rate of addition at the plus end is several times higher than that at the minus end (Figure 1.2). G-actin monomers contain tightly bound either ATP or ADP. ATP hydrolysis lowers the affinity of ADP-bound G-actin for the filament ends as compared to ATP-bound actin (Pollard, 1986). As a consequence, incorporation of ADP-bound actin to existing filaments is slower than incorporation of ATP-bound actin.

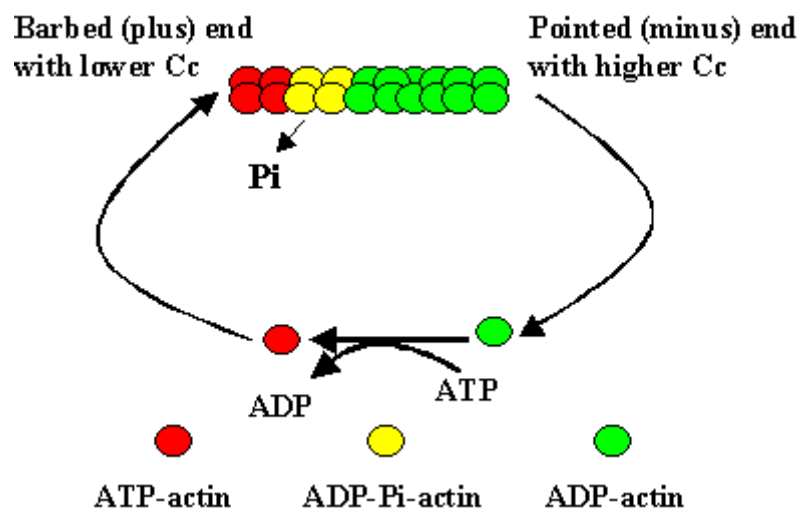


**Figure 1.2 The turnover of an actin filament.** The actin filament is a polar structure with two different ends. The slow growing pointed end has a higher critical concentration ( $C_c$ ) than the fast growing barbed end. At steady state, the net assembly at the barbed end equals the net disassembly at the pointed end (treadmilling).

ATP-actin subunits are added at the fast growing or plus end (the barbed end), whereas ADP-actin disassembles at steady state from the slow growing or minus end (the pointed end). Thus ATP hydrolysis is the basis for a turnover of the filament without net change of filament length, a process termed treadmilling (Kirschner, 1980; Wegner, 1976; Wegner, 1977). ADP-actin disassembly from the pointed end constitutes the rate-limiting step and determines the concentration of monomeric actin and thereby the rate of barbed end growth.

### **1.3.3. Cellular organization of the actin cytoskeleton**

The best known assemblies of the actin cytoskeleton in cultured cells are *stress fibers*, *lamellipodia*, *microspikes* and *filopodia*, but others like dorsal arcs and peripheral, concave or convex bundles of actin filaments as well as geodesic arrays (Heath and Holifield, 1993; Small, 1988; Small et al., 1999; Small et al., 1998) and less obvious networks between stress fiber

bundles, also occur frequently. These assemblies can be divided in two groups, according to whether they exhibit unipolar or bipolar arrays of actin filaments.

Thick bundles of parallel microfilaments are called *stress fibers*. Stress fibers that delimit the cell edge or form the base of non motile lamellipodia, contain bipolar arrays of actin and myosin type II and thus possess the ability to contract and to exert tension (Goeckeler and Wysolmerski, 1995; Huxley, 1973). They serve mainly to maintain the cellular structure (Schoenwaelder and Burridge, 1999). Contraction of stress fibers leads to the rounding of the cells and increased permeability of the endothelium (Goeckeler and Wysolmerski, 1995). Stress fibers are common in fibroblasts, endothelial cells and epithelial cells and are anchored to the substratum *via focal adhesions* (Bretscher, 1991; Wong et al., 1983).

Cell movement is initiated by the veil-like protrusion of a thin cytoplasmic sheet of about 200 nm thickness, termed the *lamellipodium* (Small et al., 2002). Lamellipodia are filled with a dense network of actin filaments (Small, 1988) that are oriented such that their fast growing barbed ends are located next to the membrane (Small et al., 1978). Lamellipodial protrusion is powered by actin assembly, involving a rapid turnover of actin filaments operating by a treadmilling mechanism, which has been demonstrated in many cell types such as endothelial cells, and fibroblasts (Ettenson and Gotlieb, 1994; Small, 1994; Small et al., 1993).

Electron-microscopic studies of the lamellipodia showed an extensively branched array of actin filament network (called dendritic brush) at the leading edge with Y-shaped branches averaging 70° and a lack of detectable free pointed ends (Svitkina and Borisy, 1999; Svitkina et al., 1997). The main actin filament nucleator, the Arp2/3 complex (comprising seven subunits) was found to be present at many branch points (Svitkina and Borisy, 1999). This model is consistent with binding of the Arp2/3 complex can bind to pointed ends (Mullins et al., 1998) and to the sides of actin filaments, where it nucleates new filaments (dendritic nucleation model (Mullins et al., 1998)), as well as branched filaments (Blanchoin et al., 2000; Gournier et al., 2001). A branched network that arises from a tightly coupled nucleation and cross-linking of actin filaments at the leading edge is proposed to provide the structural basis for polymerization-driven protrusion.

Lamellipodia are involved in the formation of adhesions to the substrate, and of ruffles, which form when lamellipodia lift upwards and detach from the substratum and fold back (Abercrombie et al., 1970). Lamellipodia are important in macropinocytosis as well as in the engulfment of particles during phagocytosis (Coppolino et al., 2001).

Many cells also extend *microspikes*, which are embedded radially in lamellipodia and are able to move laterally within lamellipodia (Wessells et al., 1973), fuse and divide into new microspikes (Small et al., 1996). Microspikes have been proposed to serve in the initiation of contacts with the substratum (DePasquale and Izzard, 1987). Similar needle-like, highly motile structures termed *filopodia* extend far beyond the border of lamellipodia (Small, 1989). They can protrude 5 to 50µm beyond the edge of the cell in all three dimensions and can kink and fold back. Filopodia

have been most recognized in the neural growth cone as a guidance apparatus located at the tip of growing neurons, but they are also present in other cell types, and may fulfill sensory functions (Gallo and Letourneau, 1998; Jacinto and Wolpert, 2001; Suter and Forscher, 1998). The controlled polymerization of actin filaments at the leading edge creates a force to push the cell membrane outwards, with the concomitant protrusion of lamellipodia, filopodia or microspikes. In migration, new cell-substratum attachments are established at the front of the cell, the cell body is then translocated by intracellularly generated forces, and in a last step all connections to the substratum at the back end are broken (Figure 1.3).

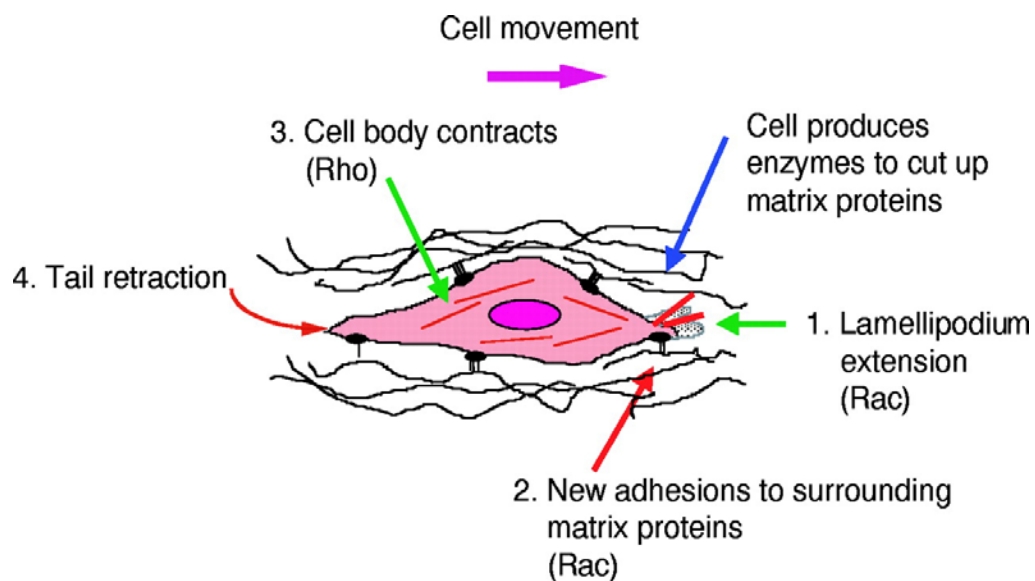


**Figure 1.3 A model for the different steps of cell migration.** A migrating cell extends a lamellipodium at the front. This extension is stabilized through the formation of new adhesions to the extra-cellular matrix. Rac induces actin polymerization and integrin adhesion complex assembly at the cell periphery, leading to membrane protrusion. The cell body is moved forward by actomyosin-mediated contraction (Rho dependent). Finally, the tail of the cell detaches from the substratum and retracts. Migrating cells also secrete proteases that cut extra-cellular matrix proteins, and this is important for cell movement (Ridley, 2001).

#### **1.3.4. Regulation of actin dynamics by actin binding proteins**

Under *in vitro* conditions, the slow addition at the barbed end and even slower dissociation at the pointed end of the filaments produces a rate of treadmilling of monomers ( $\sim 2\mu\text{m}/\text{h}$ ) that is  $\sim 200$ -fold slower than that observed *in vivo* (dos Remedios et al., 2003). The higher rate of treadmilling *in vivo* is due to proteins, which interact with actin filaments or monomers, called *actin-binding proteins (ABPs)*. ABPs present *in vivo* regulate different aspects of the assembly/ disassembly process of actin filaments into two and three-dimensional arrays (Ayscough, 1998). ABPs ultimately convey signals to the actin cytoskeleton. A large number of ABPs have been identified, about  $\sim 162$  distinct and separate proteins without including their many synonyms or isoforms (dos Remedios et al., 2003). Attempts to classify these ABPs leave many "orphans" that do not fit into families, so any attempt to group them is bound to be somewhat arbitrary.

Classification according to the function of ABPs can be problematic due to functional overlap. Functional classification distinguishes seven groups of ABPs (Figure 1.4). 1) Monomer-binding proteins sequester G-actin and prevent its polymerization (e.g., thymosin  $\beta$ 4, profilin, DNase I). 2) Filament-depolymerizing proteins induce the conversion of F- to G-actin (e.g., ADF/Cofilin). 3) Filament end-binding proteins cap the ends of the actin filament preventing the exchange of monomers at the pointed end (e.g., tropomodulin) and at the barbed end (e.g., CapZ). 4) Filament severing proteins shorten the average length of filaments by binding to the side of F-actin and cutting it into two pieces (e.g., gelsolin). 5) Cross-linking proteins contain at least two binding sites for F-actin, thus facilitating the formation of filament bundles, branching filaments, and three-dimensional networks (e.g., Arp2/3  $\alpha$ -actinin). 6) Stabilizing proteins bind to the sides of actin filaments and prevent depolymerization (e.g., tropomyosin). 7) Motor proteins use F-actin as a track upon which to move (e.g., the myosin family of motors). Some ABPs are not limited to one class. For example, gelsolin is capable of severing and capping the barbed end of actin filaments, and the Arp2/3 complex that consists of seven proteins, can nucleate and elongate filaments, and establish branch points in actin networks.

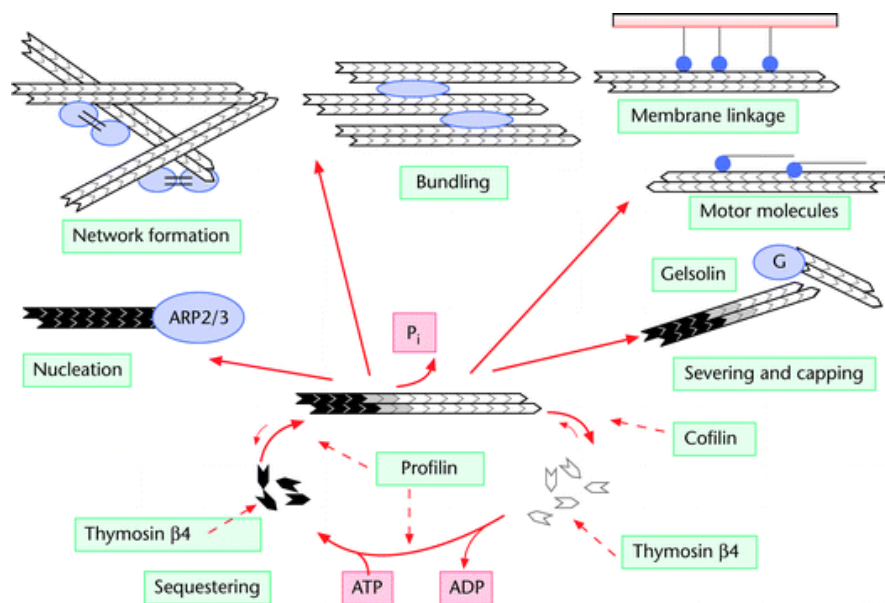


**Figure 1.4 Actin polymerization and actin-binding proteins.** The actin cycle (lower part) and modulation by actin-binding proteins. ATP-actin (black chevrons) will incorporate at the fast-growing ends. Protomers will hydrolyze ATP to ADP- $P_i$  (grey chevrons) and subsequently release inorganic phosphate, yielding ADP-protomers (white chevrons). Several actin-binding proteins modulate the cycle by typical activities. Other actin-binding proteins mediate linkage to other filaments or to membranes or proteins.

### 1.3.5. ADF/Cofilin Family

The actin depolymerization factor (ADF)/Cofilin (A/C) family of proteins is expressed in virtually all eukaryotic cells. These proteins are relatively small (15-19kDa) and exist in multiple isoforms. ADF/Cofilin is one of the essential factors for enhancing actin filament turnover. ADF/Cofilin weakly severs actin filaments without capping ends, thereby increasing the number of free filament ends where polymerization and depolymerization occur. It also enhances the rate

of monomer dissociation from the pointed ends (Bamburg et al., 1999; Carrier et al., 1997; Maciver et al., 1998). There are over 28 members of the A/C protein family, including invertebrate depectin (depolymerises actin), porcine ADF or destrin (destroys F-actin), cofilin (cosediments with filamentous actin). They are distributed across the complete spectrum of eukaryotic organisms. All of these proteins share considerable (30-40%) amino acid sequence identity. Furthermore, two other major protein families are related to ADF through the presence of an ADF homology domain. One protein has a duplication of this domain and is consequently called twinfilin; the other contains a single ADF homology domain linked to another motif and encodes the drebin family of proteins. Vertebrates have genes for only two forms, ADF and cofilin. Only one isoform of ADF is known in mammals (and birds), whereas two are known for cofilin (cofilin 1 and cofilin 2). Cofilin 1 is expressed in most embryonic tissues and adult cells, cofilin 2 is expressed in muscle cells, and ADF expression is limited to epithelial and endothelial cells (Vartiainen et al., 2002). Human ADF and cofilin have 72% sequence identity. ADF has a much higher depolymerizing activity than cofilin at pH 8.

The multiple sequence alignment in Figure 1.5 shows the conservation within these A/C family members. The vertebrate proteins are somewhat larger than the other three: human cofilin contains 166 residues, whereas plant, yeast, and actophorin contain 139, 143, and 137 residues, respectively. The vertebrate-specific residues are located principally in loop regions, and include a nuclear localization signal (NLS). These residues are found mainly between  $\alpha$ -helix 1: $\beta$ -strand 1 and  $\beta$ -strand 2:  $\alpha$ -helix 3 (Figure 1.5).

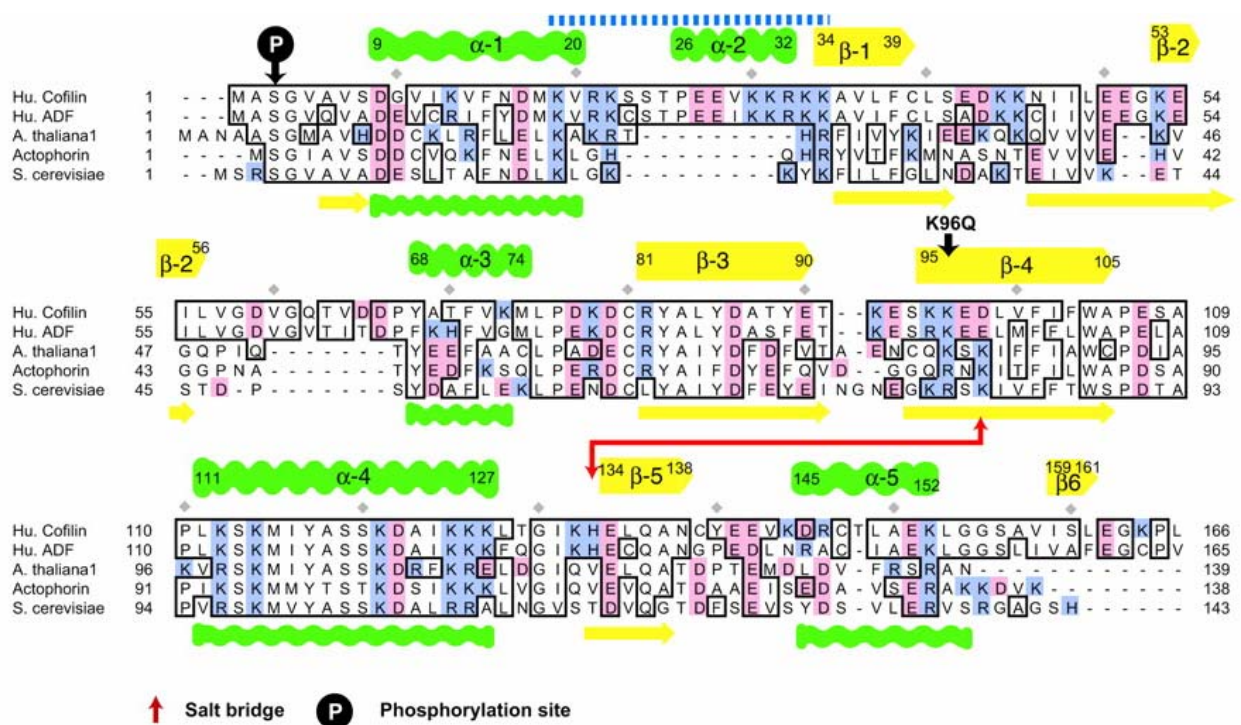


**Figure 1.5** Sequence alignment of A/C family with known three-dimensional structures. The alignment show homologous sequences (*boxed*), basic/acidic residues (*blue/red*, respectively),  $\alpha$ -helices (*green*) and  $\beta$ -strands (*yellow*; above for human cofilin with residue numbering and below for yeast cofilin), the salt bridge (*red arrows*), the phosphorylation site (*circled P*), the NLS (*blue dotted line*, residues 18-34), and every tenth residue (*gray diamonds*).

These two inserts are spatially proximal to a vertebrate-specific C-terminal extension that together define a contiguous “horseshoe-shaped” surface around the loop between  $\beta$ -strand 3 and 4, contributing 22% of the total solvent accessible area and giving stability to the loop (Figure 1.6B). The first vertebrate insert contains a putative NLS that is believed to be responsible for the nuclear translocation of the AC upon cellular stress (Figure 1.6B) (Abe et al., 1993).

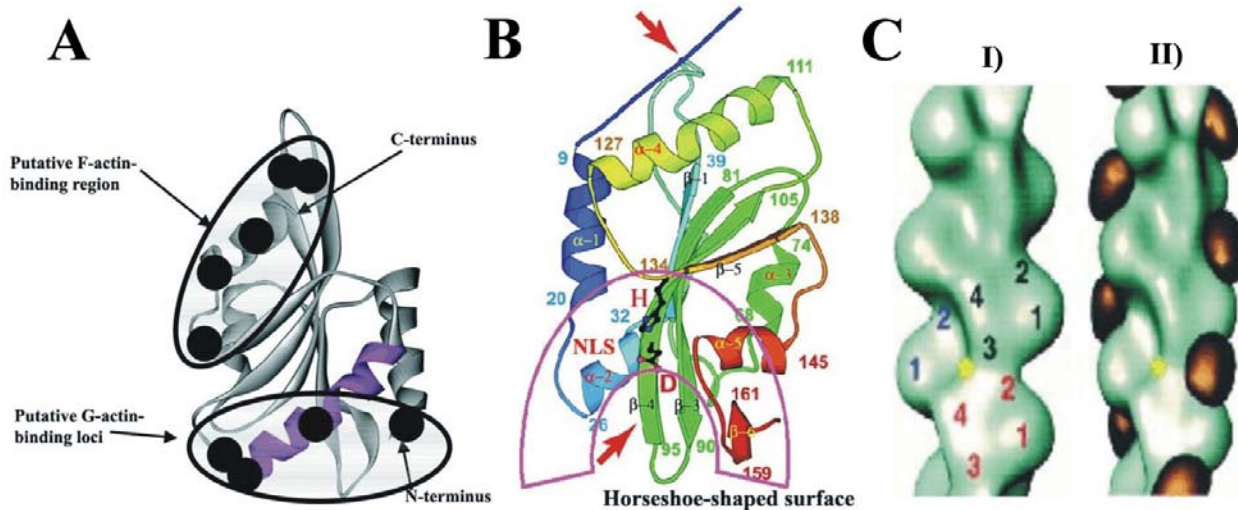


**Figure 1.6** **A**) The atomic structure of yeast cofilin solved at 1.8 Å showing the NH<sub>2</sub> and COOH termini. Putative sites for binding F-actin and G-actin (purple helix) are located in the COOH-terminal region of the molecule. The solid spheres identify residues that are essential for actin binding. **B**) It is a ribbon diagram of the lowest energy structure of human cofilin. The *red arrows* indicate the positions of Ser<sup>3</sup> and Lys<sup>96</sup>, whose mutation affects G-actin and F-actin binding, respectively. The nuclear localization signal and vertebrate specific inserts together make a horseshoe-shaped surface (Pope et al., 2004). **C**) Reconstructed image of F-actin and F-actin with cofilin binding site (based on electron cryomicroscopy (McGough et al., 1997). **I**) The sub-domains of actin and the phalloidin-binding site (*yellow asterisk*) are indicated on reconstructed actin filament. **II**) Cofilin molecules are shown as copper-colored and rugby ball-shaped mass of dimensions 32×37×43Å, decorated on actin filament. Cofilin is centered (axially) at about the position of subdomain 2 of the lower actin subunit and radially at the cleft between subdomains 1 and 3 of the upper actin subunit.

Porcine destrin (identical in sequence to human ADF) was the first structure in this family of proteins to be solved by NMR spectroscopy (Hatanaka et al., 1996) and the structures for yeast cofilin (Figure 1.6) (Fedorov et al., 1997) *Acanthamoeba* actophorin (Leonard et al., 1997) and ADF1 from *Arabidopsis thaliana* (Bowman et al., 2000) were solved by x-ray crystallography. Recently the structure of human cofilin was determined by NMR spectroscopy (Pope et al., 2004). The structural sites to which cofilin binds along the outside of the actin filament, are not known in atomic details, but are based on chemical cross-linking and other data. Cofilin binds cooperatively between two actin subunits along the filament. F-actin binding by A/Cs requires two sites, a G-actin binding site that interacts with subdomains 1 and 3 of the “upper” actin and an F-actin binding site that interacts with subdomains 1 and 2 of the “lower” actin (Figure 1.6A, C) (McGough and Chiu, 1999). Together these interactions induce a twist change in F-actin and weaken both lateral and longitudinal contacts between subunits, preparing the filament for severing. One ramification of this structural change is to alter the phalloidin-binding site; thereby preventing its binding and making it ineffective as a probe for F-actin (McGough et al., 1997).

The weakened actin-actin contacts lead to an increase rate of dissociation at filament pointed ends. Both effects contribute to the depolymerizing activities of ADF/cofilin.

Cofilin binds to ADP-actin with an affinity which is two orders higher than the binding to ATP-actin or ADP-P<sub>i</sub>-actin, and this is true for both the G- and F-actin at pH 7.8 (Carlier et al., 1997). Thus cofilin not only promotes the disassembly of ADP-actin monomers from filaments, but it also binds to release ADP-actin monomers and inhibits the exchange of their bound nucleotide (Nishida, 1985). Besides its binding to actin, cofilin binds to the membrane lipids phosphatidyl inositol 4-phosphate (PIP) and phosphatidylinositol 4,5-bisphosphate (PIP<sub>2</sub>) (Yonezawa et al., 1990) which inhibit actin binding of cofilin (Kusano et al., 1999), suggesting that transmembrane signaling by PIP<sub>2</sub> can regulate the function of ADF/cofilin.

The ability of cofilin to bind G-actin is inhibited by phosphorylation of Ser-3 that is achieved by LIM-kinase (LIMK) family of protein kinases. When cofilin is phosphorylated, there is sharp fall in its affinity to actin (Yang et al., 1998b).

### **1.3.6. Rho GTPases and actin dynamics**

The Rho-family GTPases are key regulators in signaling pathways that link extra-cellular stimuli or matrix proteins to the assembly and organization of the actin cytoskeleton (Hall, 1994). Signaling through Rho-family GTPases can be initiated by activation of many different types of plasma membrane receptors, such as tyrosine kinase receptors, and G-protein-coupled receptors. Receptors of cell adhesion molecules such as integrins, cadherins, and Ig superfamily members can also affect the Rho-family GTPases (Braga, 2002; DeMali et al., 2003). Cell proliferation is normally limited to specific conditions that include stimulation by mitogenic growth factors and adhesion to the extra-cellular matrix. Rho-family GTPases can regulate the mitogenic pathways that control G1-phase cell cycle progression (Welsh et al., 2001).

GTPases are molecular switches that use a simple bio-chemical strategy to control complex cellular processes. They cycle between two conformational states: one bound to GTP ('active' state), the other bound to GDP ('inactive' state), and they hydrolyze GTP to GDP. In the 'on' (GTP) state, GTPases recognize target proteins and generate a response until GTP hydrolysis returns the switch to the 'off' state. The cycling between the active and inactive states is regulated by GDP/GTP exchange factors (GEFs), GTPase-activating proteins (GAPs), and guanine nucleotide dissociation inhibitors (GDIs) (Figure 1.7).

The Rho GTPases family belongs to the Ras superfamily of small GTPases and can roughly be divided into 5 groups, the **Rho-like**, **Rac-like**, **Cdc42-like**, **Rnd**, and **RhoBTB** subfamilies (Burrige and Wennerberg, 2004). Rho, Rac and Cdc42, the three best-characterized members of the family, stimulate different signaling pathways. The Rho proteins induce the formation of stress fibers in response to mitogens such as lysophosphatidic acid (LPA), bombesin, or fetal calf serum (FCS) (Ridley and Hall, 1992). Rac proteins stimulate the formation of lamellipodia and

membrane ruffles through the activation of Arp2/3 mediated actin polymerization via the indirect activation of the WAVE/Scar proteins (Eden et al., 2002; Miki et al., 2000; Ridley et al., 1992). Activation of Cdc42-like GTPases by bradykinin, stimulates its binding to WASP inducing a conformational change that activates these proteins such that they stimulate Arp2/3 to nucleate actin polymerization leading to the formation of peripheral-actin microspikes, filopodia (Kozma et al., 1995; Nobes and Hall, 1995).

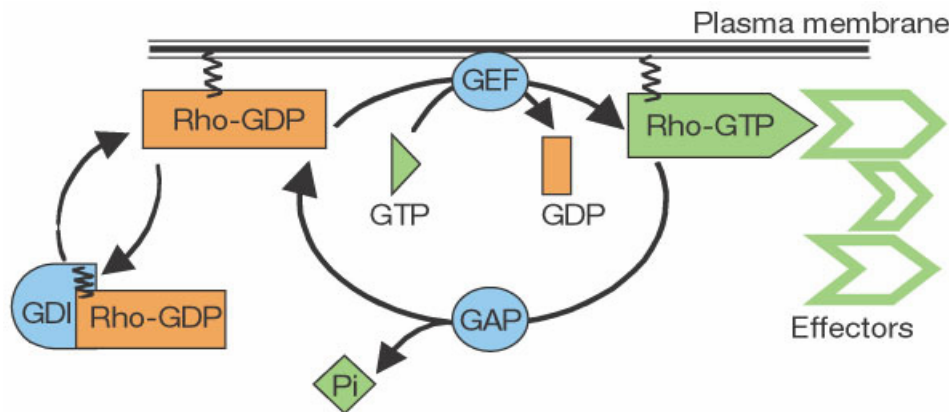


**Figure 1.7 The Rho GTPase cycle.** They cycle between an active (GTP-bound) and an inactive (GDP-bound) conformation. In the active state, they interact with one of over 60 target proteins (effectors). The cycle is highly regulated by three classes of proteins: GEFs (guanine nucleotide exchange factor) catalyze nucleotide exchange and mediate activation; GAPs (GTPase activating protein) stimulate GTP hydrolysis, leading to inactivation; and GDIs (guanine nucleotide dissociation inhibitors) extract the inactive GTPase from membranes. All Rho GTPases are prenylated at their C terminus, and this is required for function (Burrige and Wennerberg, 2004).

### **1.3.7. Rho-GTPases activated protein Kinases**

The extra-cellular signals are relayed from the plasma membrane to specific intracellular targets mostly through several phosphorylation events catalyzed by different protein kinases. Each of these kinases should possess individual target recognition specificity and localization specificity in order to ensure the specificity of the signaling flux. Protein kinases are enzymes, which catalyze the phosphorylation of the amino acids serine, threonine, or tyrosine in their substrate by transfer of the  $\gamma$ -phosphate of ATP to the acceptor amino acid. The regulation of protein activities by phosphorylation is a reversible process, with the reverse direction catalyzed by protein phosphatases.

Analysis of the phylogenetic tree of kinase domain alignments, revealed four subfamilies (Hanks et al., 1988). Each subfamily consists of protein kinases with related substrate specificities (serine/threonine-specific or tyrosine-specific) and modes of regulation (cAMP-dependent, calcium/calmodulin-dependent, calcium/diacylglycerol-dependent etc.). The rest of the kinases falling outside these major groups are difficult to classify.

All active Rho GTPases stimulate specific kinases. Rho stimulates several kinases, such as the Rho-kinase (p160 ROCK), and cistron kinase. Rho-kinase elevates myosin-light chain (MLC) phosphorylation by phosphorylating and inhibiting the MLC phosphatase (Kimura et al., 1996). It

can also directly phosphorylate the MLC *in vitro* (Amano et al., 1996). MLC phosphorylation stimulates ATPase activity the interaction of myosin with actin filaments leading to stress fiber formation and actin-myosin driven contractility. Cistron kinase, which, like Rho-kinase, stimulates MLC phosphorylation and myosin activity, appears to function primarily following mitosis in the cleavage furrow of dividing cells (Madaule et al., 1998). Rho-kinase also phosphorylates LIM-kinases (LIMKs) and enhances the ability of LIMKs to phosphorylate cofilin at Ser3 (Maekawa et al., 1999). Cofilin phosphorylation blocks its actin-depolymerization activity.

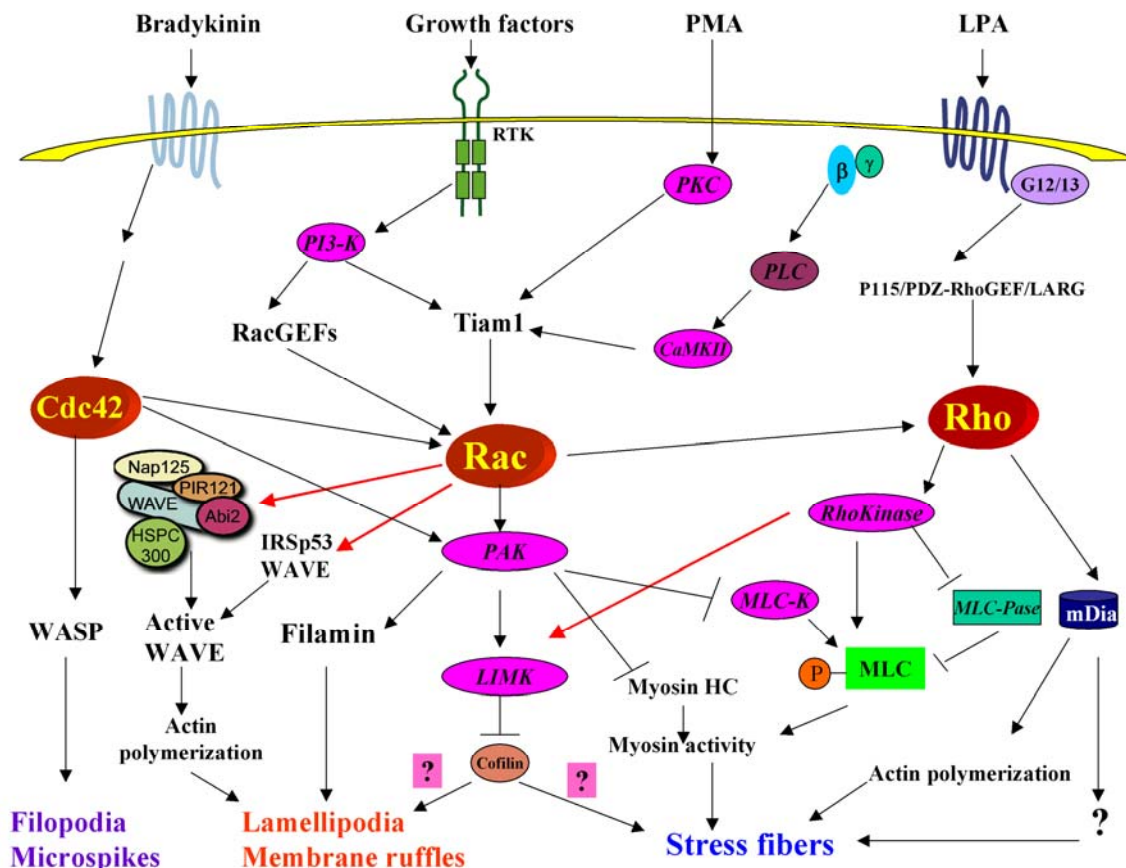


Figure 1.8 Schematic representation of Rho, Rac, and Cdc42 signaling pathways to the cytoskeleton in mammalian cells.

Both Rac and Cdc42, are known to stimulate p21-activated kinases (PAKs). Overexpression of PAKs can promote the formation of lamellipodia (Sells et al., 1997) and lead to the loss of stress fibers and focal adhesions (Manser et al., 1997). Several PAK substrates or binding partners have been implicated in the effects of PAK, including the actin binding protein filamin, LIM-kinase, myosin, the paxillin/Pix/PKL complex, and the adaptor protein Nck. PAK may contribute to the loss of stress fibers and focal adhesions by phosphorylating and inhibiting MLCK activity, thereby leading to a decrease in MLC phosphorylation. The effect of PAK on MLC phosphorylation is particularly controversial (Bokoch, 2003). Additionally, phosphorylation of the myosin heavy chain by PAK has also been reported as a mechanism to inhibit myosin function and cause the disassembly of actomyosin structures (van Leeuwen et al., 1999).

Growth factors such as platelet-derived growth factor (PDGF), epidermal growth factor (EGF), Phorbol-12-myristate-13-acetate (PMA) and insulin, were observed to stimulate Rac, leading to a subsequent Rho activation. PMA stimulates Rac through a PKC-dependent phosphorylation and activation of Tiam1 (T-lymphoma invasion and metastasis) (Mertens et al., 2003).

As shown above, the LIMKs are downstream targets of different pathways, as Rho, Rac, and Cdc42 have been linked to the LIMK activation. LIMKs may play an important role in endothelial cell biology.

## 1.4. LIM-kinase

LIM-kinase (LIMK) was initially identified in a screen for novel members of the c-Met/HGF receptor tyrosine kinase family (Mizuno et al., 1994). The LIMK family of proteins is a novel class of serine/threonine protein kinase family that plays an important role in actin cytoskeleton reorganization (Arber et al., 1998), and, as it has been recognized only recently, in cell proliferation (Roovers et al., 2003).

### 1.4.1. Structure of LIM-Kinases

LIMK is a unique protein kinase that has two repeats of the LIM domain at the N-terminus, followed by a PDZ domain and an unusual protein kinase domain at the carboxy terminus. A proline/serine-rich (P/S) region separates the PDZ domain from the kinase domain, which comprises approximately half of the 70 kDa masses of the LIMK proteins (Figure 1.9). The LIMK protein family is comprised of two members, LIMK1 and LIMK2. Both LIMKs have been found in human, rat, mouse, chicken, and *Xenopus*. Furthermore, the genetic structure of LIMK1 and LIMK2 genes in human and mouse is well conserved: both genes contain 16 exons and have identical intron/exon boundaries (Bernard et al., 1996; Ikebe et al., 1997). Human LIMK1 and LIMK2 have 92% homology with mouse LIMK1 and LIMK2, respectively.

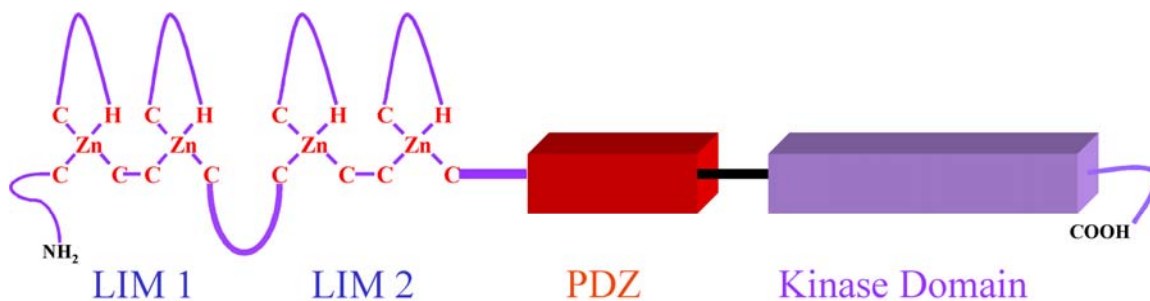


**Figure 1.9 Schematic structure of LIMK.** LIMKs feature two LIM double zinc finger domains at the N-terminus followed and one PDZ are separated from the kinase domain by serine/proline spacer region.

In the mouse, alternative splicing of exon 11 of LIMK1 yields a shorter isoform, LIMK1 (-) truncated in the kinase domain (Bernard et al., 1994), which is catalytically inactive (Arber et al., 1998). LIMK2 is transcribed from two independent sites, which results in the full-length LIMK2a

and an N-terminal truncated LIMK2b that lacks the first zinc finger of the first LIM domain. LIMK2b may be transcriptionally processed to yield two C-terminal truncated isoforms that contain only the LIM and PDZ domains (LIMK2c) or only the LIM domains (LIMK2d) (Nunoue et al., 1995). Testis-specific LIMK2 isoform (tLIMK2) lacks the two LIM domains and a portion of the PDZ domain (Ikebe et al., 1998; Takahashi et al., 1998).

Comparisons of selected LIMK homologue protein sequences reveal variations in amino acid conservation both within and between domains. The kinase domains are most highly conserved between LIMK1 and LIMK2 (~70%), followed by the LIM (~50%) and PDZ domains (~46%). Within the LIM domains, the second zinc finger of LIM1 and the first finger of LIM2 are the most conserved between the two LIM domains of LIMK1 and LIMK2.

#### 1.4.1.1. LIM domain

The LIM domain, as a conserved zinc finger motif, has been found in a variety of different proteins from ascidians to man. LIM domains contain 50 to 60 amino acids forming a double zinc-finger motif with the consensus sequence (C-X<sub>2</sub>-C-X<sub>16-23</sub>-H-X<sub>2</sub>-C)-X<sub>2</sub>-(C-X<sub>2</sub>-C-X<sub>16-21</sub>-C-X<sub>2</sub>-H/D/C). LIM is an acronym of the three transcription factors Lin-11, Isl-1, and Mec-3, in which the motif was first identified (Freyd et al., 1990; Karlsson et al., 1990). The conserved cysteine, histidine, and aspartic acid residues form two tetrahedral zinc-binding pockets, which stabilize the secondary and tertiary structure of the protein. The LIM domain is predominantly made up of  $\beta$ -sheets with a short C-terminal  $\alpha$ -helix. They are arranged in the order  $\beta$  I-IV, and  $\alpha$ -helix, where  $\beta$ -sheets I and II are oriented orthogonal to each other and comprise the CCHC zinc binding module. Similarly, the orthogonal  $\beta$ -sheets III and IV, together with the  $\alpha$ -helix, form the C-terminal CCCC subdomain (Figure 1.10B).

NMR studies of the cytoplasmic LIM proteins CRP1 and CRIP revealed that the LIM domain is structurally similar to GATA-type zinc fingers (Perez-Alvarado et al., 1996; Perez-Alvarado et al., 1994). However, unlike GATA-type zinc fingers, the LIM domains of animal LIM proteins do not seem to bind DNA. Rather, the LIM domain has been implicated in conferring specific protein-protein interactions (Arber and Caroni, 1996; Feuerstein et al., 1994; Schmeichel and Beckerle, 1994).

LIM proteins contain one, two or multiple LIM domains and have been divided into three groups according to the amino acid homology between their LIM domains. LIM domains were classified as types A-E (Figure 1.10) (Dawid et al., 1998). Group 1 LIM proteins contain paired N-terminal type A and B LIM domains either alone (Lmo proteins), or in association with a C-terminal homeodomain (LIM-homeodomain proteins) or a kinase domain (LIM-kinase). The LIM domains of LIMK1 interact with PKC, cytoplasmic domain of the transmembrane ligand neuregulin and Bone morphogenetic proteins (BMPs) II (Foletta et al., 2003; Kuroda et al., 1996; Wang et al., 1998).

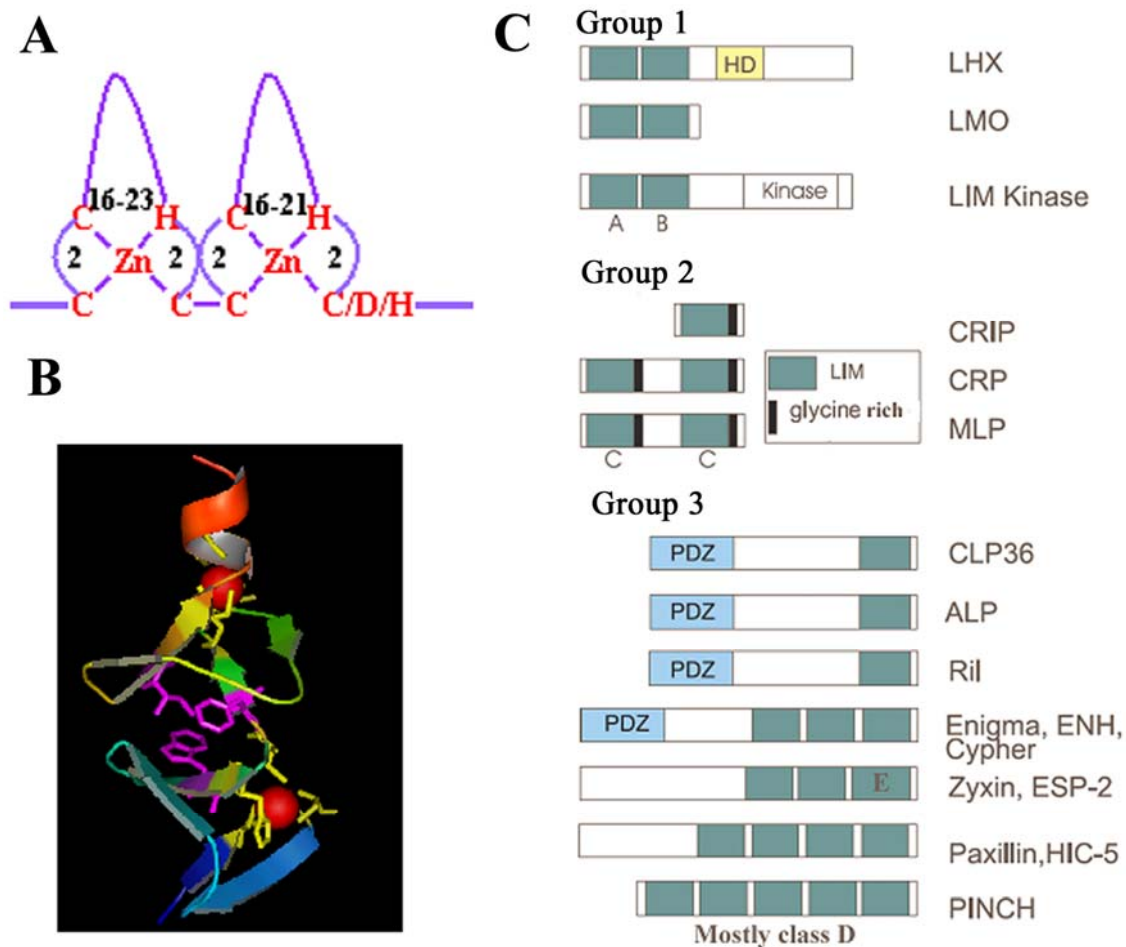


**Figure 1.10 LIM protein structure and classification.** **A:** Schematic representation of a LIM domain. The highly conserved cysteine and histidine amino acids form two zinc binding pockets. The two zinc fingers are always separated by two amino acids. **B:** NMR structure of the LIM2 domain of quail CRP2 also showing the zinc ions (red sphere, PDB code 1QLI) Both finger domains are constituted by two antiparallel  $\beta$ -sheets in the N-terminal module, these are followed by a tight turn that forms the linker to the following module. At the C-terminus of the second module, the  $\beta$ -sheets (yellow) is followed by a short  $\alpha$ -helix (red). Side chains of the hydrophobic core residues are shown in magenta color. (Prepared with the program PyMol (DeLano, 2004)). **C:** Classification of LIM domains (dark green, A-E) and groups of LIM domain proteins (Group 1-3) (Please refer text for more details) (Bauer, 2000).

Group 1 LIM proteins are predominantly nuclear, with the exception of LIMKs. LIM-homeodomain protein (LHX) perform a critical role embryonic development, tissue differentiation, and transcriptional regulation (Bach, 2000). LIM-homeodomain proteins bind DNA via their homeodomain (HD), yet their associated LIM domains bind other protein transcription factors. The LIM domain appears to have an inhibitory effect on the associated homeodomain's ability to bind DNA (Sanchez-Garcia et al., 1993).

Group 2 LIM proteins contain one or two type C LIM domains followed by a glycine-rich region with no other significant signaling domains. They include muscle LIM protein (MLP/CRP3). MLP localizes to the cardiac Z-lines where it binds the important actin-binding protein,  $\alpha$ -actinin and  $\beta$ -spectrin, interactions that are critical for the structural integrity of the cardiac cytoskeleton (Flick and Konieczny, 2000; Pomies et al., 1997). MLP also localizes in the nucleus of myoblasts and binds the myogenic transcription factor MyoD, to promote muscle differentiation (Kong et

al., 1997), targeted deletion of which has been shown to cause dilated cardiomyopathy in mice, due to marked disruption of the cardiac cytoarchitecture (Arber et al., 1997).

Group 3 LIM proteins contain 1 to 5 predominantly C-terminal type D and E LIM domains either alone or in association with other signaling domains such as PDZ or proline-rich motifs. Many LIM proteins of group 3 interact with the cytoskeleton and they include the focal adhesion proteins paxillin and zyxin. Members of the recently identified FHL protein family also known as skeletal muscle LIM proteins (SLIMS) have been shown to localize not only to the cytoskeleton but also to the nucleus, where they interact with transcription factors (Brown et al., 1999; Fimia et al., 2000).

#### 1.4.1.2. PDZ domain

PDZ domains function as protein-protein interaction modules. PDZ domains were first identified as regions of sequence homology found in diverse signaling proteins (Kim et al., 1995; Woods and Bryant, 1993). The name PDZ derives from the first three proteins in which these domains were identified: PSD-95 (a 95 kDa protein involved in signaling at the post-synaptic density), DLG (the *Drosophila melanogaster* Discs Large protein) and ZO-1 (the zonula occludens 1 protein involved in maintenance of epithelial polarity). These domains have also been referred to as DHR (Discs large homology repeat) domains or GLGF repeats (after the highly conserved four-residue GLGF sequence within the domain). The primary amino acid sequences of PDZ domains may differ considerably (down to some 20% sequence identity), but their three-dimensional structures appear strikingly similar. Like many other protein-protein interaction domains, PDZ domains are relatively small ( $\leq 90$  residues), show a compact globular structure and have N- and C-termini that are close to each other. Thus the domains are highly modular and have been integrated into existing proteins without significant structural disruption through the course of evolution. The PDZ fold consists of six  $\beta$ -strands ( $\beta$ A- $\beta$ F) and two  $\alpha$ -helices ( $\alpha$ A and  $\alpha$ B) (Figure 1.11A). PDZ domains recognize specific C-terminal sequence motifs that are usually about five residues in length, although in some rare cases specificity of recognition extends beyond these terminal five residues. The structures of several PDZ-peptide complexes reveal that peptide ligands bind in an extended groove between strand  $\beta$ B and helix  $\alpha$ B by a mechanism referred to as  $\beta$ -strand addition. Specifically, the peptide serves as an extra  $\beta$ -strand that is added onto the edge of a pre-existing  $\beta$ -sheet within the PDZ domain (Figure 1.11B). The peptide ligand backbone participates in the extensive hydrogen-bonding pattern normally observed between main-chain carbonyl and amide groups in a  $\beta$ -sheet structure (Figure 1.11C). The structure of the PDZ domain does not change upon ligand binding. Structures of PDZ-peptide complexes also reveal a loop termed the 'carboxylate-binding loop' at the end of the peptide-binding groove. This loop contains the well-conserved sequence motif R/K-X-X-X-G-L-G-F. Within the complex, the ligand terminal carboxylate is coordinated by a network of hydrogen bonds binding to main-chain amide groups in this loop, as well as an ordered water molecule that is coordinated by the side chain of a conserved arginine/lysine residue at the beginning of the loop (Figure 1.11). The

coordination of the terminal carboxylate, as well as the extensive  $\beta$ -strand- $\beta$ -strand interactions between the peptide and strand  $\beta$ B, firmly positions the peptide in the binding groove. PDZ domains can also recognize internal motifs. This second mode of interaction can be recognized, if they are presented within the specific tertiary structure context that conformationally mimics a chain terminus e.g. interaction of PDZ domain of nNOS with PSD5.

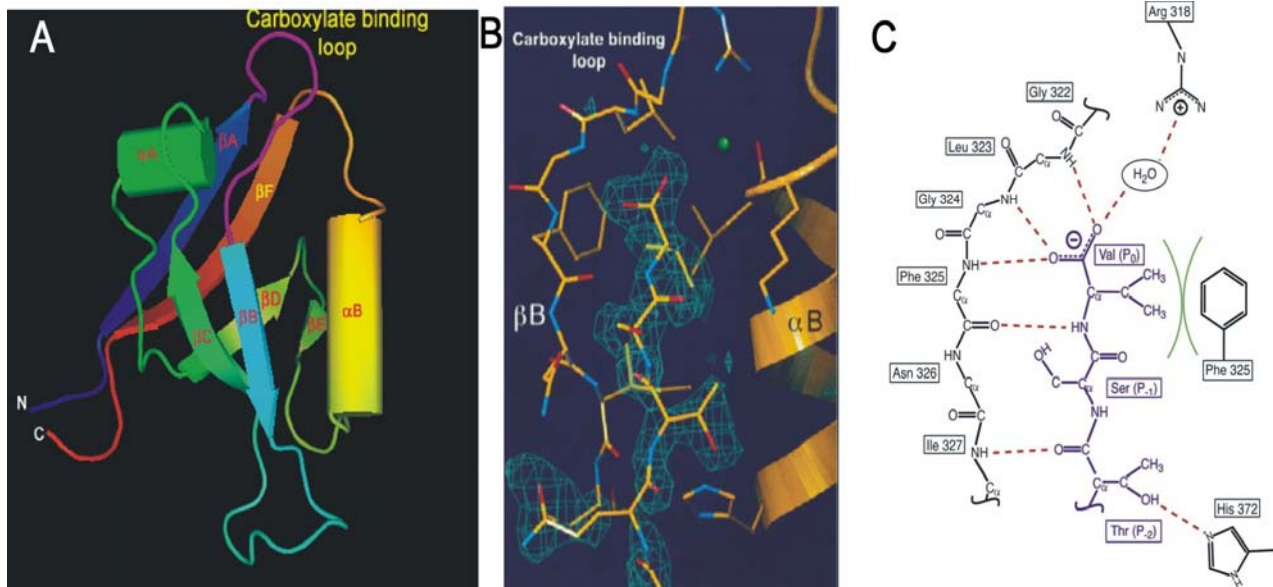


**Figure 1.11 Three-dimensional structure of a PDZ domain with or without its peptide ligand.** **A:** solution structure of the second PDZ domain of mouse PTP-BL (PDB accession code: 1GM1) showing the 6  $\beta$ -sheets and 2  $\alpha$ -helices composing the modular structure characteristic for PDZ domains. The second  $\beta$ -sheet, second  $\alpha$ -helix and the carboxylate-binding loop (magenta) involved in ligand binding are indicated **B:** The model of the peptide and surrounding domain structure is shown. The electron density map, contoured at  $3\sigma$ , defines the peptide carboxylate group and the last four C-terminal peptide residues. A water molecule, involved in the interaction of the peptide carboxylate group with the PDZ domain, is shown as a green sphere. The C-terminal sequence of the peptide is KQTSV (Doyle et al., 1996). **C:** Diagram of the peptide-binding pocket. Residues in the PDZ-domain-binding pocket are shown in black; the peptide is shown in blue. Hydrogen bonds are drawn as red dotted lines, and hydrophobic packing is indicated by green arcs (Harris and Lim, 2001)

PDZ domains can be divided into at least three main classes on the basis of their preferences for residues in recognition site: class I PDZ domains recognize the motif S/T-X- $\Phi$ -COOH (where  $\Phi$  is a hydrophobic amino acid and X is any amino acid); class II PDZ domains recognize the motif  $\Phi$ -X- $\Phi$ -COOH; and class III PDZ domains recognize the motif X-X-C-COOH. There are a few other PDZ domains that do not fall into any of these specific classes.

The multidomain structure of many PDZ-containing proteins enables them to interact with multiple binding partners simultaneously, thereby assembling larger protein complexes. PDZ-mediated protein complexes are often localized to specific sub-cellular compartments. Such PDZ-based scaffolds have been shown to organize signal transduction pathways such as phototransduction in *Drosophila*, where ion channels and signaling molecules are co-assembled by the multi-PDZ protein InaD (Montell, 1998). PDZ proteins have also been implicated in the establishment of cell polarity. In *Drosophila*, two PDZ-containing proteins, Bazooka and PAR-6, form a ternary complex with an atypical protein kinase C that is required for proper establishment and maintenance of apical-basal polarity in epithelial tissues (Ohno, 2001).

PDZ domains may also serve in coupling cytoplasmic signaling processes to nuclear events through nucleocytoplasmic shuttling. Many PDZ containing proteins, like PTP-BL, MAGUK and LIMK1, shuttle between nucleus and cytoplasm. The nuclear export of LIMK1 is mediated by two leucine rich nuclear export signals within the PDZ domain that might explain the predominant cytoplasmic localization of the enzyme (Yang and Mizuno, 1999). The PDZ domain of LIMK1 does not contain the carboxylate binding loop and does not bind with the S/TXV peptide (Yang et al., 1998a). Thus, the PDZ domain of LIMK1 may have other specific modes of protein interaction.

#### 1.4.1.3. Kinase domain

The kinase domain of eukaryotic protein kinases, which is well conserved among serine/threonine and tyrosine kinases, contains 12 conserved subdomains (Figure 1.12A). These subdomains fold into a common catalytic core structure, that is separated into two lobes (Figure 1.12B) (Hanks et al., 1988). The smaller N-terminal lobe (subdomains I-IV), or N lobe, is composed of a five-stranded  $\beta$  sheet and one prominent  $\alpha$  helix, called helix  $\alpha$ C. The C lobe (subdomains VIa-XI) is larger and is predominantly helical. ATP is bound in a deep cleft (subdomain V) between the two lobes and sits beneath a highly conserved loop connecting strands  $\beta$ 1 and  $\beta$ 2 (Figure 1.12B). This  $\gamma$ -phosphate binding loop, or P loop, contains a conserved glycine-rich sequence motif (GXGX $\phi$ G) where  $\phi$  is usually tyrosine or phenylalanine. The glycine residues allow the loop to approach the phosphates of ATP very closely and to coordinate them via backbone interactions. The conserved aromatic side chain caps the site of phosphate transfer. The glycine residues make the P loop very flexible in the absence of ATP (Zheng et al., 1993).

Peptide substrate binds in an extended conformation across the front end of the nucleotide-binding pocket, close to the  $\gamma$ -phosphate of ATP. A centrally located loop known as the “activation loop,” typically 20–30 residues in length, spanning conserved sequences DFG and APE, provides a platform for the peptide substrate. In most kinases, this loop is phosphorylated when the kinase is active. Phosphorylation of the activation loop stabilizes it in an open and extended conformation that is permissive for substrate binding.

Optimal phosphotransfer requires the precise spatial arrangement of several catalytic residues that are absolutely conserved among all known kinases. Asp<sup>166</sup> and Asn<sup>171</sup> (PKA numbering, Asp<sup>451</sup> and Asn<sup>456</sup> of LIMK2) emanate from a highly conserved loop structure at the base of the active site, called the catalytic loop. Asp<sup>166</sup> interacts with the attacking hydroxyl side chain of the substrate, while Asn<sup>171</sup> engages in hydrogen bonding interactions that orient Asp<sup>166</sup> (Figure 1.12C). Asn<sup>171</sup> and another absolutely conserved catalytic residue, Asp<sup>184</sup> (Asp<sup>469</sup> of LIMK2), are also required for the binding of two divalent cations involved in nucleotide recognition (Figure 1.12C). Asp<sup>184</sup> forms part of the highly conserved DFG motif situated at the base of the activation loop. The structure of this motif, and in particular the conformation of Asp<sup>184</sup>, is tightly coupled

to phosphorylation of the activation loop. In the N lobe, Lys<sup>72</sup> (Lys<sup>360</sup> of LIMK2) makes crucial contacts with the  $\alpha$ - and  $\beta$ -phosphate groups, positioning them properly for catalysis. Lys<sup>72</sup> is buried deep within the inter lobe cleft, where it is stabilized and oriented properly by an ionic interaction with Glu<sup>91</sup> (Glu<sup>376</sup> of LIMK2), a residue in the  $\alpha$ C helix.

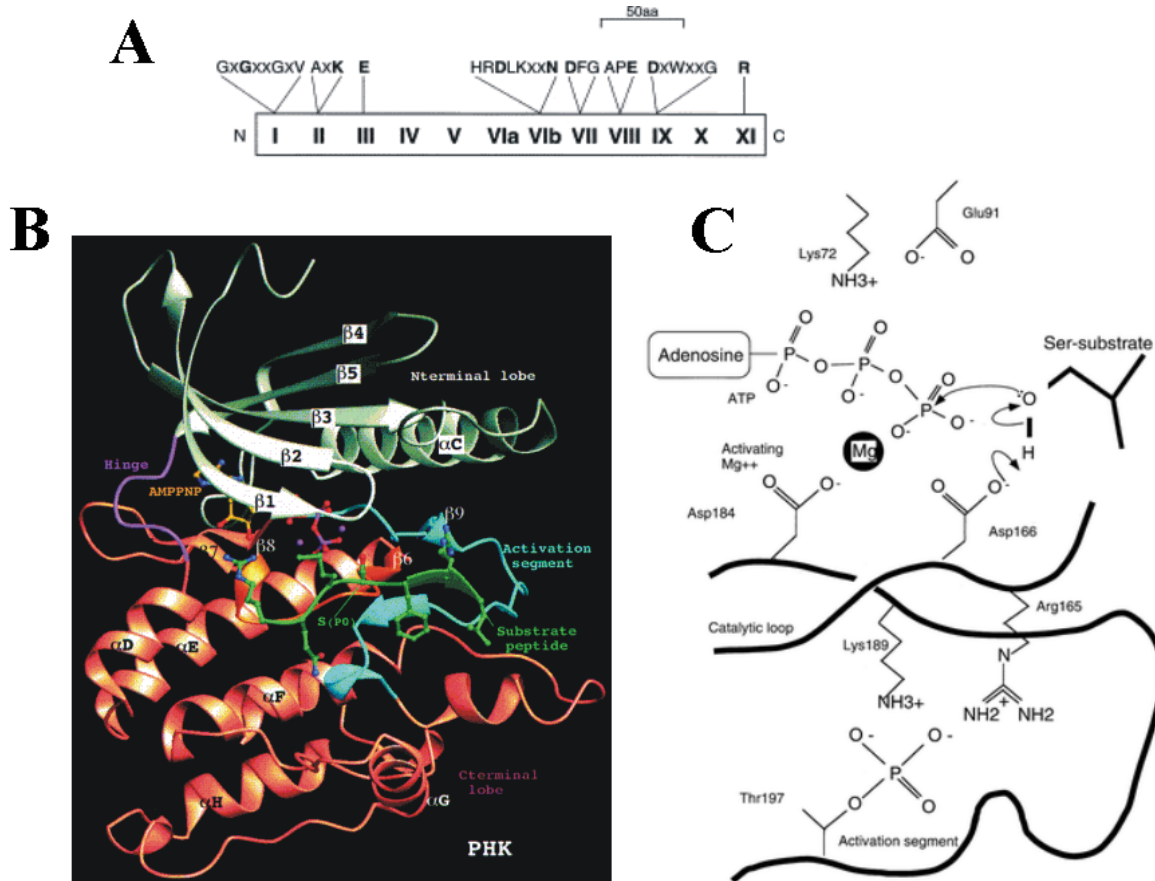


**Figure 1.12** **A:** Typical 300 amino acid protein serine/threonine kinase catalytic domain. The 12 conserved subdomains are indicated by Roman numerals. Consensus sequences found in the subdomains are shown with invariant or nearly invariant residues in bold. **B:** Schematic diagram of the fold of phosphorylase kinase (PhK), illustrating a typical protein kinase fold. The N-terminal lobe is shown in white, the hinge region in magenta and the C-terminal lobe in salmon. The catalytic loop is shown in gold and the activation segment in cyan.  $\alpha$ -Helices are labeled from  $\alpha$ C to  $\alpha$ I ( $\alpha$ I is obscured by  $\alpha$ F).  $\beta$ -Strands are labeled  $\beta$ 1– $\beta$ 9. The substrate peptide is shown in green with all residues displayed and the serine to be phosphorylated marked by S (P0). AMPNP and two manganese atoms (magenta) are shown with all atoms displayed (Johnson et al., 1998). **C:** A Schematic Representation of ATP and Some of the Key Residues at the Catalytic Site and Activation Segment of cAPK. A possible mechanism is shown in which base-catalyzed attack by Asp-166 on the substrate serine promotes the formation of an alcoholate ion, which can then attack the  $\gamma$  phosphate of ATP. The catalytic mechanism is not definitively established (Johnson et al., 1996).

The characteristic short sequence motif (DLKXXN) of a serine/threonine kinase family, present in subdomain VIb, is highly conserved among all the members of this family. This motif is also present in subdomain VIb of LIM-kinases. Almost all known serine/threonine-specific protein kinases, including the kinases with dual specificity, contain the highly conserved lysine residue at the third position of this motif (DLKXXN). In contrast both LIMK1 and LIMK2 contain the sequence DLNSHN in this motif, which does not carry either the arginine or the lysine residue at the third position, but does have a histidine residue at the fifth position: (Nunoue et al., 1995).

### **1.4.2. Gene expression and subcellular localization of LIM-kinases**

Northern and in situ hybridization (ISH) analyzes from different studies revealed that the highest levels of LIMK1 are found in fetal and adult neural tissues, such as the brain, spinal cord, and various sensory organs (Bernard et al., 1994; Cheng and Robertson, 1995; Mizuno et al., 1994). In contrast, LIMK2 isoforms (see section 1.4.1) display significant variation of expression in mouse in tissue distribution. The LIMK2a transcript is ubiquitously expressed in a variety of tissues such as kidney, lung heart, including neural tissues, and LIMK2b is predominantly expressed in the brain (Koshimizu et al., 1997; Mori et al., 1997). Furthermore, the testis-specific LIMK2 isoform (tLIMK2) is specifically expressed in differentiated, meiotic stages of spermatogenic cells, therefore suggesting that it contributes to spermatogenesis (Takahashi et al., 1998). Recently Foletta et. al. (Foletta et al., 2004) demonstrated, using a specific LIMK1 monoclonal antibody that the expression of LIMK1 is not only limited to neural tissues but is present in all tissues, although the levels of expression varied. In this study, LIMK1 in every cell and tissue type had an apparent mobility of about 70kDa. In some tissues, notably stomach, human fibroblasts and pig kidney cells, smaller bands of 45-50kDa were also evident like LIMK2 short isoforms. They also observed a high molecular weight form of 80kDa in the mouse brain.

LIMKs display a unique subcellular localization. LIMK1 and LIMK2a are localized mainly in the cytoplasm and to a lesser extent in the nucleus. In contrast, LIMK2b shows exclusive cytosolic distribution (Osada et al., 1996). tLIMK2 lacking both LIM domains was found to be preferentially localized in the nucleus (Takahashi et al., 2002). In mouse tissues, nuclear localization of LIMK1 was more pronounced than reported previously and found in a wide range of cell types including epithelial cells, spermatocytes, neuronal cells and muscle fibers. Immunofluorescence analysis of cultured cells revealed LIMK1 localization at focal adhesions in many adherent cell types suggesting a role in cell attachment and motility. In cultured hippocampal neurons, LIMK1 was found highly localized in axonal and dendritic growth cones and exhibited strong Golgi staining.

### **1.4.3. Regulation of LIMK activation**

The catalytic activity of many protein kinases is usually suppressed in cells and is activated only in response to certain upstream stimuli. The extra-catalytic region of the kinase often serves as the domain that negatively regulates the kinase activity. Moreover, liberation from its suppressive effect by events, such as binding of activators to the extra-catalytic region or phosphorylation of residues in catalytic and/or extra-catalytic regions by upstream kinases or by autophosphorylation results in activation of the enzyme (Johnson et al., 1996).

The N-terminal LIM domains play an inhibitory role in the regulation of the kinase activity of LIMK1 by direct interaction with the kinase domain (Nagata et al., 1999). The LIM domains may fix the kinase domain in an inactive conformation, or inhibit the access of substrates by masking

the kinase catalytic site or substrate-binding site. Many serine/threonine kinases are phosphorylated on a residue(s) in the activation loop (Figure 1.12B). LIMK1 and LIMK2 have threonine at 508 and 505 respectively in the activation loop. Rho-kinase, PAK1 and PAK4 phosphorylate LIMK1 at Thr508 (Dan et al., 2001; Edwards et al., 1999; Sumi et al., 2001a). Rho-kinase phosphorylates LIMK2 at Thr505 thereby activating it. LIMK2 is also phosphorylated at Thr505 by MRCK $\alpha$  (Myotonic dystrophy kinase-related Cdc42-binding kinase) (Sumi et al., 2001b).

## **1.5. Regulation of protein transport between nucleus and cytoplasm**

Eukaryotic cells are characterized by distinct nuclear and cytoplasmic compartments that are separated by the nuclear envelope, a double membrane that is continuous with the endoplasmic reticulum. Protein transport between nucleus and cytoplasm is an integral part of eukaryotic cells processes such as differentiation, proliferation and the control of gene expression. (Jans and Hubner, 1996) Because gene transcription and translation take place in separate sub-cellular compartments, specific transport events occur: a) mRNA and ribonucleoproteins take away from the nucleus into the cytoplasm, b) the proteins that are required in the nucleus need to be specifically transported into the nucleus. Therefore, many molecules shuttle continuously between the nucleus and the cytoplasm through the nuclear pore complexes (NPCs), which penetrate the nuclear envelope. NPC consists of a central core with a ring-spoke structure exhibiting 8-fold radial symmetry. From this central ring, 50-100nm fibrils extend into the nucleoplasm and the cytoplasm (Akey and Radermacher, 1993; Pante and Aebi, 1994). It is estimated that the average mammalian nucleus contains approximately 5600 pores. Small proteins (<40-60kDa), and small molecules such as lipid, ions and metabolites passively diffuse through the NPC by following a concentration gradient. Macromolecules larger than 40-60 kDa are, in most cases, actively transported across the NPC. NPCs of higher eukaryotes have a mass of ~125MDa and are estimated to be composed of ~50-100 different proteins that are often collectively called nucleoporins (Gorlich and Kutay, 1999; Ohno et al., 1998). The active nuclear import and export of proteins is mediated by specific amino acid sequences, which are referred to as nuclear localization signals (NLSs) and nuclear export signals (NESs), respectively, and which are usually present within the primary structure of each cargo.

Nuclear import signals are often characterized by essential basic amino acids, which lead to the proposal of consensus import signal. The basic types of NLS are mainly either monopartite or bipartite (Gorlich and Kutay, 1999). A monopartite NLS consists of a single short cluster of consecutive basic amino acids, while a bipartite NLS comprises two clusters of basic amino acids separated by a 10–12 amino acid spacer. Many transporters belong to the importin superfamily, and, frequently, the interactions of importin with cargo protein via NLS and NPC proteins (nucleoporins) are orchestrated by the small GTP-binding protein Ran guanosine triphosphatase

(Ran GTPase). Because of the spatial distribution of its GAP and GEF proteins, cytoplasmic Ran is primarily in the GDP-bound state, whereas nuclear Ran is primarily in the GTP-bound state (Figure 1.13) (Weis, 2003). Cargo proteins destined for import are attached to importin- $\beta$  via the importin- $\alpha$  adaptor protein (although a minority of cargo proteins bind to importin- $\beta$  directly) (Wozniak et al., 1998). Importin- $\alpha$  consists of two functional domains, a short basic N-terminal importin- $\beta$  binding domain (the IBB domain), and an NLS-binding domain built of armadillo (arm) repeats motifs (Kobe, 1999). Importin- $\alpha$  is autoinhibited by its N-terminal segment containing the IBB domain. Importin- $\beta$  binding to importin- $\alpha$  removes the N-terminal autoinhibitory segment from the NLS-binding site in importin- $\alpha$ . This importin- $\alpha/\beta$  heterodimer is then active and importin- $\alpha$  binds to a NLS-containing cargo protein in the cytoplasm (Figure 1.13). The passage of importin- $\beta$  cargo complexes through NPCs is mediated by transient interactions with nucleoporins that have characteristic FG sequence repeats (Bayliss et al., 2000). Therefore, importin- $\alpha$  acts as an adapter molecule between the cargo and importin- $\beta$ , and it is importin- $\beta$ , which actually carries the cargo from the cytoplasm into the nucleus. After translocation of the cargo/importin complex through the NPC, nuclear RanGTP binds to importin- $\beta$ , inducing release of its cargo and facilitating the recycling of both importins back to the cytoplasm (Gorlich et al., 1996). Importin- $\beta$ , bound to RanGTP, returns to the cytoplasm. Whereas importin- $\alpha$  forms a trimeric complex within the nucleus with CAS (one of the importin- $\beta$  related molecules) and RanGTP, and then migrates into the cytoplasm (not shown in Figure 1.13) (Kutay et al., 1997). For the next import cycle, in the cytoplasm, the GTP hydrolysis of Ran bound to importin- $\beta$  or CAS triggers the dissociation of the complex, resulting in recycling of the carrier molecules.

On the other hand, the leucine-rich NESs, which contain export cargoes, are complexed with their export receptor, CRM1 (Chromosomal Region Maintenance 1) and RanGTP in the nucleus. CRM1 (designated exportin 1) is also related to importin- $\beta$  with Ran-binding activity and binds the export cargo cooperatively with RanGTP. The NES-cargo/CRM1/RanGTP trimeric complex is translocated through the NPC towards the cytoplasm without GTP hydrolysis of Ran (Fornerod et al., 1997; Fukuda et al., 1997; Stade et al., 1997). After the translocation, the trimer dissociates in the cytoplasm or on the cytoplasmic side of the NPC via the conversion of RanGTP to the GDP-bound form. The drug leptomycin B inhibits this pathway by binding to CRM1 (Kudo et al., 1998). Therefore, this drug is very useful for the identification of CRM1-dependent export cargoes and for verifying whether proteins are shuttled continuously between the cytoplasm and the nucleus, when the proteins are exported in a CRM1-dependent manner.

Ran GTPase cycle is regulated by various interacting proteins. The GEF of Ran (RanGEF), RCC1, accelerates the dissociation of guanine nucleotide from Ran, resulting in the conversion of RanGDP to RanGTP because of a higher levels of GTP compared with GDP in cells. RCC1 is a chromatin protein and is located in the nucleus. Thus, the generation of the GTP-bound form of

Ran occurs only in the nucleus. Ran GTPase activity is stimulated by the GAP of Ran (RanGAP) in the cytoplasm.

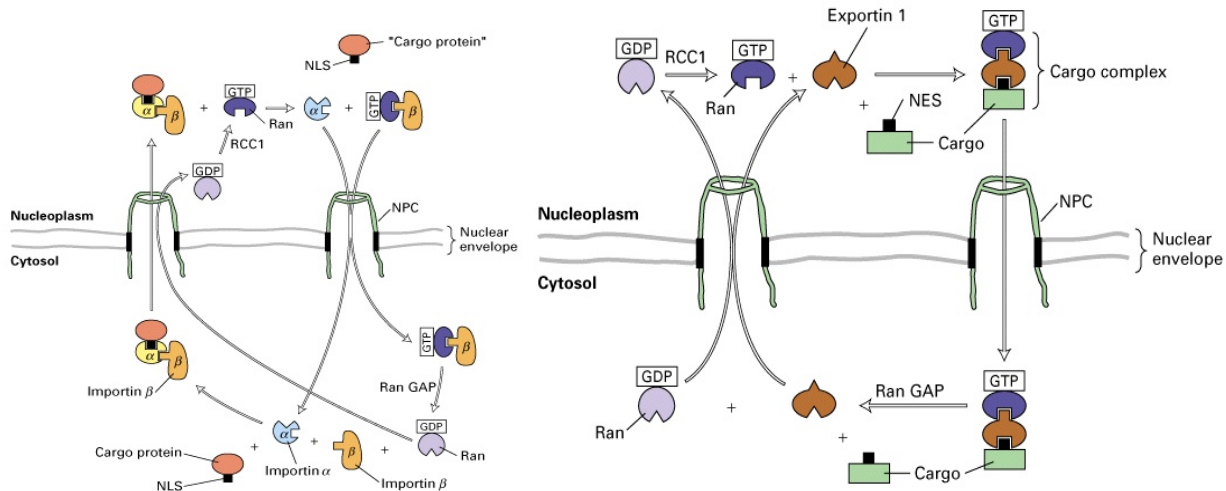


**Figure 1.13 Scheme for nuclear import and export of proteins.** Cargo proteins are transported by importin or exportin and Ran coordinates their transport. NLS: nuclear localization signal, NES: nuclear export signal.

A large number of proteins shuttle between the nucleus and the cytoplasm. The intracellular localization of these proteins is highly regulated and dependent on extra-cellular signals and the cell cycle. Extra-cellular signal-regulated kinases 1 and 2 (ERK1/2) translocate into the nucleus after activation of the cells with epidermal growth factor (EGF), and phosphorylate specific transcription factors such as Jun and Fos that control cell proliferation, differentiation and apoptosis (Thomson et al., 1999). Essential cell cycle regulators such as cyclins and cyclin-dependent kinases (CDKs) shuttle continuously between the nucleus and cytoplasm, and the final localization of these proteins regulates the cell cycle progression (Yoneda, 2000). Overexpression studies demonstrated that LIMKs are found not only in the cytoplasm but also in the nucleus. The cytoplasmic localization of LIMK1 is due to the presence of two functional leucine rich NESs, which are sensitive to LMB (Yang and Mizuno, 1999). Therefore, LIMK1 shuttles between the nucleus and the cytoplasm. However, the mechanism by which the nucleocytoplasmic shuttling occurs is completely unknown.

## 1.6. Cellular functions of LIMK-kinases

Overexpression of LIMKs in a variety of cultured cell types resulted in actin stabilization and subsequent aggregation of F-actin (Amano et al., 2001; Arber et al., 1998). This effect of LIMKs can be explained by cofilin phosphorylation at Ser-3 (inactivation of cofilin) and inhibition of actin depolymerization (Arber et al., 1998). Overexpression studies of LIMKs also observed that LIMKs play an important role in stress fiber formation, stabilization of focal adhesion, and ruffle formation in various cells (Amano et al., 2001).

Furthermore, evidence is accumulating that LIMKs are involved in transducing signals from extracellular stimuli to cytoskeletal networks that regulate various functions, such as cell division, motility, and the maintenance of specialized structures in differentiated cells.

For example LIMK1 interacts with the tail region of BMPR-II (Bone Morphogenetic Proteins Receptor); a transmembrane serine threonine protein kinase phosphorylates BMPR1 and regulates the Smad transcription factor. This interaction between LIMK1 and BMPR-II inhibited LIMK1's ability to phosphorylate cofilin (Foletta et al., 2003). A BMPR-II mutant containing the truncation of the tail region described in the rare autosomal dominant disorder primary pulmonary hypertension (PPH), is characterized by the proliferation of pulmonary artery smooth muscle cells and endothelial cells, resulting in an increased blood pressure followed by heart failure. The level of LIMK1 protein is increased in PPH patients, and truncated BMPRII, which mimics the PPH patient's mutants of BMPRII, failed to bind or inhibit LIMK1. These results together suggest that dysregulation of LIMK activity could lead to the hyperproliferation of endothelial and smooth muscle cell, a characteristic of PPH.

Various reports showed that LIMK1 is upregulated in adenocarcinomatous prostatic epithelium and prostate cancer cell lines, and that it is essential for the invasive property and growth of prostate cancer cells. Interestingly, this effect is not mediated through phosphorylation of cofilin (Davila et al., 2003; Yoshioka et al., 2003). These findings suggest a possible correlation of LIMK1 expression with prostate cancer progression. A recent study shows that LIMK1 cleaved by caspases at Asp-240, and that cleaved LIMK1 fragment induces membrane blebbing in apoptotic Jurkat and HeLa cells. These results suggest that LIMK1 might play a critical role in membrane bleb formation during apoptosis (Tomiyoshi et al., 2004).

In Williams syndrome, the chromosomal region containing the LIMK1 gene is deleted, a neurodevelopmental disorder characterized by mental retardation, difficulties in visuospatial constructive cognition, and skeletal abnormalities. This syndrome raised the questions regarding a specific neuronal function of LIMK1 (Frangiskakis et al., 1996). LIMK1- and LIMK2-deficient mice have been developed, to explore the function of LIMK *in vivo*. LIMK1-deficient mice developed quite normally, but they showed abnormalities in the hippocampal dendritic spine structure (Meng et al., 2002). In addition, these mice showed a significant deficit in relearning spatial information, strongly suggesting that LIMK1 might be implicated in Williams syndrome. Somewhat surprisingly, the LIMK1-deficient mice, and the LIMK2-deficient mice, which have all three LIMK2 isoforms disrupted, did not exhibit embryonic lethality. In addition, there was no marked phenotypic abnormality in postnatal growth and development in these mice (Takahashi et al., 2002). Apart from a smaller testis size, LIMK2-deficient mice older than two years showed no pathological symptoms, abnormal behavior, or significant increase in tumor development. A possible explanation for these normal phenotypes may be a functional redundancy of the two LIMKs i.e. LIMK1 fulfills the function of LIMK2 and *vice versa*. LIMK1- and LIMK2-double-deficient mice might answer this question.

## **2. Aim of the study**

The activation of the endothelium with various stimuli such as thrombin leads to cell shape change, migration, and proliferation that involve dynamic changes of the actin cytoskeleton. The Rho family GTPases activate Rho-kinase and PAK, which stimulate LIM-kinases. LIM-kinases regulate the actin cytoskeleton through phosphorylation of cofilin. Only very few studies reported about other functions of LIM-kinases, such as its possible role in cell cycle regulation. The function of the LIM-kinases is unknown in endothelial cells.

The aim of the present study was to answer the following two major questions:

A) Which LIM-kinase(s) are expressed in endothelial cells? What is the role of LIM-kinases and cofilin phosphorylation in thrombin-induced stress fiber formation and contraction of endothelial cells? How is the LIMK/cofilin pathway regulated in endothelial cells?

B) Does LIMK2 shuttle between the cytosol and the nucleus in endothelial cells? If yes, which are the responsible nuclear localization signals (NLSs) and nuclear export signals (NESs)? How is the nucleocytoplasmic shuttling of LIMK2 regulated in endothelial cells?

### **3. Materials and methods**

Protocols were adapted from standard methods (Sambrook and Russell, 2001) unless otherwise mentioned.

All solutions and media were prepared with ultra-pure water (Milli-Q Plus ultra purification pak, Milli-RO Plus purification pak; Millipore, Molsheim, France).

#### **3.1. General equipments**

Autoclave	Autoclave 23; MELAG Medizintechnik (Berlin, Germany) Bioclav; Schütt Labortechnik GmbH (Göttingen, Germany)
Centrifuges	Biofuge pico, Omnifuge 2.OR, Megafuge 1.ORS, Heraeus (Osterode, Germany) Centrikon H-401, with Rotors A8.24 and A6.9; Kontron-Hermle (Gosheim, Germany)
Chromatography System	Automated Econo System; Biorad (Hercules, CA)
Electroporation apparatus	Gene pulser II; Biorad (Hercules, CA)
Freezer, -70°C	ULT1706; Revco Scientific (Asheville, NC),
Gel documentation camera	Polaroid MP-4 land camera; Polaroid USA
Gel Electrophoresis	Biorad (Hercules, CA) Hera freeze; Heraeus (Osterode, Germany)
Incubators	WTB Binder (Tuttlingen, Germany), Forma Scientific (USA) JULABO Labortechnik GmbH
Liquid nitrogen tank	BT40; L'air liquide (Champigny, France) LSM 510META confocal microscope; Zeiss (Jena Germany)
Magnetic stirrer	MR3001; heidolph (Kelheim, Germany)
Microscope	IX50; Olympus Optical GmbH (Hamburg, Germany) Model RI60P; Sartorius (Göttingen, Germany)
pH meter	Model 765 Calimatic; Knick (Berlin, Germany)
Scales	Model BP 2100S; Sartorius (Göttingen, Germany)
Sonicator	SONOPLUS Bandelin electronic GmbH (Berlin, Germany)
Spectrophotometer	UVICON 930; Kontron instruments (Echingen, Germany)
Thermocycler	Mastercycler gradient; Eppendorf (Hamburg, Germany)
Thermomixer	Thermomixer compact; Eppendorf (Hamburg, Germany)
Ultracentrifuge	Optima <sup>TM</sup> TLX, with rotor TLA 100.4; BeckMan Instruments Fullerton, CA
Vortexer	REAX top; Heidolph (Kelheim, Germany)
Water baths	GFL GmbH (Burgwedel, Germany)
Densitometer	Pharmacia LKB (Sweden)

UV illuminator Model N90M; UniEquip (Martinsried, Germany)

## 3.2. Materials

### 3.2.1. Chemicals

Acryl/Bis 37.5:1; 40% (w/v) Solution	AMRESCO Inc. USA
Acetic acid	Merck Biosciences GmbH, Schwalbach, Germany
Agar	Mo Bio Laboratories, USA
Agarose	Sigma, Munich, Germany
Ammonium persulphate	Sigma, Munich, Germany
Ampicillin	Sigma, Munich, Germany
Aprotinin	Sigma, Munich, Germany
ATP	Amersham Biosciences, Freiburg, Germany
BrdU	Sigma, Munich, Germany
Bromophenol blue	Sigma, Munich, Germany
BSA (bovine serum albumin)	Sigma, Munich, Germany
G250 Brilliant Blue	Serva, Heidelberg, Germany
Dideoxynucleotides	Stratagene Inc USA
DMSO	Sigma, Munich, Germany
DTT	Sigma, Munich, Germany
EDTA	Sigma, Munich, Germany
Ethanol	Merck Biosciences GmbH, Schwalbach, Germany
Isopropanol	Sigma, Munich, Germany
Ethidium Bromide	Sigma, Munich, Germany
Formamide	Fluka AG, Neu-Ulm, Germany
G418 (Geneticin)	Invitrogen, Karlsruhe, Germany
Glycerol	Merck Biosciences GmbH, Schwalbach, Germany
Glutathione-Sepharose	Amersham Biosciences, Freiburg, Germany
HEPES	Sigma, Munich, Germany
Hoechst 3342	Molecular Probe, USA
IPTG	peqLab Biotechnologie, Erlangen, Germany
Lipofectamine®	Invitrogen, Karlsruhe, Germany
L-Glutamine	Invitrogen, Karlsruhe, Germany
Leptomycin B	Sigma, Munich, Germany
Kanamycin	Sigma, Munich, Germany
Methanol	Merck Biosciences GmbH, Schwalbach, Germany
Protein A Sepharose CL-4B	Sigma, Munich, Germany
SDS	Sigma, Munich, Germany
Sodium Azide	Serva, Heidelberg
Sodium Fluoride	Sigma, Munich, Germany
Sodium Orthovanadate	Aldrich, Steinheim, Germany
PMA	Sigma, Munich, Germany
PMSF	Sigma, Munich, Germany
Ponceau S	Sigma, Munich, Germany
Propidium Iodide	Sigma, Munich, Germany
TEMED	Sigma, Munich, Germany
Triton X-100	Sigma, Munich, Germany
Tryptone	Sigma, Munich, Germany

Tween 20	Sigma, Munich, Germany
Yeast extracts	Sigma, Munich, Germany

### **3.2.2. Enzymes and reagents for molecular biology**

Restriction enzymes	New England Biolabs GmbH, Frankfurt, Germany
<i>Taq</i> DNA polymerase	New England Biolabs GmbH, Frankfurt, Germany
<i>Pfu</i> Ultra HF DNA polymerase	Stratagene, Netherlands
Thermoscript reverse transcriptase	Invitrogen GmbH, Karlsruhe, Germany
Calf Intestine alkaline phosphatase	Roche Diagnostic, Mannheim, Germany
T4 DNA ligase	New England Biolabs GmbH, Frankfurt, Germany
RNaseA	Sigma, Munich, Germany
DNase I	Roche Diagnostic, Mannheim, Germany
DNase (RNase free)	Qiagen, Hiden, Germany
Lysozyme	Sigma, Munich, Germany
dNTP	Stratagene, Netherlands
T4 Polynucleotide kinase	New England Biolabs GmbH, Frankfurt, Germany

### **3.2.3. Antibodies**

#### **3.2.3.1. Primary antibodies**

LIM-kinase 1	Rabbit IgG, directed against KLH conjugated synthetic peptide corresponding to the C-terminal residues of LIMK1 Western Blotting 1:1000, Immunoprecipitation 1:25
LIM-kinase 2	Rabbit IgG, directed against KLH conjugated synthetic peptide corresponding to the C-terminal residues of LIMK2 Western Blotting 1:1000, Immunoprecipitation 1:25
Phospho-LIM-kinase	Rabbit IgG, directed against KLH conjugated synthetic phospho-peptide corresponding to residues surrounding Thr508 of LIMK1. Western Blotting 1:1000, Immunoprecipitation 1:25
Cofilin	Rabbit IgG, directed against KLH conjugated synthetic peptide corresponding to residues surrounding Ser3 of human cofilin. Western Blotting 1:12000
Phospho-Cofilin	Rabbit IgG, directed against KLH conjugated synthetic phospho-peptide corresponding to residues surrounding Ser3 of human cofilin. Western Blotting 1:1000.
Phospho-MYPT1	Rabbit IgG, directed against KLH conjugated synthetic peptide corresponding to residues 848-858 of human MYPT1. Western Blotting 1:3000.
Phospho-(Ser) PKC Substrate	Rabbit IgG, directed against synthetic phospho-PKC substrate PKC peptides consensus sequences library. Western Blotting 1:1000

**3.2.3.2. Secondary antibodies**

Anti-rabbit IgG HRP conjugated	F(ab') <sub>2</sub> fragment, from donkey, Amersham Biosciences, Freiburg, Germany. Western blot 1:5000
Anti-mouse IgG HRP conjugated	F(ab') <sub>2</sub> fragment, from sheep, Amersham Biosciences, Freiburg, Germany. Western blot 1:5000

**3.2.3.3. IgG isotype controls and sera**

Rabbit IgG	Sigma, Munich, Germany
Mouse IgG	Sigma, Munich, Germany
Donkey serum	Sigma, Munich, Germany
Goat serum	Sigma, Munich, Germany

**3.2.4. Inhibitors**

Y27632 (Rho-kinase)	Merck Biosciences GmbH, Schwalbach, Germany
Gö6976 (PKC isoforms)	Merck Biosciences GmbH, Schwalbach, Germany
Gö6983 (PKC isoforms)	Merck Biosciences GmbH, Schwalbach, Germany
Gö6950 (PKC isoforms)	Merck Biosciences GmbH, Schwalbach, Germany
Phosphatase inhibitor cocktail	Roche Diagnostic, Mannheim, Germany
Proteases inhibitor cocktail	Roche Diagnostic, Mannheim, Germany

**3.2.5. Ligands**

Thrombin	Sigma, Munich, Germany
LPA	Avanti polar lipids Inc. USA
PMA	Sigma, Munich, Germany

**3.2.6. Commercial Kits and other materials**

QIAquick™ PCR-Purification kit	Qiagen, Hiden, Germany
QIAquick™ Gel-extraction kit	Qiagen, Hiden, Germany
QIA® Spin Miniprep kit	Qiagen, Hiden, Germany
Endofree® Plasmid Maxi kit	Qiagen, Hiden, Germany
RNeasy® mini kit	Qiagen, Hiden, Germany
QuickChange® XL Site directed mutagenesis kit	Stratagene, Netherlands
Rapid DNA ligation kit	Roche Diagnostic, Mannheim, Germany
Expend High Fidelity PCR system	Roche Diagnostic, Mannheim, Germany
Thermoscript™ RT-PCR system	Invitrogen GmbH, Karlsruhe, Germany
Zero Blunt® TOPO® PCR cloning kit	Invitrogen GmbH, Karlsruhe, Germany
DotMetric™ -1µl Protein assay kit	Genotech Inc. USA

Lowry Protein assay kit	Sigma, Munich, Germany
Hybond™-C extra blotting membrane	Amersham Biosciences, Germany
SuperSignal® West Pico chemiluminiscent Substrate	Pierce, Rockland, USA
Photographic film	Polapan; Polaroid, Offenbach, Germany

### 3.2.7. Primers

#### 3.2.7.1. For preparation of cDNA inserts

Primer	Sequence*	Type, restriction site
CLIK2F	ATTGAATTCATGTCCGCGCTG	Sense, <i>EcoR</i> I
CPDZF	ATTGAATTCGTTCAGGAGCAG	Sense, <i>EcoR</i> I
KinaseF	GCTCAGAATTCCTTCGTTGTTCCAGC	Sense, <i>EcoR</i> I
SalML-2	AATAAGAATGTCGACTAGGGAGGTGAGTCCCGG	Antisense, <i>Sal</i> I
NLIK2F	ATTCTCGAGGCCACC ATGTCC GCG CTG GC	Sense, <i>Xho</i> I
NLIMPDZR	TTAATACCGGTGGAAGGGATTCTGAGCG	Antisense, <i>Age</i> I
Ckinase_LIK1_F	ATTGAATTCCTTCTCCGGGCGCTGGC	Sense, <i>EcoR</i> I
CPDZK_LIK1_F	ATTGAATTCGTGCATCGAGCAGATC	Sense, <i>EcoR</i> I
CLIK1_R	ATAATGTCGACTCAGTCGGGGACCTCAGG	Antisense, <i>Sal</i> I

\* Restriction sites are shown in red.

#### 3.2.7.2. For deletion mutation

Primer	Sequence	Description
LIMI-PDZK_R	GAAC TCCCCAAACTTCCCCAGTAGTCC	Antisense, LIM2 deletion
PDZ-del-LIMII_F	CACAATGAGGTGGTGGTGGCACCCATG	Sense, LIM2 deletion
LIMII_PDZK_F	GGGAGTTCTGTCATGGGTGCTCCCTGCTG	Sense, LIM1 deletion
EGFP_C1_R	AGAATTCGAAGCTTGAGCTCGAGATCTGAG TCC	Antisense LIM1 and N-term of kinase domain deletion
NLS_F	CTCATAGTGGAAGAGAGGAAAAGGGCCCCC	N-term of kinase domain deletion
EGFP_C1_F	GTCGACGGTACCGCGGGCCCGGGATCCACC	GFP-NLS preparation
NLS_R_stop	CTAGGGGTTTCCCACCACCGTGTAGCGC	GFP-NLS preparation

## 3.2.7.3. For site directed mutagenesis

Primer	Sequence*	Description (position of wild type amino acid mutated)
MutantD451A-F	ATCATCCACCGG <b>GCC</b> CTGAACTCGCAC	Sense (451 to A)
MutantD451A-R	GTGCGAGTTCAG <b>GGCC</b> CGGTGGATGAT	Antisense (451 to A)
ML2-3	CAAGAAGCGCTAC <b>GAAGA</b> AGTGGTGGGAAAC	Sense (505 to A)
ML2-4	GTTTCCCACC A <b>CTTCTT</b> CGT AGCGCTTCTT G	Antisense (505 to A)
Mutant505TF	AAGAAGCGCTAC <b>GCG</b> GTGGTGGGAAAC	Sense (505 to EE)
Mutant505TR	GTTTCCCACCAC <b>CGC</b> GTAGCGCTTCTT	Antisense (505 to EE)
Mut_S283A_F	CTGAGGAGACGT <b>GCC</b> CTAAGGCGCAGT	Sense (283 to A)
Mut_S283A_R	ACTGCGCCTTAG <b>GGC</b> ACGTCTCCTCAG	Antisense (283 to A)
Mut_S283EE_F	CACTGAGGAGACGT <b>GAGGAG</b> CTAAGGCGCAGT AAC	Sense (283 to EE)
Mut_S283EE_R	GTTACTGCGCCTTAG <b>CTCCTC</b> ACGTCTCCTCAGT G	Antisense(283 to EE)
Mut-T494A_F	ACCACCAAGAAACGC <b>GCC</b> TTGCGCAAGAAC	Sense (494 to A)
Mut_T494A_R	GTTCTTGCGCAA <b>GGC</b> GCGTTTCTTGGTGGT	Antisense (494 to A)
Mut-T494EE_F	ACCACCAAGAAACGC <b>GAGGAG</b> TTGCGCAAGAA CGAC	Sense (494 to EE)
Mut_T494EE_R	GTCGTTCTTGCGCAA <b>CTCCTC</b> GCGTTTCTTGGTG GT	Antisense (494 to EE)
NLSmutantF	AAGAACGAC <b>GCCGCCGCCGCT</b> TACACGGTG	Sense, mutant1
NLSmutantR	CAC CGT GTA <b>GGCGGCGGCGGC</b> GTCGTTCTT	Antisense, mutant1
Mut_RK496AA_F	CGCACCTTG <b>GCCGCGA</b> ACGACCGCAAG	Sense, mutant2
Mut_RK496AA_R	CTTGC GGTCGTT <b>CGCGGCCA</b> AGGTGCG	Antisense, mutant2
Mut_KKR_F	AAGGCCACCACC <b>GCCGCCGCC</b> ACCTTGC GCAAG	Sense, mutant3
Mut_KKR_R	CTTGC GCAAGGT <b>GGCGGCGGC</b> GGTGGTGGCCTT	Antisense, mutant3
Mut_RKR_F	ATAGTGGAAGAG <b>GCCGCCGCC</b> GCCCCATGGAG	Sense, mutant4
Mut_RKR_R	CTCCATGGGGGC <b>GGCGGCGGC</b> CTCTTCCACTAT	Antisense, mutant4
RK496_RK500_F	CGCACCTTG <b>GCCGCGA</b> ACGAC <b>GCCGCC</b>	Sense, mutant5
RK496_RK500_R	<b>GGCGGCG</b> GTCGTT <b>CGCGGCCA</b> AGGTGCG	Antisense, mutant5
RK496_RK500_KR	<b>GCC</b> ACCTTG <b>GCCGCGA</b> ACGAC <b>GCCGCC</b>	Sense, mutant8
492_F		
RK496_RK500_KR	<b>GGCGGCG</b> GTCGTT <b>CGCGGCCA</b> AGGT <b>GGC</b>	Antisense, mutant8
492_R		

\* The mutated bases are shown in red

### 3.2.7.4. Primers for gene expression analysis

Primer	Sequence	Description
5-bAct	AGAGATGGCCACGGCTGCTT	Sense, $\beta$ -actin
3-bAct	ATTTGCGGTGGACGATGGAG	Antisense, $\beta$ -actin
MS-3	CTACTGGATGGATCCTGAGAT	Sense, LIMK1
Limk1_3'	CAGTCGGGGACCTCAGGGTGGGCAG	Antisense, LIMK1
LIMK2_13	GTGGAAGAGAGGAAAAGGGCC	Sense, LIMK2
Limk2_3'	CTAGGGAGGTGAGTCCCGGGTCAGG	Antisense, LIMK2

### 3.2.8. Plasmids

#### 3.2.8.1. Original plasmids

Plasmid	Description	Reference
pEGFP-C1	Expression vector, EGFP tag at the N-terminal of the gene, CMV promoter, Kan <sup>r</sup> , Neo <sup>r</sup>	Clontech, Palo Alto, USA
pEYFP-N1	Expression vector, EYFP tag at the C-terminal of the gene, CMV promoter, Kan <sup>r</sup> , Neo <sup>r</sup>	Clontech, Palo Alto, USA
pGEX5X-2	Expression vector, GST tag at the N-terminal of the gene, Tac promoter, Amp <sup>r</sup>	Amersham Biosciences, Freiburg, Germany
pDsRed2-N1	Expression vector, dsRed tag at the C-terminal of the gene, CMV promoter, Kan <sup>r</sup> , Neo <sup>r</sup>	Clontech, Palo Alto, USA

#### 3.2.8.2. Plasmid with insert

Plasmid	Insert	Reference
pEGFP-Actin	Human cytoplasmic $\beta$ -actin gene cloned in pEGFP-C1	Clontech, Palo Alto, USA
pUC-SR $\alpha$ -LIMK2	Wild type human LIMK2 gene	Dr. K. Mizuno, univ. of Tokyo Japan
pEGFP-LIMK2	Full length (amino acids 1-638) LIMK2 in pEGFP-C1	This work
pEGFP- $\Delta$ LIM1-LIMK2	LIM1 domain truncated LIMK2 in pEGFP-C1 (amino acids 69-638)	This work
pEGFP-- $\Delta$ LIM2-LIMK2	LIM2 domain truncated LIMK2 in pEGFP-C1 (deleted amino acids 72-124)	This work
pEGFP-PDZK2	PDZ and kinase domain of LIMK2 in	This work

pEGFP-Kinase2	pEGFP-C1 (amino acids 142-638) Kinase domain of LIMK2 in pEGFP-C1 (amino acids 315-638)	This work
pEYFP-LIM-PDZ	LIMs and PDZ domains of LIMK2 in pEGFP-C1 (amino acids 1-239)	This work
pEGFP-PDZK1	PDZ and kinase domain of LIMK1 in pEGFP-C1 (amino acids 146-647)	This work
pEGFP-Kinase1	Kinase domain of LIMK2 in pEGFP-C1 (amino acids 302-647)	This work

### 3.2.8.3. Plasmid with mutated insert

Plasmid	Insert	Reference
pEGFP-LIMK2-D451A	Amino acid 451 mutated to alanine	This work
pEGFP-LIMK2-T505A	Amino acid 505 mutated to alanine	This work
pEGFP-LIMK2-T505EE	Amino acid 505 mutated to two glutamic acid	This work
pEGFP-LIMK2-S283A	Amino acid 283 mutated to alanine	This work
pEGFP-LIMK2-S283EE	Amino acid 283 mutated to two glutamic acid	This work
pEGFP-LIMK2-S283A- T494A	Amino acids 283 and 494 were mutated to alanine	This work
pEGFP-LIMK2-S283EE- T494EE	Amino acids 283 and 494 were mutated to two glutamic acids	This work
pEGFP-PDZK2-S283A	Amino acid 283 mutated to alanine	This work
pEGFP-PDZK2-S283EE	Amino acid 283 mutated to two glutamic acid	This work
pEGFP-PDZK2-T494A	Amino acid 494 mutated to alanine	This work
pEGFP-PDZK2-T494EE	Amino acid 494 mutated to two glutamic acid	This work
pEGFP-PDZK2-S283A- T494A	Amino acids 283 and 494 were mutated to alanine	This work
pEGFP-PDZK2-S283EE- T494EE	Amino acids 283 and 494 were mutated to two glutamic acids	This work
pEGFP-PDZK2-S283EE-	Amino acids 283 and 494 were mutated to	This work

---

T494A	two glutamic acids and alanine respectively	
pEGFP-PDZK2-S283A-T494EE	Amino acids 494 and 283 were mutated to two glutamic acids and alanine respectively	This work
pEGFP-Kinase2-mutant1	Amino acids 500-503 were mutated to alanines	This work
pEGFP-Kinase2-mutant2	Amino acids 496-497 were mutated to alanines	This work
pEGFP-Kinase2-mutant3	Amino acids 491-493 were mutated to alanines	This work
pEGFP-Kinase2-mutant4	Amino acids 480-482 were mutated to alanines	This work
pEGFP-Kinase2-mutant5	Amino acids 496-497 and 500-503 were mutated to alanines	This work
pEGFP-Kinase2-mutant6	Amino acids 491-493 and 500-503 were mutated to alanines	This work
pEGFP-Kinase2-mutant7	Amino acids 480-482 and 491-493 were mutated to alanines	This work
pEGFP-Kinase2-mutant8	Amino acids 491-493, 496-497 and 500-503 were mutated to alanines	This work
pEGFP-PDZK2-mutant1	Amino acids 500-503 were mutated to alanines	This work
pEGFP-PDZK2-mutant2	Amino acids 496-497 were mutated to alanines	This work
pEGFP-PDZK2-mutant6	Amino acids 491-493 and 500-503 were mutated to alanines	This work
pEGFP-PDZK2-mutant8	Amino acids 491-493, 496-497 and 500-503 were mutated to alanines	This work

---

### 3.3. Work with *E.coli*

#### 3.3.1. Bacterial strains

<i>Escherichia coli</i> DH5 $\alpha$	F <sup>-</sup> $\phi$ 80dlacZ $\Delta$ M15 $\Delta$ (lacZYA-argF)U169 <i>deoR</i> <i>recA1</i> <i>endA1</i> <i>hsdR17</i> (r <sub>k</sub> <sup>-</sup> , m <sub>k</sub> <sup>+</sup> ) <i>phoA</i> <i>supE44</i> $\lambda$ - <i>thi-1</i>
<i>XL10-Gold</i>	Tet <sup>R</sup> $\Delta$ ( <i>mcrA</i> )183 $\Delta$ ( <i>mcrCB</i> - <i>hsdSMR</i> - <i>mrr</i> )173 <i>endA1</i> <i>supE44</i> <i>thi-1</i> <i>recA1</i> <i>gyrA96</i> <i>relA1</i> <i>lac</i> Hte [F' <i>proAB</i> <i>lacI</i> <sup>q</sup> Z $\Delta$ M15 Tn10 (Tet <sup>R</sup> ) Amy Cam <sup>R</sup> ]

#### 3.3.2. Media for bacterial culture

<b>LB-medium</b>	1.0 % tryptone 0.5 % yeast extract 1.0 % NaCl pH 7.2
------------------	---

<b>Terrific Broth</b>	1.2 % tryptone 2.4 % yeast extract 0.4 % glycerol 17mM KH <sub>2</sub> PO <sub>4</sub> 72mM K <sub>2</sub> HPO <sub>4</sub>
-----------------------	---

1.5 % agar was added to the media for production of agar plates.

The following concentrations of the antibiotics were used if required:

Antibiotic	Stock solution	Working concentration
Ampicillin	100mg/ml in water	100 $\mu$ g/ml
Kanamycin	10mg/ml in water	30 $\mu$ g/ml
Chloramphenicol	30mg/ml in ethanol	30 $\mu$ g/ml

**Table 3.1** Antibiotic stock solutions and its working concentration

#### 3.3.3. General

*E. coli* were cultured at 37°C with LB medium or terrific broth. Bacteria transformed with an antibiotic resistance-conferring plasmid were selectively propagated by supplementing the LB medium with respective antibiotic (see Table 3.1). All solutions and supplements used for work with *E. coli* were autoclaved for 20 min at 121°C or filter-sterilized. Bacterial strains were long-term stored at -70°C in LB medium supplemented with glycerol to a final concentration of 15 %.

### **3.3.4. Culturing bacteria**

#### **3.3.4.1. Growth on solid media**

Dry LB agar plates were used as solid media. Single bacterial colony or bacterial suspension was inoculated by spreading with a sterile inoculation loop or a glass spreader, respectively, to achieve single colony growth. The plates were incubated inverted overnight at 37°C.

#### **3.3.4.2. Growth of liquid cultures**

For small liquid culture, 5-10 ml LB or LB/antibiotic medium was inoculated with a single bacterial colony and incubated overnight at 37°C on a shaking platform. Starter culture was incubated for 8-12h and used to inoculate fresh liquid medium. For large liquid culture 100-250 ml LB or LB/antibiotic medium was inoculated with a starter culture to a dilution of 1:50-1:100 and incubated overnight at 37°C with shaking. Bacteria were harvested by centrifugation.

#### **3.3.4.3. Monitoring the bacterial growth**

The growth of the bacteria in liquid culture was measured at a wavelength of 600 nm (OD<sub>600</sub>) in plastic cuvettes against pure medium as a blank in a spectrophotometer. Each 0.1 OD<sub>600</sub> unit corresponds to approx. 10<sup>8</sup> cells/ml for OD<sub>600</sub> < 1.

### **3.3.5. Transformation of plasmid in *E.coli***

#### **3.3.5.1. Preparation of competent cells by CaCl<sub>2</sub> method**

LB medium (100 ml) was inoculated with an overnight culture of *E. coli* DH5α and grown at 37°C with shaking to an OD<sub>600</sub> of 0.4. This culture was transfer to sterile, disposable, ice-cold 50-ml plastic tubes and store on ice for 10 minutes. After incubation, cells were centrifuged at 4,000 rpm for 15 min at 4°C. The pellet was resuspended in 50 ml ice-cold 100 mM MgCl<sub>2</sub>, incubated for 30 min on ice, and centrifuged at 4°C. The cells were resuspended in 2 ml ice-cold 100 mM CaCl<sub>2</sub>, incubated for 24 h at 4°C, supplemented with ice-cold 0.6 ml glycerol and 2.4 ml 100 mM CaCl<sub>2</sub> and stored in 200μl aliquots at -70°C.

#### **3.3.5.2. Heat shock transformation of the plasmid**

Treatment of competent bacterial cells with a brief heat shock enables transformation of DNA. Plasmid DNA or a plasmid ligation reaction (not more than 15ng or in a volume 2.5μL) was mixed with 50μl thawed competent bacteria and incubated for 30 min on ice. The bacteria were treated for 90sec by heat shock of 42°C, placed on ice for 1-2 minutes, diluted with 950 μl LB medium and incubated for 1 h at 37°C with shaking. An aliquot of 50-200 μl or resuspended pellet was spread on LB/antibiotic agar plate and incubated overnight at 37°C to select for transformed bacteria. In case of ligation mixture, the transformed cells were pelleted by centrifugation at 13,000rpm for 30 seconds, and the pellet was resuspended in 100μl of LB medium. The whole suspension was spread on the agar plate.

### **3.4. Recombinant DNA processing and manipulation**

#### **3.4.1. DNA amplification of LIMK1 and LIMK2 cDNA**

The polymerase chain reaction (PCR) constitutes an enzymatic *in vitro* amplification of specific cDNA segments. Amplification occurs in automated, temperature-controlled cycles of denaturation, annealing and elongation in a thermal cycler. Initially, double-stranded template DNA is separated into its complementary single strands by heating (denaturation). At a lower temperature two oligonucleotides primers, flanking the DNA region to be amplified, hybridize to their respective complementary sequences on opposite strands (annealing) and serve as primers for DNA synthesis in a 5'→3' direction (elongation). Primer extension is catalyzed at a slightly increased temperature by a thermostable DNA polymerase that add deoxyribonucleotide triphosphates (dNTPs) to the recessed 3'-hydroxyl end of extending strands, thereby generating new double-stranded DNA across the primer-flanked region. The products of each reaction cycle are then denatured to permit a new amplification cycle. Theoretically, for n cycles a 2<sup>n</sup>-fold amplification of a specific DNA sequence is obtained.

Primers for amplification of LIMK1 and LIMK2 cDNA were commercially synthesized (MWG Biotech, Ebersberg, Germany). They were designed corresponding to the DNA segment to be amplified, provided with restriction sites for endonuclease digestion. Pairs of primers were designed to have equivalent melting temperatures (T<sub>m</sub>), calculated according to the formula<sup>1</sup>  $T_m [^{\circ}\text{C}] = (A+T) \times 2 + (G+C) \times 4$ . The annealing temperature for each PCR was typically estimated by experimentally. For preparative DNA amplification as part of cloning strategies, High fidelity DNA polymerase was used in preference to *Taq* DNA polymerase, due to its 3'→5' proofreading exonuclease activity which minimizes the risk of nucleotide misincorporation during elongation.

PCR reaction composition for DNA amplification was as follows:

Template DNA	20-50ng (Plasmid PUC-SRα-LIMK2 or cDNA of LIMK1)
Sense primer (forward)	100 pmoles
Antisense primer (reverse)	100 pmoles
dNTPs	200μM each
PCR reaction buffer	1x
DMSO	5-10% (Optional, to increase yield, specificity, consistency)
DNA polymerase	1-2.5 units
Final reaction volume	100μl (preparative PCR), 20-50μl (analytical PCR)

The PCR amplified products of LIMK1 and LIMK2 gene were analyzed by agarose gel electrophoresis, they were further proceed for cloning into the EGFP-C1 vector.

---

<sup>1</sup> A, T, G, C: number of the 2'-deoxyribonucleosides adenosine (A), thymidine (T)guanosine (G) and cytidine (C) with in the primer sequence

Thermal cycle parameters for PCR were as follows:

Lid temperature	105°C
Initial denaturation	94°C, 5 minutes
Denaturation	94°C, 30 seconds
Annealing	50-55°C (primer pair and template specific), 1 minute
Elongation	72°C, 1 minute/kb
Cycles	30
Final elongation	72°C, 10 minutes

### **3.4.2. Buffers and solutions**

TBE buffer (5X) (Working solution 0.5X)	Tris-base 54 g boric acid 27.5 g EDTA 20 ml of 0.5 M, pH 8.0      Final volume 1 Liter
TE	10mM Tris (pH 7.6), 1mM EDTA (pH8.0)
DNA loading buffer (6X)	0.25% (w/v) bromophenol blue 0.25% (w/v) xylene cyanol 30% (v/v) glycerol 50 mM EDTA
Ethidium bromide	1% (w/v) in water
DNA standard	SmartLadder™ Eurogentec GmbH, Germany

### **3.4.3. Restriction endonuclease digestion of DNA**

Type II restriction endonucleases were used to digest double-stranded DNA for analytical or preparative purposes. These restriction enzymes bind to short, specific nucleotide sequences and cleave the DNA within this region by hydrolyzing a phosphodiester bond in each strand. The recognition sequences (palindromes) possess twofold rotational symmetry. Staggered cleavage generates complementary, cohesive 5' and 3' ends (sticky ends). Cleavage in the axis of symmetry yields blunt ends.

For preparative purposes, 1-5 µg PCR amplified DNA and EGFP-C1 vector were digested with 1-20 U of restriction enzymes (see section 3.2.7.1) in a volume of 10-50 µl of reaction buffer. Complete digestion was confirmed by agarose gel electrophoresis. For analytical purposes, 0.2-1 µg DNA were digested with 1-5 U of enzyme in a volume of 10-20 µl of reaction buffer. In both cases digests were incubated for 3h at 37°C. Reaction buffers were supplied by the manufacturer. Enzymes were heat-inactivated as recommended by the supplier or removed by purification of the digested DNA by column chromatography.

#### **3.4.4. Purification of the digested DNA**

To inactivate and remove the proteins e.g. restriction enzymes, digested DNA was purified by using the QIAquick PCR purification kit (Qiagen) according to the manufacturer's instructions with slight modification. Buffers were provided in the kit and all centrifugation steps were carried out at 13,000 rpm at RT in a tabletop microcentrifuge. The 5 volume of the buffer PB and one volume of isopropanol were added to the DNA solution. The sample was then applied to QIAquick spin column (Qiagen) and centrifuged for 1 min in order to bind DNA to the column. For washing of DNA on the column, 0.75 ml of buffer PE was added to the column and spun down for 1 min. The flow-through was removed and the column was centrifuged for an additional 1 min to remove the residual ethanol. The column was then placed into a clean 1.5 ml tube and the DNA was eluted by the addition of 30-50  $\mu$ l of buffer EB (10 mM Tris/HCl, pH 8.5) or dH<sub>2</sub>O to the column followed by centrifuging for 1 min. If needed the DNA could be concentrated by precipitating with ethanol.

#### **3.4.5. Ethanol precipitation of DNA**

In the presence of relatively high concentrations of monovalent cations, ethanol induces a structural transition in nucleic acid molecules, which causes them to aggregate and precipitate from solution. Ethanol precipitation was used to concentrate and/or desalt DNA solutions and to remove any residual impurity.

5 M NaCl solution was added to the DNA sample to a final concentration of 250 mM. Three volumes of ethanol (-20°C) were added to the solution and stored on ice for 30 min and then centrifuged at 13,000 rpm for 15 min at 4°C. The pellet was washed with one volume of ice-cold 70 % ethanol, recentrifuged for 5 min and dried at room temperature on desk. The DNA was dissolved in water or TE (pH 8) for 20 min at 37°C at an appropriate concentration.

#### **3.4.6. Dephosphorylation of linearized plasmid DNA by CIP**

In order to prevent self-ligation of vector ends in cloning strategies linearized plasmid DNA was treated with calf intestine alkaline phosphatase (CIP). CIP catalyzes the hydrolysis of 5'-phosphate residues to 5'-hydroxyl ends. Since T4 DNA ligase requires 5'-phosphate residues to catalyze new phosphodiester bonds, ligation is only possible between vector ends and inserts, but not between vector ends themselves. Dephosphorylation was carried out directly following plasmid linearization. CIP was added to the digestion mixture at a concentration of 1 U per pmole linearized vector DNA. After 45 min incubation at 37°C, CIP and the restriction enzymes were removed as described previously.

### **3.4.7. Ligation of DNA fragments**

DNA fragments of bearing either sticky or blunt ends can be ligated *in vitro* with bacteriophage T4 DNA ligase. This enzyme catalyzes the formation of new phosphodiester bonds between a 5'-phosphate residue of one and a 3'-hydroxyl residue of another double-stranded DNA fragment generated by restriction endonucleases.

Ligation was carried out using Rapid DNA ligation kit (Roche) according to the manufacturer's instructions with slight modification. All the buffers were provided with the kit. The insert DNA (LIMK1 or LIMK2 PCR amplified DNA) was employed at a 2-5 molar excess relative to the linearized and dephosphorylated EGFP-C1 vector DNA. The vector DNA and insert mixture were diluted in dilution buffer to a final volume of 10 $\mu$ l. 10 $\mu$ l of ligation buffer was added in diluted DNA mixture. 5unit of T4 DNA ligase was added and mix thoroughly. The ligation reaction mixture was incubated 5-10 minutes at 15-25°C. Ligation reaction mixture (5 $\mu$ l) was used directly for transformation of the 200 $\mu$ l competent cells.

### **3.4.8. Miniprep: small-scale preparation of plasmid DNA**

Plasmid DNA was purified from bacteria cultures by alkaline lysis of the bacterial cells by using QIAprep Spin miniprep kit according to the manufacture instructions. In brief, a small culture (10ml) of bacteria was grown in order to amplify the plasmid of interest *in vivo*. The bacteria were harvested by centrifugation at 13,000 rpm for 1 min at room temperature. This pellet was resuspended in 250 $\mu$ l buffer P1 (50 mM Tris·Cl pH 8.0, 10 mM EDTA, 100  $\mu$ g/ml RNase A). Lysis buffer P2 (250 $\mu$ l; 0.2 N NaOH, 1 % SDS) was added in resuspended pellet followed by gently mixing and incubated for 5 minutes at room temperature. It causes denaturation of the DNA by NaOH and of the bacterial proteins by SDS. The alkaline mixture was neutralized by 350 $\mu$ l of buffer N3 (containing guanidine hydrochloride, 3M potassium acetate, pH 5.5) causing reannealing of plasmid DNA and precipitation of SDS. The white precipitate, containing proteins, chromosomal DNA, SDS and cell debris was removed by centrifugation for 10 minutes at 13,000 rpm while the plasmid DNA was left in solution. The supernatant was passed through the spin column by centrifugation at 13,000 rpm for 1 minute. After washing of the column with 0.75ml buffer PE, the column was additionally centrifuged for 1 minute to remove residual buffer. The DNA was eluted by adding 50 $\mu$ l water or TE and centrifugation of the column at 13,000 rpm for 1 min.

### **3.4.9. Endofree Maxiprep: Large scale preparation of plasmid DNA**

Endotoxins or Lipopolysaccharides (LPS) are cell membrane components of Gram-negative bacteria (e.g., *E.coli*). During lysis of bacterial cells for plasmid preparations, endotoxin molecules are released from the outer membrane into the lysate. There tendency to form micellar

structures lead to co-purification of endotoxins with the plasmid DNA. Endotoxins strongly influence transfection of DNA into primary cells like endothelial cells and increased endotoxins levels leads to sharply reduced transfection efficiencies. To solve this problem, Endofree Plasmid maxi kit was used for large-scale purification.

Bacterial culture (100 ml) was centrifuged at 4,000 rpm for 15 min at 4°C. The pellet was resuspended in 10 ml of P1 (50mM Tris.Cl, pH 8.0; 10mM EDTA; 100µg/ml RNase A). The resuspended pellet was lysed with 10 ml P2 (200mM NaOH, 1% SDS) by incubating for 5 min at room temperature. The lysis was stopped by adding 10 ml ice-cold P3 (3M potassium acetate, pH 5.5) and the white precipitated mixture was poured into the barrel of QIAfilter cartridge and incubated. After 10 minutes, the plunger was inserted into the QIAfilter cartridge and the cell lysate was filtered into a 50ml tube. 2.5ml of buffer ER (endotoxin removal buffer) was added to the filtered lysate and incubated on ice for 30 minutes. The ER buffer treated lysate was loaded on an equilibrated anion exchange column that was subsequently washed twice with 30 ml of buffer QC (1.0M NaCl, 50mM MOPS, pH7.0; 15% isopropanol). The bound DNA was eluted with elution buffer QN (1.6M NaCl, 50mM MOPS, pH7.0; 15% isopropanol) by gravity flow. The eluted DNA was precipitated by adding 0.7 volumes isopropanol at room temperature and subsequent centrifugation at  $\geq 15,000 \times g$  for 30 min at 4°C. The pellet was washed with 5 ml 70 % ethanol, re-centrifuged for 10 min, dried under vacuum and re-dissolved in 1ml of endothelial electroporation buffer or TE.

#### **3.4.10. Quantification of DNA and RNA solutions**

The concentration of nucleic acid solutions was determined by spectrophotometry. The ultraviolet (UV) absorption was measured at a wavelength of 260 nm ( $OD_{260}$ ) using a quartz cuvette of 1 cm width. For double-stranded DNA an  $OD_{260} = 1.0$  corresponds to approximately 50 µg DNA/ml. For RNA an  $OD_{260} = 1.0$  corresponds to approximately 40 µg RNA/ml. In addition the  $OD_{260}$  was measured to estimate the purity of the nucleic acid sample. A ratio  $OD_{260}/OD_{280}$  of significantly less than 1.8-2.0 indicates protein contamination.

#### **3.4.11. Agarose gel electrophoresis**

Agarose gel electrophoresis was used for analytical and preparative purposes. The method is based on the migration of negatively charged DNA towards the anode in an electric field. The fragments migrate through the gel matrix at rates inversely proportional to the logarithm ( $\log_{10}$ ) of the number of base pairs. DNA bands were visualized within an agarose gel by staining with the intercalating fluorescent dye ethidium bromide and subsequent illumination under UV light. The length of a DNA fragment is determined by comparison of its mobility to that of DNA standards. For casting gel, 1-2 % (w/v) agarose was melted in 0.5xTBE electrophoresis buffer and supplemented with 0.5 µg/ml ethidium bromide and casted in a tray of desired size. The gel was

placed in an electrophoresis tank and submerged in 0.5xTBE buffer. The DNA samples were mixed with DNA loading buffer and loaded into the gel wells. In addition 5 µl of a DNA standard was loaded in parallel with the samples. Horizontal electrophoresis was carried out at approximately 100 V. The stained gel was photographed under UV light.

#### **3.4.12. DNA recovery from agarose gel**

For preparative purposes DNA fragments of interest were cut out from stained agarose gels with a razor blade under UV illumination. The gel slices were solubilized and DNA was purified by using the QIAquick Gel extraction kit (Qiagen) according to the manufacturer's instructions.

Agarose gel slices were weighed (= 1 volume) and dissolved each slice in 3 volumes of solubilization buffer QG by incubation for 10 min at 50°C. 1 volume isopropanol was added and the solution was applied to a silica-gel QIAquick spin column. The column was centrifuged at 13,000 rpm for 1 min, washed with washing buffer PE and centrifuged again. The extra centrifugation was done to remove residual buffer. DNA was eluted by adding 30-50µl water or TE on the column and centrifugation of the column at 13,000 rpm for 1 min. All the buffers were provided by the manufacturer.

#### **3.4.13. DNA sequencing**

The sequence of specific target regions in recombinant plasmid DNA was determined by a commercial sequencing service (Agowa GmbH Berlin, Germany). The sequence data were verified on the basis of the corresponding fluorescence electropherogram and subjected to computer analysis.

### **3.5. Mutagenesis of the LIMK2 gene**

#### **3.5.1. PCR based site-directed mutagenesis**

The QuikChange™ Site-Directed Mutagenesis method (QCS) developed by Stratagene (La Jolla, CA, USA) is a widely used PCR-based site directed mutagenesis system that eliminates the necessity to subclone the amplified mutated DNA fragment. This procedure starts with a supercoiled, dsDNA vector with an insert of interest and two synthetic oligonucleotide primers containing the desired mutation (see section 3.2.7.3). The oligonucleotide primers, each complementary to opposite strands of the vector, are extended during temperature cycling by *PfuUltra*® high-fidelity DNA polymerase. After incorporation of the oligonucleotide primers, a mutated plasmid containing staggered nicks is generated. After temperature cycling, the product is treated with *Dpn1*. *Dpn1* is used to digest the parental DNA template and select for the synthesized DNA containing mutations. Since DNA isolated from most *E. coli* strains is dam

methylated, it is susceptible to *Dpn*I digestion, that will cut only fully or hemimethylated 5'-G<sub>m</sub>6ATG-3' DNA sequences<sup>2</sup>. The nicked vector DNA incorporating the desired mutations is then transformed into the commercial XL10-Gold cells<sup>3</sup>. This method is very rapid and generates mutants with the efficiency greater than 80%.

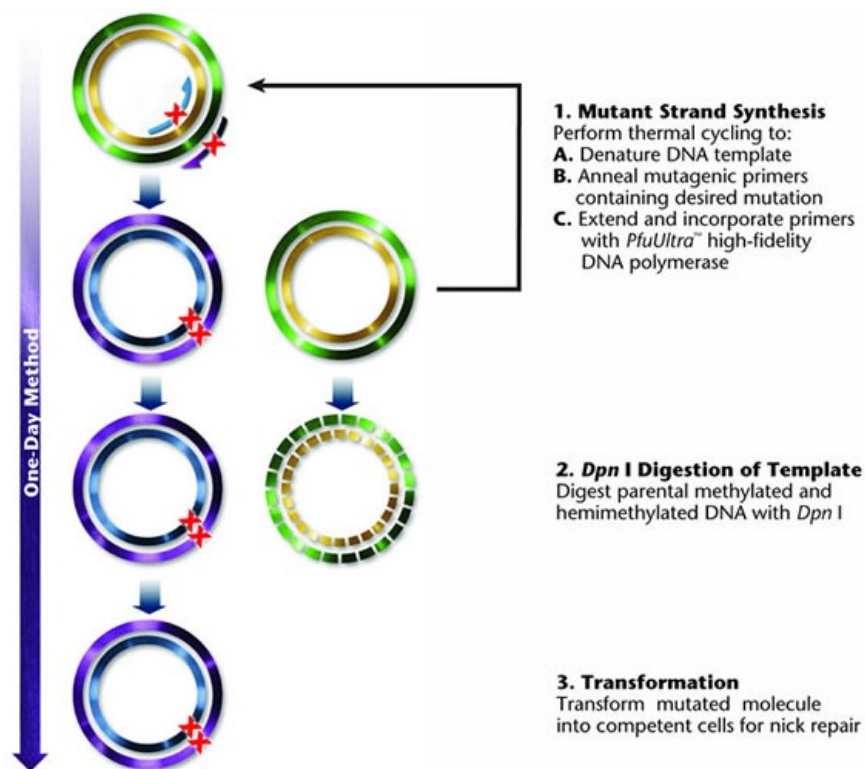


**Figure 3.1 The QuickChange® One-Day Site-Directed Mutagenesis Method:** 1. Mutant strand synthesis. 2. *Dpn*I Digestion of parental DNA template. 3. Transformation of the resulting annealed double-stranded nicked DNA molecules. After transformation, the XL-1 Blue *E. coli* cell repairs nicks in the plasmid.

The mutant strands synthesis reaction was setup for PCR according to the manufacturer's instructions. The PCR reaction composition and PCR cycling parameter were as follows.

Template DNA	30ng (EGFP-LIMK2 plasmid)
Sense primer <sup>4</sup> (forward)	125ng
Antisense primer (reverse)	125ng
dNTPs	200μM each or 1μl (supplied with the kit)
PCR reaction buffer	1x
Quick solution reagent	3μl (supplied with the kit)

Water was added to a final volume of 50μl

<sup>2</sup> While plasmid DNA isolated from almost all the commonly used *E. coli* strains such as DH5α (*dam*<sup>+</sup>) is methylated and is suitable for mutagenesis, plasmid DNA isolated from the exceptional *dam*<sup>-</sup> *E. coli* strains, including JM110 and SCS11, is not suitable.

<sup>3</sup>The DH5α chemical competent cells prepared in our lab also worked well with this protocol.

<sup>4</sup> The primers were design according to the mutagenic primer design rules, which were given in instruction manual.

Then 1µl of PfuUltra HF DNA polymerase was added and PCR was done with the following thermal cycling parameters.

Lid temperature	105°C
Initial denaturation	94°C, 2 minutes
Denaturation	94°C, 50 seconds
Annealing	60°C, 1 minute
Elongation	68°C, 1 minute/kb
Cycles	18
Final elongation	68°C, 10 minutes

After the PCR the reaction mixture was cooled to  $\leq 37^\circ\text{C}$  on ice. 1µl of *Dpn1* was added directly to reaction mixture and kept for 2 hours for digestion at 37°C. 2.5µl of the digested reaction mixture was transformed into competent cells and the mutant clone was selected and confirmed by DNA sequencing.

### 3.5.2. Deletion mutagenesis

This is the modified method of the QuikChange™ Site-Directed Mutagenesis kit with additional steps to generate deletion or insertion mutation. The reaction composition for PCR and the thermal cycling condition is the same as described before except primer amount and designing rules. The specific primer design consideration was applied as follows.

1. Both the primers must anneal to different strands of the plasmid.
2. Primers should be >22 bases in length
3. The mismatched portions should be at or near the 5' end of one or both of the primers with 15 or more bases of correct sequence on the 3' end.
4. For deletion, the primers should be designed in frame of the coding sequence of the gene. The forward primer and reverse primer should be designed at 3' and 5' end of the deletion sequence, respectively.

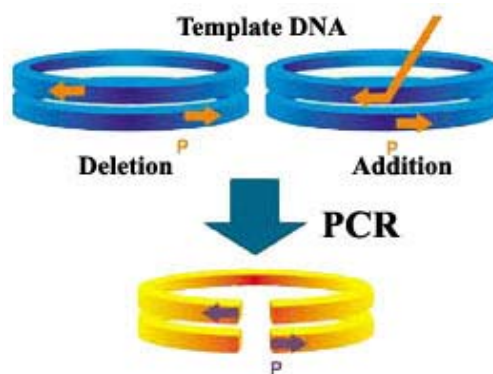


**Figure 3.2 Primer design considerations.** Mutagenesis primer oligonucleotides can be designed individually according to the desired mutation. Based on primer design, the ExSite mutagenesis method can allow for the mutagenesis of dsDNA templates resulting in large or small deletions and/or 5'-end oligonucleotide-directed base insertions.

5. One or both of the primers must be 5' phosphorylated. T4 polynucleotide kinase used for the 5' phosphorylation of an oligonucleotide primers.

The reaction composition of the phosphorylation reaction is as follows

Primer	1 $\mu$ l (100pmole)
Kinase buffer	0.5 $\mu$ l (1x)
T4 polynucleotide kinase	1 $\mu$ l (10 units)
Water	2.5 $\mu$ l

The reaction mixture was incubated for 1 hour. The 1.25 $\mu$ l of the reaction mixture was directly used for PCR.

The PCR product was digested with *Dpn1* and purified by PCR purification kit as described before. Purified PCR product (5 $\mu$ l) was ligated using rapid DNA ligation kit and transformed into DH5 $\alpha$  cells. The positive clone was confirmed by DNA sequencing.

### **3.6. Gene expression analysis at the RNA level using RT-PCR**

Gene expression analysis at the RNA level, i.e. determination of target-specific mRNA transcripts in the cell, includes isolation of total RNA, reverse transcription of mRNA to cDNA and amplification of the target cDNA by PCR.

#### **3.6.1. RNA isolation from HUVEC<sup>5</sup>**

The total cellular RNA was purified by RNeasy mini kit. In the RNeasy procedure, biological samples are first lysed and homogenized in the presence of a highly denaturing guanidine isothiocyanate (GITC)-containing buffer, which immediately inactivates RNases to ensure isolation of intact RNA. A specialized high-salt buffer system allows up to 100  $\mu$ g of RNA longer than 200 bases to bind to the RNeasy silica-gel membrane. Ethanol is added to provide appropriate binding conditions, and the sample is then applied to an RNeasy mini column where the total RNA binds to the membrane and contaminants are efficiently washed away. High-quality RNA is then eluted in water.

Cells ( $5 \times 10^6$ ) were harvested and washed with PBS and resuspended in 600 $\mu$ l of buffer RLT containing  $\beta$ -mercaptoethanol (supplied with the kit). The cell lysate was homogenized by using QIAshredder spin column. The cell lysate was loaded on QIAshredder and centrifuged at maximum speed for 2 minutes. One volume of 70% ethanol was added in homogenized sample and loaded on the RNeasy spin column and centrifuged at high speed for 15seconds. The flow-through was discarded and the column was washed with 350 $\mu$ l RW1 buffer. Then 80 $\mu$ l of DNase

---

<sup>5</sup> All the RNA work was done in RNase free conditions. All the precautions were taken during the work with RNA.

(10 $\mu$ l DNase I stock solution (30 units) + 70 $\mu$ l RDD buffer) was added onto the column and kept for 15 minutes at room temperature. After DNA digestion the column was again washed with 350 $\mu$ l RW1 buffer and then the column was finally washed two times with 700 $\mu$ l of RPE buffer and centrifuged for one minute at high speed to remove residual buffer. Finally, total RNA was eluted in 50 $\mu$ l RNase free water.

### **3.6.2. Gel electrophoresis of RNA**

#### **3.6.2.1. Buffers and solutions**

10x MOPS electrophoresis buffer	200 mM 3-[N-morpholino]propanesulfonic acid (MOPS) (free acid) 50 mM sodium acetate 10 mM EDTA DEPC-treated water, pH to 7.0 with NaOH
1x MOPS Gel Running Buffer	100 ml MOPS electrophoresis buffer 20 ml 37% (12.3 M) formaldehyde 880 ml DEPC-treated water <sup>6</sup>
5x RNA Loading Buffer	16 $\mu$ l saturated bromophenol blue solution 80 $\mu$ l 500 mM EDTA, pH 8.0 720 $\mu$ l 37% (12.3 M) formaldehyde* 2 ml 100% glycerol 3084 $\mu$ l formamide 4 ml 10 x MOPS electrophoresis buffer DEPC-treated water to 10 ml  Stability: Approximately 3 months at 4°C

The integrity and the size distribution of total RNA were checked by denaturing-agarose gel electrophoresis and ethidium bromide staining. 1.2 g agarose was dissolved in 72 ml H<sub>2</sub>O by boiling in microwave. The solution was cooled to about 60 °C, and 10 ml 10x MOPS electrophoresis buffer, ethidium bromide, and 18 ml of formaldehyde were added. The gel was cast in chemical hood, and was equilibrated in 1x MOPS electrophoresis buffer for at least 30 min. RNA sample (2-5  $\mu$ g total RNA) was prepared in RNA loading buffer (1x in final volume) by incubating at 65 °C for 5 min. The samples were then loaded onto the gel. The gel was run at 5-7 V/cm (running buffer 1x MOPS electrophoresis buffer) until the bromophenol dye has migrated two-thirds the length of the gel. The RNA was visualized by placing the gel on UV transilluminator.

---

<sup>6</sup> The water was supplemented with DEPC to final 0.1% (v/v), incubated overnight at room temperature and autoclaved. The utilized glassware was baked overnight at 140°C prior to use.

### **3.6.3. Synthesis of cDNA from total RNA and analysis of LIMK gene expression**

Total RNA (~3µg) and Oligo(dT)<sub>20</sub> primers (1µL, 50 pmole) were mixed with RNase-free water to a final volume of 12 µl and incubated for 10 min at 70°C. Master reaction mix (8 µl, composition as shown below) was added to the denatured RNA tube and the RT-PCR was performed for 60 min at 50°C. The enzyme was heat-inactivated for 15 min at 85°C and the first strand cDNA samples were stored at -20°C.

Master reaction mix composition for one RNA tube

5x cDNA synthesis buffer	4µl
0.1M DTT	1µl
RNaseOUT™ (40U/µl)	1µl
DEPC-treated water	1µl
Thermoscript™ RT (15U/µl)	1µl

In the negative control, 1µl of DEPC treated water was added to the master mix instead of reverse transcriptase enzyme

Subsequently, for gene expression analysis of LIMK1 and LIMK2, 10% of a cDNA-containing first strand reaction mix (with negative control) was subjected to analytical PCR in order to amplify cDNA fragments derived from expressed target gene-specific mRNA transcripts, i.e. LIMKs-related cDNA and as a control  $\beta$ -actin cDNA. Primers used for amplification of LIMK1 and LIMK2 cDNA and  $\beta$ -actin cDNA were shown in section (see section 3.2.7.4).  $\beta$ -actin primers allowed amplified  $\beta$ -actin fragments derived from genomic DNA contamination or spliced mRNA transcripts to be distinguished.

## **3.7. Protein analysis**

### **3.7.1. Buffers and solutions**

SDS sample buffer (2x)	100 mM Tris·Cl (pH 6.8) 20 % (v/v) glycerol 4 % (w/v) SDS 0.01 % (w/v) bromophenol blue 10% $\beta$ -mercaptoethanol
acrylamide/bis-acrylamide	40% (w/v) acrylamide/bis-acrylamide (ratio 37.5:1)
Stacking gel buffer	0.5 M Tris-HCl, pH 6.8
Resolving gel buffer	1.5 M Tris-HCl, pH 8.8
APS	10% (w/v) APS in water, (aliquots were stored at -20°C)
SDS	10% (w/v) SDS in water
Electrophoresis Buffer (10x)	30g Tris-base 142g glycine

	10g SDS Water was up to 1 liter
Transfer buffer	5.82g (48mM) Tris-base 2.93g (39mM) glycine 200ml methanol Water was added up to 1 liter
TBST buffer	10mM Tris-base (pH 7.6) 150mM NaCl 0.05% (v/v) Tween 20
Blocking solution	5% blocking milk (BioRad) in TBST
Cell lysis buffer (2x)	2 % NP-40 300mM NaCl 20 mM Tris (pH 7.5) 2 mM EGTA 5 mM Na <sub>3</sub> VO <sub>4</sub> Complete mini protease inhibitor tablet (Roche) 1/5ml Phosphatase cocktail (1:100) 0.1% SDS
Coomassie staining solution	0.25% Coomassie Brilliant Blue R-250 10%Acetic acid 40% methanol in water (filtered)
Coomassie destaining solution	10%Acetic acid 40% methanol in water

### **3.7.2. Measurement of protein concentration**

#### **3.7.2.1. Enhanced alkaline copper (Lowry) protein assay**

The method is based on Peterson's modification of the micro-Lowry method (Peterson, 1977). An alkaline cupric tartrate reagent (Lowry reagent) complexes with the peptide bonds of proteins and becomes reduced to cuprous ( $\text{Cu}^+$ ). The  $\text{Cu}^+$  as well as the R groups of tyrosine, tryptophan, and cysteine residues then react with the Folin reagent. The reagent reacts by first producing an unstable product which is slowly reduce to become molybdenum/tungsten blue color complex. The absorbance is read at a suitable wavelength between 500 nm and 800 nm (preferably 750nm) for spectroscopic quantification of proteins in aqueous solution.

Lowry protein assay kit (Sigma) was used for protein quantification according to the manufacturer instructions. Using BSA stock solution (400  $\mu\text{g}/\text{ml}$ ), a set of protein standards with 0-300  $\mu\text{g}/\text{ml}$  was prepared. The protein samples (containing with or without 1% SDS) were dilute to 1.0 ml with water. To each set of protein standards and samples, 1 ml of Lowry reagent was added and incubated for 20 minutes at room temperature. With rapid and immediate mixing, 0.5 ml of Folin & Ciocalteu's phenol reagent was added in each tube and the color was allowed to develop for 30 minutes. The absorbance was measured at the wavelength of 750 nm in a

spectrophotometer. Based on the absorption values of the protein standards a calibration curve was calculated and used for determination of the protein concentrations in the samples. All protein standards and samples were prepared in duplicate.

### 3.7.2.2. dotMETRIC™ 1 $\mu$ l Protein assay

This is in effect a chromatographic capture method where the flat surface of the test strip acts as the solid matrix or support. Protein solution is applied on a specific protein binding test strip by point of contact capillary action. Under a specific buffer condition as the protein enters into the matrix of the test strip it binds instantly and saturates as protein solution diffuses into the test strip in a circular manner. A circular protein imprint is produced which is developed into visible protein spots with a protein specific dye. The diameter of the protein spot is proportional to protein concentration. By measuring the diameter of the protein spots with a pre-developed measuring gauge the amount of protein in the spot can be estimated (Figure 3.3). This method requires only 1 $\mu$ l of the sample and is resistant to most common laboratory reagents such as Triton-X100, Triton-X114, Tween-20, NP-40 and SDS, reducing agents such as beta-mercaptoethanol and DTT, sugars, cobalt, EDTA, Tris buffers, and others. This assay is independent of protein-to-protein variation and can be performed even if the protein sample is in a SDS-PAGE gel-loading buffer.

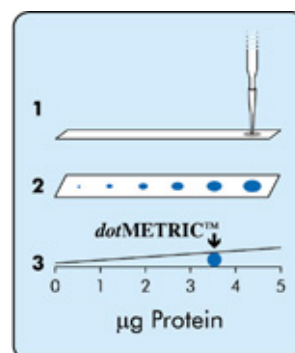


**Figure 3.3** **A)** Method of spotting of the protein sample on the test strip. **B)** Steps involved in protein estimation. 1- 5 $\mu$ l protein solution is applied to the test strip (1), it produces compact and symmetrical spots on the strip; the diameter of protein spots is proportional to their protein concentration (2). Thus, by measuring the diameter of protein spots with the dotMETRIC™ scale, supplied with each kit, protein amount can be estimated.

The protein was estimated by dotMETRIC™ 1 $\mu$ l Protein assay kit according to the manufacturer's instructions. 2  $\mu$ l of protein sample was diluted in 10  $\mu$ l of dilution buffer (provided in the kit). 2  $\mu$ l and 4  $\mu$ l of diluted samples were spotted on the test strip by using the common pipette man with ultra fine tip. The loaded protein sample was fixed on test strip by incubating the strip in diluted fixer (0.8 ml of Fixer-A stock + 7 ml water) for 2 minutes at room temperature. The fixed strip was transferred into diluted developer (0.8 ml of developer-B stock + 7 ml water) and shake gently for 30 seconds and incubated for 2-4 minutes or longer at room temperature to develop the spot. The spots were read by using dotMETRIC™ scale to match the diameter of each spot to its corresponding protein concentration. 2-3 spot were produced from each sample and the mean average was calculated.

### **3.7.3. Whole cell lysates**

Endothelial cells were washed with ice cold PBS. Approximately  $1.5 \times 10^6$  cells (25mm<sup>2</sup> flask) were lysed in 500µl of cell lysis buffer (1x, see section 3.7.1) for 45 minutes on ice. To remove the insoluble part, the lysate was collected in eppendorf tube and centrifuged at 16000xg 4°C for 15 minutes. The clear lysate was immediately processed for immunoprecipitation or kinase assay.

### **3.7.4. Immunoprecipitation**

The underlying strategy behind the immunoprecipitation is to use the high affinity of antibodies for their antigens as a method to locate and bind target molecules in the proteins mixture. Once the antibody-antigen complexes are formed in solution, they are collected and purified by using small agarose or polyacrylamide beads with covalently attached protein A or protein G. Both protein A and protein G specifically interacts with conserved regions of the antibodies, thus forming an immobilized complex of antibody-antigen bound to beads. Irrelevant molecules in the starting protein mixture are removed by washing the beads.

For immunoprecipitation, the clear whole cell lysate of endothelial cells was prepared as described above. To remove the nonspecific sepharose bind proteins, 50% protein A sepharose slurry was added to clear lysate in the ratio 1:20 respectively and incubated at 4°C for one hours end over end mixing. A-sepharose was prepared by incubating the beads in swelling buffer (20mM NaH<sub>2</sub>PO<sub>4</sub>, 0.15M NaCl, and 0.1% NaN<sub>3</sub>) containing 2% BSA to block unspecific binding. The beads were removed by centrifugation at 13,000rpm for 20 seconds and the pre-cleared supernatant was further processed. The specific antibody was added in supernatant in appropriate amount (see section 3.2.3) and was incubated overnight at 4°C with end over end mixing. 50% slurry of protein a sepharose was added (1:10), and incubated for 2 hrs at 4°C with end over end mixing. The antigen-antibody bound beads were purified by centrifugation at 13,000 rpm for 30 seconds and the beads were washed 2 times with 1 ml ice-cold cell lysis buffer (without protease and phosphatase inhibitor) followed by two washing with 1 ml ice cold PBS. The pellets containing antigen-antibody bound beads were solubilized in 1x SDS-sample buffer and heated at 95°C for 5 minutes and stored at -20°C.

### **3.7.5. SDS-PAGE**

Protein samples were resolved for analytical purposes by polyacrylamide gel electrophoresis (PAGE). The use of the anionic detergent sodium dodecyl sulfate (SDS) enables separation according to the molecular mass of the proteins. It binds to the polypeptides and confers a negative charge, which is in direct proportion to their mass. The gel matrix is prepared by polymerization of acrylamide and *N,N'*-methylenebisacrylamide via free radicals. Initial radicals arise from chemical decay of ammonium persulphate (APS) catalyzed by *N,N,N',N'*-

tetramethylethylenediamine (TEMED). The electrophoresis towards the anode is carried out in a discontinuous buffer system that first concentrates SDS-protein complexes within a stacking gel before they migrate into the resolving gel. The size of proteins is determined by comparing their mobility with that of a protein standard.

The resolving gel solution was prepared, poured between two clean glass plates and overlaid with water or butanol. After polymerization, the top of the gel was washed with water and the residual water was removed by filter paper. Freshly prepared stacking gel solution was filled and allowed to polymerize. The plastic comb was inserted in poured stacking gel to prepare the wells for sample loading. After polymerization the comb was removed and the wells were washed with water to remove unpolymerized acrylamide. Subsequently the gel was placed in a vertical electrophoresis apparatus filled with 1x electrophoresis buffer. SDS-PAGE protein samples were prepared by mixing protein samples with 2x SDS sample buffer in the ratio of 1:1, if not already prepared with 1x SDS sample buffer. The SDS-PAGE protein samples and a protein standard were denatured at 95°C for 5 min and loaded onto the gel. Electrophoresis was carried out at 200 V. The resolving gel was subsequently subjected to western blot analysis or gel staining.

Components	Stacking gel 5% (5ml final vol.)	Resolving gel 10% (10ml final Vol.)	Resolving gel 12% (10ml final vol.)
Water	3.2ml	4ml	3.3ml
Acrylamide mix	0.83 ml	3.3ml	4ml
1.5M Tris (pH8.8)		2.5ml	2.5ml
1.0M Tris (pH6.8)	0.63 ml		
10% SDS	0.05 ml	0.1ml	0.1 ml
10% ammonium persulphate	0.05 ml	0.1ml	0.1 ml
TEMED	0.005 ml	0.004ml	0.004 ml

**Table 3.2** Composition of stacking and resolving gel.

### **3.7.6. Detection of protein on gel**

#### **3.7.6.1. Silver staining of the polyacrylamide gels**

Silver staining of polyacrylamide gels allows the detection of proteins separated by SDS-PAGE to a limit of 2-5ng protein/band. The staining relies on differential reduction of silver ions bind various chemical groups such as sulfhydryl, carboxyl moieties in proteins.

The various steps involved are as follows:

Fixation	2 x 30 min	CH <sub>3</sub> OH/H <sub>2</sub> O/glacial acetic acid (4:3:1)
	2 x 10 min	H <sub>2</sub> O wash
Extra fixation	1 x 15 min	2.4 g sodium tetraborate (Na <sub>2</sub> B <sub>4</sub> O <sub>7</sub> ) decahydrate ad 148 ml H <sub>2</sub> O

		2 ml 25 % glutaraldehyde
	3 x 30 min	H <sub>2</sub> O wash
Incubation	1 x 15 min	merge in order as indicated:
		24 ml H <sub>2</sub> O
		2.3 ml 1 M NaOH
		2.5 ml 25 % NH <sub>3</sub> solution
		5 ml 20 % (w/v) AgNO <sub>3</sub>
		ad 125 ml H <sub>2</sub> O
	2 x 5 min	H <sub>2</sub> O wash
Development		until desired staining level with:
		13 ml ethanol
		750 µl 1 % (w/v) citric acid
		90 µl 37 % formaldehyde
		ad 150 ml H <sub>2</sub> O
Reduction termination		
	1 x 10 min	3.7 g Tris·Cl
		2.5 g Na <sub>2</sub> S <sub>2</sub> O <sub>3</sub>
		ad 100 ml H <sub>2</sub> O
Background destaining		exposure until desired background attenuation
		with Farmer's Reducer:
		2.5 ml 20 % (w/v) Na <sub>2</sub> S <sub>2</sub> O <sub>3</sub>
		2.5 ml 1 % (w/v) K <sub>3</sub> [Fe(CN) <sub>6</sub> ]
		ad 220 ml H <sub>2</sub> O
	3 x 10 min	H <sub>2</sub> O wash

For storage purpose the stained polyacrylamide gel was incubated in 20 % glycerin for 2 h. The gel was then placed between a wet Whatman 3MM paper and cellophane sheet on the top and dried under vacuum for 2 h at 85°C.

### 3.7.6.2. Coomassie staining of the polyacrylamide gels

Coomassie Brilliant Blue is an aminotriarylmethane dye that forms strong covalent complexes with proteins, most probably by a combination of van der Waals forces and electrostatic interactions with NH<sub>3</sub><sup>+</sup> groups. The uptake of dye is approximately proportional to the amount of protein.

The polyacrylamide gel was immersed in at least 5 volumes of the coomassie staining solution and placed on a slowly rotating platform for 15-30 minutes at room temperature. The gel was destained in coomassie destaining solution on a slowly rotating platforms, changing the destaining solution three to four times. The rapid destaining can also achieved by keeping the staining gel in hot water (80°C). The reaming background was removed by leaving the gel overnight in water.

### 3.7.7. Western blot analysis

Western blotting consists of the transfer of electrophoretically separated proteins from a SDS-PAGE gel to a nitrocellulose membrane by electroblotting. The membrane-immobilized target

protein is identified by an appropriate primary antibody and a horseradish peroxidase (HRP)-conjugated secondary antibody directed against the primary antibody. Detection of the antigen-antibody-antibody complex occurs by HRP-mediated oxidation of the chemiluminescent substrate luminol, a cyclic diacylhydrazide. The reaction product exhibits an excited state which decays to ground state via a light emitting pathway, and is detectable by exposure of the membrane to an autoradiography film.

After SDS-PAGE, the gel, nitrocellulose membrane pads and electrode papers were equilibrated with pre chilled transfer buffer. The gel cassette was placed with the gray side down on a clean surface. The fiber pad, electroblotting papers (7papers on each side), gel and nitrocellulose membrane were arranged in the cassette as shown in Figure 3.4.

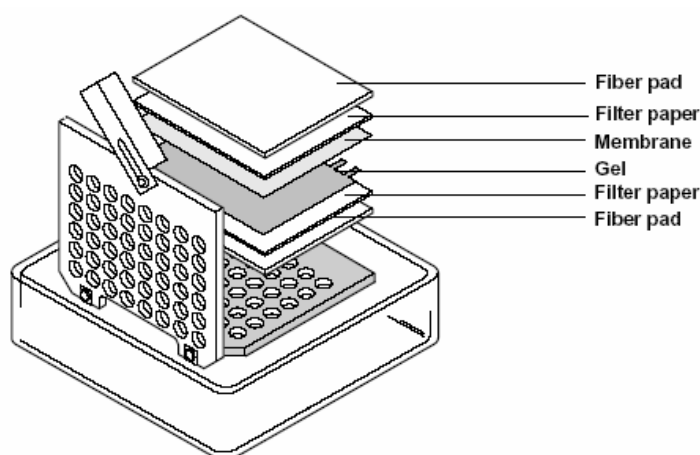


**Figure 3.4** Arrangement of the gel and the membrane in the cassette.

The firmly closed cassette was put into the blotting module and then placed into the electroblotting buffer tank with ice cooling unit. The proteins were transferred to the membrane towards the anode at 200 mA for 1 h at 4°C in ice-cooled transfer buffer with continuous stirring. Non-specific binding sites on the blotted membrane were blocked by shaking in blocking solution for 2 h at room temperature. After blocking, the membrane was washed thrice with TBST for 5 minutes each wash. The washed membrane was sealed in polybag along with the primary antibody and incubated at 4°C for over night with an end-to-end shaking. The membrane was washed thrice for minutes each washing and incubated with the secondary antibody in blocking solution for 45 minutes. The membrane was washed thrice for 5 minutes each washing. The freshly prepared chemiluminescent substrate working solution was added to the surface of the membrane (approx. 0.2 ml/cm<sup>2</sup>) and incubated for 4 min at room temperature. The membrane was wrapped in plastic foil and exposed in the darkroom for 10 s to 30 min to an autoradiographic film that was subsequently developed in dark room conditions.

### **3.7.8. Densitometric analysis of immunoblots**

Densitometric analysis of the proteins was done using the public domain of National Institutes of Health (NIH) ImageJ (1.32j) software. Using as reference image of the Kodak step tablet, the calibration to an optical density scale of scanner was performed. The densitometric values of phosphorylated proteins were divided by the corresponding values of unphosphorylated proteins respectively. Absorption of proteins in unstimulated control samples was set to 100%. Data are presented as mean±SEM of three independent experiments.

## **3.8. Endothelial cells**

### **3.8.1. Buffers and solutions**

Endothelial growth medium	Endothelial cell basal medium with supplement mix
Supplement Mix	ECGS/H 0.4 %, ECGS/H 0.4 %, FCS 2 %, Epidermal Growth Factor 0.1 ng/ml, Hydrocortison 1 µg/ml, basic Fibroblast Factor 1 ng/ml Amphotericin B 50 ng/ml, Gentamicin 50 µg/ml
Electroporation buffer	20mM, Hepes 137mM NaCl 5mM KCl 0.7mM Na <sub>2</sub> HPO <sub>4</sub> 6mM D-Glucose final pH 7.0
Freezing medium	10% DMSO in heat inactivated FCS
Trypan blue	0.4% trypan blue solution
PBS	Dulbecco's phosphate buffered saline, w/o calcium and magnesium; PAA Laboratories (Linz, Austria)
Collagen solution	Collagen G, 75µg/ml in PBS
PHEM buffer	60mM Pipes pH 6.1 25mM Hepes 10mM EGTA 3mM MgCl <sub>2</sub>
Trypsin/EDTA	0.5 g porcine trypsin 0.2g EDTA 1 liter of Hanks' Balanced Salt Solution with phenol red

### **3.8.2. General**

Cell culture work was performed in sterile conditions under a laminar flow hood using sterile disposable plastic ware. Unless purchased sterile, all media, solutions and supplements used in cell culture work were sterilized with a vacuum-driven 0.2-µm filter membrane filtration system or a 0.2-µm syringe filter. They were stored at 4°C and prewarmed to 37°C prior to use.

### **3.8.3. Isolation of human umbilical vein endothelial cells (HUVECs)**

Human ECs were isolated from the veins of umbilical cords according to (Jaffe et al., 1973). From each end of the freshly obtained umbilical cord (obtained from Frauenklinik, Roten Kreuz, Munich) 1 cm was cut off, and the cord was hung up vertically. The upper end of the umbilical vein was cannulated and then sealed with artery clips. The vein was perfused with sterile PBS to wash out blood and sealed at the remaining end.  $\alpha$ -chymotrypsin (approx. 5 ml 0.1 % w/v in PBS) was infused to slight flatulence in order to detach the HUVECs from the interior vein wall. After 20 min of incubation at 37°C and a short cord massage the solution was flushed from the vein by perfusion with 10 ml PBS into 2ml FCS or in endothelial complete growth medium that neutralizes  $\alpha$ -chymotrypsin activity.

HUVECs were harvested by centrifugation at 1000 rpm for 5 minutes at room temperature, and resuspended in 15 ml of endothelial growth medium, and cultured at 37°C in collagen-coated 75-cm<sub>2</sub> flasks as described below. After 3 h, the blood residuents were removed from adherent cells by washing with PBS and the fresh medium was added to the flask. The medium was changed after 24 h and cells were grown to confluence (passage 0) and then subcultured.

### **3.8.4. Culturing**

HUVECs were placed in polystyrene culture flasks provided with 0.2- $\mu$ m hydrophobic vent caps and maintained in a humidified 5 % CO<sub>2</sub> atmosphere in an incubator at 37°C. Endothelial growth basal media were supplemented to complete media with growth factors, FCS and antibiotics (see section 3.8.1) to avoid bacterial contamination. The medium was changed twice a week. Adherent cells were grown to confluence and then detached by trypsinization by using trypsin/EDTA-treatment (3ml per 75-cm<sup>2</sup> culture flask) for 1-2 minutes. After incubation, the cell suspension was diluted with 1 volume of complete medium to inactivate the trypsin. Subsequently, the cells were harvested by centrifugation at 1,000 rpm for 5 min at room temperature. The supernatant was removed, and cells were resuspended in fresh medium and reseeded in culture flasks at a density of approx.  $6 \times 10^4$  cells/ml. Endothelial cells of passage 1-4 were used for experiments.

### **3.8.5. Collagenization**

For adhesive growth, all cell culture flasks, and petri-dishes, subjected to HUVEC monolayer seeding, were collagen-coated by incubation with a sterile collagen G solution of final (75  $\mu$ g/ml in PBS) for 30 min at room temperature.

### **3.8.6. Cell number determination**

If cell density was to be determined, 50  $\mu\text{l}$  of the cell suspension was mixed with 50  $\mu\text{l}$  0.4 % trypan blue solution to visualize non-viable cells. The cell numbers in four 0.1-mm<sup>3</sup> volumes chamber were counted in a Neubauer hemacytometer under a binocular microscope and used to determine the mean cell density (cells/ml) by multiplying 10,000 with average cell number/chamber and dilution factor.

### **3.8.7. Freezing and thawing of endothelial cells**

Endothelial cells of passage 1 were stored in 2-ml cryovials in a liquid nitrogen storage freezer. Cells were harvested at a concentration of  $10^6$ - $10^7$  cells/ml, washed with PBS and resuspended in freezing medium. Before use of FCS in freezing medium, FCS was treated for 30 min at 56°C to inactivate complement and stored at -20°C. The cryovials were insulated with Styrofoam cloth (to avoid rapid cooling) and placed in a -70°C freezer overnight and transferred to liquid nitrogen for long-time storage.

Cryopreserved cells were thawed rapidly in a 37°C water bath, transferred in 5 volumes of prewarmed medium and seeded in collagen-coated flask. After 3-5 hours the DMSO-containing medium was removed and fresh endothelial growth medium was added into the flask.

### **3.8.8. Transfection of endothelial cells**

#### **3.8.8.1. Electroporation method**

The technique of electroporation is widely used as a means to transfect cells. It consists in applying a brief electric field across a cell which leads to the polarization of the plasma membrane. The resulting difference in potential induces reversible loss of plasma membrane integrity, as long as a critical threshold has been reached, resulting in the formation of pores large enough to allow the diffusion of macromolecules such as DNA and Dextran. However, in the absence of optimized combinations of field strength (V/cm), time constant (determined by the resistance and capacitance in the complete circuit) and electroporation buffer composition, irreversible damage to the plasma membrane will occur and lead to cell death.

Adherent endothelial cells were removed from 100-mm Petri dishes by trypsin/EDTA treatment as described above and washed with PBS. Endothelial cells ( $1.4 \times 10^6$  cells/400 $\mu\text{l}$ ) were suspended in electroporation buffer. 20  $\mu\text{g}$  of plasmid (EGFP-LIMK2 or its constructs) in electroporation buffer (30–60  $\mu\text{l}$ ) was mixed with the cell suspension and incubation was done for 10 min at room temperature. The final volume of incubation mixture was exactly 400  $\mu\text{l}$  in all experiments. The cell suspension was placed in a 4 mm gap electroporation cuvette. Cells were electroporated at a fixed capacitance of 1000  $\mu\text{F}$  and, 210V using a BioRad Gene Pulser instrument. Instrument readings showed that the time constant varied between 20 and 30 ms. Prewarmed endothelial

growth basal medium supplemented with 2x supplements (400  $\mu$ l; without antibiotics) was added to each cuvette then transferred to glass bottom petri dishes (4 Petri dishes of 10mm diameter/per transfection) for confocal microscopy and placed in the incubator. After 30 minutes, fresh endothelial growth medium was added to the Petri dishes and the medium was replenished after 24 h.

### 3.8.8.2. Nupherin<sup>TM</sup>-neuron mediated transfection

Lipofection mediated transfection of primary cells is inefficient because much of the transfected DNA is retained in endosomes, and that which escapes to the cytoplasm, enters the nucleus at low rates. Nupherin<sup>TM</sup>-neuron is a peptide-based reagent that combines a non-classical nuclear localization signal (NLS) containing the M9 sequence of heterogeneous nuclear ribonucleoprotein (hnRNP) A1, with a cationic peptide scaffold derived from a scrambled sequence of the SV40 T-antigen consensus NLS (ScT). The ScT was added to improve DNA binding of the M9 sequence. This reagent helps to transport DNA into the transfected cell's nucleus. Nupherin<sup>TM</sup>-neuron with lipid mediated transfection protocol dramatically enhances the transfection efficiency of primary cells such as HUVECs.

HUVECs were grown in 6-well plate up to the 90-100% confluency. The following solutions were prepared for transfection of HUVECs in each well.

Solution A For each transfection, 2 $\mu$ g of DNA was diluted into 150 $\mu$ l serum-free medium OPTI-MEM<sup>®</sup>I. 20 $\mu$ l (60 $\mu$ g) of the Nupherin<sup>TM</sup>-neuron reagent was added to tube A and gently mixed by pipetting (do not vortex). The solution was incubated for 15 min at room temperature before mixing with solution B.

Solution B 10 $\mu$ l cationic lipid lipofectin<sup>TM</sup> was added to a final volume of 150 $\mu$ l of OPTI-MEM<sup>®</sup>I medium.

The solutions A and B were mixed gently by pipetting (do not vortex) and incubated at room temperature for 40 minutes. After incubation 500 $\mu$ l of OPTI-MEM<sup>®</sup>I medium was added. The final volume of transfection solution was 800 $\mu$ l. Cells were washed twice with OPTI-MEM<sup>®</sup>I medium and then overlaid with transfection solution (800 $\mu$ l). Cells were centrifuged at 100xg for 5 minutes at room temperature and were incubated for 4 hours in CO<sub>2</sub> incubator. The fresh endothelial complete medium was replaced after incubation.

### 3.8.9. Actin staining

HUVECs in 8-chamber Falcon<sup>®</sup> culture slide or in glass bottom dishes (for transfected cells) were either left untreated or stimulated with LPA (20 $\mu$ M) or thrombin (1U/ml) for different times (0-45 min) in the presence or absence of Rho-kinase inhibitor Y27632 (20 $\mu$ M). Rho-kinase inhibitor Y27632 was added to the cells 40 min before stimulation. Cells were washed two times with PBS and fixed with 3.7% paraformaldehyde in PHEM buffer for 10 min at room

temperature. After washing twice with PBS, cells were permeabilized for 5 min with 0.1% Triton X-100 at room temperature, and washed again three times with PBS. In the case of transfected cells, cells were fixed and permeabilized with 50 $\mu$ l of BD Cytotfix/cytoperm<sup>TM</sup> buffer with an incubation of 15 minutes at 4°C and washed three times with PBS. Cells were incubated with a 1% solution of BSA (30 min) at room temperature, and stained with rhodamine-phalloidine or Alexa 546-phalloidine (1:100 dilution) for 20 min at 4°C in the darkness. After washing, stained F-actin was visualized using a Zeiss Axiovert 25 microscope or confocal microscope Zeiss LMS510 Meta.

### 3.9. Microscopy

#### 3.9.1. Live cell imaging by confocal microscopy

Most cellular processes occur in three dimensions overtime. To get a complete picture, we need to image cells in four dimensions. In 4D microscopy, time-lapse observations of fluorescent molecules are collected as three-dimensional data sets rather than as one image in a single focal plane. Live-cell imaging technology using fluorescent proteins (green fluorescent protein and its homologues) and confocal microscopy has revolutionized the study of cellular dynamics because an auto fluorescent molecule can be genetically encoded by fusion of GFP with the cDNA of interest.

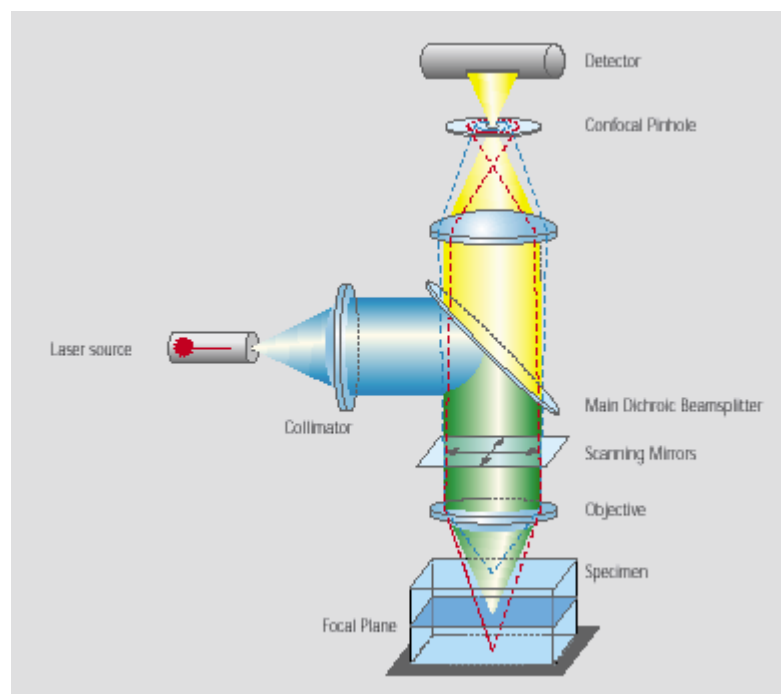
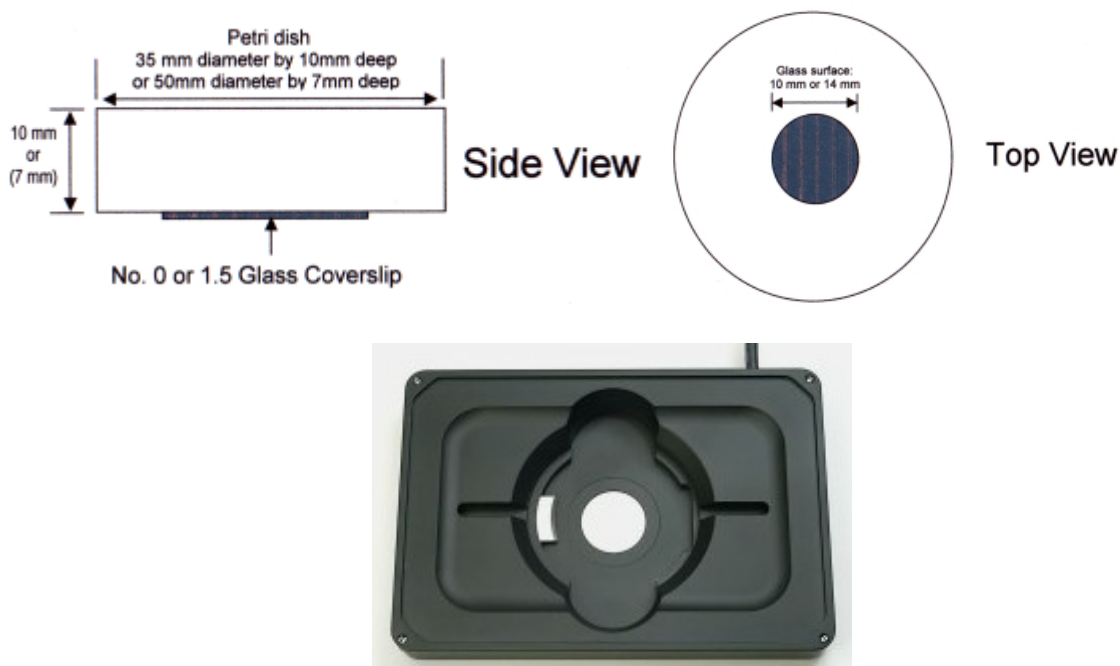


Figure 3.5 Beam path in the confocal laser scanning microscope

In confocal laser scanning microscopes, a light beam with short wave length generated by laser is reflected by a beamsplitter/diachronic mirror and is led by flexible mirrors over the object field to

scan a custom region. Excited chromophores scatter light of a longer wavelength back through the beamsplitter/diachronic mirror and produce in the focal plane a characteristic diffraction pattern from which the center, the so called “Airy disc” is selected by a detector pinhole. Because light beams projected from regions above and below the focal plane will not pass the detector pinhole (red line path in Figure 3.5), this step leads to a strong suppression of out-of-focus information, known as the confocal principle. A laser beam scans the specimen pixel-by-pixel and line-by-line. The pixel data are then assembled into an image that is an optical section through the specimen, distinguished by high contrast and high resolution in x, y and z. A number of images generated with the focal plane shifted in small steps can be combined into a 3-dimensional image stack, which is available for digital processing.

Successful observations of living cells under the microscope depend on several requirements: (a) for optimal growth, most mammalian cell types have to be kept within a distinct temperature range (36.5 to 37°C). (b) The pH value of the medium should be kept within the physiological range (pH 7.2 to 7.4). In most growth media this is accomplished by a CO<sub>2</sub>-NaHCO<sub>3</sub> based buffer system requiring a 5% CO<sub>2</sub> atmosphere. In addition, media may contain HEPES buffer to increase the buffer capacity. (c) Evaporation of water leading to a harmful increase of the ion concentration has to be prevented. (d) The microscope should be able to record time series of 3D image stacks automatically with a high aperture objective (optical surface should be uniform and thin). (e) Focus drift should be automatically corrected. Vibrations during imaging should be carefully avoided. (f) Light exposure of the cells should be kept to the possible minimum to avoid phototoxic effects.



**Figure 3.6 A)** Side and top view of glass bottom dishes. A glass coverslip was attached to the bottom of the dish. The dimensions of the dish are shown. The thickness of the bottom glass is 0.085-0.13mm. **B)** This solid heating element is made of one piece of aluminium with uniform heat distribution and a high thermal conductivity.

To minimize these artifacts, the cells were grown on glass bottom culture dishes (Figure 3.6). After 24 hrs of transfection cells were washed with OPTI-MEM<sup>®</sup>I medium and kept for two hours in the same medium. To keep the temperature constant, after incubation, the culture dishes were placed in heating elements (Figure 3.6), set at 37°C and left for 15 minutes to equilibrate the temperature so that the focus drift is minimized. The cells were focused on a microscope using the Xenon light source. The microscope functions were controlled by light manager through the software LSM 510 Meta. The desired lasers were switched on. After focusing on the cells of interest, the parameters of laser intensity and detectors gains were optimized to reduce the photo-damage and to acquire the good quality images. For Z-stacking the top and the bottom position were selected and the number of slices was determined according to the pinhole size and scanning time. After adjusting all the parameters live cell imaging was done on the microscope

### **3.9.2. Photobleaching techniques**

Photobleaching techniques were used in combination with green fluorescent protein (GFP) chimeras to analyze protein dynamics in living cells. Photobleaching is the photoinduced alteration of a fluorophore that abolishes the fluorophore's fluorescence signal. The diffusive characteristics of fluorescently tagged proteins or organelles in the cell can be studied by photobleaching a selected region of a fluorescently labeled cell with intense light and then quantitating the movement of nonbleached fluorescent molecules into the photobleached area using an attenuated light source. In this study, two photobleaching techniques of confocal laser scanning microscope were used to study the nucleocytoplasmic shuttling of LIMK2: FRAP (fluorescence recovery after photobleaching) and FLIP (fluorescence loss in photobleaching).

#### **3.9.2.1. FRAP**

In FRAP, a distinct region of interest in a cell expressing a GFP chimera is briefly photobleached with a high-intensity laser, and the movement of unbleached fluorescent molecules into the bleached region is followed with low-intensity laser light.

#### **Establishing FRAP conditions**

This protocol was adapted from Snapp et al., 2003. The cells were prepared on glass bottom with phenol red free medium (OPTI-MEM<sup>®</sup>I medium) at 37°C. The cell of interest was selected. The whole cell image was scanned at the desired excitation light intensity, line averaging, zoom, and other parameters (modify pinhole and detector gain for maximal fluorescence signal with no pixel saturation (pixel intensities that exceed the detector scale, i.e., >255 for an 8-bit image). The region-of-interest (ROI) for the photobleaching was selected which is usually a 2- to 4- $\mu$ m strip across the width of the cell. The photobleaching conditions (i.e., scan speed, zoom, laser power, microscope objective, and the minimal number of laser iterations required for photobleaching) were empirically determined so that after photobleaching, the fluorescent signal of the photobleached ROI decreases to background intensity levels. The imaging software LSM 510

META or NIH J was used to quantitate fluorescence intensity in the photobleached ROI and the whole cell prior to bleaching. For acquisition of fluorescence recovery time points, those imaging conditions that do not significantly photobleach were empirically determined.

Note: ROI. Recommended conditions for photobleaching with 25mW argon laser are 45% to 60% power with 100% transmission. For acquisition of recovery time points, use the same power with 0.1% to 1.0% transmission. For quantitative FRAP, the whole cell is usually scanned at scan speed 8 to 10 (0.798 to 3 sec per  $512 \times 512$  frame) with either two-line averaging or no-line averaging. In qualitative FRAP experiments, where the goal is to obtain high-quality images, the intervals at which images are collected during recovery are longer.

### Collecting FRAP data

To perform data analysis of a FRAP experiment, the prebleach image of the cell, a series of postbleach images of the whole cell that extend from an immediate postbleach image to several images after the bleach ROI fluorescence intensity reaches a plateau, and a table of fluorescence intensity values including the photobleach ROI, the whole-cell ROI, and a background ROI were collected. Multiple prebleach images were collected to establish the prebleach fluorescence intensity and to confirm that the prebleach fluorescence intensities of the cell and the bleach ROI do not fluctuate significantly.

Using the predetermined conditions; the ROI was photobleached with intense laser illumination. The whole cell imaging was continued at low laser illumination (the same conditions as the prebleach images) until the recovery process has reached a steady state. At least 10 to 20 data sets were collected for each fluorescently labeled protein for statistical analysis.

Note: A fraction of the data sets are usually discarded because of problems that potentially bias imaging results (e.g., recovery was not complete, the focal plane shifted, or the recovery curve-fitting method failed).

The postbleach intensity was corrected for overall loss of fluorescence determined from total fluorescence in the whole-cell images taken at the beginning and the end of the experiment.

Overall loss of fluorescence is given by  $(I\Sigma_0 - I\Sigma_\infty) / I\Sigma_0$  with  $I\Sigma_0$  = total cumulative pixel values in pre bleach whole cell image;  $I\Sigma_\infty$  = total cumulative pixel values in post bleach whole cell image. Due to this loss, postbleach fluorescence intensities in the ROI can never reach 100% of the prebleach value and need to be corrected by multiplication with  $I\Sigma_0 / I\Sigma_\infty$ . The mean fluorescence intensities per area over time were plotted.

#### 3.9.2.2. FLIP

This technique provides a powerful means for examining the boundaries of a compartment, whether it is the endoplasmic reticulum, nucleus, or cytoplasm. Using this method, a ROI is bleached repeatedly and fluorescence loss outside the ROI is monitored over time. The extent of which areas outside the ROI lose fluorescence overtime describes the boundaries over which the

fluorescent molecule is capable of diffusing. Three to five prebleach images were collected to establish the prebleach fluorescence intensity and to confirm that the prebleach fluorescence intensity does not significantly fluctuate. The cell of interest was identified. The ideal situation is to have two adjacent cells of similar fluorescence intensity in the imaging field. The cell that is not bleached provides a control to ensure that the imaging conditions do not cause nonspecific photobleaching. The imaging conditions were determined as described in FRAP. A region-of-interest (ROI) for the photobleach was defined which was between 5% and 20% of the structure of interest. The imaging conditions photobleaching conditions (i.e., scan speed, zoom, laser power, number of laser iterations required for photobleaching, and microscope objective) were determined that photobleach 90% or more of the fluorescent signal in the ROI, without causing significant photobleaching outside of the ROI. The photobleaching module in Zeiss LSM 510 Meta software was used to automate these processes. 20-40 iterations were set to photobleach the ROI to reduce the intensity to background level. Images were collected after photobleaching the area. Image were Collected at least three to five data sets for each fluorescently labeled protein and treatment. A fraction of data sets may be unusable because the focal plane shifted, the cell moved, or other reasons.

### **3.9.3. Fluorescence data analysis**

All experiments were done from cells of at least three different independent cell preparations. The fluorescent intensity measurements were carried out with 20 cells randomly selected in each experiment. Mean $\pm$ SEM was calculated for each experiment.



## 4. Results

### 4.1. Expression of LIMKs in endothelial cells

Protein sequences of LIMK1 (Entrez accession no. NP\_002305) and LIMK2 (Entrez accession no. NP\_005560) were aligned using ClustalW multi sequence alignment tool (Thompson et al., 1994). The homologies of LIM1 domains and LIM2 domains of human LIMK1 and LIMK2 were found to be 50% and 62%, respectively. The homology between the PDZ domains of human LIMK1 and LIMK2 was 48%. The highest homology (71%) was found between their kinase domains.

The information on the expression of human LIMK1 and LIMK2 genes was obtained from Unigene database (<http://www.ncbi.nlm.nih.gov/UniGene/>). 119 ESTs (Expressed Sequence Tags) were found for the human LIMK1 gene. The ESTs for human LIMK1 were obtained from tissues like brain, placenta, colon and different organ tumors (lung tumor, neuroblastoma, and retinoblastoma). 400 ESTs were found for human LIMK2, which are present in most of the body organs such as spleen, testis, ovary, skin, brain, heart, liver, and kidney. LIMK2 ESTs were also found in various cells such as human lung epithelial cells, T cells (Jurkat cell line), and B cells (Ramos cell lines). In endothelial cells, no ESTs of LIMK1 and LIMK2 were found using these databases.

Therefore, the expression of LIMKs in endothelial cells was analyzed at the transcriptional level by reverse transcriptase polymerase chain reaction (RT-PCR) using total RNA isolated from human umbilical cord vein endothelial cells (HUVECs).

Agarose gel electrophoresis of the PCR products revealed fragments of the expected size for human LIMK1 (405bp) and LIMK2 (490bp). Therefore, endothelial cells express a transcript for both LIMKs (Figure 4.1A). These amplified products of LIMKs were confirmed by DNA sequencing. Possible DNA contamination of RNA preparation leading to false-positive detection of genomic LIMKs sequences instead of *in vivo* transcribed LIMKs mRNA, was excluded by designing the LIMKs specific primers at exon boundaries (exon-intron informations of LIMK1 and LIMK2 were obtained from Ensembl database <http://www.ensembl.org/>), and by using negative controls of RT-PCR samples (reverse transcriptase polymerase enzyme was excluded during the RT-PCR). No amplification was obtained in negative RT-PCR controls. No additional amplification of LIMKs genomic fragments including the introns between exon 13 and 16 sequences (5.37kb with LIMK1 sets of primers MS3 and Limk1\_3' and 5.86kb with LIMK2 sets of primers LIMK2\_13 and Limk2\_3'; data not shown) was obtained in addition to the fragments derived from LIMKs mRNA transcripts.

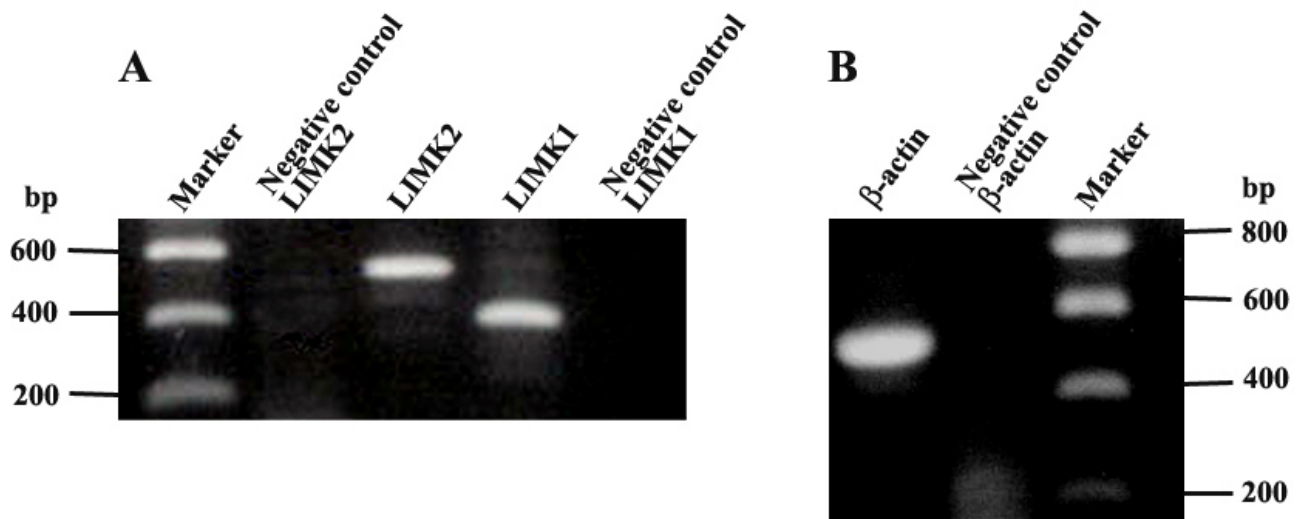


**Figure 4.1** **A) Expression of LIMKs in endothelial cells.** (A) 490bp PCR product was amplified with LIMK2 specific primers (lane 3) and a 405bp PCR product was amplified with LIMK1 specific primers (lane4). No PCR products were obtained in the negative controls of LIMK1 (lane5) and LIMK2 (lane2). **B)** Expression analysis of the  $\beta$ -actin RNA transcript (446bp) in endothelial cells (lane1). DNA contamination was excluded by the absence of a longer 652-bp fragment amplified from the intron-containing genomic  $\beta$ -actin DNA (lane1). No PCR product was seen in negative control (lane2). DNA molecular weight marker is shown in lane1 (A) and lane3 (B).

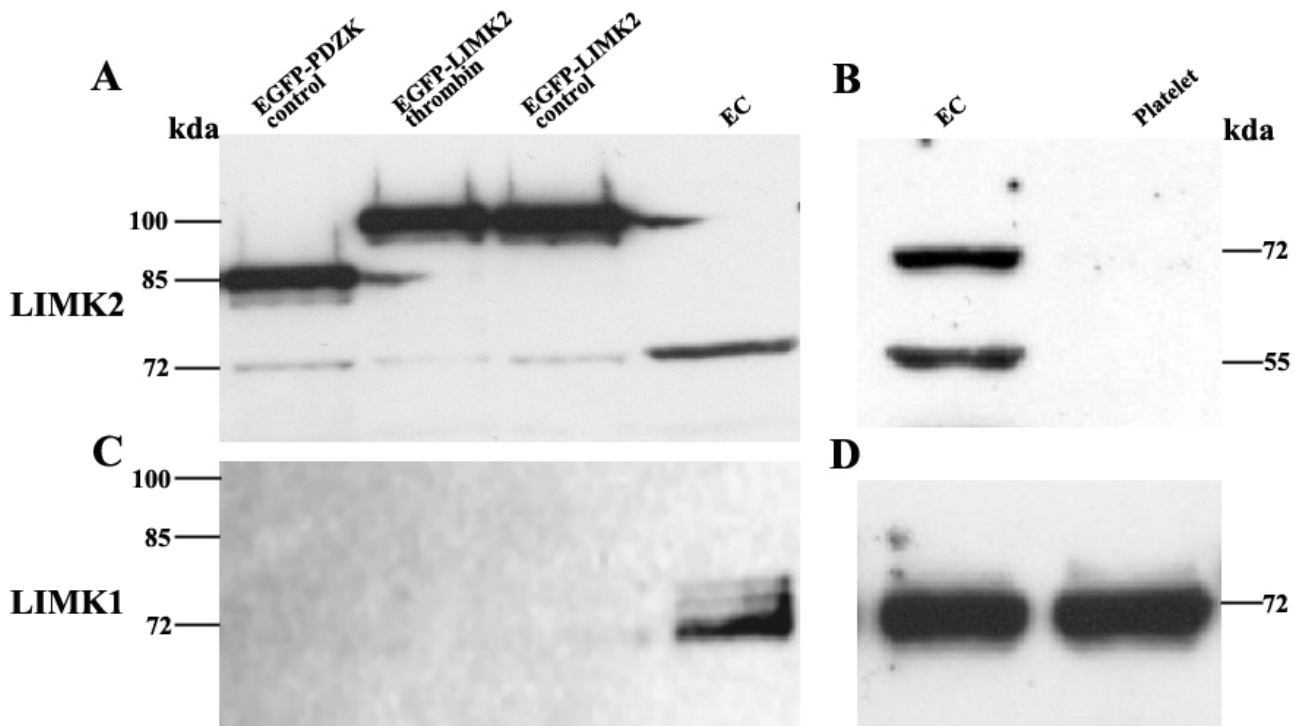


**Figure 4.2** **LIMK1 and LIMK2 protein expression in endothelial cells (EC) and platelets.** Confluent unstimulated or stimulated (thrombin, 1U/ml) endothelial cells ( $1.8 \times 10^6$  cells) and platelets ( $2 \times 10^5$  platelets/ $\mu$ l) were lysed in 500 $\mu$ L SDS PAGE sample buffer. **A)** The ~100kDa (27kDa EGFP + 72 kDa LIMK2) and ~85kDa (27kDa EGFP + 56.5 kDa PDZ-kinase (PDZK) of LIMK2) bands were detected in EGFP-LIMK2 (lane2; and lane3) and EGFP-PDZK (lane1) transfected cells respectively. The faint endogenous LIMK2 (~72 kDa) bands were also seen in the same blot. **B)** Endogenous LIMK2 protein (~72 kDa) was detected in endothelial cells but not in platelets **C)** No bands were detected in EGFP-LIMK2 transfected cells by blotting with the anti-LIMK1 antibody. Endogenous LIMK1 (~72kDa) was detected in untransfected cells (EC, lane 4). **D)** Endogenous LIMK1 protein was detected in both endothelial cells and platelets.

A PCR of negative RT-PCR controls and the RT-PCR samples was also performed with the primers of housekeeping gene  $\beta$ -actin (Figure 4.1B). In the case of the DNA contamination, PCR would lead to an additional amplification of a genomic  $\beta$ -actin fragment including the intron sequence (652bp) in addition to the fragments (446bp) derived from spliced  $\beta$ -actin mRNA transcripts. PCR with the  $\beta$ -actin primers showed only a fragment of 446bp (Figure 4.1B). These results indicate that the RNA preparation was free from genomic DNA contamination.

The expression of LIMK1 and LIMK2 proteins in endothelial cells was also analyzed by western blotting using LIMK1 and LIMK2 specific antibodies. Anti-LIMK2 specific antibody identified a band of ~72kDa in endothelial cells (lane 4, Figure 4.2A; Figure 4.2B) but not in platelets. In endothelial cells, a specific lower band (~55kDa) was also observed in immunoblots with a specific anti-LIMK2 antibody (Figure 4.2B). The anti-LIMK1 specific antibody identified the 72kDa band in both endothelial cells and platelets (lane 4 Figure 4.2; lane 1 and 2, figure 1.2D).

The specificity of the LIMK1 and LIMK2 antibodies was analyzed by immunoblotting of endothelial cells that had been transfected with different EGFP constructs of LIMK2 (pEGFP-LIMK2, pEGFP-PDZK). The anti-LIMK2 antibody but not the anti-LIMK1 antibody identified the specific bands of EGFP-LIMK2 and EGFP-PDZK (Figure 4.2A, C). The anti-LIMK1 and anti-LIMK2 antibodies but not specific IgG control antibody recognized specific bands of 72kDa in untransfected endothelial cells indicating the expression of both LIMKs in these cells (Figure 4.2B, and D, data not shown). LIMK2 was not expressed in platelets (Figure 4.2B). The endogenous proteins of LIMK1 and LIMK2 were barely detected in transfected cells (Figure 4.2A, and C). Possible reasons for this observation are that 1) the total proteins amount of the transfected cells loaded was approximately 50% of the amount of the non-transfected cells, 2) that the exposure time of the film after western blotting was less due to the high expression of EGFP-LIMK2 constructs in endothelial cells, and 3) that the transfection suppresses expression of the endogenous LIMKs.

## **4.2. LIMKs regulate actin dynamics in thrombin-stimulated endothelial cells**

### **4.2.1. Thrombin induces stress fiber formation by Rho-kinase activation**

The effect of thrombin on actin dynamics in endothelial cells was studied by live cell imaging. After 30 hours of transfection with EGFP- $\beta$ -actin plasmid, endothelial cells were serum starved for two hours and then activated with thrombin

In the control state, ruffle formation at the cell periphery and few stress fibers were observed. The EGFP- $\beta$ -actin protein was diffusively distributed throughout the cytoplasm, and also found in the ruffles as small aggregates.

Within 5 minutes of activation by thrombin, the transfected cells started contracting. After 15 to 22 minutes, the contracted cells were often rounded and a F-actin ring was seen at the periphery of cells. In addition, thrombin stimulated ruffle formation. In the upper cell, that did not contract, stress fiber formation was prominent. Some of the cell-cell contacts were disrupted and the F-actin fibers connecting the two cells were broken, possibly due to the contraction of the contractile F-actin rings (Figure 4.3 and supplementary movie 1).

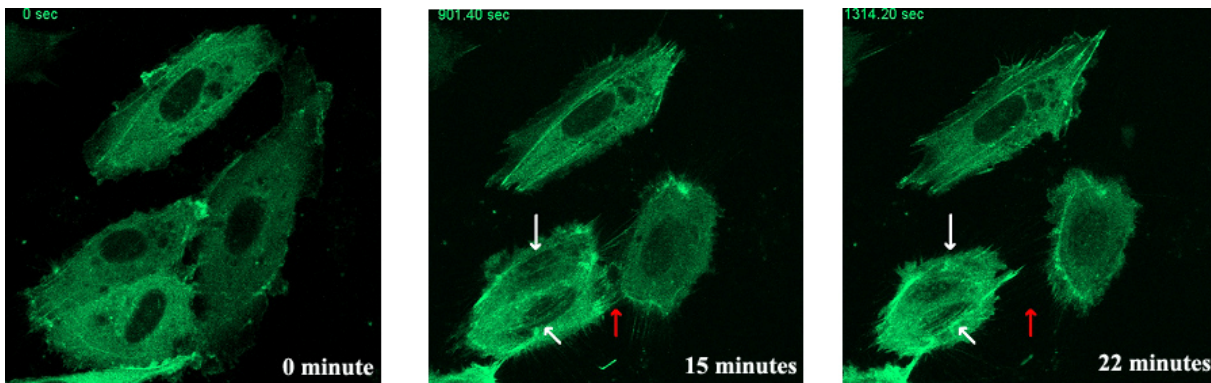


**Figure 4.3 The effect of thrombin on actin dynamics in endothelial cells.** The images show the same cells at 0 minute (control), 15 minutes, and 22 minutes after thrombin (1U/ml) activation. The white arrows indicate actin ring formation. The red arrow shows the place where the cells separated and actin fibers broke leading to cellular gap formation.

To investigate whether thrombin activates Rho-kinase in endothelial cells, Rho-kinase activation was measured by MYPT1 phosphorylation (Myosin Phosphatase Targeting Subunit1). The myosin light chain phosphatase (MLCP) consists of the delta isoform of type 1 protein phosphatase and the regulatory subunit (MYPT1). MYPT1 is phosphorylated at Thr696 and Thr853 by Rho-kinase (Ito et al., 2004). Thrombin-stimulated MYPT1 phosphorylation was increased within 2 minutes, reaching a maximum (2.4 fold) after 5 minutes. MYPT1 phosphorylation subsequently decreased (Figure 4.4A). In the presence of the Rho-kinase inhibitor Y-27632, MYPT1 phosphorylation in control cells was drastically decreased (Figure 4.4A) and the increase of MYPT1 phosphorylation after thrombin stimulation was inhibited. These data indicate that Rho-kinase is already active in unstimulated cells and further activated by thrombin. Furthermore, thrombin-induced stress fiber formation is dependent on Rho-kinase activation; since it was completely blocked by pretreatment of the cells with Y-27632 (Figure 4.4B).

#### **4.2.2. Rho-kinase stimulates phosphorylation of LIMK leading to subsequent cofilin phosphorylation in thrombin-stimulated endothelial cells**

Cofilin is an actin binding protein, which promotes actin depolymerization. Its function is inhibited by phosphorylation at Ser-3 by LIM-kinase. In studies of cell lines, it has been shown that Rho-kinase can phosphorylate LIMK1 at Thr508, and LIMK2 at Thr505, leading to the activation of these enzymes (Ohashi et al., 2000; Sumi et al., 2001a).

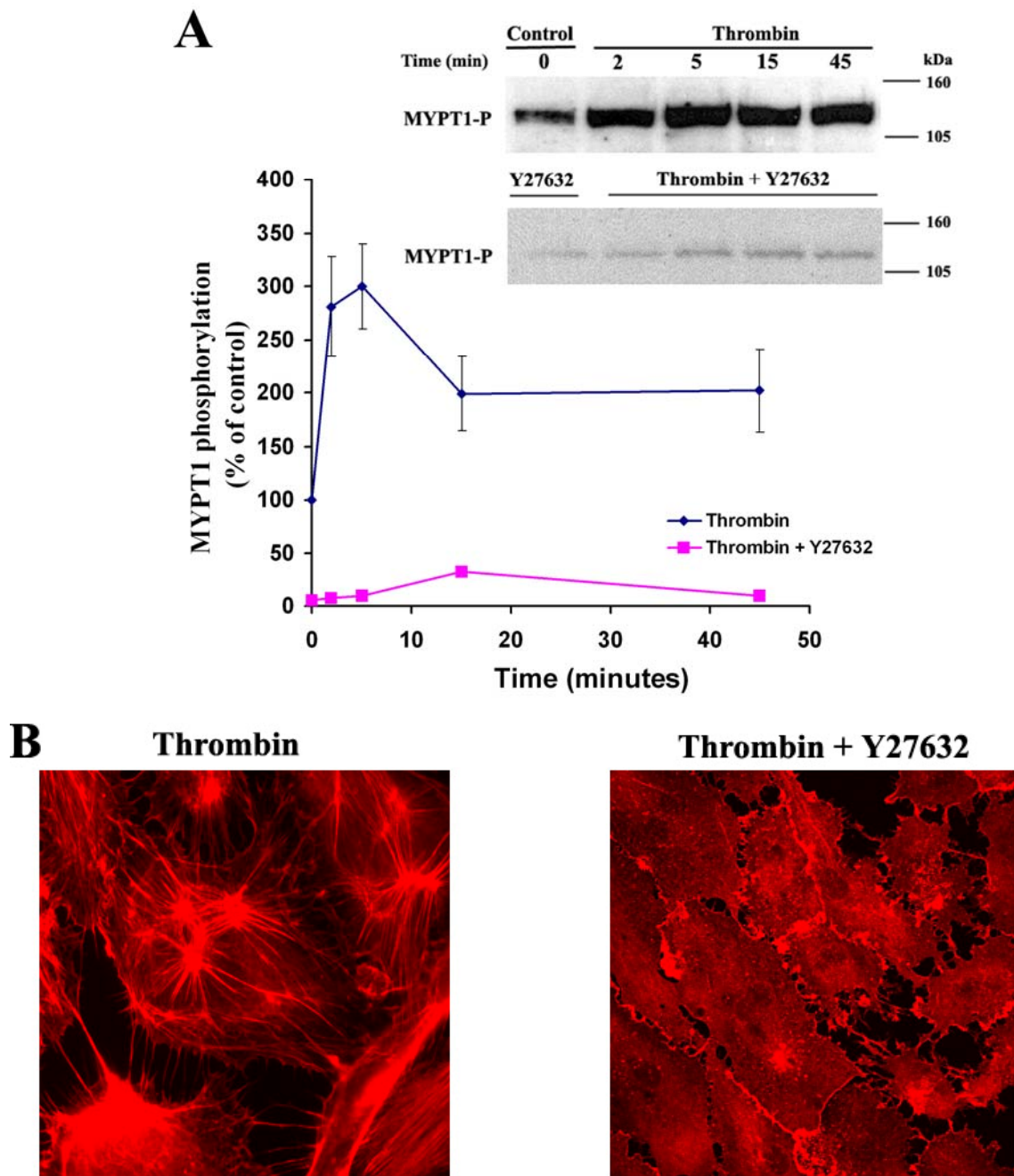


**Figure 4.4 Thrombin stimulates Rho-kinase and stress fiber formation in endothelial cells.** Endothelial cells, pretreated with or without the Rho-kinase inhibitor Y27632 (20 $\mu$ M, 45 minutes), were stimulated with thrombin (1U/ml) and immunoblotted with specific anti-phospho-MYPT1 (Thr853) specific antibody. **A)** The activation of Rho-kinase was measured by MYPT1 phosphorylation and plotted against time. **B)** Stress fiber formation was analyzed 15 minutes after thrombin stimulation using rhodamine-phalloidin staining.

To analyze the activation of LIMK1 and/or LIMK2 in thrombin-stimulated endothelial cells, LIMK-kinase phosphorylation was measured by a specific anti-phospho-LIMK antibody.

LIM-kinase phosphorylation was rapidly stimulated (7.3 fold). The maximum level was reached 2 minutes after thrombin activation. Subsequently, LIM-kinase phosphorylation decreased slowly (Figure 4.5A). LIMK phosphorylation was completely absent in Y27632-treated unstimulated and thrombin-stimulated endothelial cells (Figure 4.5A).

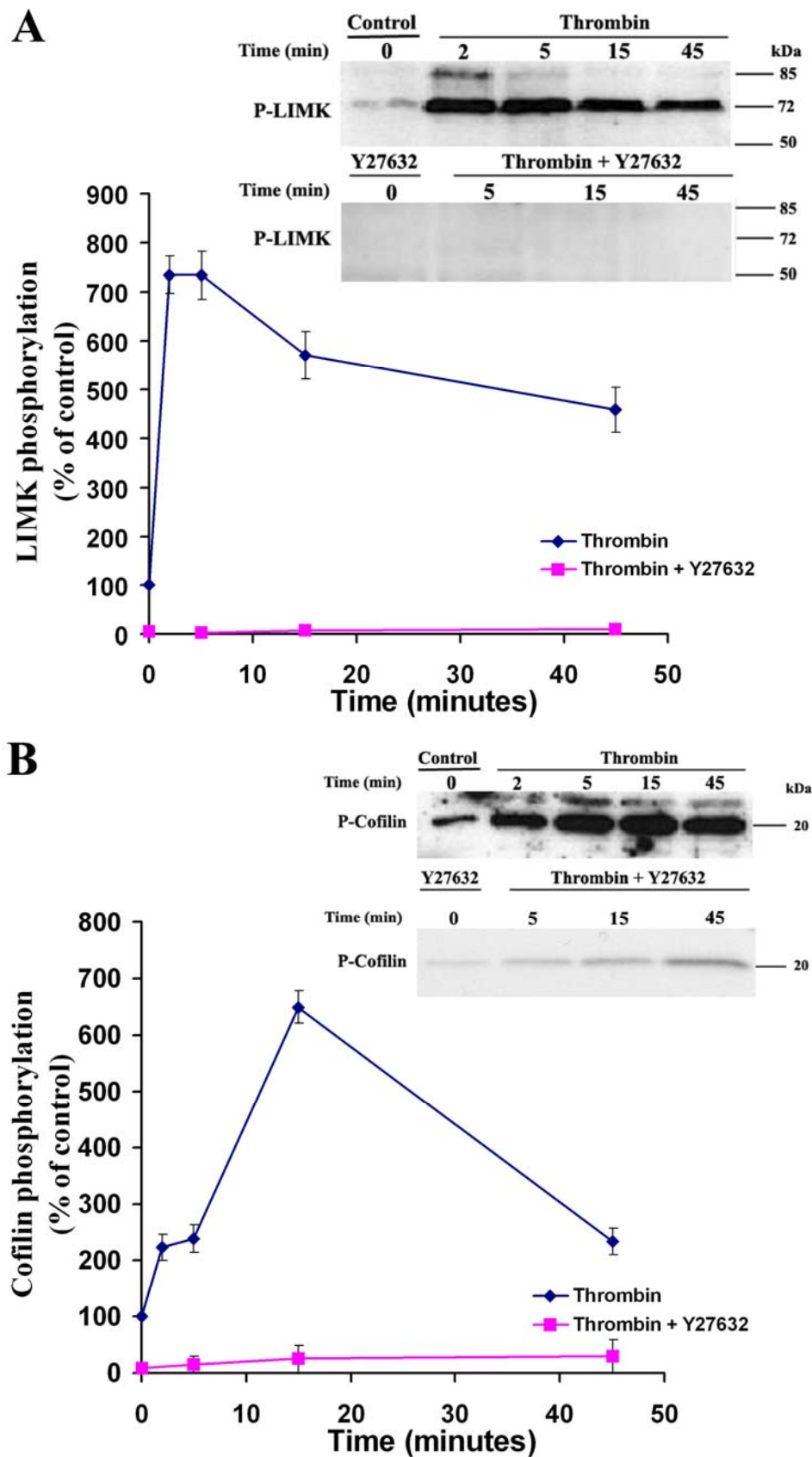


**Figure 4.5** Effect of Rho-kinase activation on LIMK activation and cofilin phosphorylation in thrombin-stimulated endothelial cells. Endothelial cells pretreated without or with Y27632 (20 $\mu$ M; 45 minutes), were stimulated with thrombin (1U/ml) for different times. **A)** LIMK phosphorylation was analyzed by blotting with anti-phospho-LIMK antibody. **B)** Cofilin phosphorylation was analyzed by blotting with a specific anti-phospho cofilin antibody. Values represent mean $\pm$ SEM of 3 experiments.

To investigate whether LIM-kinase activation might phosphorylate cofilin in thrombin-stimulated endothelial cells, cofilin phosphorylation was measured by using a specific anti-phospho cofilin antibody. In thrombin-stimulated cells, cofilin phosphorylation gradually increased up to 15 minutes and then decreased until 45 minutes after activation (Figure 4.5B). In the presence of the Y27632, cofilin phosphorylation was drastically reduced in unstimulated and stimulated cells (Figure 4.5B).

These results show that in thrombin-stimulated endothelial cells, Rho-kinase activates LIM-kinase, leading to cofilin phosphorylation.

### **4.2.3. Role of LIMKs in stress fiber formation**

To demonstrate the functional relevance of LIM-kinase activation for stress fiber formation, a kinase negative mutant (D451A) of EGFP-LIMK2 was prepared and transfected in endothelial cells. For comparison, endothelial cells were transfected with wild type EGFP-LIMK2. These cells were stimulated with thrombin for 10 minutes and analyzed for actin staining along with EGFP fluorescence by confocal microscopy.

In non-transfected cells and in wild type EGFP-LIMK2 transfected cells, dense and thick stress fibers were observed after thrombin stimulation. In contrast, in cells transfected with dominant negative mutant of EGFP-LIMK2, actin stress fiber formation was absent; instead actin aggregates were observed (Figure 4.6). These data suggest that the Rho-kinase/LIMK/cofilin pathway regulates stress fiber formation in thrombin-stimulated endothelial cells.

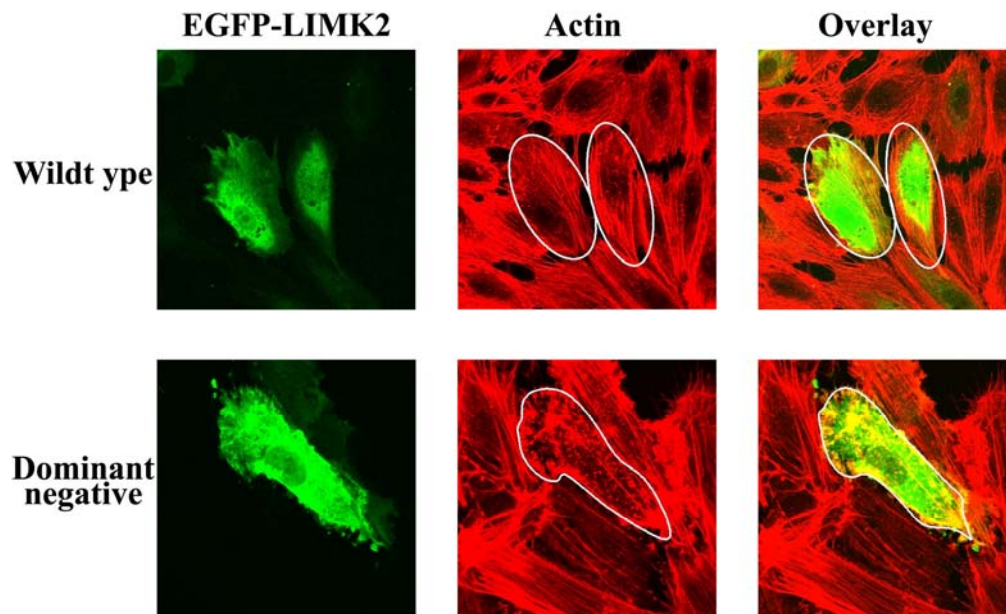


**Figure 4.6** The effect of dominant negative mutant of LIMK2 on stress fiber formation in thrombin-stimulated cells. Endothelial cells transfected with wild type EGFP-LIMK2 and dominant negative EGFP-LIMK2 (D451A) were activated with thrombin for 10 minutes. Stress fiber formation was analyzed using F-actin staining after thrombin stimulation (red). EGFP fluorescence of wild type and mutant LIMK2 is shown in green.



The unique basic amino acid-rich motifs of LIMK1 and LIMK2 in the kinase domain are shown in Figure 4.7 (amino acids, yellow). The basic nature of these motifs suggests that they may function as a nuclear localization signal (NLS). The basic amino acid-rich motif of LIMK2 has more arginine and lysine residues than LIMK1. To characterize the functional NLS in LIMK2, the basic amino acids-rich motif of LIMK2 was scanned in the Prosite database (<http://www.expasy.org/prosite/>) (Hulo et al., 2004) and compared with known NLSs of different proteins. Three types of unique potential NLSs were predicted which were designated as NLS1, NLS2, and NLS3 (Figure 4.8A).

NLS1 was predicted by comparing the motif of LIMK2 with well-characterized monopartite NLSs (consisting of a single short consecutive basic amino acids) of different proteins. The alignment with selected monopartite NLSs of different proteins is shown in Figure 4.8B (Jans and Hubner, 1996). NLS2 and NLS3 were predicted based on bipartite NLSs. Bipartite NLSs have two series of basic residues separated by a 10 to 12 amino acid spacer (Robbins et al., 1991).

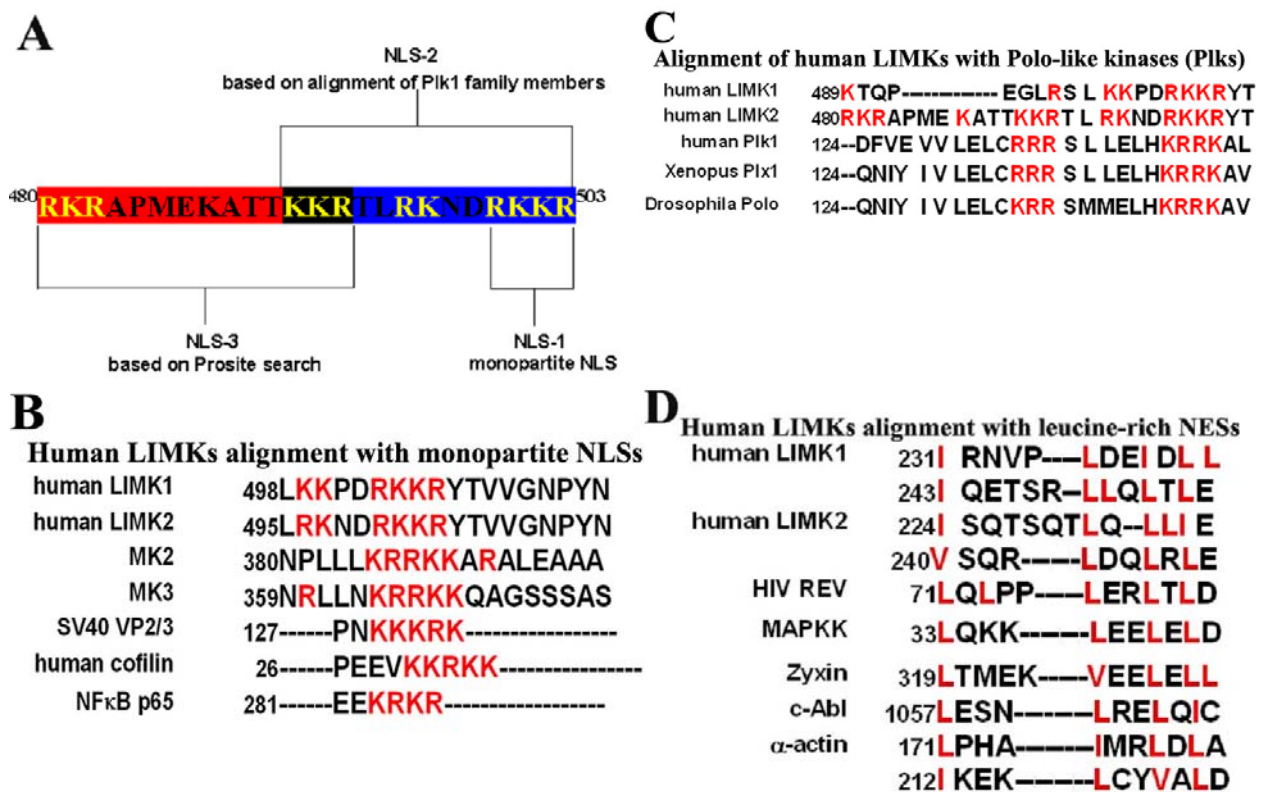


**Figure 4.8 Prediction of the nuclear localization and nuclear export signals in LIMK2.** **A)** The location of different predicted NLSs (NLS1, NLS2, and NLS3) in basic amino acid-rich motif of LIMK2. The basic amino acid-rich motifs of LIMKs were aligned with monopartite NLSs from different proteins (**B**) and bipartite NLSs of the Polo-like kinase family members (**C**). The numbering of amino acids in the Plk sequences is based on human Plk1. The basic amino acids are shown in red. **D)** NES in LIMK1 and LIMK2. The leucine rich regions of LIMK2 were aligned with LIMK1 NESs and other selected known NESs from different proteins. Leucine, isoleucine, and valine are shown in red.

Polo-like kinase 1 (Plk1), a mammalian ortholog of *Drosophila* Polo, is a serine-threonine protein kinase involved in the regulation of multiple aspects of mitosis. Plk1 bipartite NLS has an unusually short spacer (6 amino acids) sequence between two clusters of basic amino acids (Taniguchi et al., 2002). NLS2 was determined by aligning Plk1 with the basic amino acid motifs

of LIMK1 and LIMK2 (Figure 4.8C). In LIMK2, the 6 amino acid spacer is uniquely interrupted by two basic amino acids (RK). The bipartite NLS3 with an 8 amino acid spacer was predicted in LIMK2 by analyzing the Prosite database. In LIMK1, no bipartite type of NLS sequence (NLS2 or NLS3) was found. The predicted NLS1, NLS2, and NLS3 in LIMK2 are shown in Figure 4.8A.

LIMK1 has two nuclear export signals in the PDZ domain (NES1 and NES2) as shown in Figure 4.7 and Figure 4.8D (Yang and Mizuno, 1999). The two NESs in LIMK2 were predicted based on alignment with LIMK1 and the consensus sequences ( $\psi$ -X<sub>2,3</sub>- $\psi$ -X<sub>2,3</sub>-L-X- (LI),  $\psi$  represent any hydrophobic amino acid) of NES (Figure 4.7 and Figure 4.8D) The putative NES1 of the LIMK2 is present at the C-terminal of the PDZ domain and NES2 is localized immediately after the PDZ domain. The numerous NLSs and NESs in LIMK2 suggest that this kinase may actively shuttle between the nucleus and the cytoplasm.

### 4.3.2. Prediction of PKC phosphorylation sites in LIMK2

Besides the LIM-, PDZ-, and the kinase-domains, LIMKs have structurally flexible or “intrinsically disordered”<sup>7</sup> regions. The majority of known disordered proteins or domains are involved in cell signaling or transcriptional or translational regulation via non-catalytic interactions with DNA, RNA or other proteins (Iakoucheva et al., 2002). Disordered regions have a much higher frequency of known phosphorylation sites than ordered regions (Iakoucheva et al., 2004).

PONDR	LIMK1		LIMK2	
	Position	Length	Position	Length
VL-XT	147-201	55	132-157	26
	259-328	70	209-234	26
			267-307	41
			473-506	34
XL1-XT	216-245	30	269-310	42
	265-289	25	474-507	34
	299-324	26		

**Table 4.1 Prediction of disordered regions in LIMKs.** PONDR VL-XT predictor shows that LIMK1 and LIMK2 have two highly disordered regions (>30 amino acids). LIMK2 has shorter disordered regions than LIMK1. PONDR XL1-XT analysis of LIMK2 shows the same results as before. In contrast, it did predict any disordered region (longer than 30 amino acids) in LIMK1.

<sup>7</sup> Disordered regions (DRs) are entire proteins or regions of proteins, which lack a fixed tertiary structure, essentially being partially or fully unfolded.

To predict the disordered regions, LIMKs protein sequences were analyzed by using PONDR (Predictors Of Natural Disordered Regions) VL-XT and XL1-XT predictors (<http://www.pondr.com/>). The accuracy of predictions by PONDR is highest in the predicted regions of > 30 amino acids length. The results are summarized in Table 4.1.

The regions longer than 30 amino acids were selected for the further analysis. The disordered regions in LIMKs might be potential targets for phosphorylation that leads to their transition into an ordered region, and might control the functions of these enzymes.

To predict the phosphorylation sites in LIMKs other than Thr505 (LIMK2) or 508 (LIMK1) (target for Rho-kinase, refer introduction for details), Scansite (Obenauer et al., 2003), a motif based bioinformatics tool was used. The amino acid sequences of LIMK1 and LIMK2 were analyzed by using high stringency settings<sup>8</sup>. Two potential PKC phosphorylation sites (Ser283, and Thr494) were found in the predicted disordered regions of LIMK2 (Table 4.2). These sites were absent in the same corresponding regions of LIMK1. Interestingly, the second PKC phosphorylation site (Thr494) was found in the predicted NLS2 region. The two PKC sites have the consensus sequences of substrates of specifically the PKC- $\alpha$  and PKC- $\beta$  isoforms (Brinkworth et al., 2003). The positions of NLS, NES and PKC sites in LIMK2 are shown in Figure 4.9.

PKC site	Sequence	Disordered region	
		VL-XT	XL1-XT
PKCI	278TLRRR <sup>283</sup> SLRRSNSI	267-307	269-310
PKCII	489TTKKR <sup>494</sup> TLRKNDRK (NLS2)	473-506	474-507

**Table 4.2 The positions of predicted PKC phosphorylation site in LIMK2.** Two phosphorylation sites in the disordered regions of LIMK2 were predicted by Scansite program. The phosphorylation target sites are shown in red. The PKCII site is present in NLS2.

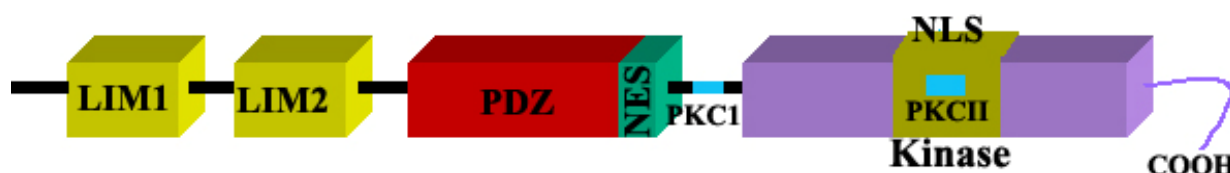


**Figure 4.9 Localization of NES, NLS, PKCI and PKCII sites in LIMK2.** The predicted NES and NLS are shown in green and dull yellow respectively. The putative PKC phosphorylation sites are shown in sky blue.

<sup>8</sup> High stringency setting is the most restrictive and reports a 'hit' only if the score falls within the top 0.2% of scores when the motif matrix of interest was applied to the vertebrate subset of SWISS-PORT.

#### 4.4. Nucleocytoplasmic shuttling of LIMK2 in endothelial cells

In order to analyze whether the predicted NLSs and NESs in LIMK2 are functional, the full-length LIMK2 cDNA was cloned into the pEGFP-C1 plasmid and the sub-cellular distribution were examined in live cells by confocal fluorescence microscopy.

The EGFP protein was diffusely distributed throughout the cytoplasm and the nucleus (Figure 4.10A), probably reflecting the unfacilitated diffusion of EGFP (~27kDa) through the nuclear pore. The EGFP-LIMK2<sup>9</sup> protein was mainly localized in the cytoplasm (92±2%, Mean±SEM) and only 6±2% was in the nucleus (Figure 4.10C). The intensity of EGFP-LIMK2 expression in the nucleus and the cytoplasm was measured by ImageJ software (<http://rsb.info.nih.gov/ij>) and LSM 510 META confocal software. The measurements were carried out in three independent experiments with 20 cells randomly selected in each experiment. The same approach was followed in all the subsequent experiments.

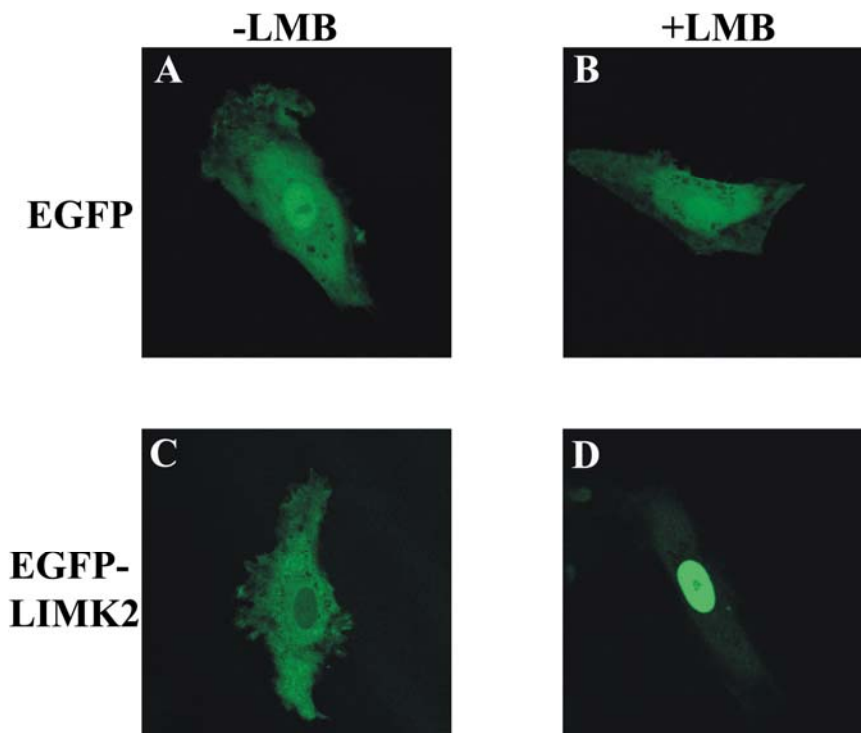


**Figure 4.10 Nucleocytoplasmic shuttling of EGFP-LIMK2 but not EGFP.** Endothelial cells were transfected with plasmid EGFP-C1 or plasmid containing the full length LIMK2 gene. EGFP was diffused throughout the cell (I) and EGFP-LIMK2 protein was mainly localized in the cytoplasm (III). After inhibition of nuclear export with leptomycin B (LMB; 10ng/ml; 60 minutes), the distribution of EGFP was not affected (II), but EGFP-LIMK2 was located exclusively in the nucleus (IV).

The nuclear export of many proteins is governed by the exportin protein CRM1. CRM1 dependent nuclear export is blocked specifically by the *Streptomyces* metabolite leptomycin B (LMB) (Kudo et al., 1998; Wolff et al., 1997). To determine whether LIMK2 is continuously

<sup>9</sup> The correct expression of the different EGFP-constructs of LIMK2 was controlled by immunoblotting with anti-LIMK2 antibody (shown in Figure 4.2).

shuttled between the nucleus and cytoplasm in resting endothelial cells and whether its export is dependent on CRM1, EGFP-LIMK2 transfected endothelial cells were treated with LMB (10ng/ml). It was found that EGFP-LIMK2 was located exclusively in the nucleus (Figure 4.10D). The cytoplasmic distribution of EGFP was not affected by the LMB treatment. These results indicate that the cytoplasmic EGFP-LIMK2 continuously goes into the nucleus, and that CRM1 transports EGFP-LIMK2 actively and continuously out of the nucleus. The continuous nucleocytoplasmic shuttling of LIMK2 is likely to be regulated by its NLSs and NESs.

#### **4.4.1. LIM domains of LIMK2 regulate its cytoplasmic localization**

Since LIMK2 is found mainly in the cytosol in resting endothelial cells, the NLS of LIMK2 might be masked. It has been found that LIM domains bind with the kinase domain of LIMK1 containing the NLS (Nagata et al., 1999). Therefore, the cytoplasmic localization of LIMK2 may be due to the interaction of LIM domains and the kinase domain. This interaction may be either intramolecularly or intermolecularly and may block the NLS function. To investigate this, different constructs of LIMK2 were made with EGFP in which either one or both LIM domains were deleted. The nuclear localization of  $\Delta$ LIM1-LIMK2 (LIM1, amino acids 1-62 were deleted) protein was approximately 2 times ( $15\pm 3\%$ ) higher than the wild type EGFP-LIMK2 (Figure 4.11A). This indicates that LIM1 partially inhibits the NLS and plays a role in the cytoplasmic localization of LIMK2. In contrast, the  $\Delta$ LIM2-LIMK2 protein (LIM2 domain, amino acids 72-124 were deleted) was localized mainly in the cytoplasm similarly to the full length EGFP-LIMK2 protein (Figure 4.11B).

The nuclear localization of EGFP-PDZK (both LIM domains, amino acids 1-141 were deleted) was drastically increased in the nucleus ( $40\pm 5\%$  of the total protein) (Figure 4.11C). This result suggests that both LIM domains contribute to the cytoplasmic localization of LIMK2. This might be due to the partial inhibition of NLS by the interaction between both the LIM domains and the kinase domain.

It was found that EGFP-LIMK1 after LMB treatment of endothelial cells was also localized in the nucleus (data not shown). However, in contrast to LIMK2, deletion of the two LIM domains of LIMK1 did not enhance the nucleus localization of LIMK1. The EGFP-PDZK (amino acids 146-647) of LIMK1 was still localized in the cytoplasm (Figure 4.11). This indicates that the LIM-domains of LIMK1 do not regulate the nucleocytoplasmic shuttling of LIMK1.

After 30 hrs of EGFP-PDZK of LIMK2 plasmid transfection, the endothelial cells were treated with LMB, and the nuclear accumulation of the protein was observed at different time intervals. Ten minutes after LMB treatment,  $80\pm 6\%$  of the total protein was shifted to the nucleus (Figure 4.12). After 30 minutes, almost all the EGFP-PDZK was localized in the nucleus. EGFP-PDZK entered the nucleus faster than the full length EGFP-LIMK2 (data not shown). These results suggest that LIMK2 rapidly shuttles between the nucleus and cytoplasm, and that cytoplasmic

localization of LIMK2 is due to the partial inhibition of the NLS by the two LIM domains and due to the active CRM1 dependent nuclear export of LIMK2.

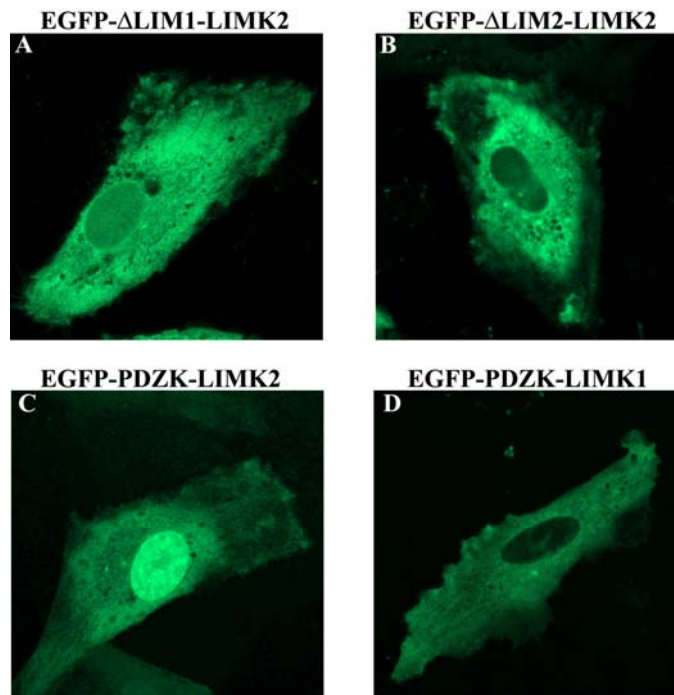


**Figure 4.11 The LIM-domains of LIMK2 inhibit nuclear localization of LIMK2, but not LIMK1.** A) Deletion of LIM1 domain (EGFP-ΔLIM1-LIMK2, amino acids 1-62 deleted) of LIMK2 partially enhanced the nuclear localization of EGFP-LIMK2. B) The deletion of LIM2 domain ((EGFP-ΔLIM2-LIMK2, amino acids 72-124 deleted) did not affect the cytoplasmic localization of LIMK2. C) Deletion of both LIM1 and LIM2 domains (EGFP-PDZK, amino acids 1-141 deleted) of LIMK2 drastically increased its localization in the nucleus. D) EGFP-PDZK of LIMK1 (amino acids 146-647) was localized exclusively in the cytoplasm.

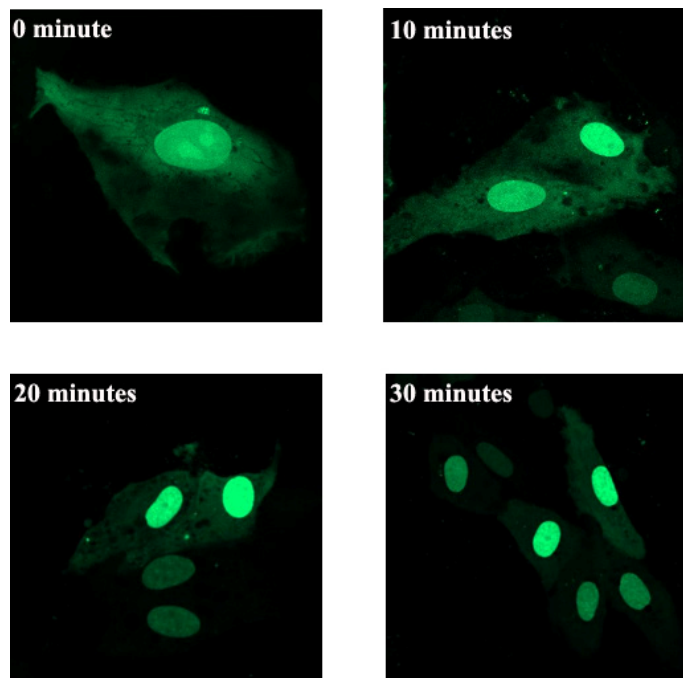


**Figure 4.12 Time course of nuclear accumulation of EGFP-PDZK after LMB treatment.** After 30hrs of transfection, cells were treated with LMB (10ng/ml) for different times, and the localization of EGFP-PDZK in the nucleus was observed by confocal microscopy.

#### 4.4.2. PDZ-kinase domain of LIMK2 is localized in the nucleus and cytosol: Analysis of shuttling by FRAP and FLIP

The shuttling of EGFP-PDZK of LIMK2 between the nucleus and the cytoplasm was analyzed by FRAP and FLIP. Fluorescence Recovery After Photobleaching (FRAP) is a tool to study the diffusive properties of molecules in living cells (Lippincott-Schwartz et al., 2003). Using this technique, a region of interest is selectively photobleached with high-intensity of laser light. The recovery that occurs as the fluorescent-labeled molecules move into the bleached region is monitored over time with low intensity laser light. EGFP-PDZK plasmid transfected cells were used for FRAP as described in materials and methods.

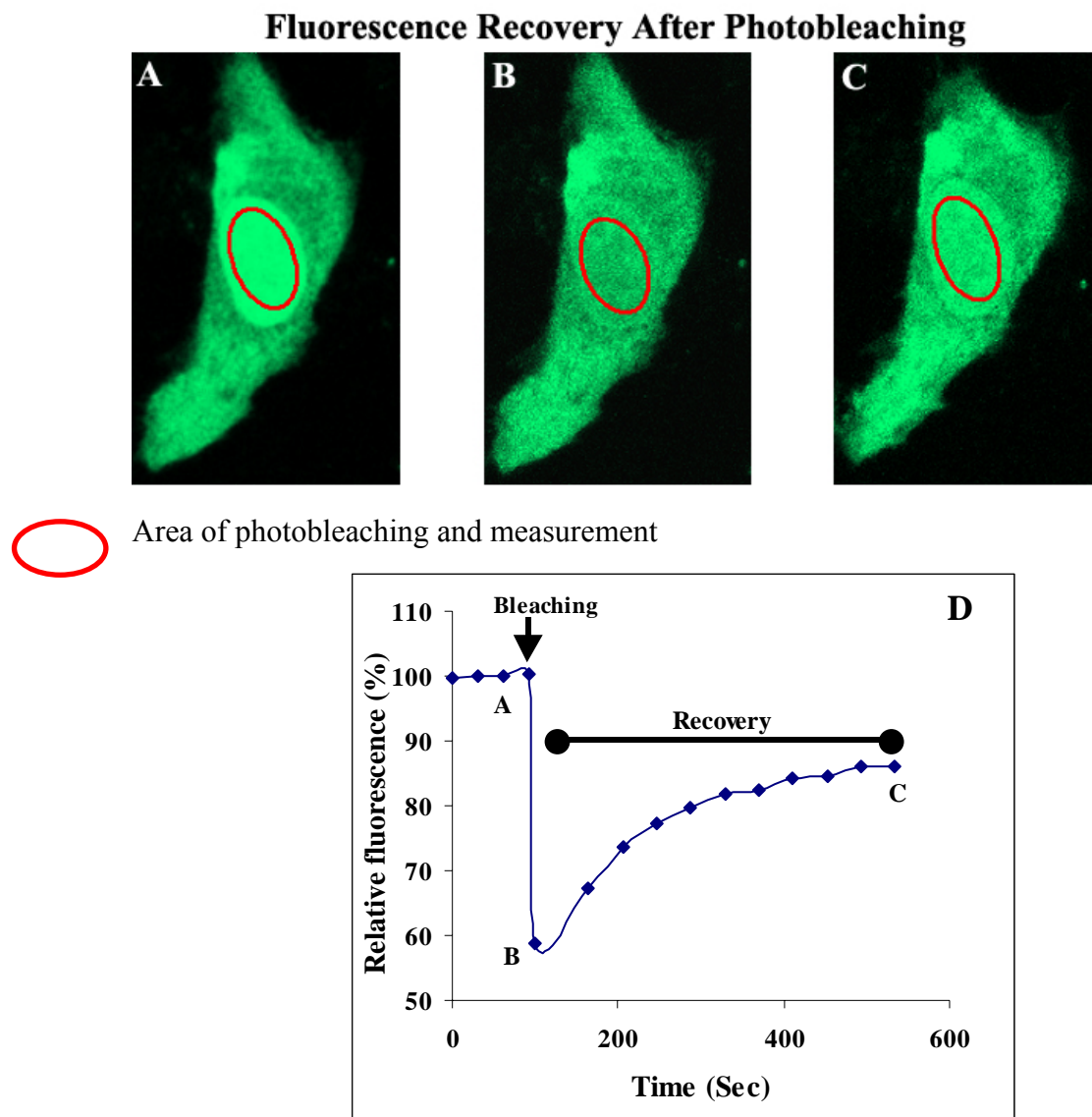


**Figure 4.13 Nuclear FRAP analysis of EGFP-PDZK in the endothelial cells.** The transfected endothelial cells were pretreated for 30 minutes with cycloheximide (10 $\mu$ g/ml) before the experiment to inhibit new EGFP-PDZK synthesis. **A)** The target cell expressing EGFP-PDZK protein is shown before bleaching. The green fluorescence was specifically photobleached in the nucleus (red circle). **B)** Image immediately after photobleaching. **C)** Final image of the bleached cell at the end time point (534 seconds) of the experiment. **D)** The recovery of the nuclear fluorescence (fluorescence intensity, control 100%) was measured in the graph at different times after photobleaching. The images A, B, and C are also indicated at the respective time points of the graph

The nucleus region was selected as the “region of interest” (ROI) and photobleached with high intensity laser light. The recovery was monitored in the same ROI. A graph was plotted as shown in Figure 4.13. The time for 50% recovery ( $\tau_{1/2}$ ) of fluorescence was determined from the graph. The  $\tau_{1/2}$  of EGFP-PDZK was calculated as 205 seconds. This means that after 3.5 minutes half of the total nuclear accumulating fluorescent EGFP-PDZK proteins have entered the nucleus. These results suggest that the NLS within the kinase domain drive the EGFP-PDZK into the nucleus. In addition, it was observed that the recovery in the ROI could not reach 100%. One possible explanation is that part of the cytosolic EGFP-PDZK is not free to move into the nucleus, perhaps due to binding with other proteins or due to auto inhibition caused by dimerization.

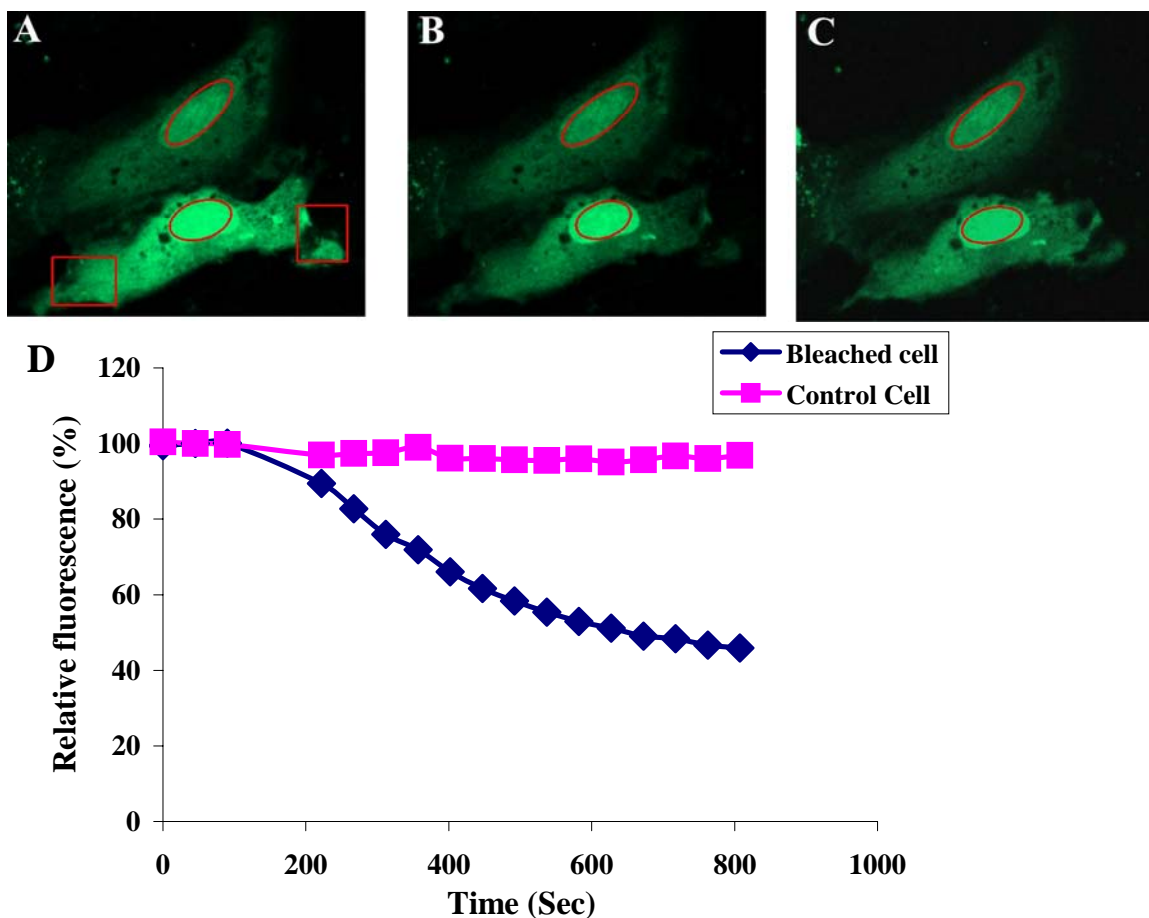


**Figure 4.14 FLIP analysis of EGFP-PDZK transfected endothelial cells.** Two regions of the cytosol of the lower cell (marked as red squares) were repeatedly photobleached (as described in Materials and Methods). Images were scanned before photobleaching (A), immediately after photobleaching (B) and at the final time point (C). D) Fluorescence in the nucleus of the lower bleached cell (blue diamond), and in the nucleus of the upper control cell (pink square) was measured at the indicated times. Cells were pretreated with cycloheximide for 30 minutes before starting the FLIP experiment.

In order to study whether EGFP-PDZK was exported from the nucleus to the cytoplasm, the technique Fluorescence Loss In Photobleaching (FLIP) was used. An area of the cytoplasm of a cell expressing the EGFP-PDZK protein was photobleached, and fluorescence intensity in the nucleus of the photobleached cell was monitored. As control, the fluorescence intensity in the nucleus of an adjacent unbleached cell was measured. The level of nuclear fluorescence in the photobleached cell gradually decreased over time (Figure 4.14C). In contrast, the nuclear

fluorescence in the adjacent cell (unbleached) was unaffected. (D) This indicates that EGFP-PDZK was exported from the nucleus in endothelial cells.

#### **4.4.3. EGFP-kinase of LIMK2 is localized in nucleus and nucleolus: comparison with the EGFP-kinase of LIMK1**

The kinase domain of LIMK2 has several predicted NLSs (NLS1, NLS2, NLS3; Figure 4.8). A NES consensus sequence was not detected in the kinase domain, suggesting that the kinase domain of LIMK2 should localize into the nucleus. To confirm this prediction, the EGFP-kinase domain (amino acids 315-638) construct was transfected into the endothelial cells. As expected, more than 95% protein accumulated in the nucleus (Figure 4.15A). Notably, EGFP kinase was also concentrated as dense bodies in the nucleus (white arrow Figure 4.15A), indicating that EGFP-kinase might associate with specific nuclear sub-compartments. The mammalian nucleus has various sub-compartments such as the nucleolus, the cajal bodies and nuclear speckles. Of these sub-compartments, the nucleolus is a highly dense nuclear compartment that can be easily detected by phase contrast microscopy. The phase contrast image of EGFP-kinase transfected endothelial cells (Figure 4.15B) showed an exact overlap of the nucleoli with the intensely stained EGFP-kinase dense bodies (Figure 4.15). This indicates that the EGFP-kinase not only accumulated in the nucleus but also in the nucleolus. To ensure that the EGFP-kinase stained dense bodies are not nuclear membrane bulge or bleb like structures, the cell was scanned by confocal microscopy. This revealed that the EGFP-kinase dense bodies were inside the nucleus (data not shown).

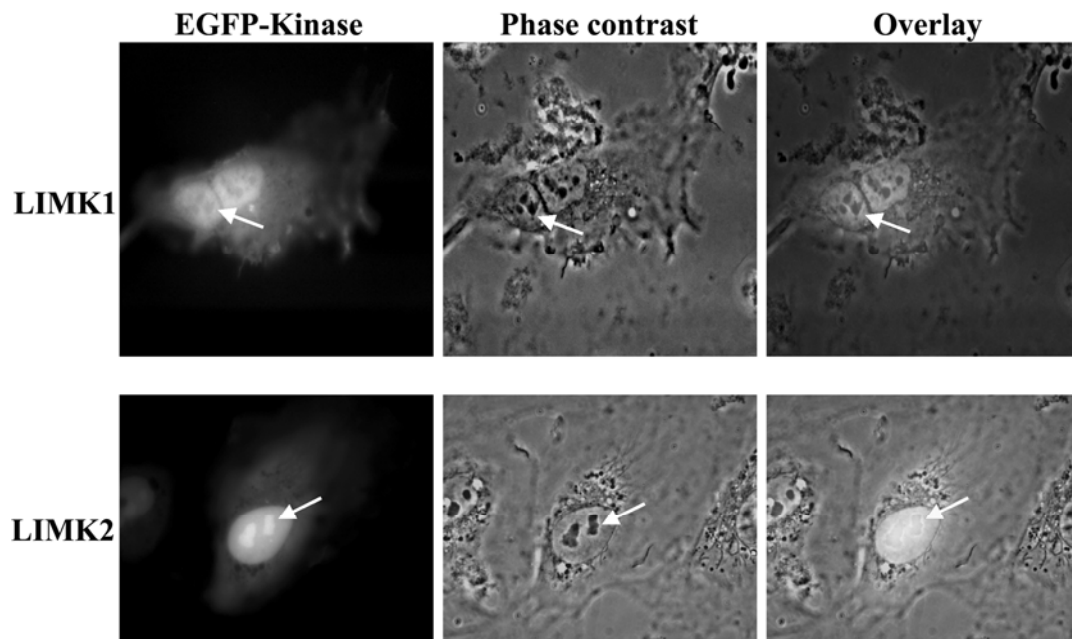


**Figure 4.15 Sub-cellular localization of EGFP-kinase of LIMK1 and LIMK2.** The EGFP-kinase domains of LIMK1 (amino acids 302-647) and LIMK2 (amino acids 315-638) mainly localized in the nucleus of the transfected endothelial cells. The fluorescence and phase contrast images of the respective EGFP-kinase transfected cells are shown. The nucleolus is indicated by white arrow. The dense fluorescent bodies of EGFP-kinase of LIMK2 exactly overlay with the nucleolus. EGFP-kinase of LIMK1 is absent in the nucleolus (white arrow).

The nuclear localization of the kinase domain of LIMK2 was compared with localization of the kinase domain of LIMK1. In LIMK1, the basic amino acid motif in the kinase domain has less arginine and lysine than the respective sequence of LIMK2 (Figure 4.7) that may affect the nuclear localization of the LIMK1. In contrast to the results obtained with LIMK2, only about 75% of the EGFP-kinase of LIMK1 was localized in the nucleus. However, it did not localize to the nucleolus (Figure 4.15).

These results suggest that the LIMK2 has more potential of being localized to the nucleus than LIMK1. They also show that the kinase domain of LIMK2, but not LIMK1, has a specific nucleolar localization signal (NoLS).

#### **4.4.4. Site directed mutagenesis of the unique basic amino acid-rich motif in LIMK2**

<b>Mutants of EGFP-kinase</b>	<b>Amino acid sequence</b>
Wild Type	480 <u>RKR</u> APMEKATT <u>KKR</u> TL <u>RKND</u> <u>RKKR</u> 503 <div style="text-align: center;"> <span style="margin-right: 100px;">NLS2</span> <span style="margin-right: 100px;">NLS1</span> </div> <div style="text-align: center;"> <span style="margin-right: 100px;">NLS3</span> </div>
Mutant 1 (NLS1)	480RKRAPMEKATTKKRTLAKNDAAA503
Mutant 2	480RKRAPMEKATTKKRTLAAADRKKR503
Mutant 3	480RKRAPMEKATTAAATLRKNDRKKR503
Mutant 4	480AAAAPMEKATTKKRTLAKNDRKKR503
Mutant 5	480RKRAPMEKATTKKRTLAAANDAAA503
Mutant 6 (NLS2)	480RKRAPMEKATTAAATLRKNDAAA503
Mutant 7 (NLS3)	480AAAAPMEKATTAAATLRKNDRKKR503
Mutant 8 (NLS2 + RK)	480RKRAPMEKATTAAATLAAANDAAA503
<b>Mutants of EGFP-PDZK</b>	<b>Amino acid sequence</b>
Mutant 9 (NLS1)	480RKRAPMEKATTKKRTLAKNDAAA503
Mutant 10	480RKRAPMEKATTKKRTLAAADRKKR503
Mutant 11 (NLS2)	480RKRAPMEKATTAAATLRKNDAAA503
Mutant 12 (NLS2 + RK)	480RKRAPMEKATTAAATLAAANDAAA503

**Table 4.3 Mutants of EGFP-kinase and EGFP-PDZK constructs.** In the wild type sequence, the putative NLS1, NLS2, and NLS3 were underlined. The basic amino acids are shown in blue, and were mutated to alanine (red). Mutant 1 (9 of EGFP-PDZK), 6 (11 of EGFP-PDZK) and 7 are generated to inhibit the function of the putative NLS1, NLS2 and NLS3 respectively.

The unique basic amino acid-rich motif within the kinase domain of LIMK2 has three putative nuclear localization signals (Figure 4.8), and the results in the previous section show that it may also contain a nucleolus localization signal. These NoLS are also generally built by sequences rich in arginine and lysine. In contrast to the NLS, the sizes of NoLS are highly variable, ranging

5 amino acids to 100 amino acids. Therefore, amino acid sequence analysis fails in predicting putative NoLS especially also because they overlap with NLS.

The unique basic insert of LIMK2 may thus have both functional NLS and NoLS. Therefore, different mutants of EGFP-kinase and EGFP-PDZK were generated in which the basic amino acids were mutated into alanine. The characteristics of the mutants are shown in Table 4.3.

#### 4.4.4.1. Site directed mutagenesis in EGFP-kinase domain of LIMK2

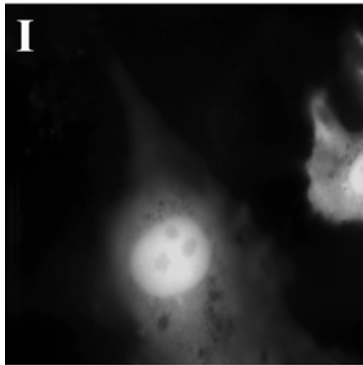
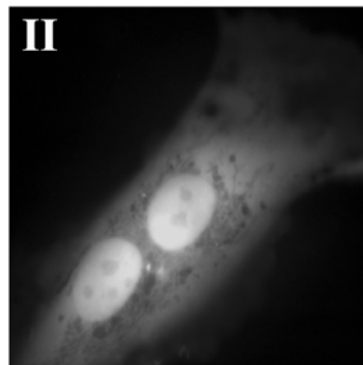
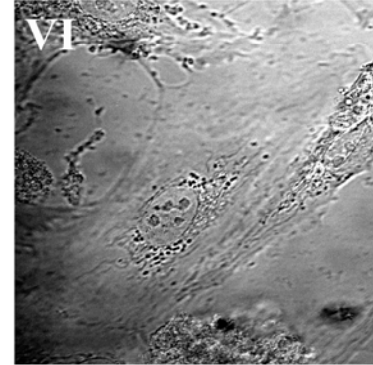
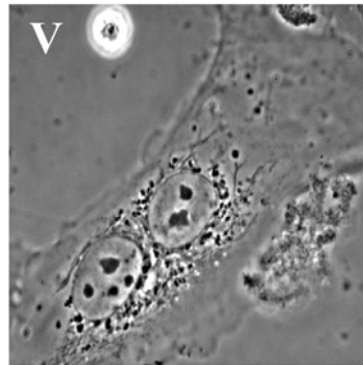
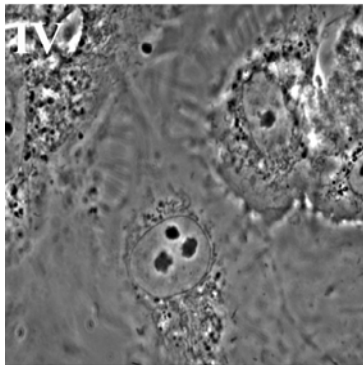
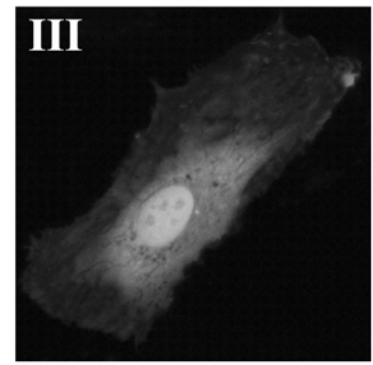
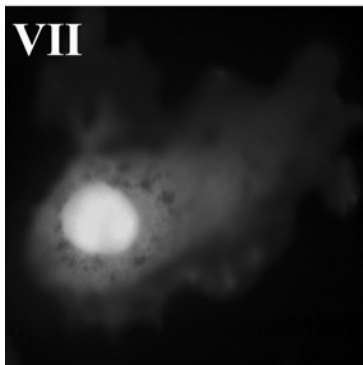
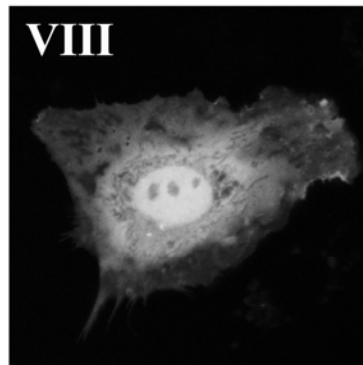
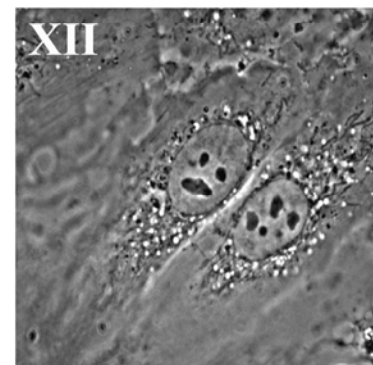
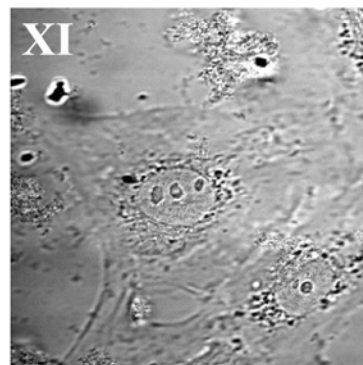
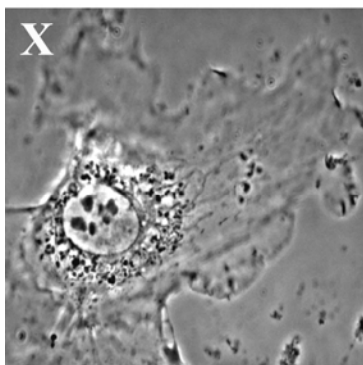
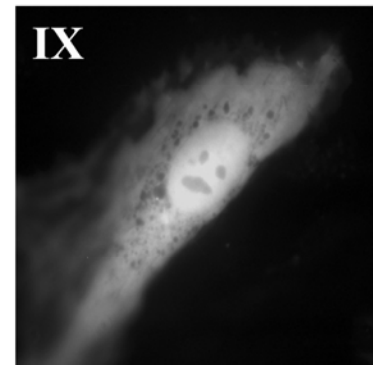
The different mutants of EGFP-kinase constructs were transfected in endothelial cells, and their sub-cellular localization was studied. Mutant 1 affecting NLS1 (RKKR, amino acids 500-503) was mainly localized in the nucleus similarly as the wild type kinase domain of LIMK2. However, the nucleolus staining was drastically reduced (Figure 4.16A I, IV). The nuclear localization of mutant 2 (RK, amino acids 496-497) and 3 (KKR, amino acids 491-493) was decreased by  $20\pm 6\%$ , and the nucleolus localization was absent similarly to the mutant 1 (Figure 4.16A II, III and its corresponding phase contrast images V and VI respectively). These results indicate that NLS1 (RKKR) and the basic amino acids RK and KKR are an important part of the NoLS.

Mutant 4 (RKR, amino acids 480-482) was mainly in the nucleus as the wild type kinase (Figure 4.16A VII and X). The nucleolar localization of mutant 4 was slightly reduced, and any distinct green fluorescent dense bodies could not be observed in the nucleus. This indicates that the basic amino acids 480-482 are not an important part of the NLS and NoLS.

Mutant 7 (NLS 3, amino acid 480-482 and 491-493 were mutated) was absent in the nucleolus and the nuclear localization of mutant 7 was more reduced ( $25\pm 5\%$ ) than of mutant 3 (Figure 4.16A and B). This confirms that the basic amino acids 480-482 play a minor role in nuclear localization signal (mutant 4).

These results together suggest that the basic amino acid-rich motif 491-503 (KKRTLKRN DRKKR) is the functional nucleolar localization signal. NLS1 and NLS3 are not active nuclear localization signals. To explore the NLS further, basic amino acids of NLS 2 were mutated in sequence in mutant1 (Table 4.3). The additional mutation of basic amino acids RK (mutant 5) and KKR (mutant 6, NLS2) in mutant 1 affected the nuclear localization of the mutant proteins. The nuclear localization of mutant 5 and 6 was decreased by  $25\pm 2\%$  and cytoplasmic staining was increased. These proteins were also absent in the nucleolus (Figure 4.16A). Finally, all the additional basic amino acids RK of NLS2 were mutated in mutant 6 and mutant 8 was prepared. The nuclear localization of this mutant protein was drastically reduced in the nucleus ( $20\pm 4\%$ ). these results indicate that the basic amino acids RK (amino acids 496-497) KKR (amino acids 491-493) and RKKR (amino acids 500-503) may all be part of the NLS of LIMK2.

The quantitative data of nuclear localization of the different mutants are show in Table 4.4.

**A Mutant 1****Mutant 2****Mutant3****Mutant4****Mutant5****Mutant6**

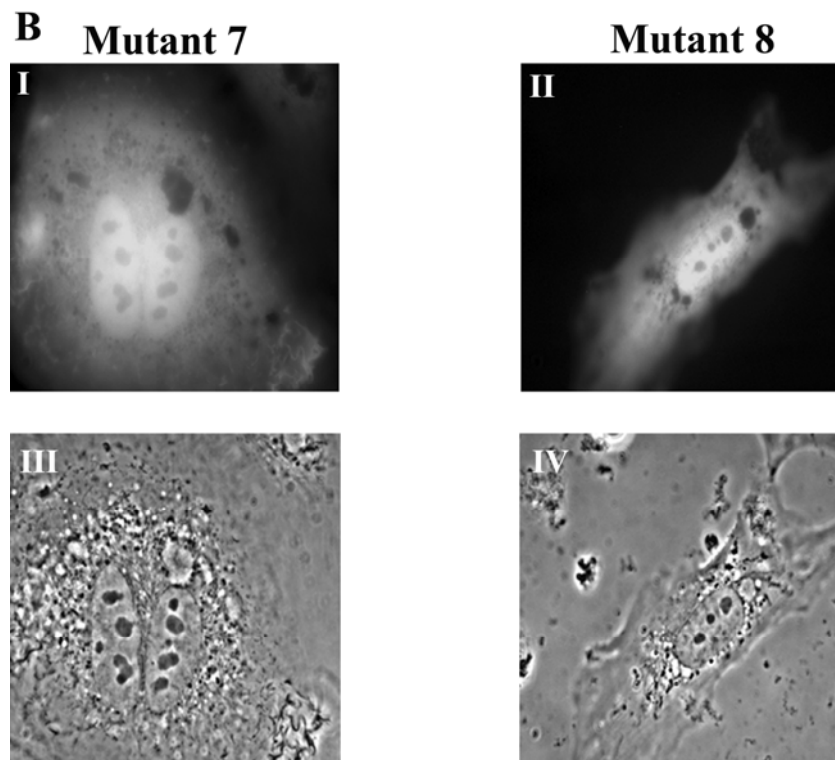


**Figure 4.16 The effect of different mutations in the basic amino acid motif of EGFP-kinase on nucleus and nucleolus localization.** A) The fluorescence images of mutant 1-6 expressions in endothelial cells are shown in figure I-III and VII-IX. The corresponding phase contrast images are shown in figure IV-VI and X-XII respectively. **B)** The expression of mutant 7 and 8 and its corresponding phase contrast images are shown in Figure I, III and figure II, IV, respectively.

The nuclear localization of the mutant 8 was not completely inhibited. This may be due to the remaining basic amino acids 480-482 being a part of NLS.

Mutants	Sub-cellular localization in %		
	Nucleus	N/C	Nucleolus
Wild type EGFP-kinase	95±2	N>>>>C	Yes
Mutant 1	85±4	N>>>>C	No
Mutant 2	80±6	N>>>C	No
Mutant 3	80±6	N>>>C	No
Mutant 4	90±1	N>>>C	Yes
Mutant 5	75±2	N>>C	No
Mutant 6	75±1	N>>C	No
Mutant 7	75±5	N>C	No
Mutant 8	20±4	N<<C	No

**Table 4.4 The summary of the mutation data of EGFP-kinase.** The sub-cellular distribution was measured as described in materials and methods and calculated as % of total expressed recombinant protein. The values of sub-cellular expression of the recombinant protein are the Mean±SEM (n=3 experiments, 20 cells per experiment were selected) N/C indicates the nuclear localization versus cytoplasmic localization of the EGFP-kinase.

#### 4.4.4.2. Site directed mutagenesis in EGFP-PDZK of LIMK2

In addition to the three NLSs in the kinase domain, PDZ-kinase contains two predicted NES, which are C-terminal of the PDZ domain. These NESs might be responsible for the decreased localization of EGFP-PDZK (40%) as compared to EGFP-kinase (95%). In comparison with the high molecular weight protein EGFP-PDZK (~84kDa), the EGFP-kinase (~62kDa) may passively diffuse into the nucleus. After LMB treatment, the wild type EGFP-PDZK completely accumulated in the nucleus. In order to explore the respective function of NLS1, NLS2 and NLS3 in the nuclear import of PDZ-kinase, specific mutants (mutants 9-12) were made. Mutant 9 (NLS 1) and mutant 11 (NLS2) were mainly in the cytoplasm (98%, Figure 4.17). The nuclear localization was increased to 20% after LMB treatment for 40 minutes.

The nuclear localization of mutant 10 was slightly higher than mutant 9. After LMB treatment, the nuclear localization of mutant 10 was only 40±6%. This indicates that the mutation of the basic amino acids 496-497 slightly reduced the rate of nuclear import, resulting in reduction of the nuclear localization of mutant protein.

The nuclear localization of mutant 12 (NLS2+RK) was mainly in the cytoplasm (98%). After LMB treatment, this sub-cellular distribution was barely affected. only 7% of mutant 12 was in the nucleus.

These results of mutation in EGFP-PDZK clearly show that the NLS2 (basic motif 491-503) is the nuclear localization signal of LIMK2. The nuclear localization of mutant 8 in contrast to mutant 12 may be due to the passive diffusion of the protein into the nucleus. The results further show that NLS1 (RKKR, amino acids 500-503) is the most important for the nuclear localization of PDZ-kinase (reduction of the nuclear localization of mutant 9 to 20% after LMB treatment). The two amino acids 496-497 (RK) contributed also to the nuclear localization (see results of mutant 10 with LMB), whereas the amino acids 491-493 (KKR) were apparently not as important for the nuclear localization of PDZ-kinase (compare results of mutant 9 with mutant 11). The summary of the results is shown in Table 4.5.

Together all these mutational data from EGFP-kinase and EGFP-PDZK show that the basic motif 491-503 is the functional NLS of LIMK2 and is also the functional NoLS.

Mutants	Sub-cellular localization in %			
	Nucleus		Cytoplasm	Nucleolus
	Control	+LMB		
Wild type EGFP-PDZK	40±5	100	60±5	Yes
Mutant 9	2±2	20±5	98±2	No
Mutant 10	2±2	40±6	98±2	No
Mutant 11	2±2	20±5	98±2	No
Mutant 12	2±2	7±3	98±2	No

**Table 4.5 The summary of the subcellular localization of the EGFP-PDZK.**

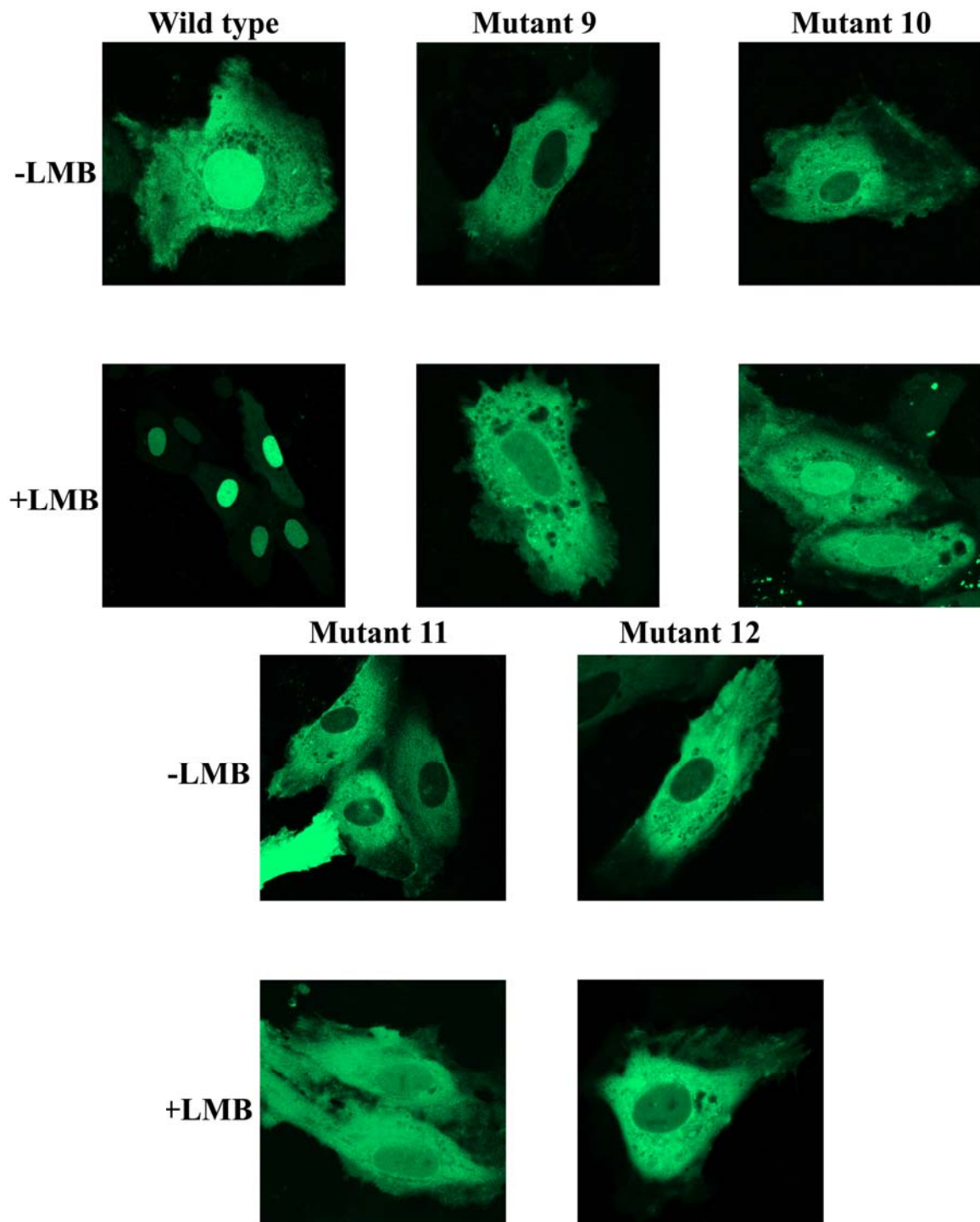


**Figure 4.17** The sub-cellular expression of different mutants of EGFP-PDZK transfected into endothelial cells. The cells transfected with mutant 9, 10, 11 and 12 plasmids are shown. These transfected cells were treated with LMB (10ng/ml, 40 minutes) to block the nuclear export.

#### **4.4.5. Sub-cellular localization of EGFP- $\Delta$ kinase-LIMK2**

The functional NLS sequence identified above lies within the kinase domain. To explore, whether there might be a further NLS present in LIMK2, the kinase domain was deleted and a EGFP- $\Delta$ kinase-LIMK2 (amino acids 1-314) construct was prepared. As expected from the mutation analysis shown before, EGFP- $\Delta$ kinase-LIMK2 protein was localized in the cytoplasm and not in

the nucleus. After one hour of treatment with LMB, to inhibit the nuclear export, the EGFP- $\Delta$ kinase-LIMK2 protein was distributed equally in the nucleus and the cytoplasm suggesting the presence of a NLS in this construct. There is a possible monopartite NLS at position 280-286 (RRRSLRR) in LIMK2. To analyze this further, the basic amino acids 280-282 (RRR) were mutated to alanine in EGFP- $\Delta$ kinase-LIMK2. The sub-cellular distribution of the mutant protein was however similar to that of the wild type construct in untreated or pretreated cells with LMB. The presence of the EGFP- $\Delta$ kinase-LIMK2 protein in the nucleus might be explained by the diffusion of this low molecular weight protein (60kDa) into the nucleus. In addition, the two putative CRM1 dependent NESs of LIMK2 localized at the end of the PDZ domain are present in the EGFP- $\Delta$ kinase-LIMK2 (Figure 4.7).

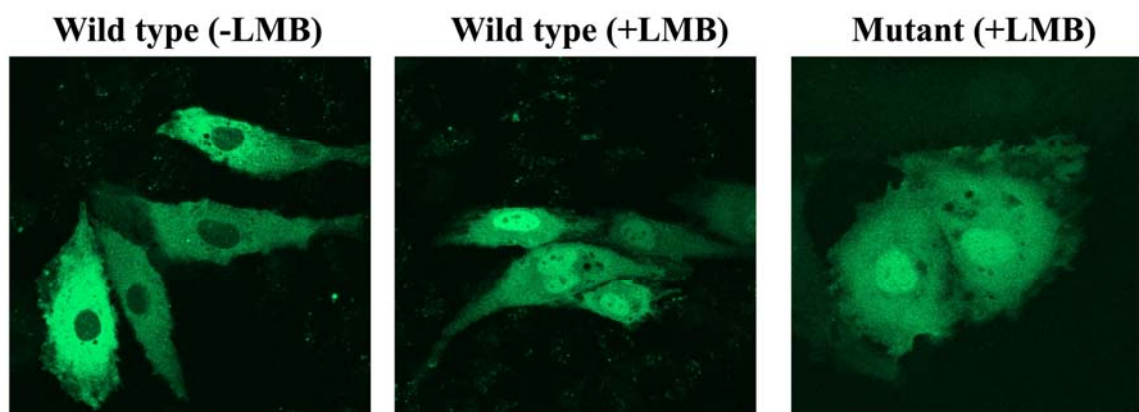


**Figure 4.18 Possible NLS of LIMK2 situated between PDZ and kinase domain is not functional.** The wild type and mutant EGFP- $\Delta$ kinase-LIMK 2 plasmids of LIMK2 were transfected into endothelial cells. The expressed EGFP- $\Delta$ kinase-LIMK2 protein was mainly localized in the cytoplasm. After LMB treatment the NLS mutant and wild type protein were equally distributed in the cytoplasm and the nucleus. The mutant EGFP- $\Delta$ kinase-LIMK2 was also localized mainly in cytoplasm and was equally distributed in the nucleus and cytoplasm after LMB treatment

## **4.5. Regulation of nucleocytoplasmic shuttling of LIMK2 by PKC-dependent phosphorylation**

### **4.5.1. Effect of PMA on sub-cellular localization of LIMK2**

Two putative PKC phosphorylation sites are present in the disordered regions of LIMK2 (Table 4.2). One (site I) is present between the PDZ and the kinase domain (amino acids 280-286), and the other (site II) is in the kinase domain within the functional NLS2 (amino acids (492-497)). To study the effect of phosphorylation by PKC, EGFP-LIMK2 and EGFP-PDZK transfected cells were stimulated with phorbol-12-myristate-13-acetate (PMA), a potent PKC activator.

Within 30 minutes of stimulation with PMA, the nuclear EGFP-LIMK2 was shifted to the cytoplasm (Figure 4.19A and D). The amount of nuclear EGFP-LIMK2 ( $6\pm 2\%$ ) was decreased to  $1\pm 0.5\%$ . The nuclear fluorescence of EGFP-PDZK (40%) also disappeared after PMA stimulation, and EGFP-PDZK was exclusively localized in the cytoplasm (Figure 4.19B and E). There was no effect of PMA on the nuclear localization of EGFP-kinase (Figure 4.19C and F)

indicating that phosphorylation of the second PKC site within NLS-2 does not alter the function of this nuclear localization signal. The effect of PKC activation on the exclusive cytoplasmic localization of EGFP-LIMK2 and EGFP-PDZK must then be due to phosphorylation of the PKC I site and might be explained either by acceleration of the nuclear export or by indirect inhibition of the nuclear localization.

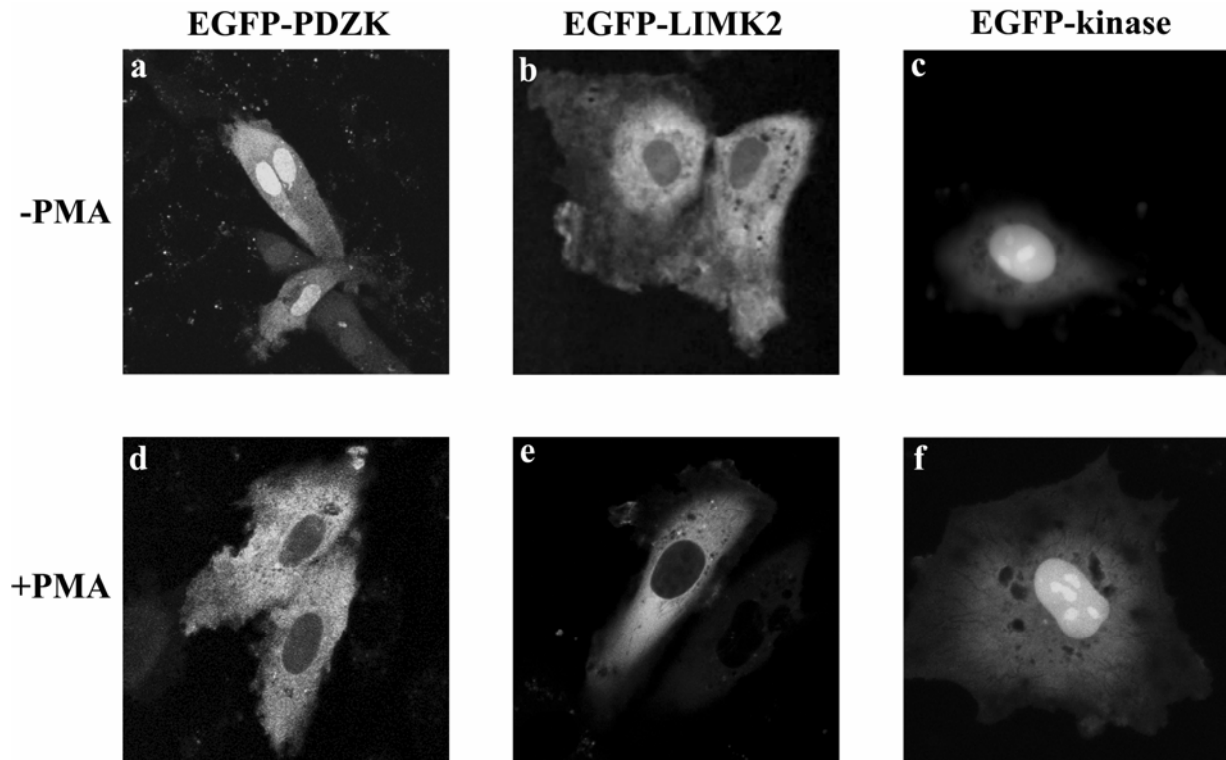


**Figure 4.19** PKC activation by PMA regulates the sub-cellular distribution of EGFP-LIMK2 and EGFP-PDZK, but not EGFP-kinase. Endothelial cells transfected with EGFP-LIMK2, EGFP-PDZK and EGFP-kinase were treated with 200nM PMA for 30 minutes. EGFP-LIMK2 is mainly present in the cytoplasm, but approximately  $6\pm 2\%$  of total expressed protein was in the nucleus (A). After treatment with PMA, the nuclear fluorescence disappeared in the nucleus (D). The nuclear fluorescence of EGFP-PDZK was higher as observed and discussed before (40%, B) and also drastically reduced to 3% by PMA treatment (E). The treatment of PMA did not affect the nuclear localization of EGFP-kinase (C and F).

#### **4.5.2. The PKC- $\alpha$ and PKC- $\beta$ isoforms regulate nucleocytoplasmic translocation of LIMK2**

PKC, a serine/threonine kinase, has various isoforms (Shirai and Saito, 2002). To find out which specific isoforms of PKC regulate the shuttling of LIMK2, the cells transfected with EGFP-PDZK were incubated with isoform specific inhibitors. Subsequently the cells were activated with PMA. Go6983, a potent PKC inhibitor, specifically inhibits PKC- $\alpha$ , PKC- $\beta$ , PKC- $\gamma$ , PKC- $\delta$  and PKC- $\zeta$  in nanomolar range, but not other PKC-isoforms (Gschwendt et al., 1996; Peterman et al., 2004). The PMA-stimulated translocation of EGFP-PDZK to the cytoplasm was completely blocked (Figure 4.20 C).

The specific inhibitor Go6976 only inhibits the PKC isoforms PKC- $\alpha$ , PKC- $\beta$ , and PKC- $\mu$ . It does not affect other PKC isoforms even at micro-molar range *in vitro* (Martiny-Baron et al.,

1993). EGFP-PDZK protein translocation to the cytoplasm by PMA stimulation was also inhibited by Go6976. These results indicate that the PMA-induced translocation of LIMK2 from the nucleus to the cytoplasm is mediated specifically by the PKC isoforms PKC- $\alpha$  and PKC- $\beta$ .

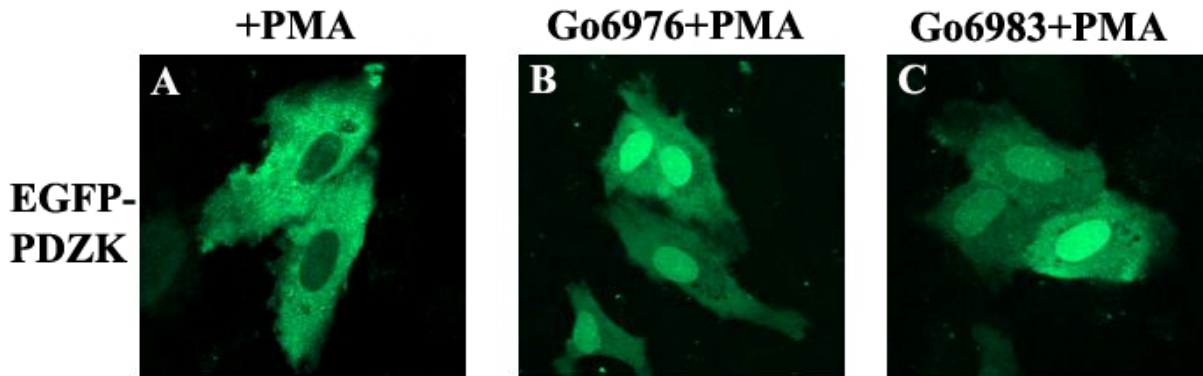


**Figure 4.20** The effect of different PKC inhibitors on the PMA induced translocation of EGFP-PDZK. Endothelial cells transfected with EGFP-PDZK were incubated with the PKC inhibitor Go6976 (2 $\mu$ M) or Go6983 (500nM) and then stimulated with PMA for 30 minutes. PMA-treatment shifted the protein from the nucleus to the cytoplasm (A). This translocation was completely blocked by the PKC inhibitors (B, C).

#### **4.5.3. Ser283 (site I) in LIMK2 is phosphorylated in PMA-stimulated endothelial cells**

Phospho-specific antibodies are powerful tool to analyze protein phosphorylation. To investigate the potential PKC phosphorylation site I in LIMK2, a specific anti-phospho-Ser PKC substrate antibody was used. This antibody has been generated against a degenerate peptide library of the PKC substrate motif CXXX(K/R)(K/R)S\*(F/L/V)(K/R)(K/R)XXX (*X* representing any amino acid except Trp and Cys, and S\* is phosphoserine) (Zhang et al., 2002) and was found to bind with high affinity to the consensus peptide sequence (XXRRRS\*LRRXX) present in LIMK2 (Table 4.2, amino acids 280-286).

To analyze, whether endogenous LIMK2 was phosphorylated, endothelial cells were untreated (control) or treated with PMA. LIMK2 in endothelial cell lysates was specifically immunoprecipitated with a specific anti-LIMK2 antibody and blotted with anti-phospho-Ser PKC substrate antibody. The phosphorylation of LIMK-2 was increased about 4.5 fold after PMA treatment (Figure 4.21A, lanes 1 and 2 and Figure 4.21B). Both PKC inhibitors Go6976 and Go6983 inhibited LIMK2 phosphorylation in control cells and PMA-stimulated cells. Go6983 was more potent than Go6976 (Figure 4.21A and B). These results strongly suggest that endogenous LIMK2 was phosphorylated on Ser283 by the PKC isoforms PKC- $\alpha$ , and PKC- $\beta$  in PMA-stimulated endothelial cells.

In addition to the PKC site at Ser283, there is a second possible PKC phosphorylation site in LIMK2 at Thr494. To confirm the specificity of the anti-phospho-Ser PKC substrate antibody, mutants of EGFP-PDZK were prepared in which Ser283, Thr494 or both sites were mutated to

alanine. The mutants were transfected into endothelial cells, which were stimulated with PMA. The anti-phospho-Ser PKC substrate antibody detected both the wild type EGFP-PDZK and the T494A mutant (Figure 4.21C lane 1-4). There was no signal on the immunoblots of the S283A mutant and the S283A/T494A double mutant in PMA stimulated or control cells (Figure 4.21 lane 5-8). These results prove that S283 in LIMK2 is phosphorylated by PKC in PMA stimulated cells.

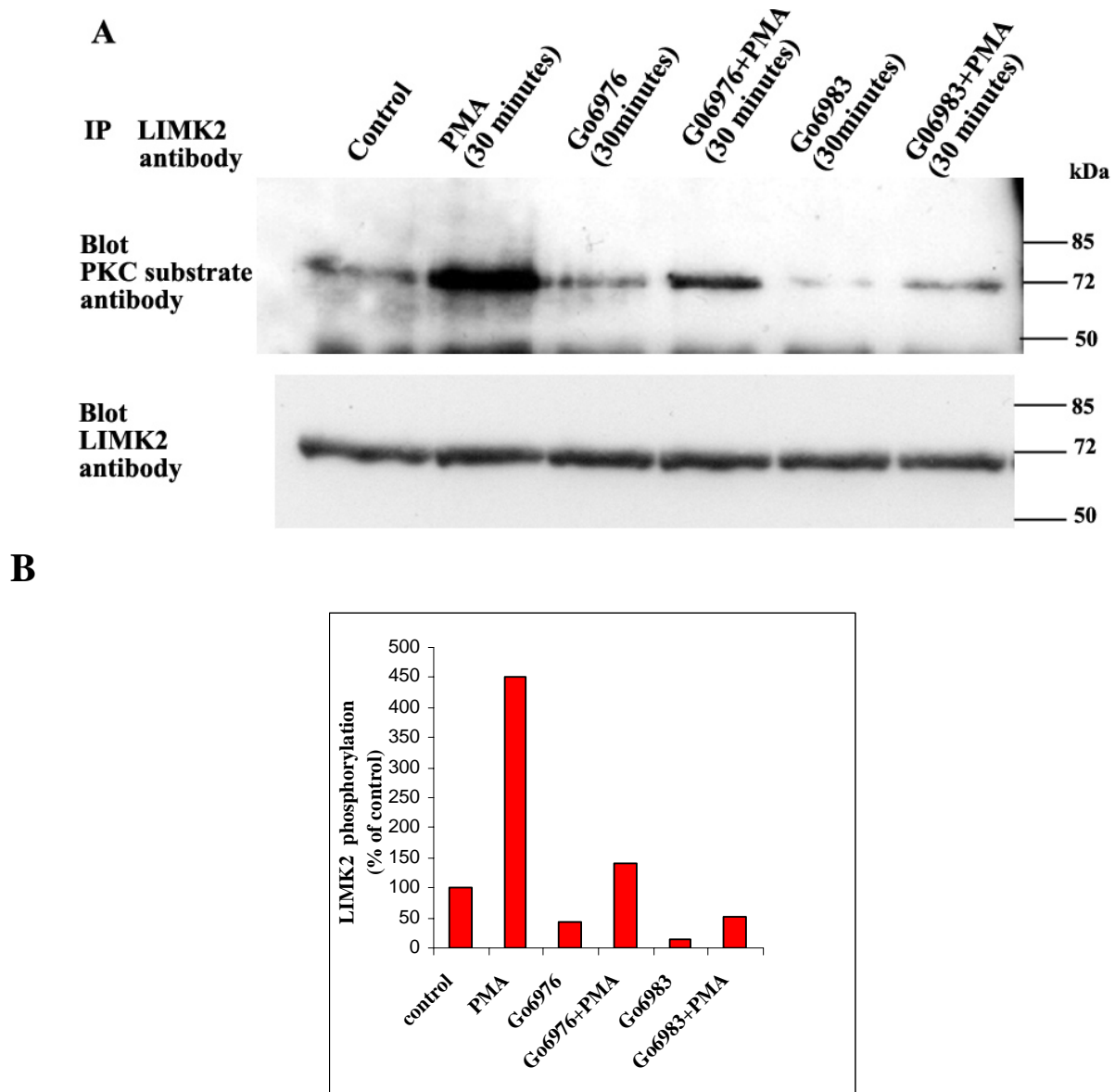


**Figure 4.21 PKC phosphorylates endogenous LIMK2 at position Ser283 in PMA-stimulated endothelial cells.** **A)** Cells were incubated at 37°C for 30 minutes with or without PKC-inhibitors (Go6983 500nM, Go6976 2µM) and then stimulated with PMA (200nM). LIMK2 in the endothelial cell lysates was immunoprecipitated with a specific anti-LIMK2 antibody. The LIMK2 immunoprecipitated samples were blotted against anti-phospho-Ser PKC substrate antibody and anti-LIMK2 antibody. **B)** Bar diagram of the densitometric analysis of the immunoblot.

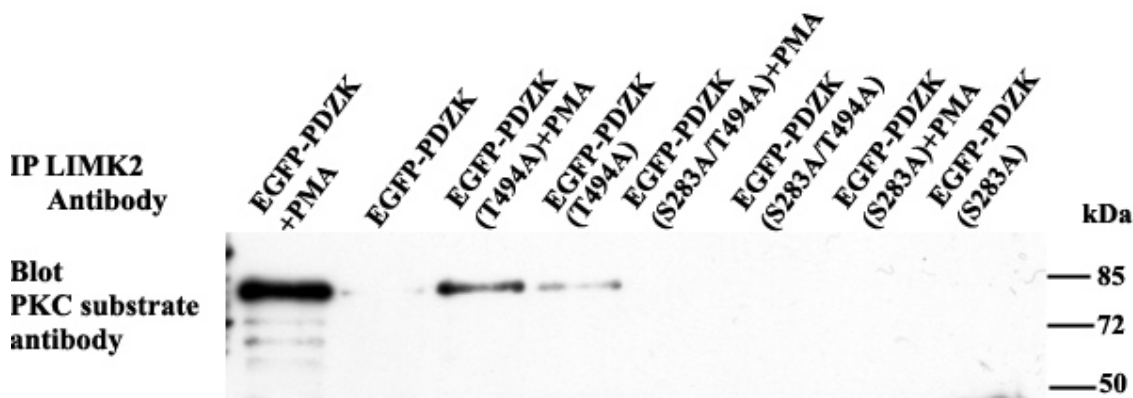


**Figure 4.22 Specificity of anti-phospho-Ser PKC substrate antibody.** Anti-phospho-Ser PKC substrate antibody recognized the EGFP-PDZK (lane 1 and 2), and threonine 494 mutated EGFP-PDZK proteins (lane 3 and 4) from both PMA treated and untreated cells. This antibody failed to recognize the protein in which Ser283 was mutated to alanine.

#### **4.5.4. PKC-mediated Ser283 phosphorylation inhibits the nuclear import of LIMK2**

In order to examine whether S283 phosphorylation is responsible for the translocation of LIMK2 from the nucleus to the cytoplasm in PMA activated cells, Ser283 was modified to either alanine (S283A) or to two glutamic acids (S283EE). Substitution of the phosphorylation site with two acidic amino acids (EE) mimics the phosphorylation of that site. LIMK2 constructs containing the S283EE mutation should be constitutively active, whereas constructs containing the S283A mutation should be inactive. The wild type EGFP-PDZK and EGFP-LIMK2 left the nucleus after PMA treatment (Figure 4.23 I, II and IV, V). After PMA stimulation of cells transfected with the S283A mutants of EGFP-PDZK and EGFP-LIMK2, the translocation of the recombinant mutant proteins to the cytoplasm was completely blocked (Figure 4.23 III, VI). In control cells, more EGFP-LIMK2 (S283A) (10%) was in the nucleus than the wild type LIMK2 (data not shown). In the cells transfected with the active S283EE mutants of EGFP-PDZK and EGFP-LIMK2, the proteins were completely localized in the cytoplasm similar to the PMA-stimulated cells (Figure 4.23B). These results indicate that PKC regulates the nucleocytoplasmic shuttling of LIMK2 in resting endothelial cells and in cells after PMA activation through phosphorylation of Ser283.

To investigate whether the S283 phosphorylation blocks the nuclear entry or accelerates the nuclear export, cells transfected with the S283EE mutant plasmid were treated with LMB. The nuclear accumulation of mutant EGFP-LIMK2 was drastically reduced (Figure 4.23B IV). More mutant EGFP-PDZK was in the nucleus and less in the cytoplasm as compared with the results of the mutant EGFP-LIMK2 (Figure 4.23B). As shown previously, wild type EGFP-LIMK2 and EGFP-PDZK accumulated in the nucleus completely in the presence of LMB. These results indicate that S283 phosphorylation inhibits nuclear accumulation of LIMK2 by reducing the rate of nuclear import of LIMK2 rather than by accelerating the nuclear export.

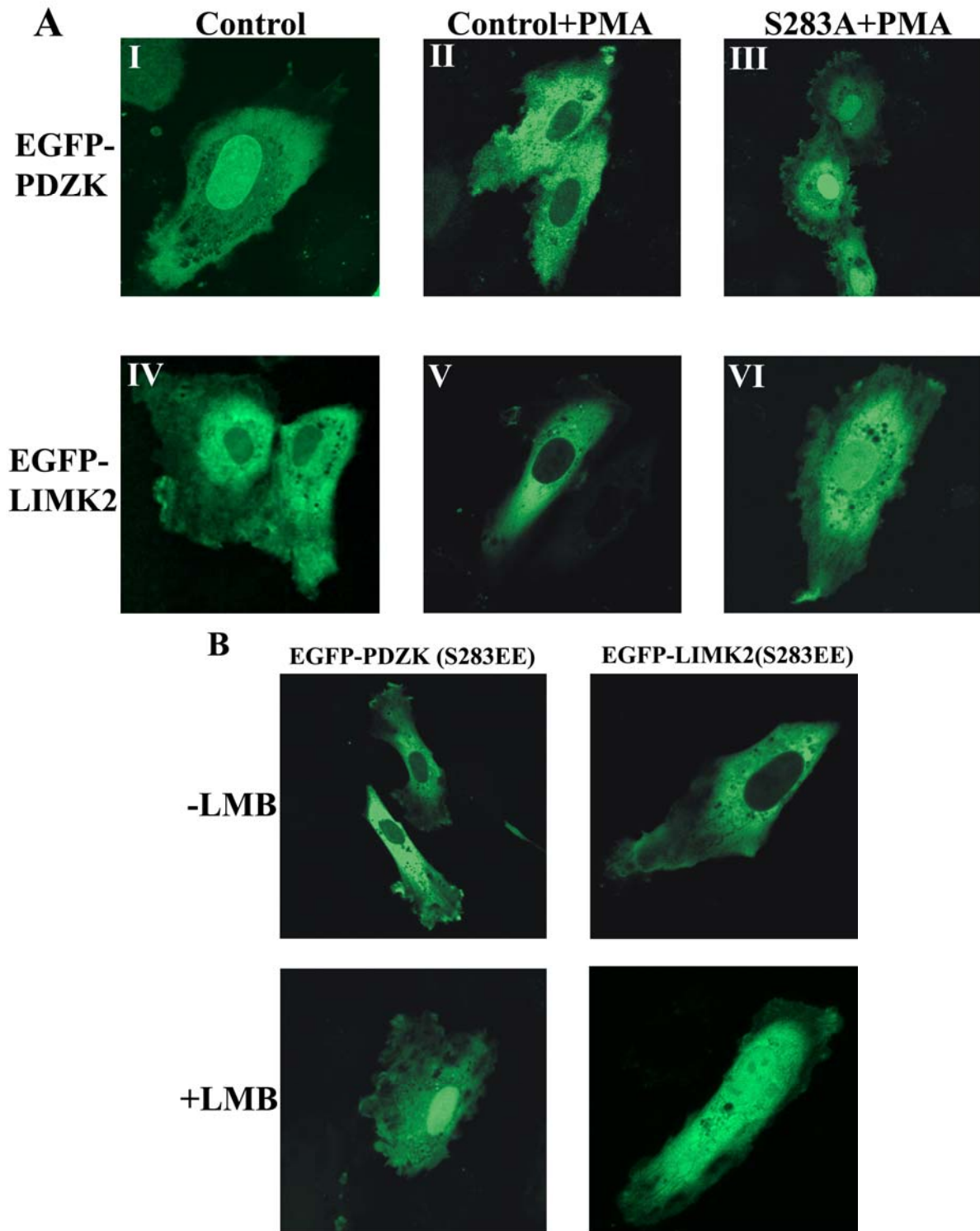


**Figure 4.23 Effect of S283 mutation on the nucleocytoplasmic shuttling of LIMK2.** The serine283 was either mutated to alanine (inactive mutation; **A** III and VI) or to two glutamic acids (active mutation; **B**). In cells transfected with the wild type EGFP-LIMK2 and EGFP-PDZK, the proteins leave the nucleus within 30 minutes of PMA treatment (II and V). S283A mutation of LIMK2 and PDZK stopped this translocation (III and VI). **B**) No nuclear localization of the active S283EE mutants of LIMK2 and PDZK was observed (III and VI). After LMB treatment (10ng/ml), the nuclear accumulation of these active mutants was reduced as compared to the results with the wild type of these constructs.

#### 4.5.5. Mutation analysis of the putative PKC phosphorylation site at Thr494 (siteII)

There is a putative second phosphorylation site by PKC: in LIMK2 at Thr494 (Table 4.2). To analyze the possible function of the phosphorylation of T494 *in vivo*, T494 was mutated to alanine (inactive mutant) or to two glutamic acids (active mutant). The T494A mutant of EGFP-PDZK was localized both in the nucleus and the cytoplasm of control cells (Figure 4.24A). After 40 minutes of PMA treatment, the T494A mutant protein was shifted to the cytoplasm similar to cells transfected with wild type EGFP-PDZK (Figure 4.24B compare with Figure 4.12). However, rate of translocation was slower than the wild type protein (30 minutes). These results suggest that the possible phosphorylation of Thr494 does not play major role in the inhibition of nuclear accumulation of EGFP-PDZK by PKC.

We also studied the sub-cellular distribution of the active mutant (T494EE) of EGFP-PDZK. LIMK2 might be also phosphorylated at this site. The results show that the active mutant of EGFP-PDZK is mainly localized in the cytoplasm not in the nucleus (Figure 4.24C) similar to the localization of S283EE mutant of EGFP-PDZK. After LMB treatment, only part of the active (T494EE) EGFP-PDZK mutant was in the nucleus. These results suggest that phosphorylation of LIMK2 at Thr494, if it was phosphorylated in endothelial cells, can also inhibit nuclear import.

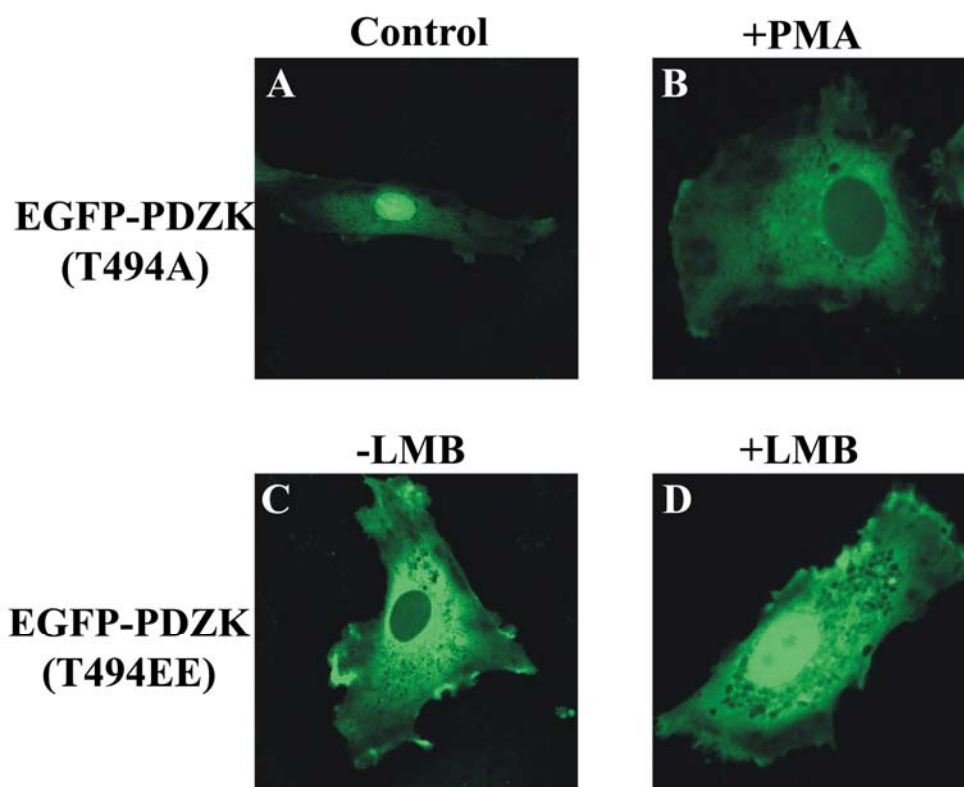


**Figure 4.24** The effect of Thr494 mutation on nucleocytoplasmic shuttling of EGFP-PDZK. Thr494 was mutated to alanine or two glutamic acids. The inactive mutant (T494A) of EGFP-PDZK was distributed both in nucleus and the cytoplasm (A), and shifted to the cytoplasm within 40 minutes of treatment with PMA (B). The active (T494EE) mutant of EGFP-PDZK was mainly localized in the cytoplasm of the control cells (C) and was partially localized in the nucleus after one hour of LMB treatment of endothelial cells.

#### **4.5.6. Phosphorylation of both Ser283 and Thr494 blocks the shuttling of LIMK2**

To study whether the phosphorylation of both PKC sites in LIMK2 (Ser283, Thr494) affects the sub-cellular distribution of LIMK2 more than the phosphorylation of one PKC site only, several double mutants of EGFP-PDZK and EGFP-LIMK2 were prepared. The S283A/T494EE (inactive/active) and the S283EE/T494A (active/inactive) mutants behaved similar to each other and to the single mutant proteins, T494EE and S283EE, respectively. The mutant proteins were found mainly in the cytoplasm (Figure 4.25A I, II) and did not completely accumulate in the nucleus after LMB treatment of the endothelial cells (Figure 4.25A IV, V). These results show that either one of the two sites reduce nuclear import of LIMK2 and regulate the nucleocytoplasmic shuttling.

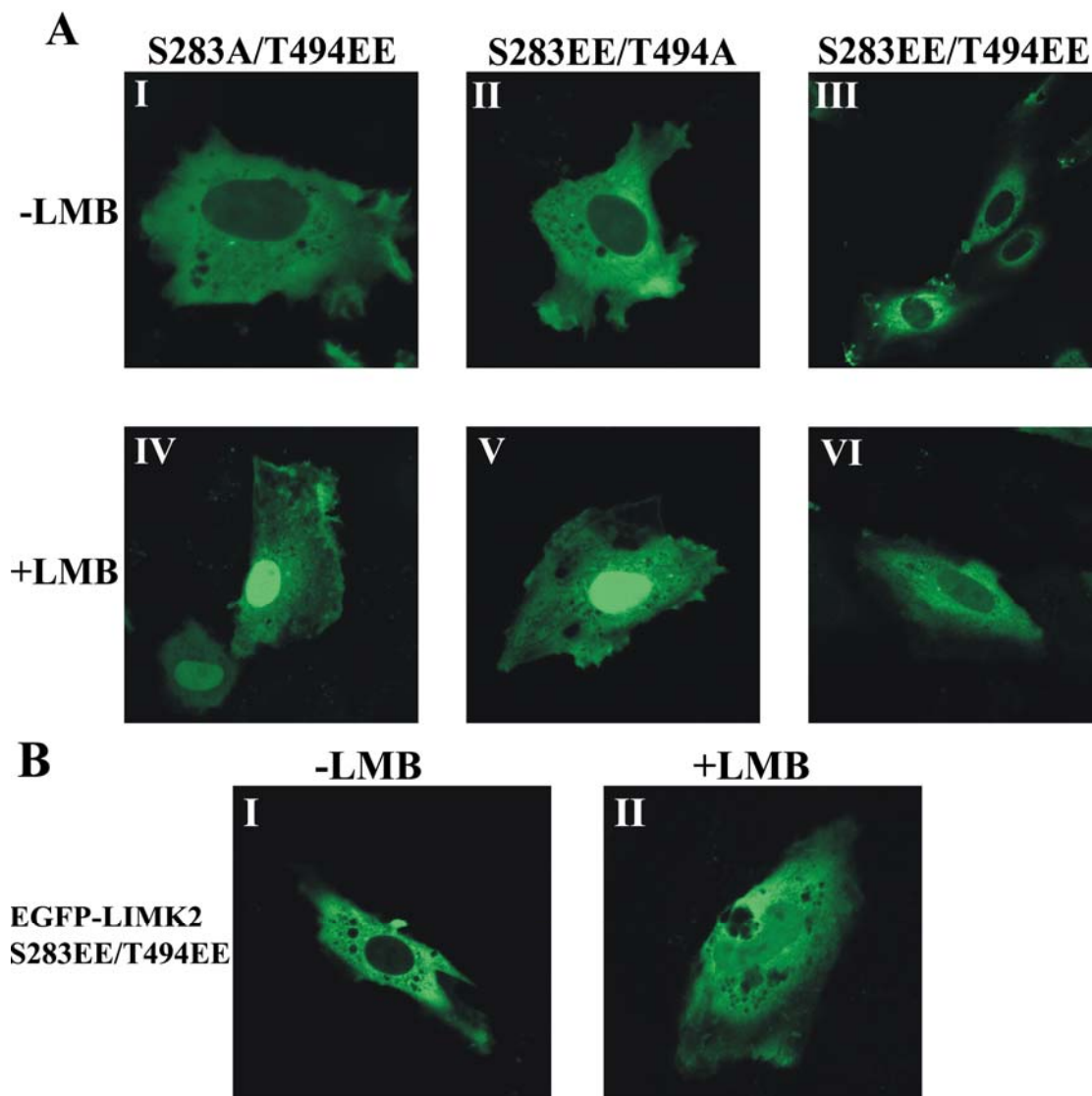


**Figure 4.25 Effect of double mutations of the two PKC sites on nucleocytoplasmic shuttling of LIMK2.** **A)** The S283A/T494EE and S283EE/T494A mutants of EGFP-PDZK mainly localized in the cytoplasm of the control cells (I and II). They partially accumulated in the nucleus after LMB treatment (IV and V). The mutant S283EE/T494EE of EGFP-PDZK was also mainly localized in the cytoplasm of the control cells (III), but failed to localize to the nucleus after LMB treatment (VI). **B)** The double mutant S283EE/T494EE of EGFP-LIMK2 was mainly localized in the cytoplasm, and after LMB treatment, did not accumulate in the nucleus

To analyze, whether phosphorylation of both sites inhibits the nuclear import completely, S283EE/T494EE double mutants of EGFP-PDZK and the EGFP-LIMK2 were prepared. S283EE/T494EE mutants of EGFP-PDZK and EGFP-LIMK2 were localized in the cytoplasm of control cells (Figure 4.25A III and Figure 4.25B I) and also after LMB treatment (Figure 4.24A, VI; Figure 4.24, II). These double active mutants were not able to enter into the nucleus. These results suggest that both PKC sites might be functional in LIMK2, and that the phosphorylation of both sites is more effective than the phosphorylation of only one site: it completely stopped LIMK2 of entering into the nucleus.

#### **4.6. PMA-induced activation of endothelial cells does not stimulate LIMK-mediated phosphorylation of cofilin**

PKC-induced phosphorylation of LIMK2 might affect the kinase activity of LIMK2 for two reasons: a) Ser283 phosphorylation might induce conformational change, b) the probable phosphorylation of Thr494 in the kinase domain is close the Thr505 in LIMK2 which is phosphorylated by Rho-kinase. Phosphorylation of Thr505 is known activate the kinase activity of LIMK2

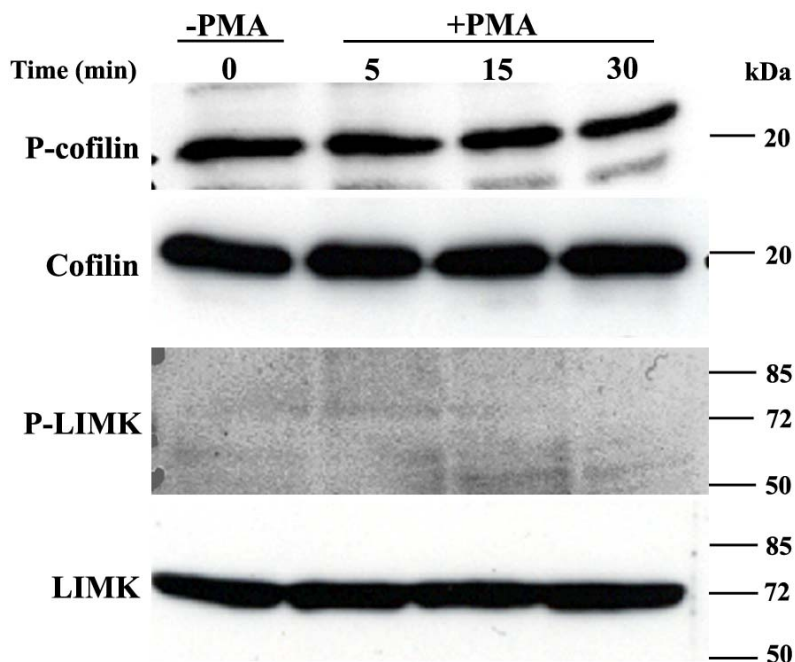


**Figure 4.26 Effect of PMA on cofilin phosphorylation in endothelial cells.** Endothelial cells were activated with PMA (200nM) and Cofilin phosphorylation was analyzed by at different time points by western blotting.

Endothelial cells were stimulated with PMA and LIMK-mediated phosphorylation of cofilin was measured. The results did not show a change of cofilin phosphorylation and also not of LIMK phosphorylation at Thr505 after PMA stimulation (Figure 4.26). Therefore the PKC mediated phosphorylation of LIMK2 affects the nucleocytoplasmic shuttling of LIMK2, but not its kinase activity.

## **5. Discussion**

### **5.1. Expression of LIMKs in endothelial cells**

Contraction, migration, and proliferation of vascular endothelial cells are essential features of vascular permeability, endothelial repair after injury, and angiogenesis (Folkman and Shing, 1992; Jackson et al., 1994), and regulated by coordinated changes of actin dynamics (Tang et al., 1997; van Nieuw Amerongen et al., 2003). The LIMK family of proteins, a member of the class of serine/threonine protein kinases, consists of LIMK1 and LIMK2 that specifically phosphorylate and inactivate cofilin, an actin-depolymerizing protein, thereby regulating actin cytoskeleton rearrangement (Arber et al., 1998; Yang et al., 1998b).

LIMK2 and as a recent study shows, also LIMK1 are ubiquitously expressed in mouse tissues (Foletta et al., 2004). The results from Unigene EST database also indicate that LIMK1 and LIMK2 are present in various tissues such as brain, placenta colon and different organ tumors. LIMK2 ESTs were also reported in various cell lines such as T cells, human lung epithelial cells. So far it has not been reported, which isoform of LIMKs is present in endothelial cells. By using RT-PCR and immunoblot, the present work demonstrates that both LIMK1 and LIMK2 are present in endothelial cells and monocytes (data not shown). However, only LIMK1 was present in platelets. In endothelial cells, an additional specific protein band of low molecular mass (~55kDa) was observed in anti-LIMK2 immunoblots. This result suggests that a low molecular mass splice variant of LIMK2 might be present in endothelial cells. Based on the AceView<sup>10</sup> database, eleven different isoforms of LIMK2 have been suggested to be present in human cells. A previous study has shown that LIMK2 has various splice isoforms in mouse tissues (Ikebe et al., 1997; Ikebe et al., 1998). The expression of LIMK2 isoforms is not yet reported in human, and the specific cellular distribution of human LIMK1 and LIMK2 is poorly studied. In the present study, only one type of endothelial cells (HUVECs) has been studied. It is possible that the expression of LIMK1, LIMK2 and their isoforms depends on the state of maturation of endothelial cells and their origin from different vascular beds. Endothelial cells in different vascular beds are heterogeneous. They show a highly different structure due to different gene expression and actin cytoskeleton rearrangement. For example, the brain and retina capillaries are lined by a layer of continuous endothelial cells connected by tight junctions that help to maintain the blood brain barrier.

---

<sup>10</sup> AceView offers an integrated view of the human, nematode and Arabidopsis genes reconstructed by alignment of all publicly available mRNAs and ESTs on the genome sequence. AceView carefully computes co-alignment and clustering of experimental cDNA data, no prediction is involved. The resulting AceView genes and their alternative variants are analyzed in terms of expression, intron-exon structure, and alternative features.

## **5.2. Thrombin-induced stress fiber formation is regulated by Rho-kinase/LIMK/cofilin pathway**

By using live cell imaging, the present study shows and confirms previous findings that thrombin induces stress fiber formation, ruffle formation and cell contraction in endothelial cells (Essler et al., 1998). This study also showed that cell-cell contacts were disrupted and F-actin fibers connecting two cells were broken after thrombin-stimulated endothelial cells. Increased permeability of endothelial monolayers results from both, disruption of tethering forces (arising from cell-cell junctions and cell-matrix interactions) and enhancement of cell retraction (Garcia et al., 1996; Lum and Malik, 1994).

Rho-like small GTPases such as Rho, Rac, and Cdc42 regulate actin dynamics in stimulated endothelial cells. Rho-kinase, a kinase downstream of Rho, plays a major role in thrombin-induced endothelial cell contraction (Goeckeler and Wysolmerski, 1995). In this study, activation of Rho-kinase in thrombin-stimulated endothelial cells was measured by a new approach; i.e. by quantifying the phosphorylation of the substrate MYPT on Thr696 or Thr853 (Hartshorne, 1998; Ito et al., 2004). The results show that MYPT phosphorylation was maximal 5 minutes after thrombin activation and decreased subsequently. This study also demonstrates that the Rho-kinase inhibitor Y27632 could completely block thrombin-stimulated MYPT phosphorylation, stress fiber formation, and cell contraction suggesting that thrombin-induced stress fiber formation and cell contraction is mediated by Rho-kinase activation. These results are consistent with the findings of previous studies, and demonstrate that thrombin induces stress fiber formation and cell rounding in endothelial cells via the Rho/Rho-kinase pathway.

The precise mechanism by which Rho-kinase regulates stress fiber formation in endothelial cells is unknown. Previous studies have shown that Rho-kinase in endothelial cells directly phosphorylates MYPT and inactivates myosin phosphatase, leading to an increase in myosin light chain phosphorylation (Essler et al., 1998). Phosphorylated myosin interacts with actin filaments, and develops actin-activated adenosine triphosphatase (ATPase) activity (Goeckeler and Wysolmerski, 1995). These properties of myosin are important for endothelial cell contraction, and may also be important for stress fiber formation. Based on transfection studies it has been proposed that Rho-kinase leads to LIMK activation and subsequent phosphorylation and inactivation of cofilin, resulting in the accumulation of actin filaments and stress fiber formation (Arber et al., 1998; Maekawa et al., 1999). In order to find out, whether in endothelial cells phosphorylation and inactivation of the actin depolymerizing protein cofilin was responsible for the F-actin increase and stress fiber formation, the LIM-kinase/cofilin pathway was analyzed in thrombin-stimulated endothelial cells.

This study showed that both LIMK1 and LIMK2 are present in endothelial cells. LIMK1 and/or LIMK2 were rapidly phosphorylated and the phosphorylation was maximal within 2 minutes after thrombin activation. Previous studies have reported that LIMKs are not only activated by

Rho-kinase, but can also be phosphorylated and activated by Rac-activated PAKs (p21 activated kinases)(Edwards et al., 1999). A previous study has however, shown that the Rac1 activity was inhibited in thrombin-activated endothelial cells (Vouret-Craviari et al., 2002). It was found in the present study that the specific Rho-kinase inhibitor Y-27632, which does not effect the activity of PAK, even at high concentrations (100 $\mu$ M) (Uehata et al., 1997), inhibited completely LIMK activation in thrombin-stimulated of endothelial cells. Therefore, LIMK phosphorylation in thrombin-stimulated endothelial cells was entirely dependent on Rho-kinase. Moreover the increase of cofilin phosphorylation in thrombin-stimulated endothelial cells was drastically decreased by pretreatment of the cells with Y27632. These results indicate that in thrombin-stimulated endothelial cells cofilin phosphorylation and inactivation is regulated by Rho-kinase mediated LIM-kinase activation.

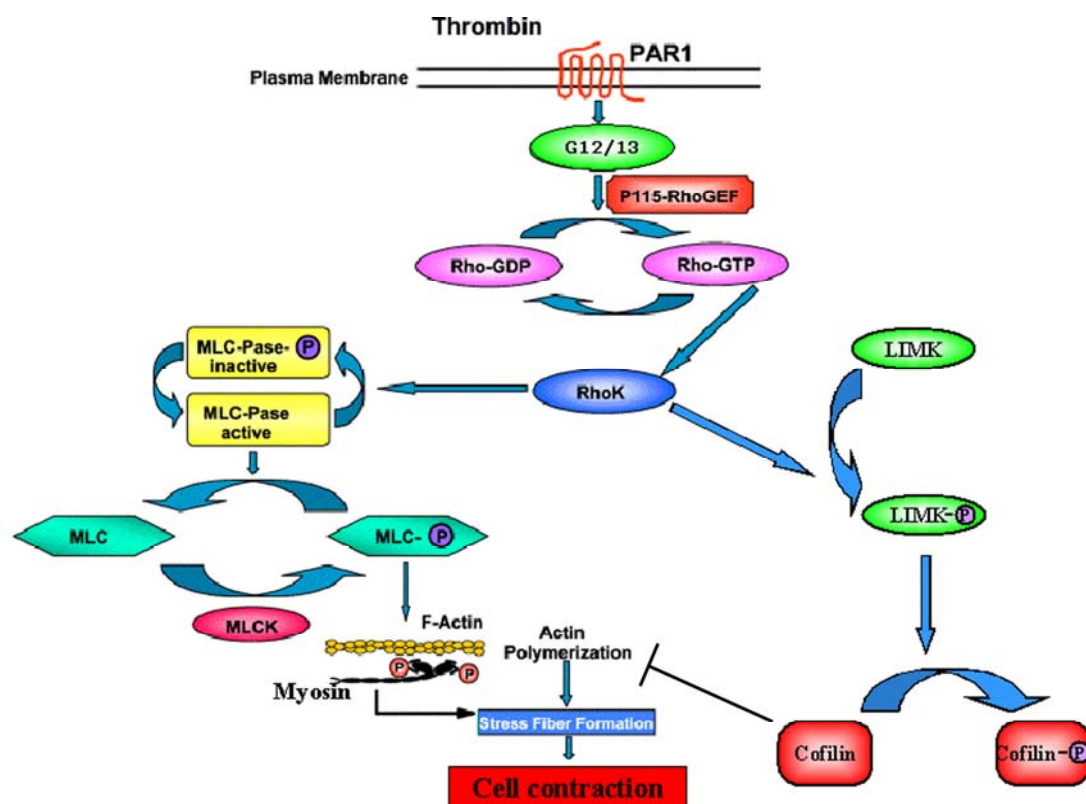


**Figure 5.1** Proposed schema of Rho-kinase/LIMK/cofilin mediated stress fiber formation in thrombin-activated endothelial cells.

To analyze more directly the role of LIMKs in stress fiber formation, a kinase inactive mutant (D451A) of LIMK2 was transfected into endothelial cells. This mutant binds to cofilin and inhibits cofilin phosphorylation by endogenous LIMKs. Stress fiber formation was blocked in these cells transfected with the dominant negative mutant of LIMK2, indicating that LIMKs play an essential role in stress fiber formation.

Together these results show that the Rho-kinase/LIMK/cofilin pathway is activated in thrombin-stimulated endothelial cells and that this pathway plays -together with the Rho-kinase/MLC-Pase/MLC phosphorylation pathway- a central role in stress fiber formation (see Figure 5.1).

### **5.3. Primary sequence analysis of LIMK**

Computational analysis of the primary sequence of a protein is a powerful method to predict the regulation of the protein function. It has been shown that the kinase domain of LIMKs has a unique basic sequence inserted between subdomain VII and VIII. The basic nature of this motif suggests a functional nuclear localization signal present in LIMKs. Of the two types of NLSs known, a monopartite NLS consists of a single short stretch of consecutive basic amino acids, like in SV40 large T-antigen (PKKKRKV), and a bipartite NLS comprises two clusters of basic amino acids separated by a 10-12-amino acid spacer, like in nucleoplasmin (KRPAATKKAGQAKKKKLDK) (Mattaj and Englmeier, 1998). Based on homology searches with NLS containing proteins and by software analysis, this study demonstrates that LIMK2 has a NLS sequence different than LIMK1. LIMK2 has three predicted NLS: one monopartite NLS (NLS1) and two bipartite NLS (NLS2, NLS3). In contrast, LIMK1 has only one monopartite NLS. This difference suggests a different mode of regulation of nuclear localization of LIMK2 and LIMK1.

Concerning the nuclear export of LIMKs, a previous study showed two leucine rich NES sequences C-terminal of the PDZ domain of LIMK1 (Yang and Mizuno, 1999). These leucine rich NES-containing proteins are exported from the nucleus by CRM1/exportin 1 (Fornerod et al., 1997). By searching homologies with NES containing proteins, two CRM1 binding NES sequences were predicted in LIMK2: one was C-terminal of the PDZ domain and the other was present immediately after the PDZ domain. These findings indicate that both LIMKs contain the signals to shuttle between the nucleus and the cytoplasm. Since LIMK1 and LIMK2 show differences in their nuclear export and import signal sequences, the two enzymes may have a different mode of regulation of nucleocytoplasmic shuttling.

Primary sequence analysis also indicated that LIMKs have a Ser/Pro-rich region between the PDZ and the kinase domain. After extensive analysis of this region, the results show that these regions are intrinsically disordered. An additional disordered region was found in the kinase domain of LIMK2, but not in LIMK1. Proteins with intrinsically unstructured regions are frequently involved in specific cell processes such as transcriptional activation, cell-cycle regulation, membrane transport, molecular recognition and signaling (Wright and Dyson, 1999). Post-translational modifications such as phosphorylation occur often in disordered regions and then lead to transition into an ordered conformation thereby regulating the function of these proteins (Dunker et al., 2001; Tompa, 2002). Both LIMKs have many serine residues in the region between the PDZ domain and the kinase domain. The disordered region in the kinase domain of LIMK2, but not LIMK1 has many threonine residues. These amino acids are potential targets for phosphorylation. Indeed this study demonstrates that LIMK2, but not LIMK1 has two potential PKC phosphorylation sites: one is present between the PDZ and the kinase domain (Ser283, site I); the other is in the kinase domain (Thr494, site II). The primary sequence analysis

suggested a unique subcellular distribution of LIMK2 and a unique mechanism of regulation of nucleocytoplasmic shuttling of LIMK2.

#### **5.4. Nucleocytoplasmic shuttling of LIMKs**

Previous reports have shown that both LIMK1 and LIMK2 are present mainly in the cytoplasm, but also in the nucleus of cell lines such as NIH3T3, and mouse embryonic fibroblast cells, indicating that the NLS and NES sequences in these enzymes are functional (Foletta et al., 2004; Roovers et al., 2003). Indeed, after blocking the CRM1-dependent export with LMB, LIMK1 was predominantly localized in the nucleus indicating that it shuttles between the nucleus and the cytoplasm (Roovers et al., 2003; Yang and Mizuno, 1999). The present study shows that LIMK2 similar to LIMK1 is also present mainly in the cytoplasm and less in the nucleus of endothelial cells. We observed that LIMK2 was completely shifted to the nucleus after treatment of endothelial cells with LMB. This indicates the existence of functional NES and NLS in LIMK2 and also, that LIMK2 is exported via the CRM1-dependent nuclear export pathway.

In order to directly visualize the nucleocytoplasmic shuttling of the PDZK construct of LIMK2, photobleaching experiments (FRAP and FLIP) were carried out. FRAP analysis indicated that EGFP-PDZK continuously entered the nucleus and has a functional NLS. The shape of the recovery curve (recovery of the fluorescence in the nucleus) is of complex type (Periasamy and Verkman, 1998). This can occur when a molecule undergoes binding and release from intracellular components, or exists as monomer and multimer. The PDZ domain generally functions as a protein-protein interacting domain (see Introduction for details), and the PDZ-kinase domain of LIMK2 might interact with other proteins in the cytoplasm and the nucleus. To analyze the export of the EGFP-PDZK in endothelial cells, the photobleaching technique FLIP was used. After cytoplasmic photobleaching, the nuclear fluorescence gradually decreased with time. This result shows that the EGFP-PDZK protein was continuously exported from the nucleus to the cytoplasm indicating the presence of functional NES in LIMK2.

#### **5.5. Subcellular distribution of LIMKs and their domains**

In mouse tissues, various isoforms of LIMK2 showing a unique sub-cellular distribution have been reported (Ikebe et al., 1998; Nunoue et al., 1995). LIMK2a (full length LIMK2) and LIMK2b (LIM1 domain deleted) were mainly found in the cytoplasm. The main LIMK2 isoform is tLIMK2, which lacks both LIM domains and is found mainly in the nucleus. The subcellular distribution of different domains of LIMK2 is not reported yet. This study shows that the full length LIMK2,  $\Delta$ LIM1-LIMK2 (LIM1 deleted, similar to LIMK2b) and  $\Delta$ LIM2-LIMK2 (LIM2 domain deleted) were mainly found in the cytoplasm. Deletion of both LIM domains (the PDZ-kinase construct, similar to tLIMK2) drastically enhanced the nuclear localization of LIMK2. In

contrast, deletion of both LIM domains of LIMK1 did not change its subcellular distribution: the PDZ-kinase construct of LIMK1 remained in the cytoplasm. These results demonstrate that the sub-cellular distribution of LIMK1 and LIMK2 is regulated differentially in endothelial cells. Studies from different groups demonstrated that the LIM domains of LIMK1 interact with the kinase domain, and that the LIM2 domain regulates its kinase activity (Edwards and Gill, 1999; Hiraoka et al., 1996). Our results suggest that the LIM domains bind to the kinase domain of LIMK2 and LIMK1 differently, masking the NLS of LIMK2 but not LIMK1.

The kinase domain of LIMKs has NLS sequences, but no NES, suggesting a nuclear localization of the kinase domain. Indeed, the kinase domain of both LIMK1 and LIMK2 was present mainly in the nucleus. The nuclear localization of the kinase domain of LIMK2 was higher than the kinase domain of LIMK1. The three NLS sequences of LIMK2 in the kinase domain seem to have higher binding affinity with importin- $\alpha$  than the one NLS in the kinase domain of LIMK1.

Interestingly, the kinase domain of LIMK2 but not LIMK1 was also present in the nucleolus suggesting a unique function of LIMK2 in this nuclear organelle. Unlike the nucleus and other membrane-bound organelles, there is no physical barrier between the nucleolus and the surrounding nucleoplasm. In principle any soluble protein should be able to diffuse in and out of the nucleoli. However, it has also become clear that many proteins that localize to the nucleolus typically possess a NoLS motif, and the NoLS usually overlaps with the NLS (Kubota et al., 1999). This indicates that the basic amino acid-rich motif of LIMK2 may also function as a nucleolar localization signal (see section 5.6).

The  $\Delta$ kinase-LIMK2 construct (kinase domain deleted) was exclusively present in the cytoplasm indicating the presence of functional NES. After LMB treatment of the cells, this construct was enriched in the nucleus but not in the nucleolus. This may be due to the presence of another NLS outside of the kinase domain. Indeed, a further basic amino acid cluster was found between the PDZ and kinase domain of LIMK2 (amino acids 280-286) which could be a monopartite NLS. However, site directed mutational analysis indicate that this possible monopartite NLS is not functional since the mutant protein behaved similar to the wild type protein after LMB treatment of endothelial cells. Another explanation for the presence of the  $\Delta$ kinase-LIMK2 construct in the nucleus after LMB treatment of the endothelial cells is that this construct may enter the nucleus by diffusion due to its low molecular mass (60kDa) after inactivation of CRM1 dependent export.

## **5.6. Identification of functional NoLS and NLS in LIMK2**

Based on the primary sequence analysis 3 types of NLS sequences were predicted in the kinase domain of LIMK2. In this study, site directed mutagenesis was used to identify key amino acid residues involved in the nuclear and nucleolar import of LIMK2. Mutation of either one of the cluster of basic amino acids RKKR (amino acids 500-503), RK (amino acids 496-497), or KKR (amino acids 491-493) to alanine indicates that each of these clusters is important for nucleolar

localization. The basic amino acids RKR (amino acids 480-482) did not play a significant role in nucleolar localization. These results identify the 13 amino acids (491-503) motif in LIMK2 containing three clusters of basic amino acids as the functional nucleolar localization signal. Analysis of the protein composition of the nucleolus in other studies did not lead to the identification of a general nucleolar localization signal (Andersen et al., 2002; Dundr and Misteli, 2002; Leung et al., 2003). Nucleolar localizing properties of eukaryotic proteins were apparently due to cooperation of several domains of the protein suggesting a complex regulation of nucleolar localization (Michael and Dreyfuss, 1996; Russo et al., 1997; Schmidt-Zachmann and Nigg, 1993). However, small NoLS sequence motifs have been identified mainly in retroviral RNA binding trans-regulator proteins. Aligning the LIMK2 NoLS with the published NoLS sequences (generally 20-40 amino acids long) (Guo et al., 2003; Horke et al., 2004; Kubota et al., 1999) revealed that all these sequences retain continuous stretches of basic residues: either one continuous stretch of three to four basic residues, or one to three stretches of three to four basic residues interrupted by one non basic residue (Table 5.1).

In some studies, it has been shown that mutation of one of these basic amino acid-rich clusters inhibited the nucleolar localization of the protein (Guo et al., 2003). In these NoLS motifs, I noted that the sequences between the basic amino acid clusters were rich in hydrophilic amino acids. However, each of these basic amino acids clusters was important, but not sufficient for nucleolar localization of the protein. The whole NoLS as shown in Table 5.1 was needed. The NoLSs described in these proteins may be regarded as members of the “compact NoLS family”.

What might be the partner in the nucleolus interacting with these compact NoLS sequences? Nucleolar localization can be accomplished by three different types of interactions: a) with nucleolar or nucleolar-associated proteins, b) with rDNA and c) with nucleolar RNA consisting mainly rRNA (Carmo-Fonseca et al., 2000; Shaw and Jordan, 1995). LIMK2 should follow one of these mechanisms to enter the nucleolus. It is hypothesized that the kinase domain of LIMK2 binds with rRNA. Arginine/lysine-rich RNA-binding domains are found in many viral proteins (Bartel et al., 1991; Dingwall et al., 1989; Lazinski et al., 1989; Slice et al., 1992). These proteins have a similar pattern of arginine distribution as in LIMK2 suggesting the binding of LIMK2 with rRNA (Table 5.2). The binding of proteins to rRNA in the nucleolus is known to regulate ribosome biogenesis necessary for cell division and transcription (Gerbi et al., 2003; Leung and Lamond, 2003).

Protein	Sequence
Werner, 1027-1058	FLVEVSRYNKFMKICALT <b>KKGR</b> NWLHKANTES
Nucleolin, 691-714	FRGGRGGGGGGGDFKPGQ <b>KKTKFR</b>
La, 323-354	QESLNKWKSK <b>RRFK</b> GKGKGNKAAQPGSGK GK
L5, 240-271	<b>YKKAH</b> AAIRENPVYE <b>KKPKKEVKKKR</b> WNRPKM
IGF-I, 161-195	GTEASLQI <b>RGKKKE</b> QRREIGSRNAECRNAECRG <b>KKGK</b>
HIV-1 Rev, 35-50	RQARRN <b>RRRR</b> WRERQR
HTLV-I Rex; 2-19	PKRT <b>RRRPRRSQRKR</b> PPTP
LIMK2, 491-503	<b>KKRTLKNDRKKR</b>

**Table 5.1** Sequence alignment NoLS sequences of different human and viral proteins with LIMK2 NoLS sequence. Clusters of basic amino acids are highlighted in red.

Protein	Arginine/Lysine-rich RNA-binding motif
P120	<b>KRLSSRAKRAAKRRLG</b>
HIV Rev	TRQA <b>RRNRRRR</b> WRERQ
HIV Tat	ALGISYGR <b>KKRRQRRR</b> P
$\lambda$ N	MDAQT <b>RRREERRA</b> EKQAQW
$\phi$ 21N	GTAKSRYKA <b>RA</b> ELIAER
P22N	GNAKT <b>RRHERRRK</b> LAIER
LIMK2	<b>KKRTLKNDRKKR</b>

**Table 5.2** Comparison of the Arginine/Lysine-rich RNA-binding domains of different proteins with the NoLS sequence of LIMK2.

The present study also identified the functional NLS of LIMK2. Based on the mutational analysis of EGFP-kinase and EGFP-PDZ-kinase, it is shown that the NLS2 containing the NLS1 (amino acids 491-503), but not the NLS3 is the functional NLS in LIMK2. When all the basic amino acids of NLS1 or NLS2 in PDZ-kinase were mutated to alanine, the mutated proteins were mainly in the cytoplasm. PDZ-kinase mutated at NLS2 was unable to enter the nucleus after LMB treatment. Mutational analysis of the kinase domain also showed that NLS2 containing NLS1 and RK (amino acids 496-497) are important for nuclear localization.

The functional NLS of LIMK2 (amino acids 491-503) is not the classical bipartite type NLS. It contains additional two basic amino acids within the sequence of 6 amino acids that separates the two clusters of basic amino acids, demonstrating a unique type of NLS.

### **5.7. Regulation of nucleocytoplasmic shuttling of LIMK2 by PKC dependent phosphorylation**

The results so far demonstrate that LIMK2 constitutively shuttles between the nucleus and the cytoplasm in resting endothelial cells. The nucleocytoplasmic shuttling is often regulated in response to specific cellular signals and influenced directly by posttranslational modifications such as phosphorylation of the cargo proteins (Kaffman and Shea, 1999). Phosphorylation often regulates the nuclear import of NLS cargo proteins by inhibiting the interaction of the cargo with the classic nuclear transport receptor importin- $\alpha$  (Harreman et al., 2004). Moreover, it has been shown that many nucleocytoplasmic shuttling proteins such as DAG kinase  $\zeta$ , Ca<sup>2+</sup>/calmodulin-dependent protein kinase II, NF- $\kappa$ B, and NF-AT contain a phosphorylation site within or adjacent to the NLS sequence, and that the phosphorylation of this site regulates nuclear localization of these proteins (Heist et al., 1998; Kaffman and O'Shea, 1999; Topham et al., 1998).

Is nuclear transport of LIMK also regulated by phosphorylation? Only one phosphorylation site (Thr505/508) was previously reported in LIMKs, which is present very near the predicted nuclear localization signal. Previous studies showed that phosphorylation of Thr505 (LIMK2) or Thr508 (LIMK1) is involved in the activation of the LIMKs, but did not affect their subcellular localization (Roovers et al., 2003; Sumi et al., 2001a).

We predicted two potential PKC phosphorylation sites in LIMK2, one at Ser283 between the PDZ and the kinase domain, and the other at Thr494 in the kinase domain, near to the predicted NLS. These sites were absent in the same homologous region of LIMK1 suggesting that only LIMK2 but not LIMK1 may be regulated by PKC. Indeed, activation of PKC by PMA stimulated the translocation of LIMK2 and the PDZ-kinase construct of LIMK2 (PDZK) from the nucleus to the cytoplasm. However, no change in the sub-cellular localization of the kinase domain of LIMK2 was observed after PMA stimulation of endothelial cells. This differential regulation of the PDZK constructs and the kinase domain of LIMK2 suggests that PKC regulates the nucleocytoplasmic shuttling of LIMK2 most probably by phosphorylation of Ser283 (present between the PDZ and the kinase domain) and not Thr494 (present in the kinase domain). We found indeed that PKC phosphorylated LIMK2 at Ser283. This was shown for the endogenous LIMK2 in endothelial cells as well as for the transfected EGFP-LIMK2 constructs. The experiments with isoform specific PKC inhibitors indicate that PKC- $\alpha$  and PKC- $\beta$  are the major PKC isoforms that regulate the translocation of LIMK2 from the nucleus to the cytoplasm.

Due to unavailability of a specific phospho-Thr PKC substrate peptide antibody, it could not be determined whether the second potential PKC phosphorylation site at Thr494 was also phosphorylated by PKC. The subcellular distribution of the kinase domain of LIMK2 was not affected by PMA treatment indicating that Thr494 may not be essential for translocation of LIMK2 from the nucleus to the cytoplasm after PKC activation.

To gain further insight into the relative importance of PKC mediated phosphorylation of the two sites in LIMK2, active and inactive mutations were introduced into the PDZ-kinase construct and the full length LIMK2. The inactive S283A mutant of PDZ-kinase did not accumulate in the cytoplasm after PMA treatment, whereas the T494A mutant of PDZ-kinase behaved similarly to the wild type PDZ-kinase: it still accumulated in the cytoplasm after PMA treatment, but at a slower rate. These results indicate that phosphorylation of Ser283 is necessary for the PMA-induced translocation of LIMK2 from the nucleus to the cytoplasm. However, phosphorylation of Thr494 is not needed, but may be involved in the nucleocytoplasmic shuttling of LIMK2.

The results with PDZK and LIMK2 constructs containing the active mutant (S283EE) mimicking serine phosphorylation were the same as after PMA treatment of endothelial cells: the mutant proteins were not in the nucleus but in the cytoplasm in resting endothelial cells. Constitutive phosphorylation of Ser283 may either stimulate nuclear export or inhibit the nuclear import of LIMK2. To study these two possibilities further, the cells transfected with the S283EE mutant were treated with LMB, which inhibits nuclear export. The nuclear localization of the mutant proteins (PDZ-kinase, LIMK2) was highly reduced after LMB treatment, indicating that Ser283 phosphorylation by PKC indeed partially inhibits the nuclear import of LIMK2. Surprisingly the T494EE mutant protein was also mainly localized in the cytoplasm; similar to the mutant S283EE. After LMB treatment the nuclear localization of T494EE mutant was also highly reduced suggesting that phosphorylation of this site might also partially inhibit the nuclear import of LIMK2.

To explain these results, the following hypothesis is made: the NES and NLS are partially masked in the PDZ-kinase domain of LIMK2 leading to equal distribution of the protein in the cytoplasm and the nucleus of resting cells. In the first step after PMA induced PKC activation, Ser283 phosphorylation by PKC leads to a conformational change of the protein, which makes the NES fully accessible to the CRM1 export receptor and/or inhibits the NLS indirectly. The rate of export of LIMK2 from the nucleus to the cytoplasm would be increased. In the second step, the Thr494 site in the NLS is accessible for PKC, and phosphorylation of this site, located in the NLS of LIMK2, inhibits directly its interaction with importin- $\alpha$ .

To further test this hypothesis, double mutants of both sites were studied. In active single mutants (S283EE, T494EE), the possibility of basal phosphorylation and the contribution of the other site cannot be ruled out. To eliminate this possibility, S283EE/T494A and T494EE/S283A double mutant proteins (active/inactive) were studied. These proteins behaved similar to the single active mutants of the same site. However, the S283EE/T494EE double active mutant remained completely in the cytoplasm after LMB treatment. These results suggest that the two phosphorylation sites are functional and by completing each other may affect nuclear import through different mechanism. Ser283 phosphorylation might through conformational change partially mask the NLS and inhibit nuclear import indirectly, whereas Thr494 phosphorylation

might directly inhibit NLS binding to importin- $\alpha$ . Phosphorylation of both the sites is required to block the nuclear import of LIMK2 completely.

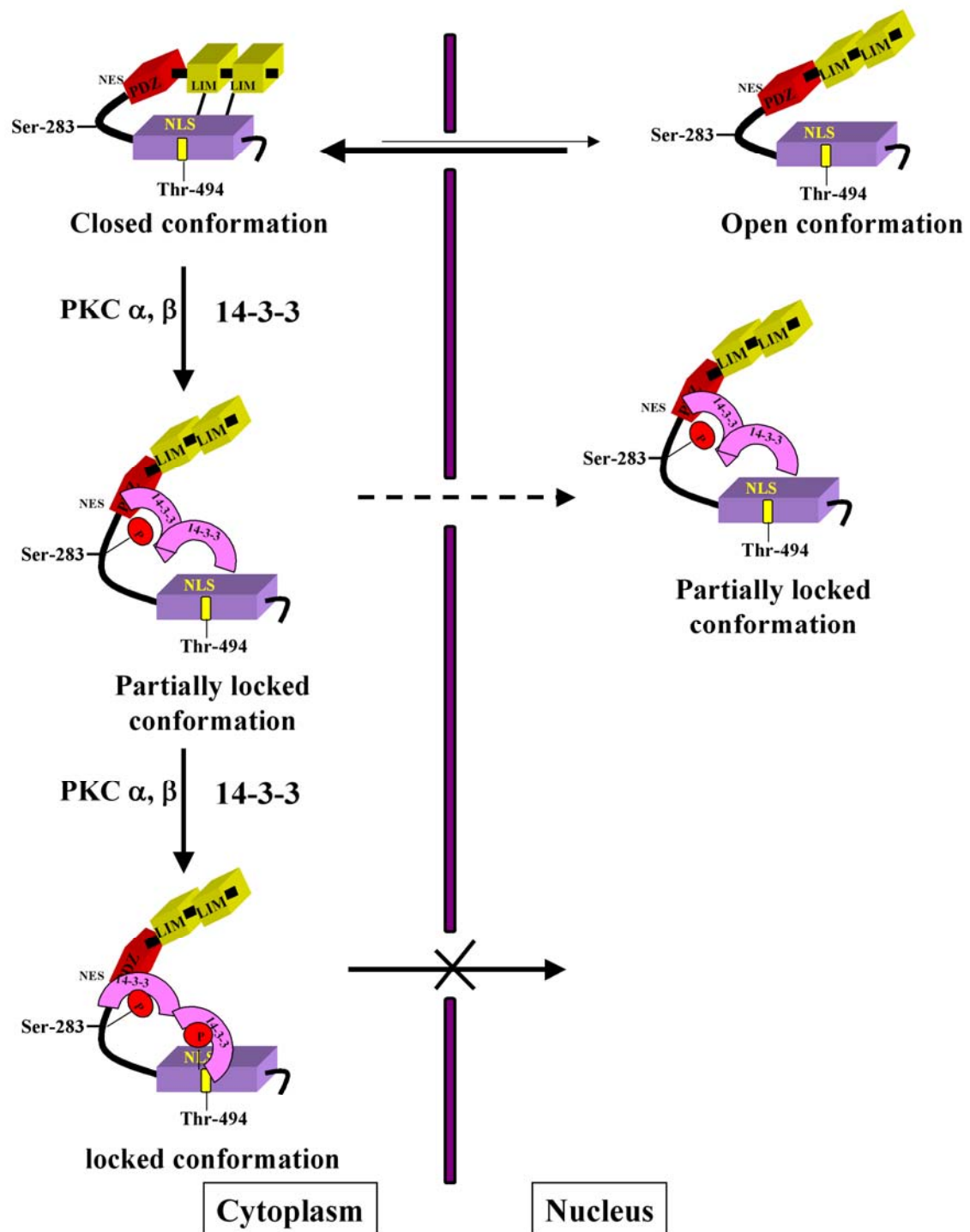


**Figure 5.2** Proposed model of the regulation of nucleocytoplasmic shuttling of LIMK2. See text for details.

14-3-3 is a protein which binds to pSer/pThr motifs present in many target proteins and modulates their subcellular localization by interfering with the function of nearby targeting sequences such as NES and NLS. Various nucleocytoplasmic shuttling proteins such as CDC25, and transcription factors such as FKHL1, are phosphorylated at Ser/Thr present near or in the NLS sequences binds to with 14-3-3. These proteins are localized mainly in the cytoplasm after

phosphorylation (Muslin and Xing, 2000). It has been reported that LIMK1 can interact with 14-3-3 (Birkenfeld et al., 2003). 14-3-3 binds as a dimer to proteins containing the consensus sequences a) R(S/Ar)XpSXP, b) RX(Ar/S)XpSXP and, c) RX<sub>1-2</sub>pSX<sub>2-3</sub>S in which pS denotes pSer/pThr and Ar denotes aromatic residues (Fu et al., 2000; Muslin et al., 1996; Yaffe et al., 1997). LIMK2 at Ser283 has the same consensus sequence of 14-3-3 binding as in c): (RRRpS<sup>283</sup>LRRS). This result suggests that 14-3-3 could bind to LIMK2 after phosphorylation at Ser283. This binding may inhibit the NLS function partially.

Based on these findings and considerations the following model of regulation of nucleocytoplasmic shuttling of LIMK2 by PKC is proposed. (Figure 5.2):

LIMK2 adopts a close conformation in resting cells and the LIM domains interact with the kinase domain thereby masking the NLS and keeping the protein mainly in the cytoplasm. PDZ-kinase (similar to the tLIMK2 isoform in mice) is more localized in the nucleus, due to lack of inhibition of the NLS by LIM domains. Activation of PKC induces phosphorylation of LIMK2 at Ser283 causing the binding of 14-3-3 to this site. This results in a partially locked conformation of LIMK2 with partial inhibition of NLS. PKC then phosphorylates LIMK2 at Thr494 and 14-3-3 also binds to this site. The binding of 14-3-3 as a dimer locks the LIMK2 conformation and inhibits completely the binding of NLS to importin- $\alpha$ . LIMK2 in this locked conformation cannot enter the nucleus and is found completely in the cytoplasm.

## **5.8. Possible nuclear function of LIMK2**

What is the possible function of LIMK2 in the nucleus? Nucleocytoplasmic shuttling of LIMK2 in resting endothelial cells and its regulation by PKC mediated phosphorylation suggests that LIMK2 might have a function in the nucleus.

It has been suggested that nuclear actin plays an important role in some nuclear functions, such as RNA transcription, RNA splicing, chromosome condensation, and chromatin remodeling (Bettinger et al., 2004; Percipalle et al., 2003; Rando et al., 2000), all of which are essential for cell survival and mitotic or meiotic division. Under conditions of cellular stress such as heat, DMSO treatment, cofilin migrates into the nucleus and forms rod like inclusions with associated actin, and such nuclear accumulation of cofilin is inhibited by phosphorylation (Bamburg, 1999). Therefore, the LIMK-cofilin system-mediated actin cytoskeleton dynamics may play a crucial role in the formation and proper function of nuclear processes. Utilizing the *Xenopus* oocyte system, it has been demonstrated that ectopic expression of LIMK1 in the nucleus clearly impaired progression of the meiotic process (oogenesis), such as organization, maintenance, and migration of specific meiotic spindle precursors (Takahashi et al., 2002). In the *Drosophila* mutant *twinstar* (*tsr*, the gene encoding *Drosophila* cofilin), migration and separation of centrosomes were severely impaired in spermatocytes because of an unusual accumulation of actin at this site (Gunsalus et al., 1995). These studies strongly demonstrated that the LIMK and

cofilin-mediated actin cytoskeleton dynamics might be a key component of gametogenesis, and abnormalities in the LIMK-cofilin system and could contribute to infertility in humans.

Furthermore, it has been demonstrated that cell cycle progression depends on the regulated activity of the LIMK-cofilin system. In HeLa cells, LIMK1 became hyperphosphorylated during prometaphase and metaphase (Amano et al., 2002; Sumi et al., 2002). Cofilin phosphorylation also peaked during this period. Both LIMK1 and cofilin phosphorylation declined to interphase levels, as cells entered the telophase and began cytokinesis. Furthermore, LIMK1 activation during mitosis is abrogated by cyclin-dependent kinase (CDK) inhibitors, suggesting that activation of CDKs directly or indirectly participates in LIMK1 activation (Sumi et al., 2002).

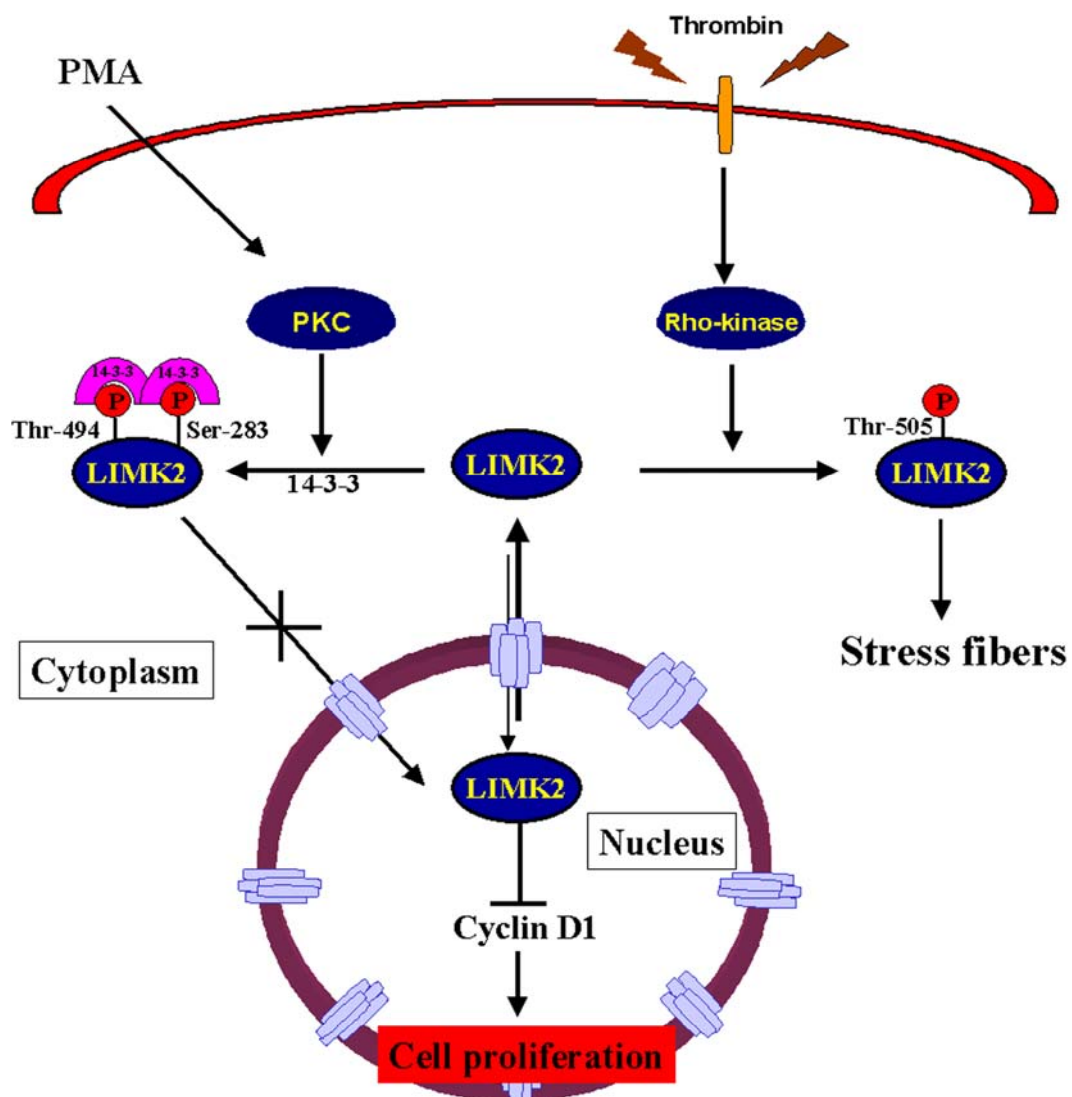


**Figure 5.3** Schematic representation of the pathway regulates the function of LIMK2. See text for details.

It has been reported recently that LIMKs control cyclin D1 expression in a manner independent of cofilin phosphorylation and actin polymerization (Roovers et al., 2003). Induction of cyclin D1 is the critical step during the G1-S phase transition of cell cycle in mammalian cells, and involves cooperative signaling by receptor tyrosine kinases, integrins, and the actin cytoskeleton (Assoian and Schwartz, 2001). In fibroblasts, cyclin D1 is induced in mid-G1 phase (~9 hr) after mitogen

stimulation of quiescent cells, and requires sustained (~5-6 hr) ERK activity (Welsh et al., 2001). Rac and/or Cdc42 can induce an early cyclin D1 expression (~3hr) in an ERK-independent manner after mitogen stimulation of quiescent cells. Rho-kinase is required for sustained ERK signaling and maintains the mid-G1 phase. Rho kinase prevents early G1 phase induction of cyclin D1 in response to Rac/Cdc42 signaling (Welsh et al., 2001). The recent study shows that LIMKs act in the nucleus to suppress Rac/Cdc42-mediated cyclin D1 expression (Roovers et al., 2003). This suggests that the regulation of nucleocytoplasmic shuttling of LIMKs may play a role in cell cycle regulation. Various studies also show that cyclin D1 expression was enhanced by the several growth stimulatory signaling pathways such as PKC (Blobe et al., 1994; Soh and Weinstein, 2003). These studies together with our findings lead us to suggest that PKC phosphorylation of LIMK2 serves to keep this protein out of the nucleus thereby relieving LIMK-mediated suppression of cyclin D1.

Based on the findings in the present study, I propose that LIMK2 has a dual function in endothelial cells. LIMK2 in the cytoplasm regulates the cofilin-mediated actin cytoskeleton rearrangement. The other function of the LIMK2 in the nucleus might be to suppress cyclin D1 expression during the G1-S phase transition thereby regulating the cell proliferation (Figure 5.3).

## 6. Summary

The endothelium regulates cellular and nutrient trafficking, maintains blood fluidity, regulates vasomotor tone, contributes to the local balance of pro-inflammatory and anti-inflammatory mediators, and participates in the generation of new blood vessels. Actin microfilaments, their associated adherens junctions and focal adhesions are important regulators of endothelial permeability and adhesiveness. After injury of the endothelium, the actin cytoskeleton is essential for endothelial cell migration and proliferation leading to wound repair. Disruption and dysfunction of the cytoskeleton may result in impairment of endothelial function, subsequently tipping the balance towards vascular disease. Thus, an understanding of the cellular and molecular biology of the endothelial cytoskeleton is important for our understanding of the pathogenesis of vascular disease such as atherosclerosis and pathological angiogenesis.

Small Rho-like GTPases such as Rho, Rac, and Cdc42 play a major role in regulating actin dynamics in stimulated endothelial cells. They often act by stimulation of specific kinases. Rho-kinase, activated by Rho, is essential for thrombin-induced endothelial stress fiber formation and cell contraction. This enzyme directly phosphorylates and inhibits myosin phosphatase leading to an increase of myosin light chain phosphorylation. Phosphorylated myosin interacts with actin filaments, and develops actin-activated ATPase-activity. Transfection studies have shown that Rho-kinase also phosphorylates LIMKs and enhances their kinase activity. LIMKs consisting of LIMK1 and LIMK2 specifically phosphorylate cofilin at Ser-3 and inactivate this actin-depolymerizing protein. The precise mechanism by which Rho-kinase regulates thrombin-induced stress fiber formation in endothelial cells is unknown.

In this study, it is found that endothelial cells express both LIMK1 and LIMK2, and a smaller isoform of LIMK2. This study for first time demonstrates the stimulation of the Rho-kinase/LIMK/cofilin pathway upon physiological cell activation. In thrombin-stimulated endothelial cells, Rho-kinase activation led to LIMK stimulation and subsequent cofilin phosphorylation. Actin stress fiber formation was blocked by dominant negative LIMK2 in thrombin-stimulated endothelial cells. These results demonstrate that in thrombin-stimulated endothelial cells, the other signal cascade downstream of Rho-kinase, i.e. the LIMK/cofilin pathway is also essential for stress fiber formation.

LIMKs have two repeats of the LIM domain at the N-terminus, followed by a PDZ domain and an unusual protein kinase domain at the carboxy terminus. A proline/serine-rich (P/S) region separates the PDZ domain from the kinase domain. In this study, it has been shown that the kinase domain of LIMK2 has a unique basic amino acid-rich motif, and that LIMK2 in resting endothelial cells shuttles between the nucleus and cytoplasm. This has been shown indirectly by inhibition of the nuclear export of LIMK2 with LMB and demonstrated directly by FRAP and FLIP analysis of the PDZ-kinase domain of LIMK2. The LIM domains of LIMK2, but not of LIMK1 inhibited its nuclear import thereby keeping LIMK2 mainly in the cytoplasm. Primary sequence analysis predicted three NLS sequences in the kinase domain of LIMK2, and two NES

sequences at C-terminal of PDZ domain. The NLS sequences of LIMK2 were very different of that of LIMK1. Interestingly the PDZ-kinase domain of LIMK2, but not of LIMK1 was enriched in the nucleus, and the kinase domain of LIMK2, but not of LIMK1 was found in the nucleolus.

Mutational analysis of the basic amino acid-rich motif (amino acids 480-503) indicated that the bipartite NLS-2 (amino acids 480-503) containing the monopartite NLS-1 (amino acids 500-503) at one end and the unique RK (amino acids 496-497) in the middle is the functional NLS and NoLS. This motif regulated the nuclear and nucleolar localization of LIMK2.

Primary sequence analysis indicated that LIMK2 has two highly disordered regions: one is present between the PDZ and the kinase domain, and the other is present in the kinase domain. Two PKC phosphorylation sites (Ser283, Thr494) were predicted in these regions. These sites were absent in the same homologous regions of LIMK1. Activation of PKC in PMA-stimulated endothelial cells stimulated the phosphorylation of LIMK2 at Ser283 and the translocation of LIMK2 and the PDZ-kinase construct of LIMK2 from the nucleus to the cytoplasm. Of the various PKC isoforms, PKC- $\alpha$  and PKC- $\beta$  were found to be mainly responsible for Ser283 phosphorylation and the regulation of translocation of LIMK2. Mutational analysis indicated that LIMK2 phosphorylation at Ser283 is functional, and revealed that phosphorylation at Thr494 might also play a role in the regulation of nucleocytoplasmic shuttling of LIMK2 by PKC.

Based on the findings of this dissertation and the data in the literature, a model of the regulation of nucleocytoplasmic shuttling of LIMK2 by PKC is proposed. LIMK2 in resting endothelial cells adopts a close conformation: the LIM domains interact with the kinase domain thereby masking the NLS and keeping the protein mainly in the cytoplasm. PDZ-kinase is more localized in the nucleus than LIMK2, due to lack of inhibition of the NLS by the LIM domains. Activation of PKCs induces phosphorylation of LIMK2 in a first step at Ser283, and probably in a second step at Thr494, causing the binding of adapter proteins such as 14-3-3. This protein complex exhibiting a locked conformation and masking the NLS might not bind to importin- $\alpha$ , and the nuclear import of this protein is inhibited.

What may be the function of LIMK2 in the nucleus? It has been reported very recently that nuclear LIMKs suppress cyclin D1 expression in a manner independent of cofilin phosphorylation and actin polymerization. Induction of cyclin D1 expression is a critical step during the G1-S phase transition of cell cycle in mammalian cells, and controlled by several growth stimulatory signaling pathways such as PKC. It is therefore suggested that the PKC-mediated inhibition of nucleocytoplasmic shuttling of LIMK2 may stimulates the expression of cyclin D1 and cell cycle progression.

Based on the findings presented in this study, I propose that LIMK2 has a dual function in endothelial cells. LIMK2 in the cytoplasm regulates the cofilin-mediated actin dynamics and stress fiber formation downstream of Rho-kinase in physiologically activated endothelial cells. Nucleocytoplasmic shuttling of LIMK2 in resting endothelial cells and its direct regulation by PKC suggests that LIMK2 might also have a function in the nucleus such as the suppression of cyclin D1 expression.

## **7. Zusammenfassung**

Das Endothel ist am Stoffaustausch zwischen Blut und umliegenden Geweben beteiligt, unterhält die Fließfähigkeit des Blutes, beeinflusst den vaskulären Tonus, trägt zum Gleichgewicht zwischen pro- und anti-inflammatorischen Mediatoren bei und ist von Bedeutung für die Angiogenese. Aktin-Mikrofilamente, die mit interzellulären *adherent junctions* und über *focal adhesions* mit der subendothelialen Matrix verbunden sind, spielen eine wichtige Rolle bei der Steuerung der endothelialen Adhäsionsfähigkeit und Barrierefunktion. Das Aktin-Zytoskelett ist vor allem nach Verletzung des Endothels essentiell für Migration und Proliferation der Zellen, was zur Wundheilung führt. Veränderungen des Zytoskeletts können somit zur Beeinträchtigung der Endothelfunktion führen, wodurch vaskuläre Erkrankungen ausgelöst werden könnten. Aufgrund dessen ist das Aufdecken der zellulären und molekularbiologischen Zusammenhänge des Endothelzytoskeletts bedeutend für das Verständnis der pathogenen Vorgänge bei Gefäßerkrankungen wie z. B. der Atherosklerose und pathologischer Angiogenese.

Eine wichtige Rolle in der Regulation der Aktindynamik stimulierter Endothelzellen spielen die kleinen Rho-ähnlichen GTPasen wie Rho, Rac und Cdc42. Diese wirken häufig über die Stimulation spezifischer Kinasen. Rho-Kinase, aktiviert durch Rho, ist bedeutend für die Thrombin - induzierte Bildung von Stressfasern und die Zellkontraktion. Dieses Enzym phosphoryliert und inhibiert direkt die Myosinphosphatase, was unmittelbar zum Anstieg der Phosphorylierung der leichten Kette des Myosin führt. Phosphoryliertes Myosin interagiert mit Aktinfilamenten und entwickelt eine Aktin-aktivierte ATPase Aktivität. In Transfektionsstudien wurde gezeigt, daß Rho-Kinase einen zweiten Signalweg stimuliert, und zwar phosphoryliert die Rho-Kinase auch LIM-Kinasen (LIMK) und erhöht deren Aktivität. LIM-Kinasen, bestehend aus LIMK1 und LIMK2, phosphorylieren Cofilin an Position Ser3 und inaktivieren dieses Aktin-depolymerisierende Protein. Der genaue Mechanismus, wie die Rho-Kinase die Thrombin - induzierte Stressfaserbildung reguliert, ist unbekannt.

In dieser Arbeit wird gezeigt, daß Endothelzellen sowohl LIMK1 als auch LIMK2 und eine kleinere Isoform von LIMK2 exprimieren. Zum ersten Mal wird die Stimulation des Rho-Kinase/ LIMK/ Cofilin-Signalwegs in physiologisch stimulierten Zellen beschrieben. In Thrombin - stimulierten Endothelzellen führte die Aktivierung der Rho-Kinase zu LIM-Kinasen Stimulierung und anschließender Cofilinphosphorylierung. Die Bildung von Aktinstressfasern wurde durch Transfektion der Endothelzellen mit dominant negativer LIMK2 blockiert. Diese Ergebnisse zeigen, daß in Thrombin - stimulierten Endothelzellen die andere Signalkaskade abwärts der Rho-Kinase, und zwar der LIMK / Cofilin-Signalweg, auch essentiell für die Ausbildung von Aktinstressfasern ist.

LIM-Kinasen haben zwei Wiederholungen der LIM-Domäne am N-Terminus, gefolgt von einer PDZ- Domäne und einer ungewöhnlichen Proteinkinase-Domäne am C-Terminus. Eine Prolin/

Serin (P/S)-reiche Region teilt die PDZ-Domäne von der Kinase-Domäne. In dieser Arbeit wurde gezeigt, dass die Kinase-Domäne von LIMK2 ein einzigartiges Motiv reich an basischen Aminosäuren enthält, und dass LIMK2 in ruhenden Endothelzellen zwischen Zellkern und Zytoplasma hin und her wandert. Das konnte indirekt durch Inhibition des Kernexports von LIMK2 mit LMB und direkt durch FRAP- und FLIP-Analysen der PDZ-Kinase-Domäne (PDZK) dargestellt werden. Die LIM-Domänen von LIMK2, nicht jedoch von LIMK1, verhinderten den Kernimport, so daß die LIM-Domänen wahrscheinlich für die vorwiegende Lokalisation der LIMK2 im Zytoplasma verantwortlich sind. Primäre Sequenzanalysen sagten drei NLS (*nuclear localization signal*) Sequenzen in der Kinase-Domäne von LIMK2 und zwei NES (*nuclear export signal*) Sequenzen C-terminal der PDZ-Domäne voraus. Die NLS-Sequenzen der LIMK2 waren sehr verschieden von denen der LIMK1. Interessanterweise war die PDZ-Domäne von LIMK2, aber nicht die von LIMK1, im Zellkern angereichert, und die Kinase-Domäne von LIMK2, aber nicht von LIMK1, wurde im Nukleolus gefunden.

Mutationsanalysen des an basischen Aminosäuren reichen Motivs von LIMK2 (AS 480-503) zeigten, dass das zweiteilige NLS-2 (AS 480-503), welches zusätzlich den einteiligen NLS-1 an einem Ende und die einmalige RK-Sequenz (AS 496-497) in der Mitte enthält, das wichtige NLS und NoLS (*nucleolus localization signal*) ist. Dieses Motiv regulierte die nukleäre und nukleoläre Lokalisation.

Weitere Sequenzanalysen zeigten zwei stark ungeordnete Regionen in LIMK2: eine zwischen der PDZ-Region und der Kinase-Domäne, die andere innerhalb der Kinase-Domäne. In diesen Regionen wurden zwei Phosphorylierungspositionen (Ser283 und Thr494) für Proteinkinase C (PKC) vorausgesagt. Diese Positionen waren nicht in LIMK1 vorhanden. Eine Aktivierung der PKC in Phorbol-12-myristat-13-acetat-stimulierten Endothelzellen stimulierte die Phosphorylierung von LIMK2 an Ser283 und die Translokation der LIMK2 und des PDZ-Kinase Konstrukts von LIMK2 vom Nukleus ins Zytoplasma. Unter den verschiedenen PKC Isoformen wurden PKC- $\alpha$  und PKC- $\beta$  als die hauptverantwortlichen Formen für die Ser283 Phosphorylierung und die Translokation identifiziert. Mutationsanalysen zeigten, dass die Phosphorylierung an Ser283 essentiell und die Phosphorylierung an Thr494 wichtig für die Regulation des Kern-Zytoplasma-*shuttle* durch PKC sind.

Basierend auf den Ergebnissen dieser Arbeit und den Daten aus der Literatur wird ein Modell der PKC-abhängigen Regulation des nukleozytoplasmatischen *shuttling* von LIMK2 vorgestellt (siehe Abb.5.2.). LIMK2 nimmt in ruhenden Endothelzellen eine geschlossene Konformation an: Die LIM-Domänen interagieren mit der Kinase-Domäne, wobei die NLS maskiert wird und das Protein im Zytoplasma verbleibt. PDZK ist eher im Zellkern lokalisiert infolge des Fehlens der NLS-Inhibition durch die LIM-Domänen. Die Aktivierung von PKC induziert in einem ersten Schritt eine Phosphorylierung von LIMK2 an Ser283, und eventuell in einem weiteren Schritt an Thr494, die eine Bindung von Adapterproteinen, wie z. Bsp. 14-3-3, verursacht. Dieser

Proteinkomplex mit maskierter NLS liegt dann in einer *locked conformation* vor und würde nicht an Importin-  $\alpha$  binden. Somit wäre der nukleäre Import dieses Proteins komplett inhibiert.

Was aber ist die Funktion von LIMK2 im Zellkern? In einer kürzlich veröffentlichten Publikation wurde gezeigt, daß nukleäre LIM-Kinasen eine Cyclin D1 Expression unterbinden, unabhängig von ihrer Wirkung auf Cofilinphosphorylierung und Aktinpolymerisation. Die Induktion der Cyclin D1 Expression ist ein wichtiger Schritt während des Übergangs der G1- zur S-Phase im Zellzyklus von Säugerzellen. Es wird deshalb vermutet, daß die PKC- vermittelte Inhibition des Imports von LIMK2 in den Zellkern die Cyclin D1 Suppression durch LIMK2 aufhebt und dadurch die Expression von Cyclin D1 stimuliert.

Basierend auf den Ergebnissen dieser Studie schlage ich eine duale Funktion der LIMK2 in Endothelzellen vor. LIMK2 reguliert im Zytoplasma die Cofilin - vermittelte Aktindynamik und Stressfaserbildung in physiologisch aktivierten Endothelzellen abwärts der Rho-Kinase. Das nukleozytoplasmatische *shuttling* der LIMK2 in Endothelzellen und dessen Regulation durch PKC suggeriert dass LIMK2 auch eine Funktion im Zellkern hat, wie z. Bsp. die Suppression der Cyclin D1 Expression.

## 8. Reference List

Abe, H., Nagaoka, R., and Obinata, T. (1993). Cytoplasmic localization and nuclear transport of cofilin in cultured myotubes. *Exp Cell Res* 206, 1-10.

Abercrombie, M., Heaysman, J. E., and Pegrum, S. M. (1970). The locomotion of fibroblasts in culture. II. "Ruffling". *Exp Cell Res* 60, 437-444.

Aird, W. C. (2001). Vascular bed-specific hemostasis: role of endothelium in sepsis pathogenesis. *Crit Care Med* 29, S28-34; discussion S34-25.

Akey, C., and Radermacher, M. (1993). Architecture of the *Xenopus* nuclear pore complex revealed by three-dimensional cryo-electron microscopy. *J Cell Biol* 122, 1-19.

Amano, M., Ito, M., Kimura, K., Fukata, Y., Chihara, K., Nakano, T., Matsuura, Y., and Kaibuchi, K. (1996). Phosphorylation and activation of myosin by Rho-associated kinase (Rho-kinase). *J Biol Chem* 271, 20246-20249.

Amano, T., Kaji, N., Ohashi, K., and Mizuno, K. (2002). Mitosis-specific activation of LIM motif-containing protein kinase and roles of cofilin phosphorylation and dephosphorylation in mitosis. *J Biol Chem* 277, 22093-22102.

Amano, T., Tanabe, K., Eto, T., Narumiya, S., and Mizuno, K. (2001). LIM-kinase 2 induces formation of stress fibers, focal adhesions and membrane blebs, dependent on its activation by Rho-associated kinase-catalyzed phosphorylation at threonine-505. *Biochem J* 354, 149-159.

Andersen, J. S., Lyon, C. E., Fox, A. H., Leung, A. K. L., Lam, Y. W., Steen, H., Mann, M., and Lamond, A. I. (2002). Directed Proteomic Analysis of the Human Nucleolus. *Current Biology* 12, 1-11.

Arber, S., Barbayannis, F. A., Hanser, H., Schneider, C., Stanyon, C. A., Bernard, O., and Caroni, P. (1998). Regulation of actin dynamics through phosphorylation of cofilin by LIM-kinase. *Nature* 393, 805-809.

Arber, S., and Caroni, P. (1996). Specificity of single LIM motifs in targeting and LIM/LIM interactions in situ. *Genes Dev* 10, 289-300.

Arber, S., Hunter, J. J., Ross, J., Jr., Hongo, M., Sansig, G., Borg, J., Perriard, J. C., Chien, K. R., and Caroni, P. (1997). MLP-deficient mice exhibit a disruption of cardiac cytoarchitectural organization, dilated cardiomyopathy, and heart failure. *Cell* 88, 393-403.

Assoian, R. K., and Schwartz, M. A. (2001). Coordinate signaling by integrins and receptor tyrosine kinases in the regulation of G1 phase cell-cycle progression. *Curr Opin Genet Dev* 11, 48-53.

- Ayscough, K. R. (1998). In vivo functions of actin-binding proteins. *Curr Opin Cell Biol* 10, 102-111.
- Bach, I. (2000). The LIM domain: regulation by association. *Mech Dev* 91, 5-17.
- Bachetti, T., and Morbidelli, L. (2000). Endothelial cells in culture: A model for studying vascular functions. *Pharmacological Research* 42, 9-19.
- Bamburg, J. R. (1999). Proteins of the ADF/cofilin family: essential regulators of actin dynamics. *Annu Rev Cell Dev Biol* 15, 185-230.
- Bamburg, J. R., McGough, A., and Ono, S. (1999). Putting a new twist on actin: ADF/cofilin modulate actin dynamics. *Trends Cell Biol* 9, 364-370.
- Bartel, D. P., Zapp, M. L., Green, M. R., and Szostak, J. W. (1991). HIV-1 Rev regulation involves recognition of non-Watson-Crick base pairs in viral RNA. *Cell* 67, 529-536.
- Bauer, K. (2000) Zellbiologische Charakterisierung des PDZ- und LIM-Domäne Proteins CLP-36, PhD Dissertation, LMU München, Munich.
- Bayliss, R., Kent, H. M., Corbett, A. H., and Stewart, M. (2000). Crystallization and initial X-ray diffraction characterization of complexes of FxFG nucleoporin repeats with nuclear transport factors. *J Struct Biol* 131, 240-247.
- Bernard, O., Burkitt, V., Webb, G. C., Bottema, C. D., Nicholl, J., Sutherland, G. R., and Matthew, P. (1996). Structure and chromosomal localization of the genomic locus encoding the Kiz1 LIM-kinase gene. *Genomics* 35, 593-596.
- Bernard, O., Ganiatsas, S., Kannourakis, G., and Dringen, R. (1994). Kiz-1, a protein with LIM zinc finger and kinase domains, is expressed mainly in neurons. *Cell Growth Differ* 5, 1159-1171.
- Bettinger, B. T., Gilbert, D. M., and Amberg, D. C. (2004). Actin up in the nucleus. *Nat Rev Mol Cell Biol* 5, 410-415.
- Birkenfeld, J., Betz, H., and Roth, D. (2003). Identification of cofilin and LIM-domain-containing protein kinase 1 as novel interaction partners of 14-3-3 zeta. *Biochem J* 369, 45-54.
- Blanchoin, L., Amann, K. J., Higgs, H. N., Marchand, J. B., Kaiser, D. A., and Pollard, T. D. (2000). Direct observation of dendritic actin filament networks nucleated by Arp2/3 complex and WASP/Scar proteins. *Nature* 404, 1007-1011.
- Blobe, G. C., Obeid, L. M., and Hannun, Y. A. (1994). Regulation of protein kinase C and role in cancer biology. *Cancer Metastasis Rev* 13, 411-431.
- Bokoch, G. M. (2003). Biology of the p21-activated kinases. *Annu Rev Biochem* 72, 743-781.

Botstein, D., Amberg, D., Mulholland, J., Huffaker, T., and Adams, A. (1997). The yeast cytoskeleton. In *Yeast III* (Cold Spring Harbor, NY: Cold Spring Harbor Lab. Press), pp. 1-80.

Bowman, G. D., Nodelman, I. M., Hong, Y., Chua, N. H., Lindberg, U., and Schutt, C. E. (2000). A comparative structural analysis of the ADF/cofilin family. *Proteins* *41*, 374-384.

Braga, V. M. (2002). Cell-cell adhesion and signaling. *Curr Opin Cell Biol* *14*, 546-556.

Bretscher, A. (1991). Microfilament structure and function in the cortical cytoskeleton. *Annu Rev Cell Biol* *7*, 337-374.

Brinkworth, R. I., Breinl, R. A., and Kobe, B. (2003). From the Cover: Structural basis and prediction of substrate specificity in protein serine/threonine kinases. *PNAS* *100*, 74-79.

Brown, S., McGrath, M. J., Ooms, L. M., Gurung, R., Maimone, M. M., and Mitchell, C. A. (1999). Characterization of two isoforms of the skeletal muscle LIM protein 1, SLIM1. Localization of SLIM1 at focal adhesions and the isoform slimmer in the nucleus of myoblasts and cytoplasm of myotubes suggests distinct roles in the cytoskeleton and in nuclear-cytoplasmic communication. *J Biol Chem* *274*, 27083-27091.

Burridge, K., and Wennerberg, K. (2004). Rho and Rac take center stage. *Cell* *116*, 167-179.

Carlier, M.-F., Laurent, V., Santolini, J., Melki, R., Didry, D., Xia, G.-X., Hong, Y., Chua, N.-H., and Pantaloni, D. (1997). Actin Depolymerizing Factor (ADF/Cofilin) Enhances the Rate of Filament Turnover: Implication in Actin-based Motility. *J Cell Biol* *136*, 1307-1322.

Carmeliet, P. (2000). Mechanisms of angiogenesis and arteriogenesis. *Nat Med* *6*, 389-395.

Carmeliet, P., and Jain, R. K. (2000). Angiogenesis in cancer and other diseases. *Nature* *407*, 249-257.

Carmo-Fonseca, M., Mendes-Soares, L., and Campos, I. (2000). To be or not to be in the nucleolus. *Nat Cell Biol* *2*, E107-112.

Cheng, A. K., and Robertson, E. J. (1995). The murine LIM-kinase gene (*limk*) encodes a novel serine threonine kinase expressed predominantly in trophoblast giant cells and the developing nervous system. *Mech Dev* *52*, 187-197.

Cines, D. B., Pollak, E. S., Buck, C. A., Loscalzo, J., Zimmerman, G. A., McEver, R. P., Pober, J. S., Wick, T. M., Konkle, B. A., Schwartz, B. S., *et al.* (1998). Endothelial Cells in Physiology and in the Pathophysiology of Vascular Disorders. *Blood* *91*, 3527-3561.

Coppolino, M. G., Krause, M., Hagendorff, P., Monner, D. A., Trimble, W., Grinstein, S., Wehland, J., and Sechi, A. S. (2001). Evidence for a molecular complex consisting of Fyb/SLAP, SLP-76, Nck, VASP and WASP that links the actin cytoskeleton to Fcγ receptor signaling during phagocytosis. *J Cell Sci* *114*, 4307-4318.

- Dan, C., Kelly, A., Bernard, O., and Minden, A. (2001). Cytoskeletal changes regulated by the PAK4 serine/threonine kinase are mediated by LIM kinase 1 and cofilin. *J Biol Chem* 276, 32115-32121.
- Darnell, J., Lodish, H., and Baltimore, D. (1986). *Molecular Cell biology*, First edn, Scientific American Books).
- Datta, Y. H., and Ewenstein, B. M. (2001). Regulated secretion in endothelial cells: biology and clinical implications. *Thromb Haemost* 86, 1148-1155.
- Davila, M., Frost, A. R., Grizzle, W. E., and Chakrabarti, R. (2003). LIM kinase 1 is essential for the invasive growth of prostate epithelial cells: implications in prostate cancer. *J Biol Chem* 278, 36868-36875.
- Dawid, I. B., Breen, J. J., and Toyama, R. (1998). LIM domains: multiple roles as adapters and functional modifiers in protein interactions. *Trends Genet* 14, 156-162.
- DeLano, W. L. (2004). *The PyMOL Molecular Graphics System*. (DeLano Scientific LLC).
- DeMali, K. A., Wennerberg, K., and Burridge, K. (2003). Integrin signaling to the actin cytoskeleton. *Curr Opin Cell Biol* 15, 572-582.
- DePasquale, J. A., and Izzard, C. S. (1987). Evidence for an actin-containing cytoplasmic precursor of the focal contact and the timing of incorporation of vinculin at the focal contact. *J Cell Biol* 105, 2803-2809.
- Dingwall, C., Ernberg, I., Gait, M. J., Green, S. M., Heaphy, S., Karn, J., Lowe, A. D., Singh, M., Skinner, M. A., and Valerio, R. (1989). Human immunodeficiency virus 1 tat protein binds trans-activation-responsive region (TAR) RNA in vitro. *Proc Natl Acad Sci U S A* 86, 6925-6929.
- dos Remedios, C. G., Chhabra, D., Kekic, M., Dedova, I. V., Tsubakihara, M., Berry, D. A., and Nosworthy, N. J. (2003). Actin binding proteins: regulation of cytoskeletal microfilaments. *Physiol Rev* 83, 433-473.
- Doyle, D. A., Lee, A., Lewis, J., Kim, E., Sheng, M., and MacKinnon, R. (1996). Crystal structures of a complexed and peptide-free membrane protein-binding domain: molecular basis of peptide recognition by PDZ. *Cell* 85, 1067-1076.
- Dundr, M., and Misteli, T. (2002). Nucleolomics: An Inventory of the Nucleolus. *Molecular Cell* 9, 5-7.
- Dunker, A. K., Lawson, J. D., Brown, C. J., Williams, R. M., Romero, P., Oh, J. S., Oldfield, C. J., Campen, A. M., Ratliff, C. M., and Hipps, K. W. (2001). Intrinsically disordered protein. *Journal of Molecular Graphics and Modelling* 19, 26-59.
- Eden, S., Rohatgi, R., Podtelejnikov, A. V., Mann, M., and Kirschner, M. W. (2002). Mechanism of regulation of WAVE1-induced actin nucleation by Rac1 and Nck. *Nature* 418, 790-793.

Edwards, D. C., and Gill, G. N. (1999). Structural features of LIM kinase that control effects on the actin cytoskeleton. *J Biol Chem* 274, 11352-11361.

Edwards, D. C., Sanders, L. C., Bokoch, G. M., and Gill, G. N. (1999). Activation of LIM-kinase by Pak1 couples Rac/Cdc42 GTPase signaling to actin cytoskeletal dynamics. *Nat Cell Biol* 1, 253-259.

Engel, J., Fasold, H., Hulla, F. W., Waechter, F., and Wegner, A. (1977). The polymerization reaction of muscle actin. *Mol Cell Biochem* 18, 3-13.

Essler, M., Amano, M., Kruse, H. J., Kaibuchi, K., Weber, P. C., and Aepfelbacher, M. (1998). Thrombin inactivates myosin light chain phosphatase via Rho and its target Rho kinase in human endothelial cells. *J Biol Chem* 273, 21867-21874.

Ettenson, D. S., and Gotlieb, A. I. (1994). Endothelial Wounds with Disruption in Cell Migration Repair Primarily by Cell Proliferation. *Microvascular Research* 48, 328-337.

Fedorov, A. A., Lappalainen, P., Fedorov, E. V., Drubin, D. G., and Almo, S. C. (1997). Structure determination of yeast cofilin. *Nat Struct Biol* 4, 366-369.

Feuerstein, R., Wang, X., Song, D., Cooke, N. E., and Liebhaber, S. A. (1994). The LIM/double zinc-finger motif functions as a protein dimerization domain. *Proc Natl Acad Sci U S A* 91, 10655-10659.

Fimia, G. M., De Cesare, D., and Sassone-Corsi, P. (2000). A family of LIM-only transcriptional coactivators: tissue-specific expression and selective activation of CREB and CREM. *Mol Cell Biol* 20, 8613-8622.

Flick, M. J., and Konieczny, S. F. (2000). The muscle regulatory and structural protein MLP is a cytoskeletal binding partner of betaI-spectrin. *J Cell Sci* 113 ( Pt 9), 1553-1564.

Foletta, V. C., Lim, M. A., Soosairajah, J., Kelly, A. P., Stanley, E. G., Shannon, M., He, W., Das, S., Massague, J., and Bernard, O. (2003). Direct signaling by the BMP type II receptor via the cytoskeletal regulator LIMK1. *J Cell Biol* 162, 1089-1098.

Foletta, V. C., Moussi, N., Sarmiere, P. D., Bamburg, J. R., and Bernard, O. (2004). LIM kinase 1, a key regulator of actin dynamics, is widely expressed in embryonic and adult tissues. *Exp Cell Res* 294, 392-405.

Folkman, J., and Shing, Y. (1992). Angiogenesis. *J Biol Chem* 267, 10931-10934.

Fornierod, M., Ohno, M., Yoshida, M., and Mattaj, I. W. (1997). CRM1 is an export receptor for leucine-rich nuclear export signals. *Cell* 90, 1051-1060.

Frangiskakis, J. M., Ewart, A. K., Morris, C. A., Mervis, C. B., Bertrand, J., Robinson, B. F., Klein, B. P., Ensing, G. J., Everett, L. A., Green, E. D., *et al.* (1996). LIM-kinase1 hemizyosity implicated in impaired visuospatial constructive cognition. *Cell* 86, 59-69.

- Freyd, G., Kim, S. K., and Horvitz, H. R. (1990). Novel cysteine-rich motif and homeodomain in the product of the *Caenorhabditis elegans* cell lineage gene *lin-11*. *Nature* *344*, 876-879.
- Fu, H., Subramanian, R. R., and Masters, S. C. (2000). 14-3-3 proteins: structure, function, and regulation. *Annu Rev Pharmacol Toxicol* *40*, 617-647.
- Fukuda, M., Asano, S., Nakamura, T., Adachi, M., Yoshida, M., Yanagida, M., and Nishida, E. (1997). CRM1 is responsible for intracellular transport mediated by the nuclear export signal. *Nature* *390*, 308-311.
- Gallo, G., and Letourneau, P. C. (1998). Axon guidance: GTPases help axons reach their targets. *Curr Biol* *8*, R80-82.
- Garcia, J. G., Verin, A. D., and Schaphorst, K. L. (1996). Regulation of thrombin-mediated endothelial cell contraction and permeability. *Semin Thromb Hemost* *22*, 309-315.
- Gerbi, S. A., Borovjagin, A. V., and Lange, T. S. (2003). The nucleolus: a site of ribonucleoprotein maturation. *Current Opinion in Cell Biology* *15*, 318-325.
- Gimbrone, M. A. J., Kume, N., and Cybulsky, M. I. (1993). Vascular endothelial dysfunction and the pathogenesis of atherosclerosis. In *Atherosclerosis Reviews.*, P. C. Weber, and A. Leaf, eds. (Raven Press, New York, NY.), pp. 1-9.
- Goeckeler, Z., and Wysolmerski, R. (1995). Myosin light chain kinase-regulated endothelial cell contraction: the relationship between isometric tension, actin polymerization, and myosin phosphorylation. *J Cell Biol* *130*, 613-627.
- Gonzalez, M. A., and Selwyn, A. P. (2003). Endothelial function, inflammation, and prognosis in cardiovascular disease. *The American Journal of Medicine* *115*, 99-106.
- Gorlich, D., and Kutay, U. (1999). Transport between the cell nucleus and the cytoplasm. *Annu Rev Cell Dev Biol* *15*, 607-660.
- Gorlich, D., Pante, N., Kutay, U., Aebi, U., and Bischoff, F. R. (1996). Identification of different roles for RanGDP and RanGTP in nuclear protein import. *Embo J* *15*, 5584-5594.
- Gournier, H., Goley, E. D., Niederstrasser, H., Trinh, T., and Welch, M. D. (2001). Reconstitution of human Arp2/3 complex reveals critical roles of individual subunits in complex structure and activity. *Mol Cell* *8*, 1041-1052.
- Gschwendt, M., Dieterich, S., Rennecke, J., Kittstein, W., Mueller, H.-J., and Johannes, F.-J. (1996). Inhibition of protein kinase C [ $\mu$ ] by various inhibitors. Inhibition from protein kinase c isoenzymes. *FEBS Letters* *392*, 77-80.
- Gunsalus, K. C., Bonaccorsi, S., Williams, E., Verni, F., Gatti, M., and Goldberg, M. L. (1995). Mutations in *twinstar*, a *Drosophila* gene encoding a cofilin/ADF homologue, result in defects in centrosome migration and cytokinesis. *J Cell Biol* *131*, 1243-1259.

- Guo, Y. X., Dallmann, K., and Kwang, J. (2003). Identification of nucleolus localization signal of betanodavirus GGNNV protein [alpha]. *Virology* 306, 225-235.
- Hall, A. (1994). Small GTP-binding proteins and the regulation of the actin cytoskeleton. *Annu Rev Cell Biol* 10, 31-54.
- Hanks, S. K., Quinn, A. M., and Hunter, T. (1988). The protein kinase family: conserved features and deduced phylogeny of the catalytic domains. *Science* 241, 42-52.
- Harreman, M. T., Kline, T. M., Milford, H. G., Harben, M. B., Hodel, A. E., and Corbett, A. H. (2004). Regulation of Nuclear Import by Phosphorylation Adjacent to Nuclear Localization Signals. *J Biol Chem* 279, 20613-20621.
- Harris, B. Z., and Lim, W. A. (2001). Mechanism and role of PDZ domains in signaling complex assembly. *J Cell Sci* 114, 3219-3231.
- Harrison, V. J., Barnes, K., Turner, A. J., Wood, E., Corder, R., and Vane, J. R. (1995). Identification of endothelin 1 and big endothelin 1 in secretory vesicles isolated from bovine aortic endothelial cells. *Proc Natl Acad Sci U S A* 92, 6344-6348.
- Hartshorne, D. J. (1998). Myosin phosphatase: subunits and interactions. *Acta Physiol Scand* 164, 483-493.
- Hatanaka, H., Ogura, K., Moriyama, K., Ichikawa, S., Yahara, I., and Inagaki, F. (1996). Tertiary structure of destrin and structural similarity between two actin-regulating protein families. *Cell* 85, 1047-1055.
- Hayward, C. P., Cramer, E. M., Song, Z., Zheng, S., Fung, R., Masse, J. M., Stead, R. H., and Podor, T. J. (1998). Studies of multimerin in human endothelial cells. *Blood* 91, 1304-1317.
- Heath, J. P., and Holifield, B. F. (1993). On the mechanisms of cortical actin flow and its role in cytoskeletal organization of fibroblast. In *Cell Behaviour: Adhesion and motility*, G. Jones, Wigley, C., and R. C. Warn, eds. (The company of Biologist Ltd), pp. 35-56.
- Heist, E. K., Srinivasan, M., and Schulman, H. (1998). Phosphorylation at the nuclear localization signal of Ca<sup>2+</sup>/calmodulin-dependent protein kinase II blocks its nuclear targeting. *J Biol Chem* 273, 19763-19771.
- Herman, I. M. (1993). Actin isoforms. *Curr Opin Cell Biol* 5, 48-55.
- Hiraoka, J., Okano, I., Higuchi, O., Yang, N., and Mizuno, K. (1996). Self-association of LIM-kinase 1 mediated by the interaction between an N-terminal LIM domain and a C-terminal kinase domain. *FEBS Lett* 399, 117-121.
- Horke, S., Reumann, K., Schweizer, M., Will, H., and Heise, T. (2004). Nuclear Trafficking of La Protein Depends on a Newly Identified Nucleolar Localization Signal and the Ability to Bind RNA. *J Biol Chem* 279, 26563-26570.

- Hulo, N., Sigrist, C. J. A., Le Saux, V., Langendijk-Genevaux, P. S., Bordoli, L., Gattiker, A., De Castro, E., Bucher, P., and Bairoch, A. (2004). Recent improvements to the PROSITE database. *Nucl Acids Res* 32, D134-137.
- Huxley, H. E. (1973). Muscular contraction and cell motility. *Nature* 243, 445-449.
- Iakoucheva, L. M., Brown, C. J., Lawson, J. D., Obradovic, Z., and Dunker, A. K. (2002). Intrinsic disorder in cell-signaling and cancer-associated proteins. *J Mol Biol* 323, 573-584.
- Iakoucheva, L. M., Radivojac, P., Brown, C. J., O'Connor, T. R., Sikes, J. G., Obradovic, Z., and Dunker, A. K. (2004). The importance of intrinsic disorder for protein phosphorylation. *Nucleic Acids Res* 32, 1037-1049.
- Ikebe, C., Ohashi, K., Fujimori, T., Bernard, O., Noda, T., Robertson, E. J., and Mizuno, K. (1997). Mouse LIM-kinase 2 gene: cDNA cloning, genomic organization, and tissue-specific expression of two alternatively initiated transcripts. *Genomics* 46, 504-508.
- Ikebe, C., Ohashi, K., and Mizuno, K. (1998). Identification of testis-specific (Limk2t) and brain-specific (Limk2c) isoforms of mouse LIM-kinase 2 gene transcripts. *Biochem Biophys Res Commun* 246, 307-312.
- Ito, M., Nakano, T., Erdodi, F., and Hartshorne, D. J. (2004). Myosin phosphatase: structure, regulation and function. *Mol Cell Biochem* 259, 197-209.
- Jacinto, A., and Wolpert, L. (2001). Filopodia. *Curr Biol* 11, R634.
- Jackson, D., Volpert, O. V., Bouck, N., and Linzer, D. I. (1994). Stimulation and inhibition of angiogenesis by placental proliferin and proliferin-related protein. *Science* 266, 1581-1584.
- Jaffe, E. A., Nachman, R. L., Becker, C. G., and Minick, C. R. (1973). Culture of human endothelial cells derived from umbilical veins. Identification by morphologic and immunologic criteria. *J Clin Invest* 52, 2745-2756.
- Jans, D. A., and Hubner, S. (1996). Regulation of protein transport to the nucleus: central role of phosphorylation. *Physiol Rev* 76, 651-685.
- Johnson, L. N., Lowe, E. D., Noble, M. E., and Owen, D. J. (1998). The Eleventh Datta Lecture. The structural basis for substrate recognition and control by protein kinases. *FEBS Lett* 430, 1-11.
- Johnson, L. N., Noble, M. E., and Owen, D. J. (1996). Active and inactive protein kinases: structural basis for regulation. *Cell* 85, 149-158.
- Jung, U., Norman, K. E., Scharffetter-Kochanek, K., Beaudet, A. L., and Ley, K. (1998). Transit time of leukocytes rolling through venules controls cytokine-induced inflammatory cell recruitment in vivo. *J Clin Invest* 102, 1526-1533.

- Kaffman, A., and O'Shea, E. K. (1999). Regulation of nuclear localization: a key to a door. *Annu Rev Cell Dev Biol* 15, 291-339.
- Kaffman, A., and Shea, E. K. (1999). Regulation of nuclear localization: A Key to a Door. *Annual Review of Cell and Developmental Biology* 15, 291-339.
- Kaplanski, G., Fabrigoule, M., Boulay, V., Dinarello, C. A., Bongrand, P., Kaplanski, S., and Farnarier, C. (1997). Thrombin induces endothelial type II activation in vitro: IL-1 and TNF-alpha-independent IL-8 secretion and E-selectin expression. *J Immunol* 158, 5435-5441.
- Karlsson, O., Thor, S., Norberg, T., Ohlsson, H., and Edlund, T. (1990). Insulin gene enhancer binding protein Isl-1 is a member of a novel class of proteins containing both a homeo- and a Cys-His domain. *Nature* 344, 879-882.
- Kim, E., Niethammer, M., Rothschild, A., Jan, Y. N., and Sheng, M. (1995). Clustering of Shaker-type K<sup>+</sup> channels by interaction with a family of membrane-associated guanylate kinases. *Nature* 378, 85-88.
- Kimura, K., Ito, M., Amano, M., Chihara, K., Fukata, Y., Nakafuku, M., Yamamori, B., Feng, J., Nakano, T., Okawa, K., *et al.* (1996). Regulation of myosin phosphatase by Rho and Rho-associated kinase (Rho-kinase). *Science* 273, 245-248.
- Kirschner, M. W. (1980). Implications of treadmilling for the stability and polarity of actin and tubulin polymers in vivo. *J Cell Biol* 86, 330-334.
- Kobe, B. (1999). Autoinhibition by an internal nuclear localization signal revealed by the crystal structure of mammalian importin alpha. *Nat Struct Biol* 6, 388-397.
- Kong, Y., Flick, M. J., Kudla, A. J., and Konieczny, S. F. (1997). Muscle LIM protein promotes myogenesis by enhancing the activity of MyoD. *Mol Cell Biol* 17, 4750-4760.
- Koshimizu, U., Takahashi, H., Yoshida, M. C., and Nakamura, T. (1997). cDNA cloning, genomic organization, and chromosomal localization of the mouse LIM motif-containing kinase gene, *Limk2*. *Biochem Biophys Res Commun* 241, 243-250.
- Kozma, R., Ahmed, S., Best, A., and Lim, L. (1995). The Ras-related protein Cdc42Hs and bradykinin promote formation of peripheral actin microspikes and filopodia in Swiss 3T3 fibroblasts. *Mol Cell Biol* 15, 1942-1952.
- Kubota, S., Copeland, T. D., and Pomerantz, R. J. (1999). Nuclear and nucleolar targeting of human ribosomal protein S25: common features shared with HIV-1 regulatory proteins. *Oncogene* 18, 1503-1514.
- Kudo, N., Wolff, B., Sekimoto, T., Schreiner, E. P., Yoneda, Y., Yanagida, M., Horinouchi, S., and Yoshida, M. (1998). Leptomycin B inhibition of signal-mediated nuclear export by direct binding to CRM1. *Exp Cell Res* 242, 540-547.

- Kuroda, S., Tokunaga, C., Kiyohara, Y., Higuchi, O., Konishi, H., Mizuno, K., Gill, G. N., and Kikkawa, U. (1996). Protein-protein interaction of zinc finger LIM domains with protein kinase C. *J Biol Chem* 271, 31029-31032.
- Kusano, K., Abe, H., and Obinata, T. (1999). Detection of a sequence involved in actin-binding and phosphoinositide-binding in the N-terminal side of cofilin. *Mol Cell Biochem* 190, 133-141.
- Kutay, U., Bischoff, F. R., Kostka, S., Kraft, R., and Gorlich, D. (1997). Export of importin alpha from the nucleus is mediated by a specific nuclear transport factor. *Cell* 90, 1061-1071.
- Lazinski, D., Grzadzielska, E., and Das, A. (1989). Sequence-specific recognition of RNA hairpins by bacteriophage antiterminators requires a conserved arginine-rich motif. *Cell* 59, 207-218.
- Leonard, S. A., Gittis, A. G., Petrella, E. C., Pollard, T. D., and Lattman, E. E. (1997). Crystal structure of the actin-binding protein actophorin from *Acanthamoeba*. *Nat Struct Biol* 4, 369-373.
- Leung, A. K., Andersen, J. S., Mann, M., and Lamond, A. I. (2003). Bioinformatic analysis of the nucleolus. *Biochem J* 376, 553-569.
- Leung, A. K., and Lamond, A. I. (2003). The dynamics of the nucleolus. *Crit Rev Eukaryot Gene Expr* 13, 39-54.
- Lippincott-Schwartz, J., Altan-Bonnet, N., and Patterson, G. H. (2003). Photobleaching and photoactivation: following protein dynamics in living cells. *Nat Cell Biol Suppl*, S7-14.
- Lum, H., and Malik, A. B. (1994). Regulation of vascular endothelial barrier function. *Am J Physiol Lung Cell Mol Physiol* 267, L223-241.
- Maciver, S. K., Pope, B. J., Whytock, S., and Weeds, A. G. (1998). The effect of two actin depolymerizing factors (ADF/cofilins) on actin filament turnover: pH sensitivity of F-actin binding by human ADF, but not of *Acanthamoeba* actophorin. *Eur J Biochem* 256, 388-397.
- Madaule, P., Eda, M., Watanabe, N., Fujisawa, K., Matsuoka, T., Bito, H., Ishizaki, T., and Narumiya, S. (1998). Role of citron kinase as a target of the small GTPase Rho in cytokinesis. *Nature* 394, 491-494.
- Maekawa, M., Ishizaki, T., Boku, S., Watanabe, N., Fujita, A., Iwamatsu, A., Obinata, T., Ohashi, K., Mizuno, K., and Narumiya, S. (1999). Signaling from Rho to the actin cytoskeleton through protein kinases ROCK and LIM-kinase. *Science* 285, 895-898.
- Manser, E., Huang, H. Y., Loo, T. H., Chen, X. Q., Dong, J. M., Leung, T., and Lim, L. (1997). Expression of constitutively active alpha-PAK reveals effects of the kinase on actin and focal complexes. *Mol Cell Biol* 17, 1129-1143.

Martiny-Baron, G., Kazanietz, M., Mischak, H., Blumberg, P., Kochs, G., Hug, H., Marme, D., and Schachtele, C. (1993). Selective inhibition of protein kinase C isozymes by the indolocarbazole Go 6976. *J Biol Chem* 268, 9194-9197.

Mattaj, I. W., and Englmeier, L. (1998). NUCLEOCYTOPLASMIC TRANSPORT: The Soluble Phase. *Annual Review of Biochemistry* 67, 265-306.

McGough, A., and Chiu, W. (1999). ADF/cofilin weakens lateral contacts in the actin filament. *J Mol Biol* 291, 513-519.

McGough, A., Pope, B., Chiu, W., and Weeds, A. (1997). Cofilin changes the twist of F-actin: implications for actin filament dynamics and cellular function. *J Cell Biol* 138, 771-781.

Meng, Y., Zhang, Y., Tregoubov, V., Janus, C., Cruz, L., Jackson, M., Lu, W. Y., MacDonald, J. F., Wang, J. Y., Falls, D. L., and Jia, Z. (2002). Abnormal spine morphology and enhanced LTP in LIMK-1 knockout mice. *Neuron* 35, 121-133.

Mertens, A. E., Roovers, R. C., and Collard, J. G. (2003). Regulation of Tiam1-Rac signalling. *FEBS Lett* 546, 11-16.

Michael, W. M., and Dreyfuss, G. (1996). Distinct Domains in Ribosomal Protein L5 Mediate 5 S rRNA Binding and Nucleolar Localization. *J Biol Chem* 271, 11571-11574.

Miki, H., Yamaguchi, H., Suetsugu, S., and Takenawa, T. (2000). IRSp53 is an essential intermediate between Rac and WAVE in the regulation of membrane ruffling. *Nature* 408, 732-735.

Mizuno, K., Okano, I., Ohashi, K., Nunoue, K., Kuma, K., Miyata, T., and Nakamura, T. (1994). Identification of a human cDNA encoding a novel protein kinase with two repeats of the LIM/double zinc finger motif. *Oncogene* 9, 1605-1612.

Montell, C. (1998). TRP trapped in fly signaling web. *Current Opinion in Neurobiology* 8, 389-397.

Mori, T., Okano, I., Mizuno, K., Tohyama, M., and Wanaka, A. (1997). Comparison of tissue distribution of two novel serine/threonine kinase genes containing the LIM motif (LIMK-1 and LIMK-2) in the developing rat. *Brain Res Mol Brain Res* 45, 247-254.

Muller, W. A. (2002). Leukocyte-endothelial cell interactions in the inflammatory response. *Lab Invest* 82, 521-533.

Mullins, R. D., Heuser, J. A., and Pollard, T. D. (1998). The interaction of Arp2/3 complex with actin: nucleation, high affinity pointed end capping, and formation of branching networks of filaments. *Proc Natl Acad Sci U S A* 95, 6181-6186.

Muslin, A. J., Tanner, J. W., Allen, P. M., and Shaw, A. S. (1996). Interaction of 14-3-3 with Signaling Proteins Is Mediated by the Recognition of Phosphoserine. *Cell* 84, 889-897.

- Muslin, A. J., and Xing, H. (2000). 14-3-3 proteins: regulation of subcellular localization by molecular interference. *Cellular Signalling* 12, 703-709.
- Nagata, K., Ohashi, K., Yang, N., and Mizuno, K. (1999). The N-terminal LIM domain negatively regulates the kinase activity of LIM-kinase 1. *Biochem J* 343 Pt 1, 99-105.
- Nathan, C. (2002). Points of control in inflammation. *Nature* 420, 846-852.
- Nilius, B., and Droogmans, G. (2001). Ion channels and their functional role in vascular endothelium. *Physiol Rev* 81, 1415-1459.
- Nishida, E. (1985). Opposite effects of cofilin and profilin from porcine brain on rate of exchange of actin-bound adenosine 5'-triphosphate. *Biochemistry* 24, 1160-1164.
- Nobes, C. D., and Hall, A. (1995). Rho, rac, and cdc42 GTPases regulate the assembly of multimolecular focal complexes associated with actin stress fibers, lamellipodia, and filopodia. *Cell* 81, 53-62.
- Nunoue, K., Ohashi, K., Okano, I., and Mizuno, K. (1995). LIMK-1 and LIMK-2, two members of a LIM motif-containing protein kinase family. *Oncogene* 11, 701-710.
- Obenauer, J. C., Cantley, L. C., and Yaffe, M. B. (2003). Scansite 2.0: proteome-wide prediction of cell signaling interactions using short sequence motifs. *Nucl Acids Res* 31, 3635-3641.
- Ohashi, K., Nagata, K., Maekawa, M., Ishizaki, T., Narumiya, S., and Mizuno, K. (2000). Rho-associated kinase ROCK activates LIM-kinase 1 by phosphorylation at threonine 508 within the activation loop. *J Biol Chem* 275, 3577-3582.
- Ohno, M., Fornerod, M., and Mattaj, I. W. (1998). Nucleocytoplasmic transport: the last 200 nanometers. *Cell* 92, 327-336.
- Ohno, S. (2001). Intercellular junctions and cellular polarity: the PAR-aPKC complex, a conserved core cassette playing fundamental roles in cell polarity. *Current Opinion in Cell Biology* 13, 641-648.
- Osada, H., Hasada, K., Inazawa, J., Uchida, K., Ueda, R., Takahashi, T., and Takahashi, T. (1996). Subcellular Localization and Protein Interaction of the Human LIMK2 Gene Expressing Alternative Transcripts with Tissue-Specific Regulation. *Biochemical and Biophysical Research Communications* 229, 582-589.
- Pante, N., and Aebi, U. (1994). Toward the molecular details of the nuclear pore complex. *J Struct Biol* 113, 179-189.
- Percipalle, P., Fomproix, N., Kylberg, K., Miralles, F., Bjorkroth, B., Daneholt, B., and Visa, N. (2003). An actin-ribonucleoprotein interaction is involved in transcription by RNA polymerase II. *PNAS* 100, 6475-6480.

Perez-Alvarado, G. C., Kosa, J. L., Louis, H. A., Beckerle, M. C., Winge, D. R., and Summers, M. F. (1996). Structure of the cysteine-rich intestinal protein, CRIP. *J Mol Biol* 257, 153-174.

Perez-Alvarado, G. C., Miles, C., Michelsen, J. W., Louis, H. A., Winge, D. R., Beckerle, M. C., and Summers, M. F. (1994). Structure of the carboxy-terminal LIM domain from the cysteine rich protein CRP. *Nat Struct Biol* 1, 388-398.

Periasamy, N., and Verkman, A. S. (1998). Analysis of Fluorophore Diffusion by Continuous Distributions of Diffusion Coefficients: Application to Photobleaching Measurements of Multicomponent and Anomalous Diffusion. *Biophys J* 75, 557-567.

Peterman, E. E., Taormina, P., 2nd, Harvey, M., and Young, L. H. (2004). Go 6983 exerts cardioprotective effects in myocardial ischemia/reperfusion. *J Cardiovasc Pharmacol* 43, 645-656.

Peterson, G. L. (1977). A simplification of the protein assay method of Lowry et al. which is more generally applicable. *Anal Biochem* 83, 346-356.

Pollard, T. D. (1986). Rate constants for the reactions of ATP- and ADP-actin with the ends of actin filaments. *J Cell Biol* 103, 2747-2754.

Pollard, T. D., and Cooper, J. A. (1986). Actin and actin-binding proteins. A critical evaluation of mechanisms and functions. *Annu Rev Biochem* 55, 987-1035.

Pomies, P., Louis, H. A., and Beckerle, M. C. (1997). CRP1, a LIM domain protein implicated in muscle differentiation, interacts with alpha-actinin. *J Cell Biol* 139, 157-168.

Pope, B. J., Zierler-Gould, K. M., Kuhne, R., Weeds, A. G., and Ball, L. J. (2004). Solution structure of human cofilin: actin binding, pH sensitivity, and relationship to actin-depolymerizing factor. *J Biol Chem* 279, 4840-4848.

Prudovsky, I., Bagala, C., Tarantini, F., Mandinova, A., Soldi, R., Bellum, S., and Maciag, T. (2002). The intracellular translocation of the components of the fibroblast growth factor 1 release complex precedes their assembly prior to export. *J Cell Biol* 158, 201-208.

Rando, O. J., Zhao, K., and Crabtree, G. R. (2000). Searching for a function for nuclear actin. *Trends in Cell Biology* 10, 92-97.

Ridley, A. J. (2001). Rho GTPases and cell migration. *J Cell Sci* 114, 2713-2722.

Ridley, A. J., and Hall, A. (1992). The small GTP-binding protein rho regulates the assembly of focal adhesions and actin stress fibers in response to growth factors. *Cell* 70, 389-399.

Ridley, A. J., Paterson, H. F., Johnston, C. L., Diekmann, D., and Hall, A. (1992). The small GTP-binding protein rac regulates growth factor-induced membrane ruffling. *Cell* 70, 401-410.

- Robbins, J., Dilworth, S. M., Laskey, R. A., and Dingwall, C. (1991). Two interdependent basic domains in nucleoplasmin nuclear targeting sequence: identification of a class of bipartite nuclear targeting sequence. *Cell* 64, 615-623.
- Roovers, K., Klein, E. A., Castagnino, P., and Assoian, R. K. (2003). Nuclear translocation of LIM kinase mediates Rho-Rho kinase regulation of cyclin D1 expression. *Dev Cell* 5, 273-284.
- Ross, R. (1993). The pathogenesis of atherosclerosis: a perspective for the 1990s. *Nature* 362, 801-809.
- Russo, G., Ricciardelli, G., and Pietropaolo, C. (1997). Different Domains Cooperate to Target the Human Ribosomal L7a Protein to the Nucleus and to the Nucleoli. *J Biol Chem* 272, 5229-5235.
- Sambrook, J., and Russell, D. W. (2001). *Molecular Cloning A Laboratory manual*, 3 edn, Cold Spring Harbor Laboratory Press, New York).
- Sanchez-Garcia, I., Osada, H., Forster, A., and Rabbitts, T. H. (1993). The cysteine-rich LIM domains inhibit DNA binding by the associated homeodomain in Isl-1. *Embo J* 12, 4243-4250.
- Schmeichel, K. L., and Beckerle, M. C. (1994). The LIM domain is a modular protein-binding interface. *Cell* 79, 211-219.
- Schmidt-Zachmann, M., and Nigg, E. (1993). Protein localization to the nucleolus: a search for targeting domains in nucleolin. *J Cell Sci* 105, 799-806.
- Schoenwaelder, S. M., and Burridge, K. (1999). Bidirectional signaling between the cytoskeleton and integrins. *Curr Opin Cell Biol* 11, 274-286.
- Sells, M. A., Knaus, U. G., Bagrodia, S., Ambrose, D. M., Bokoch, G. M., and Chernoff, J. (1997). Human p21-activated kinase (Pak1) regulates actin organization in mammalian cells. *Curr Biol* 7, 202-210.
- Shaw, P. J., and Jordan, E. G. (1995). The nucleolus. *Annu Rev Cell Dev Biol* 11, 93-121.
- Shirai, Y., and Saito, N. (2002). Activation mechanisms of protein kinase C: maturation, catalytic activation, and targeting. *J Biochem (Tokyo)* 132, 663-668.
- Slice, L. W., Codner, E., Antelman, D., Holly, M., Wegrzynski, B., Wang, J., Toome, V., Hsu, M. C., and Nalin, C. M. (1992). Characterization of recombinant HIV-1 Tat and its interaction with TAR RNA. *Biochemistry* 31, 12062-12068.
- Small, J. V. (1988). The actin cytoskeleton. *Electron Microsc Rev* 1, 155-174.
- Small, J. V. (1989). Microfilament-based motility in non-muscle cells. *Curr Opin Cell Biol* 1, 75-79.

- Small, J. V. (1994). Lamellipodia architecture: actin filament turnover and the lateral flow of actin filaments during motility. *Semin Cell Biol* 5, 157-163.
- Small, J. V., Anderson, K., and Rottner, K. (1996). Actin and the coordination of protrusion, attachment and retraction in cell crawling. *Biosci Rep* 16, 351-368.
- Small, J. V., Isenberg, G., and Celis, J. E. (1978). Polarity of actin at the leading edge of cultured cells. *Nature* 272, 638-639.
- Small, J. V., Rohlf, A., and Herzog, M. (1993). Actin and cell movement. *Symp Soc Exp Biol* 47, 57-71.
- Small, J. V., Rottner, K., and Kaverina, I. (1999). Functional design in the actin cytoskeleton. *Current Opinion in Cell Biology* 11, 54-60.
- Small, J. V., Rottner, K., Kaverina, I., and Anderson, K. I. (1998). Assembling an actin cytoskeleton for cell attachment and movement. *Biochim Biophys Acta* 1404, 271-281.
- Small, J. V., Stradal, T., Vignal, E., and Rottner, K. (2002). The lamellipodium: where motility begins. *Trends in Cell Biology* 12, 112-120.
- Snapp, E. L., Altan, N., and Lippincott-Schwartz, J. (2003). *Current Protocols in Cell Biology*, Vol 2, John Wiley & Sons, Inc.).
- Soh, J.-W., and Weinstein, I. B. (2003). Roles of Specific Isoforms of Protein Kinase C in the Transcriptional Control of Cyclin D1 and Related Genes. *J Biol Chem* 278, 34709-34716.
- Stade, K., Ford, C. S., Guthrie, C., and Weis, K. (1997). Exportin 1 (Crm1p) is an essential nuclear export factor. *Cell* 90, 1041-1050.
- Stevens, T., Garcia, J. G., Shasby, D. M., Bhattacharya, J., and Malik, A. B. (2000). Mechanisms regulating endothelial cell barrier function. *Am J Physiol Lung Cell Mol Physiol* 279, L419-422.
- Sumi, T., Matsumoto, K., and Nakamura, T. (2001a). Specific activation of LIM kinase 2 via phosphorylation of threonine 505 by ROCK, a Rho-dependent protein kinase. *J Biol Chem* 276, 670-676.
- Sumi, T., Matsumoto, K., and Nakamura, T. (2002). Mitosis-dependent phosphorylation and activation of LIM-kinase 1. *Biochem Biophys Res Commun* 290, 1315-1320.
- Sumi, T., Matsumoto, K., Shibuya, A., and Nakamura, T. (2001b). Activation of LIM kinases by myotonic dystrophy kinase-related Cdc42-binding kinase alpha. *J Biol Chem* 276, 23092-23096.
- Suter, D. M., and Forscher, P. (1998). An emerging link between cytoskeletal dynamics and cell adhesion molecules in growth cone guidance. *Curr Opin Neurobiol* 8, 106-116.

- Svitkina, T. M., and Borisy, G. G. (1999). Arp2/3 complex and actin depolymerizing factor/cofilin in dendritic organization and treadmilling of actin filament array in lamellipodia. *J Cell Biol* 145, 1009-1026.
- Svitkina, T. M., Verkhovsky, A. B., McQuade, K. M., and Borisy, G. G. (1997). Analysis of the actin-myosin II system in fish epidermal keratocytes: mechanism of cell body translocation. *J Cell Biol* 139, 397-415.
- Swinscoe, J. C., and Carlson, E. C. (1992). Capillary endothelial cells secrete a heparin-binding mitogen for pericytes. *J Cell Sci* 103 ( Pt 2), 453-461.
- Takahashi, H., Koshimizu, U., Miyazaki, J., and Nakamura, T. (2002). Impaired spermatogenic ability of testicular germ cells in mice deficient in the LIM-kinase 2 gene. *Dev Biol* 241, 259-272.
- Takahashi, H., Koshimizu, U., and Nakamura, T. (1998). A novel transcript encoding truncated LIM kinase 2 is specifically expressed in male germ cells undergoing meiosis. *Biochem Biophys Res Commun* 249, 138-145.
- Tan, P., Lusinskas, F. W., and Homer-Vanniasinkam, S. (1999). Cellular and molecular mechanisms of inflammation and thrombosis. *Eur J Vasc Endovasc Surg* 17, 373-389.
- Tang, S., Morgan, K. G., Parker, C., and Ware, J. A. (1997). Requirement for Protein Kinase C theta for Cell Cycle Progression and Formation of Actin Stress Fibers and Filopodia in Vascular Endothelial Cells. *J Biol Chem* 272, 28704-28711.
- Taniguchi, E., Toyoshima-Morimoto, F., and Nishida, E. (2002). Nuclear translocation of plk1 mediated by its bipartite nuclear localization signal. *J Biol Chem* 277, 48884-48888.
- Tarantini, F., Micucci, I., Bellum, S., Landriscina, M., Garfinkel, S., Prudovsky, I., and Maciag, T. (2001). The precursor but not the mature form of IL1alpha blocks the release of FGF1 in response to heat shock. *J Biol Chem* 276, 5147-5151.
- Thompson, J., Higgins, D., and Gibson, T. (1994). CLUSTAL W: improving the sensitivity of progressive multiple sequence alignment through sequence weighting, position-specific gap penalties and weight matrix choice. *Nucl Acids Res* 22, 4673-4680.
- Thomson, S., Mahadevan, L. C., and Clayton, A. L. (1999). MAP kinase-mediated signalling to nucleosomes and immediate-early gene induction. *Semin Cell Dev Biol* 10, 205-214.
- Tomiyoshi, G., Horita, Y., Nishita, M., Ohashi, K., and Mizuno, K. (2004). Caspase-mediated cleavage and activation of LIM-kinase 1 and its role in apoptotic membrane blebbing. *Genes Cells* 9, 591-600.
- Tomba, P. (2002). Intrinsically unstructured proteins. *Trends in Biochemical Sciences* 27, 527-533.

Topham, M. K., Bunting, M., Zimmerman, G. A., McIntyre, T. M., Blackshear, P. J., and Prescott, S. M. (1998). Protein kinase C regulates the nuclear localization of diacylglycerol kinase-zeta. *Nature* 394, 697-700.

Uehata, M., Ishizaki, T., Satoh, H., Ono, T., Kawahara, T., Morishita, T., Tamakawa, H., Yamagami, K., Inui, J., Maekawa, M., and Narumiya, S. (1997). Calcium sensitization of smooth muscle mediated by a Rho-associated protein kinase in hypertension. *Nature* 389, 990-994.

van Leeuwen, F. N., van Delft, S., Kain, H. E., van der Kammen, R. A., and Collard, J. G. (1999). Rac regulates phosphorylation of the myosin-II heavy chain, actinomyosin disassembly and cell spreading. *Nat Cell Biol* 1, 242-248.

van Nieuw Amerongen, G. P., Koolwijk, P., Versteilen, A., and van Hinsbergh, V. W. M. (2003). Involvement of RhoA/Rho Kinase Signaling in VEGF-Induced Endothelial Cell Migration and Angiogenesis In Vitro. *Arterioscler Thromb Vasc Biol* 23, 211-217.

Vartiainen, M. K., Mustonen, T., Mattila, P. K., Ojala, P. J., Thesleff, I., Partanen, J., and Lappalainen, P. (2002). The Three Mouse Actin-depolymerizing Factor/Cofilins Evolved to Fulfill Cell-Type-specific Requirements for Actin Dynamics. *Mol Biol Cell* 13, 183-194.

Vouret-Craviari, V., Bourcier, C., Boulter, E., and Van Obberghen-Schilling, E. (2002). Distinct signals via Rho GTPases and Src drive shape changes by thrombin and sphingosine-1-phosphate in endothelial cells. *J Cell Sci* 115, 2475-2484.

Wang, G. X., Cai, S. X., Wang, P. Q., Ouyang, K. Q., Wang, Y. L., and Xu, S. R. (2002). Shear-induced changes in endothelin-1 secretion of microvascular endothelial cells. *Microvasc Res* 63, 209-217.

Wang, J. Y., Frenzel, K. E., Wen, D., and Falls, D. L. (1998). Transmembrane Neuregulins Interact with LIM Kinase 1, a Cytoplasmic Protein Kinase Implicated in Development of Visuospatial Cognition. *J Biol Chem* 273, 20525-20534.

Wegner, A. (1976). Head to tail polymerization of actin. *J Mol Biol* 108, 139-150.

Wegner, A. (1977). The mechanism of ATP hydrolysis by polymer actin. *Biophys Chem* 7, 51-58.

Weis, K. (2003). Regulating access to the genome: nucleocytoplasmic transport throughout the cell cycle. *Cell* 112, 441-451.

Welsh, C. F., Roovers, K., Villanueva, J., Liu, Y., Schwartz, M. A., and Assoian, R. K. (2001). Timing of cyclin D1 expression within G1 phase is controlled by Rho. *Nat Cell Biol* 3, 950-957.

Wessells, N. K., Spooner, B. S., and Luduena, M. A. (1973). Surface movements, microfilaments and cell locomotion. *Ciba Found Symp* 14, 53-82.

- Wolff, B., Sanglier, J. J., and Wang, Y. (1997). Leptomycin B is an inhibitor of nuclear export: inhibition of nucleo-cytoplasmic translocation of the human immunodeficiency virus type 1 (HIV-1) Rev protein and Rev-dependent mRNA. *Chem Biol* 4, 139-147.
- Wong, A. J., Pollard, T. D., and Herman, I. M. (1983). Actin filament stress fibers in vascular endothelial cells in vivo. *Science* 219, 867-869.
- Woods, D. F., and Bryant, P. J. (1993). ZO-1, DlgA and PSD-95/SAP90: homologous proteins in tight, septate and synaptic cell junctions. *Mech Dev* 44, 85-89.
- Wozniak, R. W., Rout, M. P., and Aitchison, J. D. (1998). Karyopherins and kissing cousins. *Trends in Cell Biology* 8, 184-188.
- Wright, P. E., and Dyson, H. J. (1999). Intrinsically unstructured proteins: re-assessing the protein structure-function paradigm. *Journal of Molecular Biology* 293, 321-331.
- Yaffe, M. B., Rittinger, K., Volinia, S., Caron, P. R., Aitken, A., Leffers, H., Gamblin, S. J., Smerdon, S. J., and Cantley, L. C. (1997). The Structural Basis for 14-3-3:Phosphopeptide Binding Specificity. *Cell* 91, 961-971.
- Yang, N., Higuchi, O., and Mizuno, K. (1998a). Cytoplasmic localization of LIM-kinase 1 is directed by a short sequence within the PDZ domain. *Exp Cell Res* 241, 242-252.
- Yang, N., Higuchi, O., Ohashi, K., Nagata, K., Wada, A., Kangawa, K., Nishida, E., and Mizuno, K. (1998b). Cofilin phosphorylation by LIM-kinase 1 and its role in Rac-mediated actin reorganization. *Nature* 393, 809-812.
- Yang, N., and Mizuno, K. (1999). Nuclear export of LIM-kinase 1, mediated by two leucine-rich nuclear-export signals within the PDZ domain. *Biochem J* 338 ( Pt 3), 793-798.
- Yoneda, Y. (2000). Nucleocytoplasmic protein traffic and its significance to cell function. *Genes Cells* 5, 777-787.
- Yonezawa, N., Nishida, E., Iida, K., Yahara, I., and Sakai, H. (1990). Inhibition of the interactions of cofilin, destrin, and deoxyribonuclease I with actin by phosphoinositides. *J Biol Chem* 265, 8382-8386.
- Yoshioka, K., Foletta, V., Bernard, O., and Itoh, K. (2003). A role for LIM kinase in cancer invasion. *Proc Natl Acad Sci U S A* 100, 7247-7252.
- Zhang, H., Zha, X., Tan, Y., Hornbeck, P. V., Mastrangelo, A. J., Alessi, D. R., Polakiewicz, R. D., and Comb, M. J. (2002). Phosphoprotein Analysis Using Antibodies Broadly Reactive against Phosphorylated Motifs. *J Biol Chem* 277, 39379-39387.
- Zheng, J., Knighton, D. R., ten Eyck, L. F., Karlsson, R., Xuong, N., Taylor, S. S., and Sowadski, J. M. (1993). Crystal structure of the catalytic subunit of cAMP-dependent protein kinase complexed with MgATP and peptide inhibitor. *Biochemistry* 32, 2154-2161.

## **Acknowledgements**

It is my privilege to express my sincere gratitude to Prof. Dr. med. Wolfgang Siess for his expert supervision, mentorship and constant encouragement, which developed a sense of self confidence and independent thinking in computing the entire course of present work.

I would like to thank Prof. Dr. med. P.C. Weber, Director, Institut für Prophylaxe und Epidemiologie der Kreislaufkrankheiten, Universität München for accepting me to work in this institute.

I am thankful to Prof. Dr. Michael Schleicher and Dr. Ralph Gräf (Institute of Cell biology, LMU, Munich) for their expert suggestions and unlimited access to confocal microscopy.

I am also thankful to Dr. K. Mizuno for providing the LIMK2 cDNA.

I am delighted to thank Dr. Stefan Linder for many illuminating discussions, his strong intellectual and other supports throughout this work.

I am grateful to Dharmendra Pandey, without whom my stay in Germany and this research work would have not been possible. I wish to thank Navneet Tyagi and Ravi for their selfless effort and support during the preparation of this dissertation.

I am thankful to Sandra Penz, Enno Rother, Nadine Haserück, Harry Gebhard, Dr. Christian Johannes, Barbara Shell and Andreas Schröder for the mutual support and all the help whenever I needed in public relation. I am also thankful to Nicole Wilke and Barbara Böhlig for an expert technical assistance and the help in official work of the lab. Thanks also to Nada Vukorepa for taking care of all the glassware and the lab.

I am deeply indebted to all my colleagues in the IPEK institute and the friends from Munich for all their help and homely environment, which gave me a moral support and strength to work abroad, thousands of miles away from my home.

I am deeply grateful to my parents and brothers for their blessings, affections, moral support and constant encouragement.

# List of publications

## Original Articles

1. **Rother, E., Brandl, R., Baker, D. L., Goyal, P., Gebhard, H., Tigyi, G., and Siess, W.** (2003). Subtype-Selective Antagonists of Lysophosphatidic Acid Receptors Inhibit Platelet Activation Triggered by the Lipid Core of Atherosclerotic Plaques. *Circulation* 108, 741-747.
2. **Penz, S., Reininger, A.J., Brandl, R., Goyal, P., Rabie, T., Bernlochner, I., Rother, E., Goetz, C., Engelmann, B., Smethurst, P.A., Ouwehand, W.H., Farndale, R., Nieswandt, B., and Siess, W.** (2005) Human atheromatous plaques stimulate thrombusformation by activating platelet glycoprotein VI. *FASEB J* 19: 898–909
3. **Goyal, P., Pandey, D., Behring, A., and Siess, W.** (2005) Inhibition of nuclear import of LIMK2 in endothelial cells by protein kinase C-dependent phosphorylation at Ser283. *J Biol Chem*, Epub 2005 May 27.
4. **Miehe, U., Neumaier-Wagner, P., Kadyrov, M., Goyal, P., Alfer, J., Rath, W., and Huppertz, B.** (2005). Concerted upregulation of CLP36 and smooth muscle actin protein expression in human endometrium during decidualization *Cells Tissues Organs* Epub 2005 Jan 13.
5. **Pandey, D., Goyal, P., and Siess, W.** (2005). Regulation of LIM-kinase1 and cofilin in activated platelets. *Revised version resubmitted to Blood*.
6. **Goyal, P., and Siess, W.** (2005). Identification of unique nucleolar and nuclear localization signals in LIMK2. *Submitted to J Biol Chem*.
7. **Massberg, S., Konrad, I., Schürzinger, K., Lorenz, M., Schneider, S., Zohnhoefer, D., Hoppe, K., Schiemann, M., Kennerknecht, E., Sauer, S., Rudelius, M., Seidl, S., Schulz, M., Sorge, F., Langer, H., Peluso, M., Goyal, P., Vestweber, D., Emambokus, N. R., Busch, D. H., Frampton, J., and Gawaz, M.** (2005). Platelets secrete SDF-1 $\alpha$  and recruit bone marrow-derived progenitor cells to arterial thrombi *in vivo*. *Revised version resubmitted to Nature Medicine*.
8. **Tyagi, N. K., Goyal, P., Kumar, A., Pandey, D., Siess, W., Kinne, R. K. H.** (2005). Human Sodium/D-Glucose Cotransporter 1: Purification, Functional Reconstitution, and Characterization of Ligand-Induced Conformational Changes as Studied by Tryptophan Fluorescence. *Revised version resubmitted to J Biol Chem*.
9. **Goyal, P., Pandey, D., and Siess, W.** (2005). LIMKs regulate stress fiber formation in thrombin-activated endothelial cells. *In preparation*.

## Presentations at scientific meetings

### Oral Presentation

**Pankaj Goyal**, Dharmendra Pandey, Wolfgang Siess. “Dual function of LIM-Kinases in endothelial cells”. Presented at Annual Meeting of "Gesellschaft für Mikrozirkulation und Vaskuläre Biologie", Munich, Germany. (16-18 Oct., 2003), (**nominated for Young investigator Award**)

### Poster Presentations

1. **Pankaj Goyal**, Dharmendra Pandey, Wolfgang Siess. “LIM-kinases regulate actin dynamics in thrombin-stimulated endothelial cells” at Adhesion Meeting, Munich, Germany (28-30 April, 2005).
2. Dharmendra Pandey, **Pankaj Goyal**, Wolfgang Siess. “LIM-kinases regulate actin dynamics in thrombin-stimulated endothelial cells” at Adhesion Meeting, Munich, Germany (28-30 April, 2005).
3. Daniel Walz, Katharina Hüfner, Martin Aepfelbacher, **Pankaj Goyal**, Stefan Linder. “Podosome regulation through cofilin-regulatory pathways” at Adhesion Meeting, Munich, Germany (28-30 April, 2005).
4. Peruka M Neumaier-Wagner, Ulrich Miehe, Simon Black, Bertold Huppertz, Karl-Friedrich Beck, Josef Pfeilschifter, **Pankaj Goyal**. “Role of the actin modifying protein CLP36 in pregnancies complicated by preeclampsia”. International Society of Obstetric Medicine meeting (14-14 Nov, 2004).
5. P. Neumaier-Wagner, U. Miehe, Kadyrov, **P. Goyal**, J Alfer, W. Rath, B. Huppertz. “Elfin, the human CLP36, is expressed in decidualized endometrial stromal cells”. 10. European Placenta Group-Meeting IFPA-Meeting (23-28 Sept., 2003).
6. U. Miehe, S. Black, B. Huppertz, K.F. Beck, J. Pfeilschifter, **P. Goyal**, W. Rath, P., Neumaier-Wagner. “Role of the actin modifying protein CLP36 in pregnancies complicated by preeclampsia – new insights into the pathophysiology”. 10. European Placenta Group-Meeting IFPA-Meeting (23-28 Sept., 2003).
7. **Pankaj Goyal**, Dharmendra Pandey, Wolfgang Siess. “Regulation of LIM-Kinases in endothelial cells”. Presented at 4th Symposium on the Biology of Endothelial cells, Munich, Germany (18-20 July, 2003).
8. Pandey D., **Goyal P.**, Bamburg J. R., Siess W. “Analysis of the Rho-kinase/LIMkinase/cofilin signaling pathway in activated platelets” XIXth Congress of the International Society on Thrombosis and Haemostasis, Birmingham, UK (12-18 July 2003).

9. **Pankaj Goyal**, Dharmendra Pandey, Wolfgang Siess. "Regulation of LIM-Kinases and cofilin in platelets and endothelial cells". at 2nd Symposium on Cell Dynamics, Munich, Germany (9-12 Oct, 2002).
10. **Pankaj Goyal**, Neelo Singh "PCR based diagnosis for Kala-azar" at Indo-European Symposium & Workshop on Cytogenetics & Molecular Genetics, Tata Memorial Hospital, Mumbai, India (3-4 Dec, 1999).

# Curriculum vitae

## Personal Data

Name	Pankaj Goyal
Date/Place of birth	19 <sup>th</sup> April 1976/Agra, India
Nationality	Indian
Marital Status	Married

## Academic Qualification

1997-1998	M.Tech Biotechnology, Inst. of Engg. & Tech., Lucknow, India
1995-1997	M.Sc. Biotechnology, Banaras Hindu University, Varanasi, India
1992-1995	B.Sc. (Honors) Chemistry, Dayalbagh Educational Inst., Agra, India

## Scientific background

2001-present	Graduate student and research scholar at the Institut für Prophylaxe und Epidemiologie der Kreislaufkrankheiten, Universität München, Germany.
2000-2001	CSIR Junior research fellow at Indian Institute of Technology Bombay, India
1998-1998	Project assistant at Central Drug Research Institute, Lucknow, India

## Achievements

Qualified ASRB-NET examination of Agricultural sciences and awarded **Assistant Professorship/Lectureship** by Agriculture Scientist Recruitment Board.

Qualified CSIR-UGC NET examination and awarded **Junior Research Fellowship** by CSIR and **Lectureship** by UGC.



